



HAL
open science

Effective field theory studies of hadron-hadron interactions

Junxu Lu

► **To cite this version:**

Junxu Lu. Effective field theory studies of hadron-hadron interactions. High Energy Physics - Phenomenology [hep-ph]. Université Paris-Saclay; Beihang university (Pékin), 2020. English. NNT : 2020UPASP095 . tel-03187168

HAL Id: tel-03187168

<https://theses.hal.science/tel-03187168>

Submitted on 31 Mar 2021

HAL is a multi-disciplinary open access archive for the deposit and dissemination of scientific research documents, whether they are published or not. The documents may come from teaching and research institutions in France or abroad, or from public or private research centers.

L'archive ouverte pluridisciplinaire **HAL**, est destinée au dépôt et à la diffusion de documents scientifiques de niveau recherche, publiés ou non, émanant des établissements d'enseignement et de recherche français ou étrangers, des laboratoires publics ou privés.

Effective field theory studies of hadron-hadron interactions

**Thèse de doctorat de l'université Paris-Saclay et
de l'université Beihang**

École doctorale n° 576, Particules, Hadrons, Énergie, Noyau,
Instrumentation, Imagerie, Cosmos et Simulation (PHENIICS)
Spécialité de doctorat: Physique Hadronique
Unité de recherche : Université Paris-Saclay, CNRS, IJCLab, 91405, Orsay, France
Réfèrent : Faculté des sciences d'Orsay

Thèse présentée et soutenue à Pékin, le 17/12/2020, par

Junxu LU

Composition du Jury

Qing WANG Professeur, Tsinghua University	Président
Feng-Kun GUO Directeur de Recherche (HDR), Institute of Theoretical Physics, Chinese Academy of Sciences	Rapporteur & Examineur
Norbert KAISER Professeur, Technical University of Munich	Rapporteur
Cong-Feng QIAO Professeur, University of Chinese Academy of Sciences	Examineur
Qiang ZHAO Directeur de Recherche, Institute of High Energy Physics, Chinese Academy of Sciences	Examineur
Han-Qing ZHENG Professeur, Peking University	Examineur
Bachir MOUSSALLAM Directeur de Recherche, Laboratoire de Physique des 2 Infinis Irène Joliot-Curie	Directeur de thèse
Li-Sheng GENG Professeur, Beihang University	Co-Directeur de thèse
Li-Hua ZHU Professeur, Beihang University	Invité

Acknowledgements

I would like to express my sincere gratitude to my teachers, classmates, families and friends who cared about and helped me.

First of all, I would like to sincerely thank my supervisor in Beihang University, Professor Lisheng Geng. Prof. Geng is rigorous, efficient and conscientious. He is very sensitive to physics and meanwhile very experienced to find solutions. It was him who inspired my interests in effective field theory and hadron-hadron interactions. During my PhD, he provided me great guidance, great support and countless suggestions. Whenever my research was faced with troubles, Prof. Geng always took time to discuss and gave me encouragement. In addition, Prof. Geng also provided a broad platform for me, in which I can learn from outstanding colleagues in our group as well as top physicists abroad. These communications have broadened my horizons and enabled me to think from different angles.

It is a honor of me to be supervised by Dr. Bachir Moussallam in Paris-Saclay university. Dr. Moussallam is a very kind and warm elder, who is full of wisdom and always there with patience as if waiting for my, even stupid, questions. He could always provided me very nice explanations and answers. He taught me to concentrate more on the deeper details behind the mathematics from the point of view of physics. He never hesitated to help me during my stay in France with not only my researches but also my life in Paris. And he was very tolerant in the first year during which I was not able to handle the researches from both sides simultaneously. It was quite a pity of me that my stay in France was suspended because of my illness.

I would like to thank all my colleagues in the theoretical physical group in Beihang University. Prof Huaxing Chen gave me detailed advises on group theory. Prof Manuel Pavon Valderrama provided significant ideas and solutions on heavy flavor effective field theory. I would also like to thank all the group members, Xiulei Ren, Kaiwen Li, Dan Zhou, Yu Zhou, Erliang Cui, Yang Xiao, Ruixiang Shi, Tianwei Wu, Mingzhu Liu and so on for helpful discussions and suggestions. Besides, I also thank all my collaborators in my work, Prof Jujun Xie, Prof Chuwen Xiao, Prof En Wang, Prof Ulf-G Meißner, Prof Hyodo Tetsuo, Prof Zhihui Guo, and Doctor Menglin Du, Chunhua Zeng, Sanchez Sanchez Mario for their criticized advises. I would like to thank Prof Yujie Zhang, Prof Gaolong Zhang, Prof Chengping Shen, Prof Lihua Zhu, Prof Xiaoyun Le, Prof Baohua Sun in Beihang university who have ever taught me during my postgraduate.

I would also like to thank all the colleagues in the Bonn University during my three months stay there. I thank

Prof Ulf-G Meißner for providing such an opportunity and kind suggestions on meson-baryon interactions I thank Doctor Menglin Du, Qian Wang, Zhihui Guo for kind and patient guidance on my researches and life there.

I would also like to thank all the colleagues in the theoretical physical group in Paris-Saclay University. I thank Prof V. Bernard for kind advises on subthreshold parameters and Prof Udirajara van Kolck for suggestions on the unitary method for meson-baryon scattering. I thank the director IPN Orsay, Prof Michal Guidal for providing me the opportunity to visit IPN. I also thank all the members of theoretical group for their care of my stay there.

I am very grateful of my families for their constant support. I thank all my friends for their kind encouragement and motivation. I thank all the people who helped me during my illness both in China and France.

Finally I am very thankful to Beihang University, Scholarship Council of China(CSC) and Paris-Saclay University for their financial support.

RÉSUMÉ DE LA THÈSE

Étude des interactions hadron-hadron en théorie effective des champs

A. Introduction

Nous savons maintenant que notre univers est régi par 4 forces fondamentales: la gravitation, l'électromagnétisme, la force forte et la force faible. Alors que la gravitation concerne principalement les plus grandes structures de l'univers, les trois autres forces sont responsables de la dynamique des structures les plus petites, autrement dit des particules élémentaires, dont les dimensions sont inférieures de 39 ordres de grandeur à celles des grandes structures. La théorie de ces trois dernières forces constitue le fameux Modèle Standard au sein duquel l'interaction forte est décrite par la chromodynamique quantique (QCD).

La QCD a été largement développée dans la deuxième moitié du siècle dernier. La résolution d'une série de paradoxes apparents, comme le fait que l'on n'observe pas de quarks isolés, a nécessité une réflexion approfondie qui a révélé deux propriétés essentielles de la QCD. La première est l'hypothèse du confinement de la couleur qui implique que seules les particules neutres en couleur, comme les mésons ou les baryons, sont physiquement observables alors même que les degrés de liberté de base de la théorie, les quarks et les gluons, ont des charges de couleur. La deuxième propriété est la liberté asymptotique qui peut être simplement formulée comme le fait que la constante de couplage devient petite quand le moment de transfert devient grand et, au contraire, la constante de couplage augmente quand le moment de transfert devient petit. Cette propriété implique qu'à basse énergie, le couplage est grand ce qui rend le développement perturbatif inapplicable alors qu'il donne de bons résultats à haute énergie. Pour résoudre la QCD dans ce domaine des basses énergies, deux types d'approches ont été développées: d'une part les théories effectives de champs (EFT) et d'autre part, plus directement, la résolution numérique par discrétisation sur un réseau.

Le théorie effective des champs est une approximation de la QCD dans le domaine de basse énergie. L'idée principale est que les interactions dans le régime de basse énergie sont découplées de celles du domaine des hautes énergies. Par ailleurs, dans ce domaine, la présence de mésons très légers en QCD, qui peuvent s'interpréter comme des pseudo-bosons de Goldstone (associés à la brisure spontanée de la symétrie chirale) joue un grand rôle. En pratique, on introduit de nouveaux paramètres qui absorbent les contributions de ce domaine des hautes énergies. Il est alors nécessaire d'introduire une échelle d'énergie, Λ , que l'on appelle "l'échelle dure", qui définit

explicitement la délimitation entre les régimes des basses et des hautes énergies. Ainsi, l'échelle Λ caractérise avec précision le domaine d'énergie dans lequel l'EFT est applicable. D'un autre côté, on peut toujours introduire une échelle Q "molle" en référence aux impulsions externes ou aux masses des quarks légers. De cette façon s'introduit la quantité petite $Q/\Lambda \ll 1$, qui est le paramètre fondamental du développement perturbatif basé sur l'EFT. De plus, une fois ce développement effectué pour une observable, il devient possible de déterminer l'importance relative des diverses contributions.

Cette méthode est appliquée en pratique à l'aide de règles de comptage des puissances qui permettent d'évaluer l'importance de chaque diagramme de Feynman en fonction de l'ordre de chacun de ses vertex et du nombre de boucles du diagramme. Ces règles de comptage permettent de déterminer sans ambiguïté l'ordre du lagrangien qu'il est nécessaire de considérer ainsi que les diagrammes de Feynman à calculer afin d'évaluer une amplitude à un ordre donné. On peut ainsi organiser les amplitudes en fonction de leur ordre déterminé par les règles de comptage des puissances ce qui permet d'explorer les corrections d'une manière systématique. Bien que, formellement, l'EFT puisse se substituer à une résolution non perturbative de la QCD à basse énergie et donne lieu à de nombreuses prédictions, le principal inconvénient est que le nombre d'opérateurs augmente rapidement avec l'ordre, de sorte qu'en pratique, cette approche n'est applicable qu'aux premiers ordres.

Bien qu'étant un outil puissant pour l'interaction forte à basse énergie, l'EFT chirale (ou ChPT) n'en reste pas moins un développement perturbatif en fonction des masses des mésons légers et de leurs impulsions. Dans ce cadre, l'EFT n'est pas capable d'engendrer les résonances que peuvent former les systèmes de plusieurs mésons légers, qui sont des phénomènes non perturbatifs. Dans cette thèse, je présenterai deux méthodes de resommation de ce développement qui permettent de contourner cette limitation en s'appuyant sur la propriété d'unitarité des amplitudes. L'une d'elle utilise l'équation de Bethe et Salpeter associée à une prescription sur-couche et l'autre est une méthode plus générale qui s'avère efficace pour les amplitudes calculées à un ordre élevé.

Dans cette thèse, j'appliquerai la théorie effective des champs à l'étude de trois types d'interactions hadron-hadron: l'interaction entre un baryon charmé et un méson pseudo-Goldstone, l'interaction entre un baryon ordinaire et un méson pseudo-Goldstone et finalement à des interactions entre deux mésons pseudo-Goldstone, des aspects différents seront considérés dans chacun des cas. Ces trois études font l'objet de trois parties de la thèse qui sont présentées ci-dessous.

Partie I:

Des phénomènes nouveaux ont été récemment mis en évidence dans la physique des saveurs lourdes autour, par exemple, du boson $X(3872)$ découvert par la collaboration BELLE, ou du baryon $\Lambda_c(2595)$, qui ont suscité un intérêt très fort de la part des physiciens. Des explications théoriques basées sur plusieurs types de modèles ont été proposées, en particulier des modèles de type moléculaire faiblement liés et des modèles multiquarks (tetraquarks, pentaquarks) faisant appel à la symétrie chirale, l'unitarité ainsi que la symétrie de quarks lourd, qui est particulièrement utile.

Dans ce contexte nous avons étudié l'interaction entre un baryon mono-charmé et un méson pseudo-scalaire

léger dans la théorie de perturbation chirale unitarisée se basant sur les amplitudes chirales calculées à l'ordre dominant. Nous nous focalisons sur les aspects non-perturbatifs, tels que les resonances et leurs propriétés. Nos calculs montrent que les interactions sont suffisamment fortes pour que la resommation génère des résonances (génération dite dynamique). Certains états peuvent être comparés de manière naturelle à des états observés expérimentalement tels que le $\Lambda_c(2595)$ ($\Lambda_c^*(2625)$). Une fois ajusté un paramètre (constante de soustraction en régularisation dimensionnelle ou valeur du paramètre de coupure en régularisation par coupure) de manière à reproduire les masses expérimentales, nous prédisons également un certain nombre d'états supplémentaires qui n'ont pas encore été observés.

Anticipant l'arrivée prochaine de résultats sur les longueurs de diffusion provenant de simulations de QCD sur réseau, comme il en existe déjà pour les baryons légers, nous avons calculé les longueurs de diffusion entre les baryons charmés et les mésons pseudo-scalaires. La comparaison entre nos résultats et le calcul en ChPT à $O(p^3)$ confirme qu'il y a effectivement une attraction forte dans certains des canaux couplés ce qui suggère que des états puissent être générés dynamiquement.

Dans le but d'améliorer la description des interactions, nous avons utilisé l'EFT pour effectuer le calcul complet des contributions sous-dominantes (NLO) dans le développement de basse énergie. Malheureusement, on doit alors faire face à une augmentation du nombre de paramètres. Les données expérimentales disponibles ne sont pas suffisantes pour déterminer quantitativement tous les paramètres présents dans le lagrangien à cet ordre sous-dominant et on ne peut utiliser que des contraintes de naturalité sur leur ordre de grandeur. Nous n'avons donc pas pu faire de prédictions quantitatives basés sur ce calcul NLO mais nous avons pu montrer que les prédictions que nous avons faites sur l'interprétation moléculaire du $\Lambda_c(2595)$ et de son partenaire $3/2^-$ n'étaient pas remises en cause par les corrections NLO.

Afin de mieux préciser les composantes du baryon $\Lambda_c(2595)$ comme état généré dynamiquement, nous avons fait appel à deux approches communément utilisées: le critère d'état composite de Weinberg et l'évolution en grand N_c . Nos résultats montrent que si l'importance relative de chaque voie dans un système de canaux couplés ne peut pas être établie de manière non dépendante d'un modèle, l'image de base d'une composante meson-baryon essentielle pour le $\Lambda_c(2595)$ est bien confirmée. Notre étude montre que la façon habituelle de définir un état composite dépend des canaux pris en considération ainsi que du schéma de renormalisation utilisé pour éliminer les divergences des fonctions de boucle dans les approches par unitarisation. L'image moléculaire est par ailleurs renforcée par notre étude de la variation de la masse et de la largeur du $\Lambda_c(2595)$ en fonction du nombre de couleurs en QCD. Nous montrons, en effet, que cette variation est très différente de celle d'un baryon ordinaire formé de 3 quarks.

Partie II:

Les collisions élastiques entre un méson et un baryon, tous deux légers, sont des processus fondamentaux qui permettent de tester notre compréhension de l'interaction forte et qui jouent également un rôle important pour étudier les propriétés des baryons isolés et des systèmes multi-baryons. Les interactions des bosons de Nambu-

Goldstone entre eux sont fortement contraintes par la symétrie chirale ce qui implique que la puissance prédictive de la ChPT est la meilleure dans le secteur purement mésonique. Dans le secteur à un baryon la prédictivité est moins bonne à cause du nombre important de constantes de basses énergie qui s'introduisent. Une complication supplémentaire vient du problème de la brisure du comptage des puissances en régularisation dimensionnelle pour la ChPT en présence d'un baryon (BChPT). Dans les dernières décennies, plusieurs solutions ont été proposées à ce problème. Celles qui ont été le plus étudiées sont la méthode du baryon lourd (HB), la méthode de régularisation infrarouge et, enfin, l'approche dite de renormalisation étendue sur couche de masse (EOMS). Il est devenu clair dans les années récentes, à la fois formellement et empiriquement, que cette approche EOMS satisfait à la fois toutes les contraintes de symétrie ainsi que celle d'analyticité (ce qui n'est pas le cas des autres méthodes) et converge également plus rapidement que les autres.

Dans cette partie de la thèse, nous nous concentrons principalement sur les contributions à une boucle aux amplitudes de diffusion méson-baryon, sur la renormalisation et sur la convergence. Nous avons étudié la diffusion élastique avec le développement à trois saveurs (symétrie $SU(3)$) et dans le cadre chirale covariant jusqu'à l'ordre p^3 . Nous avons considéré principalement les canaux πN ($I=1/2, 3/2$) ainsi que les canaux KN ($I=0, 1$) pour lesquels des mesures expérimentales existent. Nous avons appliqué la méthode EOMS afin de rétablir le comptage correct en puissance et nous avons ensuite déterminé les constantes de couplage par fit conjoint sur les déphasages expérimentaux des deux canaux. Nous parvenons ainsi à une bonne description du canal πN jusqu'à une énergie de 1.16 GeV et du canal KN jusqu'à 1.52 GeV. Pour πN nos résultats dans le développement $SU(3)$ sont comparables en qualité aux résultats $SU(2)$ et bien meilleurs que ceux de l'approche HB en $SU(3)$. Pour les canaux KN , nous montrons que la connaissance des déphasages n'est pas suffisante pour déterminer de manière unique la totalité des constantes de couplage.

Nous avons également étudié la possibilité de reproduire à la fois les masses de l'octet des baryons et les propriétés de la diffusion méson-baryon dans le cadre du développement à l'ordre p^3 . Ainsi, nous déterminons d'abord les trois constantes de couplage b_0, b_F, b_D à l'aide des masses et effectuons ensuite le fit des déphasages des ondes partielles en les maintenant fixés. Nous trouvons qu'une description simultanée des masses et des amplitudes méson-baryon est possible avec le développement chirale EOMS à l'ordre p^3 mais une étude plus systématique des ordres supérieurs serait nécessaire.

Les longueurs de diffusion des canaux πN et KN que nous prédisons sont en bon accord avec les résultats HB ainsi qu'avec les mesures expérimentales. Par ailleurs, nous avons étudié la convergence du développement BChPT pour les amplitudes méson-baryon. On observe une cancellation importante entre les ordres NLO et NNLO ce qui pourrait suggérer une convergence lente, similaire à celle du développement en $SU(2)$. Toutefois, dans le secteur à un baryon, l'augmentation de l'ordre chirale se fait unité par unité, il est possible que des cancellations s'opèrent entre les ordres pairs et les ordres impairs adjacents. Cela a été observé dans l'étude des masses du décuplet de baryons.

Le canal particulièrement intéressant $\bar{K}N$ et sa résonance proche du seuil $\Lambda(1405)$ n'a pas été pris en compte

dans notre analyse. Dans notre travail, nous avons effectué le calcul perturbatif des amplitudes méson-baryon à l'ordre p^3 . Une extension intéressante (que nous projetons d'explorer ultérieurement) serait d'appliquer une méthode de resommation non perturbative sur notre résultat ce qui permettrait d'inclure ce canal $\bar{K}N$ dans notre analyse. Ainsi, il deviendrait possible de déterminer la totalité des constantes de couplage qui apparaissent dans le lagrangian à l'ordre p^3 .

Partie III

Dans cette dernière partie nous nous intéressons au secteur des mésons. Dans le cas de la diffusion meson-meson dans l'isospin $I=0$, des méthodes théoriques s'appuyant sur la ChPT ont permis d'établir l'existence de la résonance large $f_0(500)$ et de déterminer avec précision ses propriétés ainsi que celles de la résonance $f_0(980)$. Cela a été possible grâce à la disponibilité de résultats expérimentaux de diffusion $\pi\pi \rightarrow \pi\pi$ et $\pi\pi \rightarrow (K\bar{K})_{I=0}$ détaillés et précis. La situation est différente dans le cas de l'isospin $I = 1$ et des résonances $a_0(980)$, $a_0(1450)$ car on ne peut pas accéder expérimentalement aux amplitudes de diffusion $\pi\eta \rightarrow \pi\eta$ ou $\pi\eta \rightarrow (K\bar{K})_{I=1}$. Les propriétés de ces amplitudes et du méson $a_0(980)$ doivent être reconstruites en analysant les effets de rediffusion du système $\pi\eta$ produit dans un état final.

Dans cette partie de la thèse nous avons reconsidéré la diffusion d'une paire méson-méson isovecteur produite dans l'état final par collision de deux photons. Pour cela nous avons appliqué le formalisme des équations intégrales d'Omnès-Muskhelishvili en utilisant pour l'onde $J = 0$ un modèle de matrice de diffusion à deux canaux ($\pi\eta$, $K\bar{K}$) construit à partir des amplitudes chirales $O(p^4)$ unitarisées par une méthode de type matrice K . Notre modèle d'amplitude photon-photon prend aussi en compte l'effet des échanges de mésons vecteurs légers dans les voies croisées t , u ainsi que la résonance tenseur dans la voie directe $J = 2$, décrite simplement par la forme de Breit-Wigner. Les paramètres du modèle sont ajustés à l'aide des résultats expérimentaux récents de haute statistique sur $\gamma\gamma \rightarrow \pi^0\eta$, $\gamma\gamma \rightarrow K_S K_S$ obtenus par la collaboration Belle. Nous trouvons deux solutions différentes à la minimisation du χ^2 . Une de ces solutions produit une résonance a'_0 légère et étroite très similaire à celle trouvée dans l'analyse effectuée par la collaboration Belle. Bien que permise formellement, nous présentons des arguments indiquant que cette solution est probablement non physique et doit être rejetée. La solution correspondant au deuxième minimum contient une résonance a'_0 large.

Concernant la résonance $a_0(980)$ nous trouvons qu'elle est générée par nos amplitudes ajustées aux données $\gamma\gamma$ comme un pôle sur le deuxième feuillet de Riemann avec une masse et une largeur compatibles avec les moyennes données par le PDG et un fort couplage aux deux canaux $\pi^0\eta$ et $K\bar{K}$. La encore, nos résultats diffèrent de l'analyse effectuée par Belle avec une méthode plus naïve conduisant à une résonance $a_0(980)$ dont la masse et la largeur sont nettement plus élevées que les valeurs du PDG et qui ne se couple qu'au canal $\pi^0\eta$.

Conclusion

En résumé, la théorie effective des champs s'est imposée comme un des outils les plus performants pour l'étude des interactions hadron-hadron. Dans cette thèse, nous avons appliqué l'EFT pour étudier la génération

dynamique de baryons charmés au sein de la nouvelle famille de hadrons contenant des quarks lourds et nous avons exploré la structure d'un état typique, le $\Lambda_c(2595)$, en utilisant le critère d'état composite et le développement en grand N_c . Nous avons par ailleurs étudié la renormalisation et les propriétés de convergence du développement perturbatif chirale en considérant les amplitudes méson-baryon. Finalement, nous avons reconsidéré l'interaction méson-méson isovecteur en utilisant la production dans les collisions photon-photon et en s'appuyant sur des méthodes rigoureuses de traitement de la rediffusion dans l'état final ainsi que sur des contraintes expérimentales récentes provenant de la collaboration Belle.

Copyright

Copyright ownership belongs to the author, shall not be reproduced, copied, or used in other ways without permission. Otherwise the author will have the right to pursue legal responsibilities.

Abstract

With the development of accelerator and detector techniques, experimentalists have obtained quite a large amount of data on hadron-hadron interactions with much higher statistics based on large experimental accelerators such as BEKB, LHC, BEPC and so on, revealing a large variety of phenomena for theoretical researches. In order to provide a reliable understanding on these experimental data, theorists continually investigate new models or improve the original ones. Among all the approaches for studying hadron-hadron interactions in the low energy regime, the Effective field theory(EFT) has now become one of most popular approaches. Due to the asymptotic freedom and the color confinement, the fundamental theory for the strong interaction, quantum chromodynamics(QCD) is perturbative at high energy, while at low energies it is in a strongly coupled and confining regime and perturbation theory is not applicable. With the chiral symmetry and its spontaneous breaking fully taken into account, chiral perturbation theory and its unitary version make it possible to improve the descriptions order by order according to a certain power counting rule. One can thus improve the description systematically and evaluate the uncertainties. Applications to hadron-hadron interactions, including meson-meson, meson-baryon and baryon-baryon interactions have turned out to be very successful.

In the present work, we first briefly introduce the main idea of effective field theory. Then we study three typical scattering processes as examples to show how EFT helps to understand experimental data and further more, its power for predicting the unmeasured ones.

- Part I: In this part we investigate the interactions between singly charmed baryons and Goldstone bosons with a unitary chiral perturbation theory combined with approximate heavy quark symmetry. We compare different regularization methods for the two-point integral. In the lowest order, we fix the only free parameter in our model by reproducing the $\Lambda_c(2595)$ and predict a number of resonances. We then extend our study to include the next-to-leading order contributions. Further more, we utilize the compositeness rules and large N_c expansion to study the internal structure of $\Lambda_c(2595)$.
- Part II: In this part we study the interactions between ground state baryons and pseudoscalar mesons up to one loop level with covariant SU(3) baryon chiral perturbation theory. We apply the extended-on-mass-shell scheme to absorb the Ultraviolet divergences and power counting breaking terms. For the first time we perform a combined fit for both πN and KN scattering phase shifts. Further more, we perform a global fit to meson-baryon scattering phase shifts and baryon masses and show that it can provide a reasonable

description of the experimental data. In the end of this part we discuss in detail the convergence of covariant BChPT.

- Part III: In this part, we study the $\pi\eta$ interaction with isospin $I = 1$ as final state interactions in photon-photon scattering. Muskhelishvili-Omnès (MO) representation based on dispersion relations and analytical properties of amplitudes are applied. The most recent experimental data on $\gamma\gamma \rightarrow \pi\eta$ and $\gamma\gamma \rightarrow K_S K_S$ with much higher statistics from the Belle Collaboration are used to fix the parameters of our model, with which we calculate the positions of $a_0(980)$ and $a_0(1450)$, whose information still remains ambiguous.

Keywords: effective field theory, chiral perturbation theory, hadron-hadron interactions

Résumé

Les progrès techniques dont ont bénéficié les accélérateurs de particules ainsi que les détecteurs ont permis aux expérimentateurs de collecter des résultats sur un grand nombre d'interactions hadron-hadron, avec de grandes statistiques auprès d'accélérateurs tels que KEK, LHC, BEPC ce qui fournit de nombreux sujets d'étude pour les théoriciens. Ces derniers développent de nouveaux modèles ou améliorent de plus anciens afin de fournir des explications fiables aux divers phénomènes qui sont observés. Parmi les nombreuses approches utilisées pour décrire les interactions hadron-hadron à basse énergie, celles qui se basent sur la théorie effective des champs (EFT) deviennent les plus populaires. La théorie fondamentale des interactions fortes, la QCD, est perturbative aux grandes énergies (liberté asymptotique) mais pas aux basses énergies où la physique associée est dominée par le couplage fort et le confinement. Dans le régime de basse énergie on substitue à la QCD l'EFT dont le degrés de liberté sont les hadrons, mésons et baryons, et non plus les quarks et les gluons. Dans ce cadre, la brisure spontanée de la symétrie chirale est prise en compte et un développement perturbatif chirale est possible sur lequel sont également applicables des méthodes d'unitarisation. Des règles de comptage en puissance peuvent être introduites qui permettent la description d'une interaction hadron-hadron ordre par ordre. On peut ainsi améliorer la description de manière systématique et faire une évaluation des incertitudes. Cette approche a été appliquée avec succès aux diverses classes d'interaction hadron-hadron: méson-méson, méson-baryon et baryon-baryon.

Dans le présent travail, nous présentons tout d'abord brièvement les idées de base de la théorie effective des champs. Nous étudions ensuite trois processus de diffusion hadron-hadron, ayant chacun un intérêt particulier, dans le cadre de l'EFT. Nous montrerons ainsi la capacité de cette approche à expliquer les observables mesurées et de plus, à faire des prédictions sur des quantités qui ne le sont pas encore.

- Première partie: Dans cette partie nous examinons la possibilité d'engendrer des résonances dans les interactions entre un baryon charmé ou un baryon bottom et un boson de Goldstone en utilisant un développement chirale unitarisé et en exploitant la symétrie approximative de quark lourd. Nous comparons plusieurs méthodes de régularisation pour l'intégrale de la fonction à deux points. A l'ordre dominant, l'unique paramètre de la théorie est fixé de manière à reproduire les états $\Lambda_b(5912)$ et $\Lambda_c(2595)$. Cette étude est ensuite étendue de manière à inclure les contributions sous-dominantes. Par ailleurs, nous avons étudié la structure du $\Lambda_c(2595)$ en utilisant le critère d'état composite de Weinberg ainsi que le développement en grand N_c .

- Deuxième partie: Dans cette partie nous calculons les amplitudes d'interaction entre mésons légers et baryons de l'état fondamental dans le cadre de la théorie de perturbation chirale baryonique (BChPT) covariante et du groupe de saveur $SU(3)$ à l'ordre d'une boucle. Nous appliquons la méthode dite sur-couche étendue qui permet d'absorber à la fois les divergences ultra-violettes et les contributions qui violent la règle de comptage en puissances. Nous avons effectué, pour la première fois, un fit combiné des déphasages πN et KN . De plus, nous effectuons un fit global simultanément des déphasages méson-nucléon et des masses des baryons et nous trouvons un bon accord avec les données expérimentales. A la fin de cette partie nous discutons en détail les propriétés de convergence de la BChPT covariante.
- Troisième partie: Dans cette partie nous étudions l'amplitude d'interaction d'une paire méson-méson dans l'isospin $I = 1$ via le processus de production par des collisions photon-photon. Nous construisons les amplitudes de production en résolvant les équations d'Omnès-Muskhelishvili qui sont basées sur les propriétés générales d'analyticité et d'unitarité. Les mesures expérimentales de sections efficaces $\gamma\gamma \rightarrow \pi\eta$ et $\gamma\gamma \rightarrow K_S K_S$ de haute statistique effectuées récemment par la collaboration Belle nous permettent de contraindre les paramètres de notre modèle d'amplitude méson-méson (deux solutions sont trouvées) et d'en déduire les propriétés des résonances $a_0(980)$ et $a_0(1450)$ d'après leur position dans le plan complexe en énergie.

Mots clés: théorie effective des champs, théorie de perturbation chirale, interactions hadron-hadron

Contents

1	Introduction	10
1.1	Standard Model of particle physics	10
1.2	Quantum chromodynamics	12
1.3	Hadrons and exotic hadrons	15
1.4	Outline of the dissertation	18
2	Chiral Effective field theory	19
2.1	Effective field theory and Weinberg's power counting rule	19
2.2	Chiral effective field theory	21
2.2.1	Chiral symmetry and its breaking	21
2.2.2	Construction of chiral effective lagrangian	24
2.2.3	External sources	28
2.2.4	Chiral effective Lagrangian at NLO in the meson sector	30
2.3	Chiral effective field theory for meson-baryon interactions	31
2.3.1	The lowest order effective lagrangian	31
2.3.2	Effective Lagrangians at NLO and NNLO	32
2.3.3	Power counting breaking	34
2.4	Unitarity in hadron-hadron interactions	36
2.4.1	Unitary relation	37
2.4.2	Bethe-Salpeter equation	40
2.4.3	Unitarity in general	43
2.4.4	Resonances	44
3	Dynamically generated excited charmed baryons	47
3.1	Introduction	47
3.2	Framework	48
3.3	Results and discussions	51
3.3.1	Excited charmed baryons	52

3.3.2	Further Discussions	53
3.3.3	Scattering Lengths	56
3.3.4	An exploratory NLO study	60
3.4	The compositeness condition of $\Lambda_c(2595)$	63
3.4.1	Introduction	63
3.4.2	16 channels	65
3.4.3	Two channels	66
3.4.4	Three channels	67
3.5	N_c dependence of $\Lambda_c(2595)$	68
3.5.1	Introduction	68
3.5.2	Baryon and meson masses	69
3.5.3	Loop function	69
3.5.4	Group representation-Clebsch-Gordan coefficients	70
3.6	Summary	72
4	Meson-baryon interactions up to NNLO	74
4.1	Introduction	74
4.2	Theoretical formalism	75
4.2.1	Scattering amplitudes and partial wave phaseshifts	75
4.2.2	Power counting	77
4.2.3	Chiral Lagrangians	77
4.2.4	Feynman diagrams up to NNLO	79
4.3	Renormalization	82
4.3.1	Mass renormalization	83
4.3.2	Vertex renormalization	84
4.3.3	Chiral corrections to the decay constants	85
4.4	Ultraviolet divergence and power counting breaking terms	85
4.5	Results and discussion	86
4.5.1	Fitting strategy one: direct fit to the phase shifts	88
4.5.2	Fitting strategy two: combined study of baryon masses and meson-baryon scattering	90
4.5.3	Scattering lengths	94
4.5.4	Convergence of BChPT	94
4.5.5	Decuplet contributions	96
4.6	Summary	100

5	The $\pi\eta$ interaction and a_0 resonances in photon-photon scattering	101
5.1	Introduction	101
5.2	Framework	103
5.2.1	Scattering amplitudes and right hand cuts	103
5.2.2	Left hand cuts	105
5.2.3	Muskhelishvili-Omnès representations	108
5.3	Results and discussions	113
5.4	Conclusion	118
6	Summary and Outlook	119
A	Clebsch-Gordan coefficients	122
B	Tree amplitudes and renormalization of LECs	125
B.1	Tree level contact terms	125
B.2	Tree level Born diagrams	127
B.3	Vertex renormalization	128
B.4	Divergent parts of the LECs	131
B.5	Power counting breaking terms of the one-loop diagrams	132

List of Figures

1.1	Standard model of particle physics(from wikipedia).	11
1.2	QCD coupling constant α_s as a function of $1/Q$ or r	13
1.3	The SU(4) weight diagram for multiplets of mesons and baryons consisting of u, d, s, c quarks [1].	16
2.1	Kinematics of meson-baryon scattering.	38
2.2	Kinematics of meson-baryon scattering.	40
3.1	Loop function $G(M)$ as a function of the heavy hadron mass M in different regularization schemes: HQS (the heavy quark symmetry inspired scheme), $\overline{\text{MS}}$ (the modified minimal subtraction scheme), CUT (the cutoff regularization scheme), and HH (the exact heavy-quark limit). The subtraction constants or cutoff values have been fixed by reproducing $\Lambda_c(2595)$. In calculating the loop function G , the pseudoscalar meson mass is fixed at that of the pion $m = 138$ MeV and the renormalization scale in the dimensional regularization methods is fixed at $\mu = 1$ GeV.	51
3.2	Thresholds of the coupled channels considered in different works for the singly charmed sector with $J^P = 1/2^-$ and $(S = 0, I = 0)$: Liang et al. [2], Hofmann et al. [3], Garcia-Recio et al. [4], and Exp [5]. Two model spaces denoted by dot-dot-dashed lines (PB) and dashed lines (VB), respectively, were studied in Ref. [2].	57
3.3	Imaginary part of the $\Lambda_c(2595)$ pole position, where ‘‘Scaling’’ refers to the cutoff dependence $\mathcal{O}(\sqrt{N_c/3})$, while ‘‘No scaling’’ refers to the use of a constant cutoff $\mathcal{O}(1)$	72
3.4	Real part of the $\Lambda_c(2595)$ pole position with respect to the $\pi\Sigma_c$ threshold, where ‘‘Scaling’’ refers to the cutoff dependence $\mathcal{O}(\sqrt{N_c/3})$, while ‘‘No scaling’’ refers to the use of a constant cutoff $\mathcal{O}(1)$	73
4.1	Tree level diagrams contributing to meson-baryon scattering up to $\mathcal{O}(p^3)$. The solid lines correspond to baryons, and the dashed lines represent mesons. The vertices with filled circles and hollow blocks stem from the $\mathcal{L}_{MB}^{(2)}$ and $\mathcal{L}_{MB}^{(3)}$ Lagrangian, respectively.	79
4.2	Leading one-loop contributions to meson-baryon scattering up to $\mathcal{O}(p^3)$. Note that the wave function renormalization and crossed graphs are not shown explicitly.	80
4.3	Wave function renormalization contributions to meson (dashed) and baryon (solid) fields. Counterterms from $\mathcal{L}_{MM}^{(4)}$ are denoted by the filled block.	80

4.4	Feynman diagrams contributing to vertex renormalizations. The hollow block represents the contributions of the $\mathcal{O}(p^3)$ vertices.	84
4.5	Pion-nucleon phase shifts. The blue lines denote our results and the black dots with error bars represent the WI08 solution with empirical errors given in Eq. 4.33. The blue bands correspond to the uncertainties propagated from the errors of LECs. In some partial waves, the error bands are of the size of the thickness of the lines. For the sake of comparison, we show as well the EOMS SU(2) results [6] (green dot-dashed lines) and the HB SU(3) results [7] (red dashed lines).	90
4.6	$I = 0$ (upper panel) and $I = 1$ (lower panel) KN phase shifts. The orange long-short dashed lines and blue solid lines represent our $\mathcal{O}(p^2)$ and $\mathcal{O}(p^3)^*$ results while the red dashed lines denote those of the HB ChPT [7]. The blue bands correspond to the uncertainties of the $\mathcal{O}(p^3)^*$ results propagated from the uncertainties of the LECs. The error bands of the $\mathcal{O}(p^2)$ results are not shown here to make the figures easier to read. In some partial waves, the error bands are of the size of the thickness of the lines.	91
4.7	Same as Fig. 4.5, but the black dot-dashed lines associated with the black bands denote the EOMS results and their errors with b_0 , b_D , and b_F fixed by fitting to the physical (isospin averaged) octet baryon masses at NNLO. In some partial waves, the error bands are of the size of the thickness of the lines.	91
4.8	Same as Fig. 4.6, but the purple dotted lines and black dot-dashed lines denote the $\mathcal{O}(p^2)$ and $\mathcal{O}(p^3)^*$ results in the EOMS scheme with b_0 , b_D , and b_F fixed by fitting to the physical (isospin averaged) octet baryon masses at NNLO. The black bands correspond to the uncertainties of the $\mathcal{O}(p^3)^*$ results propagated from the uncertainties of the LECs. The error bands of $\mathcal{O}(p^2)$ results (purple) are not shown here to make the figures easier to read. In some partial waves, the error bands are of the size of the thickness of the lines.	92
4.9	Order by order decomposition of the πN phase shifts. The blue lines donate the total results, while those of the $\mathcal{O}(p)$, $\mathcal{O}(p^2)$, and $\mathcal{O}(p^3)$ are represented by the green-dashed, red-dot-dashed, and black-dotted lines, respectively.	96
4.10	Order by order decomposition of the KN phase shifts. The blue lines donate the total results, while those of the $\mathcal{O}(p)$, $\mathcal{O}(p^2)$, and $\mathcal{O}(p^3)^*$ are represented by the green-dashed, red-dot-dashed, and black-dotted lines, respectively.	97
4.11	Lowest order contribution from the intermediate decuplet. The double line refers to the spin- $\frac{3}{2}$ propagator.	97
4.12	πN phase shifts with the lowest order decuplet contribution included. The blue lines are our results in SU(3) while the green dashed lines are the results in SU(2) from Ref. [6]. The black dots denote the experimental data.	99

4.13	KN phase shifts with the lowest order decuplet contribution included. The blue solid lines are our results in SU(3) while the red dashed lines are the results without the decuplet contributions. The black dots denote the experimental data. The blue solid lines and the red dashed lines overlap each other.	99
5.1	Physical regions for $\gamma\gamma \rightarrow \pi\eta, \gamma\pi \rightarrow \gamma\eta$ scattering and $\eta \rightarrow \gamma\gamma\pi^0$ decay.	103
5.2	Born amplitudes of $\gamma M \rightarrow \gamma M$	105
5.3	Phase-shifts and inelasticity from the two-channel T matrix model using the two sets of parameters corresponding to the two χ^2 minimums.	114
5.4	Experimental $\gamma\gamma \rightarrow \pi\eta$ differential cross sections compared with the two fits.	115
5.5	Experimental $\gamma\gamma \rightarrow K_S K_S$ differential cross sections compared with the two fits.	116
5.6	Cross sections for $\gamma\gamma \rightarrow \pi\eta, K_S K_S$ integrated in the range $ \cos\theta < 0.8$. The data are from Refs. [8, 9], they are compared with the two fits.	117

List of Tables

2.1	Two scenarios of central values of L_i with $\mu = 0.77\text{GeV}$ from NLO fits [10].	30
3.1	Numerical values of isospin and SU(3)-multiplet averaged masses, the pion decay constant f_π , and the SU(3) averaged pseudoscalar meson decay constant f_0 (in units of MeV) [5].	50
3.2	Dynamically generated charmed baryons of $J^P = 1/2^-$. The subtraction constant is fixed in a way such that $\Lambda_c(2595)$ mass is produced to be 2591 MeV with $a = -8.27$. All energies are in units of MeV and $(S, I)^M$ denotes (strangeness, isospin) ^{SU(3)multiplet}	54
3.3	Same as Table 3.2, but obtained in the cutoff regularization scheme with $\Lambda = 1.35\text{ GeV}$	54
3.4	Dynamically generated charmed baryons of $J^P = 3/2^-$. The subtraction constant is fixed in a way such that $\Lambda_c^*(2625)$ mass is produced to be 2625 MeV with $a = -12.0$. All energies are in units of MeV and $(S, I)^M$ denotes (strangeness, isospin) ^{SU(3)multiplet}	55
3.5	Same as Table 3.2, but obtained in the cutoff regularization scheme with $\Lambda = 2.13\text{ GeV}$	55
3.6	ϕB scattering lengths a (in units of fm) in the charmed sector with $J^P = 1/2^-$	58
3.7	ϕB scattering lengths a (in units of fm) in the charmed sector with $J^P = 3/2^-$	59
3.8	Constants in Eq. (3.15) for the anti-triplet.	61
3.9	Constants in Eq. (3.15) for the anti-triplet (in units of GeV^{-1}).	61
3.10	Constants in Eq. (3.15) for the sextet (in units of GeV^{-1}).	61
3.11	Dynamically generated charmed baryons of $J^P = 1/2^-$ in the NLO UChPT in comparison with those in the LO. At NLO, three values for the LEC α' have been taken. The subtraction constant is fixed in the same way as in the LO case. All energies are in units of MeV and $(S, I)^M$ denotes (strangeness, isospin) ^{SU(3)multiplet}	62
3.12	Compositeness of each of the 16 coupled channels for the narrow state corresponding to $\Lambda_c(2595)$. The only parameter in the meson-baryon loop function is fixed by reproducing the nominal $\Lambda_c(2595)$ mass with the following parameter: $\alpha' = 0.97952$ [4], $q_{\text{max}} = 0.67898$ [2], and $a = -3.37865$ [11].	66
3.13	Same as Table 3.12, but for the broader sibling of the $\Lambda_c(2595)$	67

3.14	Compositeness of each of the two coupled channels for $\Lambda_c(2595)$. The only parameter in the meson-baryon loop function is fixed by reproducing the nominal $\Lambda_c(2595)$ mass with the following parameter: $\alpha' = 0.8268$ [4], $q_{\max} = 0.7969$ [2], and $a = -5.3768$ [11].	67
3.15	Compositeness of each of the three coupled channels for $\Lambda_c(2595)$. The only parameter in the meson-baryon loop function is fixed by reproducing the nominal $\Lambda_c(2595)$ mass with the following parameter: $\alpha' = 0.96048$ [4], $q_{\max} = 0.67535$ [2], and $a = -5.6365$ [11].	68
4.1	Independent (combinations of) LECs contributing to πN and KN scattering. For the sake of later reference, we introduce $\alpha_{1,\dots,8}, \beta_{1,\dots,8}, \gamma_{1,\dots,8}$ to denote different combinations of LECs. The units of the LECs are given in the last column.	78
4.2	11 coupled channels of meson-baryon scattering of conserved strangeness (S) and isospin (I). . .	87
4.3	Masses and decay constants (in units of GeV) and axial-coupling constants relevant in the present work. Note the mass of the K meson is taken to be 0.493 GeV to be consistent with the SP92 data, which were originally from K^+n scattering.	87
4.4	LECs in the πN channel.	89
4.5	LECs in the πN channel with $\alpha_4 = b_0 + \frac{b_D}{2} + \frac{b_F}{2}$ fixed by fitting to the baryon masses.	89
4.6	LECs in the πN channel including the lowest order decuplet contribution with $h_A = 2.9$	89
4.7	πN and KN scattering lengths in units of fm. Note that we did not associate any uncertainties to the $\mathcal{O}(p^3)^*$ contributions of the KN channel because we have not included the tree level contributions at this order for the KN channels.	89
4.8	LECs contributing to the $I = 0$ KN scattering.	90
4.9	LECs contributing to $I = 1$ KN scattering.	90
4.10	LECs determined by fitting to the experimental baryon masses up to NLO in the EOMS BChPT and the corresponding fitted results, in comparison with the experimental data. All of the masses are in units of GeV.	93
4.11	LECs in the $I = 0$ KN channel with $\beta_4 = b_0 - b_F$ fixed by fitting to the baryon masses.	93
4.12	LECs in the $I = 1$ KN channel with $\gamma_4 = b_0 + b_D$ fixed by fitting to the baryon masses.	93
4.13	LECs in the $I = 0$ KN channel including the lowest order decuplet contribution with $h_A = 2.9$ at $\mathcal{O}(p^3)^*$	99
4.14	LECs in the $I = 1$ KN channel including the lowest order decuplet contribution with $h_A = 2.9$ at $\mathcal{O}(p^3)^*$	99
5.1	Radiative widths of vector mesons and corresponding coupling constants. The relative signs of the couplings are determined assuming flavour symmetry.	107
5.2	Parameters of the two-channel T matrix in the two fits.	113

5.3	Positions of two a_0 resonances predicted by our model, as well as the coupling constants to each channel.	116
A.1	$(S = 1, I = 1/2)$	122
A.2	$(S = 0, I = 1)$	122
A.3	$(S = 0, I = 0)$	122
A.4	$(S = -1, I = 3/2)$	122
A.5	$(S = -1, I = 1/2)$	123
A.6	$(S = -2, I = 1)$	123
A.7	$(S = -2, I = 0)$	123
A.8	$(S = 1, I = 3/2)$	123
A.9	$(S = 1, I = 1/2)$	123
A.10	$(S = 0, I = 2)$	123
A.11	$(S = 0, I = 1)$	123
A.12	$(S = 0, I = 0)$	123
A.13	$(S = -1, I = 3/2)$	124
A.14	$(S = -1, I = 1/2)$	124
A.15	$(S = -2, I = 1)$	124
A.16	$(S = -2, I = 0)$	124
A.17	$(S = -3, I = 1/2)$	124

Chapter 1

Introduction

1.1 Standard Model of particle physics

As is well known, our world is constructed via 4 fundamental forces: gravitational, the electromagnetic, the strong and the weak force. While the gravity mainly concerns the largest structures of our universe, the rest three forces are responsible for the dynamics of the smallest structures, or in another word, elementary particles which are about 39 orders of magnitudes smaller than the former one. The theory concerning the latter one is the famous Standard Model.

Through out the latter half of the 20th century, the Standard Model of particle physics was developed, aiming to classify what the elementary particles of our world are and how they interact, with the collaborative effort of scientists all around the world. Starting from the experimental confirmation of quarks in the middle of 1970s, the last building blocks was finally accomplished till 2013 when Higgs boson was confirmed by Atlas and CMS collaboration [12, 13]. So far, there is no doubt that the Standard Model has been proved to be a huge success since it almost perfectly explains a large variety of experimental results.

The elementary particles in the Standard Model can be divided into three categories, the fermions, gauge bosons and the higgs boson. The fermions of the Standard Model, together with their anti-particle partners, are the building blocks of the matter world. They are identified via the charges they carried. Totally there are 12 different kinds including six quarks (up, down, charm, strange, top, bottom) and six leptons (electron, electron neutrino, muon, muon neutrino, tau and tau neutrino). They can further be collected into 3 generations in which each pair exhibits similar properties. Besides their own charges which are also known as flavors, quarks also carry color charges. There are three kinds of color charges, 'red', 'green' and 'blue', and the quarks participate in the strong interaction via their color charges. On the other hand, leptons do not carry color charges and hence they cannot contribute to the strong interaction. But they are crucial participants of the weak and electromagnetic force. Particularly, the three kinds of neutrinos do not carry electric charges thus only show up in the weak interaction. This is why they are extremely difficult to be detected.

The Standard Model describes a physical pattern for the fundamental forces in which matter particles exchange some kinds of other particles. These mediating particles serve as force carriers and are called gauge bosons. All of these gauge bosons have integer spins which makes them obey the Bose-Einstein statistics. Hence there is no limit on the number of gauge bosons in one single energy level. There are three kinds of gauge bosons, corresponding to three fundamental forces (except gravity) respectively. Photons mediate the electromagnetic force between particles with electrical charges. The W^+ , W^- and Z gauge bosons are responsible for the weak force between quarks with different flavors. And the gluons propagate the strong interaction among quarks with color charges.

The last building block of the standard model is the Higgs boson. It is a very massive scalar particle and the key to explain the masses of elementary particles and why photons and gluons are massless. It was first predicted by theorists Robert Brout, François Englert and Peter Higgs in 1964 [14, 15] and immediately followed by G. S. Guralnik, C. R. Hagen and T. W. B. Kibble [16]. They were rewarded by the Nobel prize after the discovery of the Higgs in 2013.

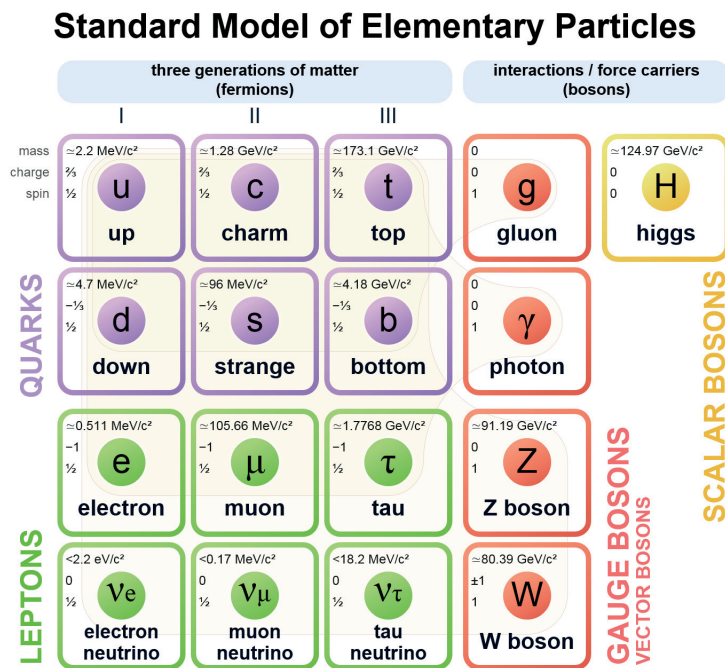


Figure 1.1: Standard model of particle physics(from wikipedia).

The theories corresponding to each of the four fundamental forces have been well established so far. The Electromagnetic force is well described by the theory of quantum electrodynamics(QED). Sheldon Glashow managed to find a way to combine the electromagnetic and the weak force [17]. Later on, Steven Weinberg [18] and Abdus Salam [19] unified the two forces into the electroweak interaction. For the strong interaction, the theory is called quantum chromodynamics(QCD).

For scientists, the Standard Model is a treasure full of symmetries and their spontaneous symmetry breaking, anomalies and non-perturbation phenomena covering a large variety of physics. It is now recognized as “the

theory of almost everything” and is the basis of more exotic models such as all kinds of effective field theory. However, with the repaid improvement of accuracy for experimental measurements, people are now very enthusiastic searching for clues beyond the Standard Model, which is, however, beyond this thesis.

1.2 Quantum chromodynamics

QCD is the modern quantum theory for the strong interaction, which has been developed for over half a century. The foundation of QCD is the quark model which could be dated back to 1960s when physicists attempted to sort out the large amount of new particles detected in 1950s according to their electrical charges, isospins and strangeness. In 1963, Gell-Mann[20, 21] and George Zweig [22] independently proposed a simple but very sufficient model in which a more elementary unit with spin one-half was introduced. At that time, with only 3 kinds, i.e., up, down and strange, one can reproduce all the new particles detected. These elementary fermions got their name ‘quark’ from Gell-mann later. From then the objects of QCD are established [23, 24].

However, people realized immediately that the understanding of quarks was far from enough when Boris Struminsky proposed the problem of Ω_{sss} , in which the three strange quarks process common value of spin, violating the Pauli exclusion rule(see Ref. [25] for the translated version). Moo-Young Han, Yoichiro Nambu and Oscar W. Greenberg [26] suggested that this antinomy indicated that quarks should carry extra charges except their flavors. This extra charge is then called ‘color’. Every quark is actually a triplet in color space. This fact also implies that the transformation of quarks should obey the 3-dimensional representations of $SU(3)$ Lie group, which is known as Yang-Mills theory proposed by Chen-Ning Yang and Robert Mills [27]. This means that totally there will be eight generators, corresponding to eight kinds of gluons who mediate the strong interaction between quarks. From then on, QCD got its initial version.

Although the quark model has been successfully applied to explain all the particles detected before 1965 and has been described with strict mathematical language, there was still doubt on whether quarks really existed or not because one never detected a single quark, which made the explanation of extra color charges an unconvincing patch. This embarrassing situation was finally terminated when a new kind of quarks, the charm quark, was discovered in mid-1970s by Ting ChaoChung [28] and Burton Richter [29] independently. The discovery of charm quark and its related physical observables verified a large amount of predictions based on the quark model, which greatly improved people’s confidence on the existence of quarks. Later on, another two heavier quarks were predicted and detected in 1977, the bottom quark [30], and in 1995, the top quark [31, 32].

The deep thinking of the antinomy that there is no isolated quark finally reveals two critical features of QCD. The first is the asymptotic freedom. Asymptotic freedom was first proposed in 1973 by David Gross, Franks Wilczek [33] and David H. Politzer [34]. They suggested that the theory of the strong interaction should be established based on non-Abelian gauge symmetry, which in turn has asymptotic behavior. Nowadays, the QCD

couplings α reads

$$\alpha_s(Q^2) = \frac{1}{1 + \alpha(\mu) \frac{\beta_0}{4\pi} \ln(\frac{Q^2}{\mu^2})}, \quad (1.1)$$

where Q is the transfer momentum, μ the renormalization scale, $\beta_0 = 11 - \frac{2}{3}N_F$ with N_F the number of flavors. When N_F is no more than 16, one has $\beta_0 > 0$, and the coupling constant decreases rapidly as the Q increases. Thus in higher energy regions, quarks behave more like free particles. Considering that the Yang-Mills theory has been proved to be renormalizable, QCD in higher energy regions can be treated strictly within a perturbative framework. On the other hand, the QCD coupling constant will rise exponentially as the distance r between quarks increases since r is inversely proportional to the transfer momentum Q . As a result, the interactions between quarks will be so strong that degrees of freedom relevant will be changed. The energy that separates quarks will produce a new quark anti-quark pair in versus. This feature of QCD is known as confinement hypothesis, which provides a explanation why isolated quark cannot be detected [35].

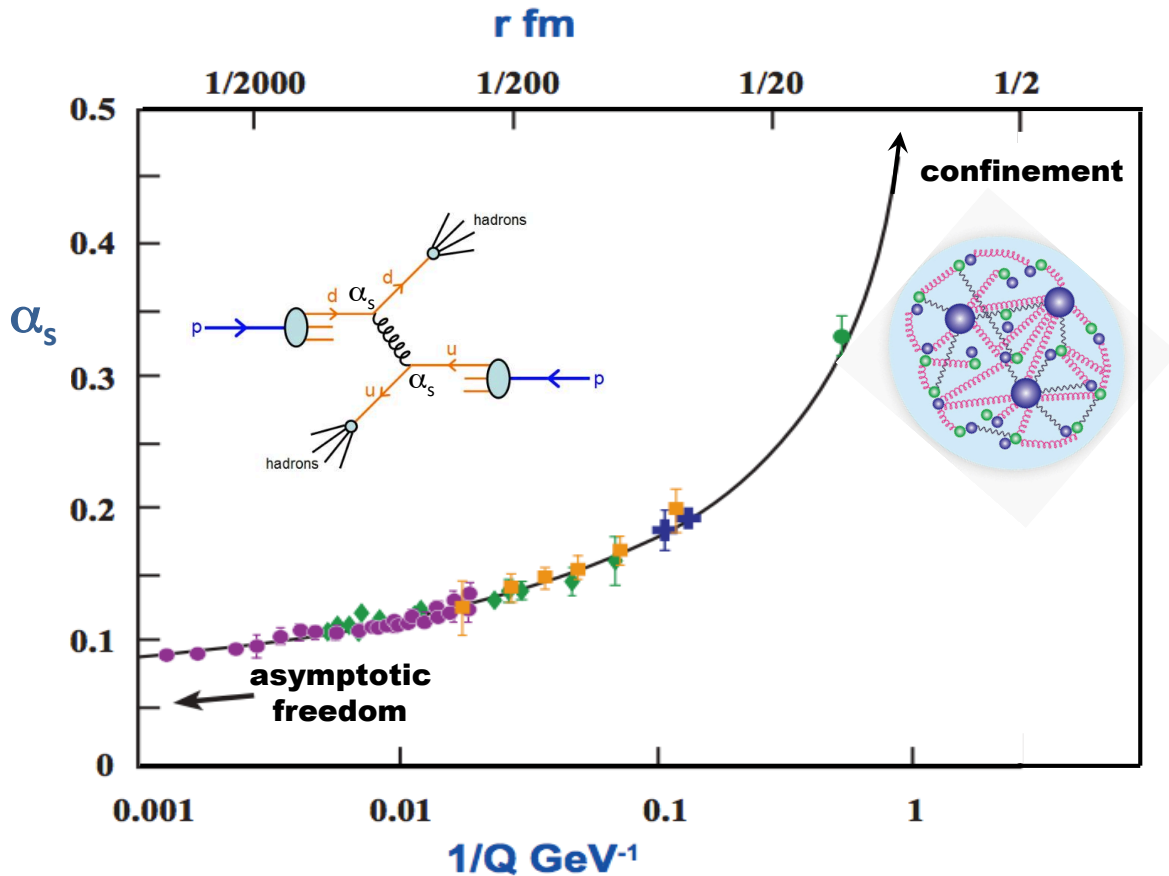


Figure 1.2: QCD coupling constant α_s as a function of $1/Q$ or r [36].

While the asymptotic freedom guarantees that QCD can be treated perturbatively in higher energy regions, the perturbative solution of QCD is no longer reliable in lower energy regions. Besides, the degrees of freedom are no longer quarks and gluons but color singlet hadrons according to the confinement hypothesis. To solve this

non-perturbative problem, people turned to effective field theory(EFT) or direct numerical solutions, that is, lattice QCD(LQCD), which will be introduced afterwards.

The modern version of QCD is a rigorous mathematical model based on quantum field theory, whose Lagrangian reads

$$\mathcal{L}_{QCD} = \sum_f \bar{q}_f^i (i\gamma_\mu D_{ij}^\mu - m_f \delta_{ij}) q_f^j - \frac{1}{4} G_{\mu\nu}^a G_a^{\mu\nu}. \quad (1.2)$$

The first term is related to quark fields with i, j the indices for color charge taking the value from 1 to 3, m_f denotes the masses of quarks, f refers to the flavors of quarks thus we have to sum over all the six kinds. The covariant derivative D_{ij}^μ reads

$$D_{ij}^\mu = \partial^\mu \delta_{ij} + ig_s \sum_{a=1}^8 A^{\mu,a} T_{ij}^a. \quad (1.3)$$

The second term on the right is the coupling of quark-quark-gluon, which contains the gluon field $A^{\mu,a}$, the generator matrix T_{ij}^a and the QCD coupling constant g . The subscript a running from 1 to 8 refers to the 8 generators of the representation of SU(3) Lie group and the 8 corresponding gluons. Usually the generators are expressed as 8 Gell-Mann Matrices $T_{ij}^a = \lambda_{ij}^a/2$,

$$\begin{aligned} \lambda_1 &= \begin{pmatrix} 0 & 1 & 0 \\ 1 & 0 & 0 \\ 0 & 0 & 0 \end{pmatrix}, \lambda_2 = \begin{pmatrix} 0 & -i & 0 \\ i & 0 & 0 \\ 0 & 0 & 0 \end{pmatrix}, \lambda_3 = \begin{pmatrix} 1 & 0 & 0 \\ 0 & -1 & 0 \\ 0 & 0 & 0 \end{pmatrix}, \\ \lambda_4 &= \begin{pmatrix} 0 & 0 & 1 \\ 0 & 0 & 0 \\ 1 & 0 & 0 \end{pmatrix}, \lambda_5 = \begin{pmatrix} 0 & 0 & -i \\ 0 & 0 & 0 \\ i & 0 & 0 \end{pmatrix}, \\ \lambda_6 &= \begin{pmatrix} 0 & 0 & 0 \\ 0 & 0 & 1 \\ 0 & 1 & 0 \end{pmatrix}, \lambda_7 = \begin{pmatrix} 0 & 0 & 0 \\ 0 & 0 & -i \\ 0 & i & 0 \end{pmatrix}, \lambda_8 = \frac{1}{\sqrt{3}} \begin{pmatrix} 1 & 0 & 0 \\ 0 & 1 & 0 \\ 0 & 0 & -2 \end{pmatrix}. \end{aligned} \quad (1.4)$$

Having $[\lambda^a, \lambda^b] = 2if^{abc}\lambda^c$, the Gell-Mann matrices lead to a Lie algebra, in which f^{abc} is the so-called structure constant for such a SU(3) Lie group.

The second term of \mathcal{L}_{QCD} denotes the gluon interaction part, also known as Yang-Mills field part. The field-strength tensor for gluons $G_{\mu\nu}^a$ reads

$$G_{\mu\nu}^a = \partial_\mu A_\nu^a - \partial_\nu A_\mu^a - g_s f^{abc} A_\mu^b A_\nu^c. \quad (1.5)$$

This term describes the vertices with three or four gluon legs. The last term of Eq. 1.5 represents the self-interaction of gluons. This is the consequence of non-Abelian character of QCD and is the main difference between a non-Abelian gauge theory and Abelian gauge theory, like QED, in which the photon mediating electromagnetic interactions does not interact with another photon. Also this is the crucial part where the asymptotic freedom comes

from, making QCD in lower energy regime a true non-perturbative theory.

With the lagrangian \mathcal{L}_{QCD} above, one can calculate the correlation function from the action $S = \int d^4x \mathcal{L}_{QCD}$ via the path integral

$$\langle 0|T\hat{\mathcal{O}}_n(x_n)\cdots\hat{\mathcal{O}}_1(x_1)|0\rangle = \frac{1}{Z} \int \mathcal{D}A\mathcal{D}\Psi\mathcal{D}\bar{\Psi} \exp[iS] \mathcal{O}_n(x_n)\cdots\mathcal{O}_1(x_1), \quad (1.6)$$

with T the time ordering operator.

$$Z \equiv \int \mathcal{D}A\mathcal{D}\Psi\mathcal{D}\bar{\Psi} \exp[iS]. \quad (1.7)$$

However, the solution for such a path integral is a tough task. In higher energy regime, perturbative methods can be applied, which makes the problem much easier to handle since one can calculate the integral up to certain orders within a renormalizable framework. But for the non-perturbative QCD, the only practical method is lattice QCD [35, 37]. Lattice QCD discretizes the space-time into lattices. The lattice points represent the quarks and the links between points are gluons. In this way, the momentum can only take discrete values inversely proportional to the size of the lattice spacing a . Hence lattice QCD can reproduce the realistic world at the limit $a \rightarrow 0$. Based on this, one can find that the smaller the size of the lattice spacing a is, the more expensive the calculations are. As a consequence, lattice QCD only makes big progress after the ground-broken progress in computer science.

1.3 Hadrons and exotic hadrons

The confinement hypothesis indicates that in the lower energy regime, the degrees of freedom are no longer quarks and gluons but hadrons. Hadrons can be divided into two kinds: baryons composed of three quarks, like proton(uud) and neutron(udd), and mesons composed of a pair of quark and anti-quark such as pion and Kaon mesons.

Among the six quark flavors, u, d and s quarks are grouped as light quarks since their masses are smaller compared to the lightest hadron ¹. In the limit of massless light quarks, the three light quarks behave almost the same in the strong interaction. Thus we can investigate them within a SU(3) symmetry of flavor space. This extra symmetry, as well as their hyperon charge which is also conserved in the strong interaction, make the SU(3) basis their eigenstates, which allows us to collect the large amount of hadrons into different groups from the point of view of group theory.

In the language of group theory, the light quarks belong to a triplet and the anti-quarks an anti-triplet. Thus the mesons containing one pair of quark-anti-quark can be sorted out as

$$\mathbf{3} \otimes \bar{\mathbf{3}} = \mathbf{8} \oplus \mathbf{1}. \quad (1.8)$$

¹The mass of s quark $m_s = 90\text{MeV}$ is somehow not much smaller than that for the lightest meson pion $m_\pi = 140\text{MeV}$. This is the main reason for the breaking of SU(3) flavor symmetry.

function must be antisymmetric under the exchange of any two of the quarks. All of these constraints guarantee that the space, spin and flavor parts of wave function must be symmetric which can be expressed as

$$|qqq\rangle_A = |color\rangle_A \times |space, spin, flavor\rangle_S \quad (1.11)$$

One can again extend the SU(3) to SU(4) flavor symmetry by introducing the fourth quark, such as the charm or the bottom quark. In this case, the decomposition of the inner product reads

$$4 \otimes 4 \otimes 4 = 20_S \oplus 20_M \oplus 20_M \oplus 4_A. \quad (1.12)$$

We also show in Fig. 1.3 the baryon multiplets with $J^P = \frac{1}{2}^+$ and $\frac{3}{2}^+$.

Besides the ordinary mesons and baryons mentioned above, there is one special kind of hadrons detected by experiments but not compatible with the traditional quark model. They are called exotic hadrons. Basically we have two kinds of exotic hadrons. Those of the first kind have quantum number which are forbidden by the traditional quark model. Taken mesons as examples, considering the conservations in the strong interaction, mesons are actually J^{PC} multiplets. For a neutral quark antiquark configuration, the quantum number $J^P = 0^{+-}$, $J^P = 1^{-+}$ are forbidden. The light excited mesons $\pi_1(1400)$ as a $J^P = 1^{-+}$ state is such an exotic state. The other kind of exotic states have the quantum number of $q\bar{q}$ or qqq but have exotic structures. The light scalars such as $a_0(980)$, $f_0(980)$, $f_0(500)$ and $K_0^*(700)$ with $J^{PC} = 0^{++}$ observed experimentally should be $q\bar{q}(L=1)$ states according to the quark model. However, such a physical pattern cannot explain why the mass of $a_0(980)$ is close to that of $f_0(980)$ and much larger than that of $f_0(500)$. Later, this problem was solved and these exotic mesons are usually considered to have an extra pair of $q\bar{q}$. The same thing happens in the baryon sector. In the classical quark model, $N(1535)(J^P = \frac{1}{2}^-)$ was expected to be the lightest excited baryons with one lowest excited quark with an orbital angular momentum $L=1$. However, experimentally the lightest baryon with the same quantum number was found to be $\Lambda(1405)$. The mass anomaly was finally explained by the multi-quark or molecule models. For a recent review of this, we refer to Refs. [38, 39].

Exotic hadrons beyond the traditional quark model were noticed quite a long time ago. Gell-Mann [21] and Zweig [22] suggested that there was no reason that complex structures such as tetraquark($qq\bar{q}\bar{q}$) with baryon number $\mathcal{B}=0$ or pentaquark($qqqq\bar{q}$) with baryon number $\mathcal{B}=1$ cannot exist. Earlier discoveries such as the scalar mesons $a_0(980)$, $f_0(980)$, $f_0(500)$, $K_0^*(700)$ and light baryons $\Lambda(1405)$, $N(1535)$ confirmed this conjecture. With huge improvement of accelerator techniques, more and more new exotic hadrons containing heavier charm quarks or bottom quarks are detected, including $X(3872)$, $Z_c(3900)$, $Y(4260)$, $Z_b(10610)$ and the exotic heavy baryons $\Lambda_c(2595)$, $\Lambda_b(5912)$ (See reviews of Particle data group [1]).

Every new exotic state turns out to be a grand banquet for scientists. Theoretically there may be various explanations for a single exotic state, such as compact multi-quark state, dynamically generated molecule, kinematic effect like cusp structure or triangle singularity, or their mixture. The compact multi-quark model starts from the

degrees of quarks and gluons, while molecule models take hadrons as the degree of freedom. On the other hand when the state locates very close to thresholds of related channels, kinematic effect will be largely enhanced. For instance, $D_{s0}^*(2317)$ is now generally recognized as a dynamically generated molecule which mainly couples to KD channel or a tetraquark state, $X(3872)$ as a $D^*\bar{D}$ molecule or tetraquark state [40]. Thus it is not easy to know for sure the internal structure of one exotic hadron. Most probably it is a mixing of various configurations but with different weight. For example, it takes scientists half of century and lots of delicate analysis before it is finally concluded that $\Lambda(1405)$ is more in favor of a dynamically generated molecule [41]. For a review of this topic, we refer to Ref. [38] and Ref. [36].

1.4 Outline of the dissertation

In Chapter 2, we first introduce the main idea for effective field theory, followed by a brief introduction of chiral symmetry and its spontaneous breaking. We take the meson-meson interactions as an example to illustrate how to construct the chiral effective Lagrangian. In the last section of this chapter, we discuss the unitary method, which is essential to interpret the non-perturbation phenomena in the scattering process.

Then we are prepared to study realistic scattering processes after all the general discussions. In this thesis, we applied effective field theory to study three typical hadron-hadron interactions, i.e., the interaction of singly charmed baryons and Goldstone mesons in Chapter 3, those of ground state baryons and Goldstone bosons in Chapter 4 and those of meson-meson as final state interactions of photon-photon scattering in Chapter 5. Finally we present a brief summary and outlook.

Chapter 2

Chiral Effective field theory

Quantum chromodynamics(QCD) is the fundamental theory of the strong interaction. However, as mentioned in the introduction, two critical features of this fundamental theory make a direct solution a difficult task, especially in the lower energy regime. One is the so-called color confinement hypothesis [35], implying that although in QCD, the basic degrees of freedom are quarks and gluons, which are color-charged, one can only observe color-neutral particles, such as mesons and baryons in nature. The other is asymptotic freedom [33, 34], which simply states that the QCD coupling constant increases fast as the decrease of transfer momentum. This feature implies that the coupling constant may be too large in the lower energy regions, declaring the failure of a perturbative treatment for QCD [42], which, however, has been applied successfully in the higher energy regions.

2.1 Effective field theory and Weinberg's power counting rule

Effective field theory is an approximation of QCD in the lower energy regions. The main idea is that interactions in the lower energy regime do not depend on those in the higher energy region, which can be integrated out in advance. Practically, one can introduce new parameters to absorb the contributions from the higher energy regime. Hence an energy scale Λ , which is usually named as 'hard scale', is required to define explicitly the dividing point between the low energy regime and the high energy regime. Therefore, the hard scale Λ accurately characterizes the energy regime in which the EFT is reliable. On the other hand, one can always define a 'soft' scale Q in contrast to the hard scale, which usually refers to the external momentum and quark masses. In this way, one finds a small quantity $\frac{Q}{\Lambda} \ll 1$, which provides the stepping stones for expansions in the framework of EFT. Further more, once the interaction can be expanded according to the small quantity, one can immediately evaluate quantitatively the importance of each part of contributions.

In Ref [43], Weinberg firstly proposed a theorem which says that although individual quantum field theories have of course a good deal of content, quantum field theory itself has no content beyond analyticity, unitarity, cluster decomposition, and symmetry. That is to say, if we calculate the matrix elements with the most general

possible Lagrangian, which includes all terms consistent with assumed symmetries up to any given order, the results will simply be the most general possible S-matrix consistent with analyticity, perturbative unitarity, cluster decomposition, and assumed symmetry principles. This theorem was then proved in Ref. [44] and Ref. [45] based on Lorentz invariance, as well as the invariance of the generating function under local transformation. As a consequence, an EFT is local invariant although originally the symmetry taken into account may be a global one.

From the theorem above, the most general Lagrangian for an EFT is expected to be

$$\mathcal{L}_{MM} = \sum_i c_i \mathcal{O}_i, \quad (2.1)$$

where \mathcal{O}_i are the operators which are usually constructed via fields, derivatives, and lorentz algebra following the principles with which one starts. The c_i are called low-energy constants(LECs). As mentioned in the beginning of this section, the LECs practically absorb the contributions from the higher energy regime. Hence these LECs can in principle be calculated out theoretically from the high energy theory, though in most cases, they are treated as free parameters determined by fitting relevant experimental data.

However, Weinberg immediately noticed that for a realistic EFT, the most general Lagrangian contains infinite series of operators of higher and higher dimensionality. Weinberg then proposed power counting rules for such an effective field theory, based on dimensional analysis [43]. With the help of power counting rules, one can estimate the importance of each Feynman diagram via the number and the order of vertices and loops with the soft energy scale Q quantitatively. This is significant. The Weinberg power counting rules formulate unambiguously that in order to obtain the amplitude up to a given order, which Lagrangian we need to know and which Feynman diagrams we need to calculate. Hence one can quantitatively re-organize the amplitudes according to their orders obtained from the power counting rules, which makes it possible to systematically explore corrections. This advantage in turn is quite helpful for testing the convergence of such a perturbation theory.

Taking the meson sector as an example, the effective Lagrangian following the power counting rules can be written as

$$\mathcal{L}_{MM} = \mathcal{L}_{MM}^2 + \mathcal{L}_{MM}^4 + \dots, \quad (2.2)$$

where the superscripts denote the chiral order. i.e., the order in the momentum and mass expansion, of corresponding terms.

Based on naive dimension analysis, the momentum of external meson legs are counted as $\mathcal{O}(p)$ and the light quark masses as $\mathcal{O}(p^2)$ considering the relations of masses between light quarks and Goldstone bosons. To be more explicit, the chiral order D for a given Feynman diagram is defined as,

$$\begin{aligned} p_i &\rightarrow \alpha p_i, & m_q &\rightarrow \alpha^2 m_q, \\ \mathcal{A}(\alpha p_i, \alpha^2 m_q) &= \alpha^D \mathcal{A}(p_i, m_q). \end{aligned} \quad (2.3)$$

Therefore

$$D = 2 + \sum_{n=1}^{\infty} 2(n-1)N_{2n} + 2N_L, \quad (2.4)$$

where N_{2n} denotes the number of vertices at order $\mathcal{O}(p^{2n})$ and N_L the number of independent loops.

It has been already noted in Ref. [46] and Ref. [47] that the effective field theory cannot be renormalized like what one does in QED. However, with the help of Weinberg power counting rules, one can calculate the ultraviolet divergences in loops order by order, which can be absorbed via LECs of corresponding order. Therefore the EFT is as a matter of fact renormalizable order by order.

Although the EFT is very sufficient as the substitute of non-perturbative QCD in the low energy regime and very powerful for making prediction, it has a main shortcoming that the number of the possible operators increases so rapidly that it can only be practically applied for lower orders.

Afterwards a series of works witnessed the huge success of the applications of chiral perturbation theory(ChPT) in the mesonic sector. In Ref. [48], Gasser and Leutwyler proposed a systematic method which allows one to extend Weinberg's S-matrix analysis to an expansion of Green functions in powers of momenta and quark masses. Shortly followed by Ref. [46] and Ref. [47], in which the most general Lagrangian up to next-to-leading order $\mathcal{O}(p^4)$ was constructed and meson-meson interactions was calculated up to one loop order not only in SU(2) but also in SU(3). So far in the mesonic sector, the original effective Lagrangian has been extended to next-to-next-to-leading order or $\mathcal{O}(p^6)$ [49] in the standard power counting rule in which two-loop diagrams arise. For a review of this, we refer to Ref. [50].

For comprehensive reviews of EFT, we refer to Refs. [51, 52, 53, 54, 55, 56, 57, 58].

2.2 Chiral effective field theory

2.2.1 Chiral symmetry and its breaking

In EFT, the basic degrees of freedom are mesons and baryons instead of quarks and gluons. Besides, it reserves more or less all the symmetries that QCD contains. Inspired by the much smaller masses [59] of u, d and s quarks in comparison with the masses of typical light hadrons such as ρ meson(770MeV) or the proton(938MeV), people find that in the limit where the masses of light quarks go to zero, the left-handed and the right-handed quark fields are decoupled from each other in the \mathcal{L}_{QCD} . This is the so-called chiral limit.

$$\begin{pmatrix} m_u = 2.16_{-0.26}^{+0.49} \text{MeV} \\ m_d = 4.67_{-0.17}^{+0.48} \text{MeV} \\ m_s = 93_{-5}^{+11} \text{MeV} \end{pmatrix} \ll 1 \text{GeV} \ll \begin{pmatrix} m_c = 1.27_{-0.02}^{+0.02} \text{GeV} \\ m_b = 4.18_{-0.02}^{+0.03} \text{GeV} \\ m_t = 172.76_{-0.30}^{+0.30} \text{GeV} \end{pmatrix}, \quad (2.5)$$

where the 1GeV is the typical masses of light hadrons mentioned above.

The QCD Lagrangian in Eq. 1.2 can be divided into two pieces,

$$\mathcal{L}_{QCD} = \mathcal{L}_{QCD}^0 + \mathcal{L}_M, \quad (2.6)$$

with

$$\mathcal{L}_{QCD}^0 = \sum_f \bar{q}_f (i\gamma_\mu D^\mu) q_f - \frac{1}{4} G_{\mu\nu}^a G_a^{\mu\nu}, \quad (2.7)$$

$$\mathcal{L}_M = \bar{q}_f \mathcal{M} q_f. \quad (2.8)$$

Note that compared to Eq. 1.2, we have already collected the quarks with different colors into a 3-dimension vector. And the quark masses are collected into a diagonal matrix $\mathcal{M} = \text{diag}(m_u, m_d, m_s)$. In the chiral limit, the \mathcal{L}_M related to quark masses vanishes.

The right and left hand projecting operators (also called chiral operators) are defined as

$$P_R = \frac{1}{2}(1 + \gamma_5), \quad P_L = \frac{1}{2}(1 - \gamma_5). \quad (2.9)$$

They are unitary operators and represent a transformation under $U(3)$ group. One can easily find the auxiliary formulae via Dirac algebra, which read

$$\gamma_5 P_R = P_R \gamma_5 = P_R, \quad \gamma_5 P_L = P_L \gamma_5 = -P_L, \quad (2.10)$$

$$\gamma_\mu P_R = P_L \gamma_\mu, \quad \gamma_\mu P_L = P_R \gamma_\mu. \quad (2.11)$$

With the operators above, the quarks field can be divided into 2 pieces, i.e., the left- and right-handed pieces,

$$q_f = \frac{1}{2}(1 + \gamma_5)q_f + \frac{1}{2}(1 - \gamma_5)q_f = P_R q_f + P_L q_f \equiv q_{f,R} + q_{f,L}. \quad (2.12)$$

Making use of the auxiliary formulae, one can immediately observe the decoupling of the left- and right-handed quark fields:

$$\mathcal{L}_{QCD}^0 = \sum_f \bar{q}_{f,R} (i\gamma_\mu D^\mu) q_{f,R} + \bar{q}_{f,L} (i\gamma_\mu D^\mu) q_{f,L} - \frac{1}{4} G_{\mu\nu}^a G_a^{\mu\nu}. \quad (2.13)$$

Since in Eq. 2.7, \mathcal{L}^0 is invariant under the classical global $U(3)$ symmetry, the left- and right-handed piece of \mathcal{L}^0 are invariant separately under their own $U(3)$ transformation $q_R \mapsto R q_R$ and $q_L \mapsto L q_L$ with $R \in U_R(3)$ and $L \in U_L(3)$. This means that the \mathcal{L}^0 actually exhibits a $U_L(3) \times U_R(3)$ symmetry. In accordance with the group

theory, a group of $U_L(3) \times U_R(3)$ can be further decomposed as

$$U(3)_L \times U(3)_R \equiv SU_L(3) \times SU_R(3) \times U_V(1) \times U_A(1), \quad (2.14)$$

where the subscripts V refers to the vector ($R + L$) and A the axial-vector ($R - L$).

With all the discussions above, we can find that the QCD hamiltonian is actually symmetric under $SU(3)_L \times SU(3)_R \times U(1)_V$, where the $U(1)_V$ symmetry is commonly related to the conservation of baryon number. The $U(1)_A$ is not preserved by the so-called anomalies [60, 61, 62, 63].

Under the symmetry of $SU(3)_L \times SU(3)_R$, one could construct 8 left- and right-handed transformation operators corresponding to the eight generators of $SU(3)$ group.

$$g_L^a = \exp(-i\Theta_L^a \frac{\lambda^a}{2}), \quad g_R^a = \exp(-i\Theta_R^a \frac{\lambda^a}{2}), \quad a = 1, \dots, 8, \quad (2.15)$$

where λ^a with $a = 1, \dots, 8$ is the Gell-Mann matrices in Eq. 1.5.

According to Noether's theorem, every invariance results in a conserved current. Therefore, one obtains 8 conserved left- and right-handed currents from the corresponding transformation, which can be expressed as

$$\begin{aligned} L^{\mu,a} &= \bar{q}_L \gamma^\mu \frac{\lambda^a}{2} q_L, & \partial_\mu L^{\mu,a} &= 0, \\ R^{\mu,a} &= \bar{q}_R \gamma^\mu \frac{\lambda^a}{2} q_R, & \partial_\mu R^{\mu,a} &= 0. \end{aligned} \quad (2.16)$$

The conserved vector and axial-vector currents as the linear combinations of $L^{\mu,a}$ and $R^{\mu,a}$ read

$$\begin{aligned} V^{\mu,a} &= R^{\mu,a} + L^{\mu,a} = \bar{q} \gamma^\mu \frac{\lambda^a}{2} q, \\ A^{\mu,a} &= R^{\mu,a} - L^{\mu,a} = \bar{q} \gamma^\mu \gamma^5 \frac{\lambda^a}{2} q, \end{aligned} \quad (2.17)$$

the name of which originates from the behavior like a vector or axial-vector under Parity transformation,

$$\begin{aligned} P : V^{\mu,a}(\vec{x}, t) &= V_\mu^a(-\vec{x}, t) \\ P : A^{\mu,a}(\vec{x}, t) &= -A_\mu^a(-\vec{x}, t). \end{aligned} \quad (2.18)$$

Corresponding to the 16 conserved currents, the charge operators can be defined as

$$\begin{aligned} Q_V^a(t) &= \int d^3x q^\dagger(\vec{x}, t) \frac{\lambda^a}{2} q(\vec{x}, t), \quad a = 1, \dots, 8, \\ Q_A^a(t) &= \int d^3x q^\dagger(\vec{x}, t) \gamma^5 \frac{\lambda^a}{2} q(\vec{x}, t), \quad a = 1, \dots, 8. \end{aligned} \quad (2.19)$$

At the chiral limit, the charge operators commute with the QCD Hamiltonian under the symmetry of $SU(3)_L \times SU(3)_R \times U(1)_V$, but with opposite parity. As a consequence, if there exists a multiplet of hadrons with positive parity, a negative partner will be expected. However, experimentally such a degeneration was never detected in the

low-energy hadron spectrum, forcing people reexamine the $SU(3)_L \times SU(3)_R \times U(1)_V$ symmetry. In ref. [64], the authors pointed out that the ground states are necessarily invariant under $SU(3)_V \times U(1)_V$ symmetry at the chiral limit. That is, the ground state vanishes under the eight vector charge operators and the baryon number operator.

$$Q_V^a |0\rangle = Q_V |0\rangle = 0. \quad (2.20)$$

This implies that the QCD Hamiltonian is invariant at least under $SU(3)_V \times U(1)_V$ at the chiral limit and the ground states can be grouped with corresponding irreducible representation.

Since the subgroup $SU(3)_V \times U(1)_V$ symmetry is necessarily observed, the coset group is then the only choice responsible for the absence of the degeneration of hadron spectrum. One naturally assumes that Q_A^a cannot annihilate the ground state

$$Q_A^a |0\rangle \neq 0. \quad (2.21)$$

All the discussions above indicate that although at the chiral limit, the QCD lagrangian is invariant under $SU(3)_L \times SU(3)_R \times U(1)_V$, the ground state is only invariant under a subgroup symmetry of $SU(3)_V \times U(1)_V$. Thus the chiral symmetry is spontaneously broken or hidden. A symmetry is spontaneously broken if the ground state of the system is no longer invariant under the full symmetry of the Hamiltonian. According to the Goldstone theorem [65, 66, 67, 68, 69], the eight symmetry breaking axial-vector currents lead to eight massless Goldstone bosons $\phi^a(x)$ with spin 0. The Goldstone bosons correspondingly follow the same behavior of parity transformation.

$$P : \phi^a(\vec{x}, t) = -\phi^a(-\vec{x}, t), \quad (2.22)$$

which implies that the Goldstone bosons are pseudoscalar mesons. The smaller masses of pseudoscalar meson octet (π, K, η) compared to the $J^P = 1^-$ vector mesons are also convincing evidences that they are actually candidates of Goldstone bosons of the spontaneous breaking of chiral symmetry.

2.2.2 Construction of chiral effective lagrangian

Generally speaking, in order to construct an effective Lagrangian for interactions of one's interest, one needs two steps. The first is to find a suitable representation of the hadron fields according to the symmetry of chiral transformation. Secondly, one applies the Weinberg theorem, finding out all possible terms satisfying all symmetries required up to a given order following power counting rules. In fact, Callan, Coleman, Wess, and Zumino have already elaborated the standard method for constructing an effective field theory with certain spontaneously symmetry breaking [70, 71]. In this section, I will briefly show the standard procedure of constructing an effective lagrangian taking the lightest octet of pseudoscalar mesons of (π, K, η) as an example.

In the preceding section, it was mentioned that the global symmetry $G = SU(3)_L \times SU(3)_R$ of the QCD lagrangian is spontaneously broken to a vectorial subgroup $H = SU(3)_V$, during which eight Goldstone bosons,

or the octet of pseudoscalar meson, are generated corresponding to the eight generators not belonging to the subgroup H . This means that the Goldstone bosons can actually be represented by a matrix \hat{U} belonging to the coset group G/H , which is isomorphic to a $SU(3)$ group. Thus what we need to do next is to find a proper representation for this coset group G/H .

For an element $g \in G = SU(3)_R \times SU(3)_L$, the Goldstone boson field ϕ^a transforms in the following way

$$\phi^a \rightarrow \phi^{a'} = F(g, \phi^a), \quad (2.23)$$

with F a representation of the group G . Considering the spontaneous symmetry breaking, the transformation $g \in G$ can be decomposed as

$$g = qh, \quad h \in H = SU(3)_V, \quad q \in G/H. \quad (2.24)$$

Associated with the left- and right-handed transformation, such a transformation $g \in G$ can be represented as

$$g = (g_R, g_L) = (g_R, g_L g_R^\dagger g_R) = (\mathbf{1}, g_L g_R^\dagger)(g_R, g_R), \quad (2.25)$$

or arbitrarily

$$g = (g_L, g_R) = (g_L, g_R g_L^\dagger g_L) = \underbrace{(\mathbf{1}, g_R g_L^\dagger)}_{(\mathbf{1}, \hat{U})} (g_L, g_L), \quad (2.26)$$

in which the second factor (g_R, g_R) or (g_L, g_L) actually belongs to $H = \{(V, V) | V \in SU(3)_V\}$.

The decomposition above indicates that under the chiral transformation, the element $\hat{U} \in G/H$ behaves as

$$(\mathbf{1}, \hat{U}) \rightarrow (\mathbf{1}, \hat{U}') = g(\mathbf{1}, \hat{U}) = (g_L, g_R)(\mathbf{1}, \hat{U}) = (g_L, g_R \hat{U}) = (\mathbf{1}, g_R \hat{U} g_L^\dagger)(g_L, g_L), \quad (2.27)$$

$$\hat{U} \rightarrow \hat{U}' = g_R \hat{U} g_L^\dagger. \quad (2.28)$$

With Eq. 2.28, the Goldstone boson matrix \hat{U} can be defined by means of exponential representation

$$\hat{U} = \exp(i \frac{\phi}{F_\phi}), \quad (2.29)$$

$$\phi = \sum_{a=1}^8 \phi^a \lambda^a = \sqrt{2} \begin{pmatrix} \frac{1}{\sqrt{2}}\pi^0 + \frac{1}{\sqrt{6}}\eta & \pi^+ & K^+ \\ \pi^- & -\frac{1}{\sqrt{2}}\pi^0 + \frac{1}{\sqrt{6}}\eta & K^0 \\ K^- & \bar{K}^0 & -\frac{2}{\sqrt{6}}\eta \end{pmatrix}, \quad (2.30)$$

where λ^a are again the Gell-mann matrices. The F_ϕ is related to the decay constant of Goldstone bosons at the

chiral limit.

Now we have obtained an appropriate representation for the pseudoscalar meson field $U(\phi)$. The derivative of U has exactly the same behavior under the chiral transformation

$$\partial_\mu \hat{U} \rightarrow \partial_\mu \hat{U}' = g_R \partial_\mu \hat{U} g_L^\dagger. \quad (2.31)$$

Therefore, the building blocks of the effective Lagrangian contains the field operator U and its derivative

$$\mathcal{L}_{\text{eff}} = \mathcal{L}_{\text{eff}}(U, \partial_\mu U, \dots). \quad (2.32)$$

Taking into account pseudoscalar mesons having $J^P = 0^-$, the parity transformation for the field operator ϕ or U reads

$$\phi \rightarrow \phi' = -\phi, \quad U \rightarrow U' = U^\dagger, \quad (2.33)$$

which implies that in the effective Lagrangian, one U must accompany one U^\dagger to guarantee the parity invariance. On the other hand, the Lorentz invariance requires that the derivatives should also appear in pairs. Thus the possible configurations are

$$\langle UU^\dagger \rangle, \quad \langle UU^\dagger UU^\dagger \rangle, \quad \langle \partial_\mu U \partial^\mu U^\dagger \rangle, \dots, \quad (2.34)$$

where the symbol $\langle \dots \rangle$ denotes the trace of flavor space. The configurations in Eq. 2.36 are all invariant under the chiral transformation since

$$\begin{aligned} \langle UU^\dagger \rangle &\rightarrow \langle g_R U g_L^\dagger g_L U^\dagger g_R^\dagger \rangle = \langle g_R^\dagger g_R U g_L^\dagger g_L U^\dagger \rangle = \langle UU^\dagger \rangle, \\ \langle \partial_\mu U \partial^\mu U^\dagger \rangle &\rightarrow \langle g_R \partial_\mu U g_L^\dagger g_L \partial^\mu U^\dagger g_R^\dagger \rangle = \langle g_R^\dagger g_R \partial_\mu U g_L^\dagger g_L \partial^\mu U^\dagger \rangle = \langle \partial_\mu U \partial^\mu U^\dagger \rangle. \end{aligned} \quad (2.35)$$

As a low-energy effective field theory, the small quantity Q can be naturally chosen to be the momentum. Thus one can organize the effective Lagrangian in powers of momenta or equivalently the number of derivatives on the meson fields. As is shown in Eq. 2.34, the lowest term with minimal meson field reads $\langle UU^\dagger \rangle$. However, this term is trivial since $UU^\dagger = 1$. Thus the lowest order non-trivial Lagrangian starts from the second order and reads

$$\mathcal{L}_\phi^{(2)} = \frac{F_\phi^2}{4} \langle \partial_\mu U \partial^\mu U^\dagger \rangle. \quad (2.36)$$

The factor $F_\phi^2/4$ comes from the normalization of the kinematic term in the standard form

$$\mathcal{L}_\phi^{(2)} = \frac{1}{2} \langle \partial_\mu \phi \partial^\mu \phi \rangle + \frac{1}{12 F_\phi^2} \langle (\phi \partial_\mu \phi) (\phi \partial^\mu \phi) \rangle + \dots \quad (2.37)$$

Now one obtains the lowest order chiral effective Lagrangian which is invariant under Lorentz, charge conjugate, parity, time reversal and, especially, chiral symmetry. However, as mentioned in the preceding section, chiral

symmetry is explicitly broken because of the finite quark masses. The mass term \mathcal{L}_M in Eq. 2.8 mixes left- and right-handed fields under the projection of chiral operators,

$$\mathcal{L}_M = -\bar{q}\mathcal{M}q = -(\bar{q}_R\mathcal{M}q_L + \bar{q}_L\mathcal{M}q_R). \quad (2.38)$$

According to the statement in Ref. [72], \mathcal{L}_M would be invariant if the diagonal matrix \mathcal{M} of quark masses transformed as the meson field U ,

$$\mathcal{M} \rightarrow g_R\mathcal{M}g_L^\dagger. \quad (2.39)$$

Under this assumption, one can construct the effective Lagrangian $\mathcal{L}(\mathcal{M}, U)$ following the same method with the two building blocks, quark mass \mathcal{M} and meson field U . Chiral symmetry requires that the sum of the number of \mathcal{M} and U in the product of $\mathcal{L}(\mathcal{M}, U)$ should be even. Besides, since \mathcal{M} itself does not carry intrinsic parity, one U must be accompanied with one U^\dagger either as a product or alternatively as a sum.

With all the discussions above, one can find a configuration $\mathcal{L}(\mathcal{M}, U)$ invariant under the assumed symmetries the same as Eq. 2.36, which reads

$$\mathcal{L}_{S.B.} = \frac{F_\phi^2 B_0}{2} \langle MU^\dagger + UM^\dagger \rangle, \quad (2.40)$$

where the subscript $S.B.$ means symmetry breaking. The new parameter $B_0 = -\langle 0|\bar{q}q|0\rangle/F_\phi^2$ is related to chiral quark condensate and then to the masses of Goldstone bosons.

$$\mathcal{L}_{S.B.} = -B_0 \langle \phi^2 \mathcal{M} \rangle + \dots, \quad (2.41)$$

Expanding the first term of Eq. 2.41 at the isospin limit $m_u = m_d = m_l$, one can obtain the masses of Goldstone bosons as functions of B_0 and quark masses

$$\begin{aligned} M_\pi^2 &= 2B_0 m_l, \\ M_K^2 &= B_0(m_l + m_s), \\ M_\eta^2 &= \frac{2}{3}B_0(m_l + 2m_s), \end{aligned} \quad (2.42)$$

which satisfy the Gell-mann-Okubo relation [73, 74]

$$4M_K^2 = M_\pi^2 + 3M_\eta^2. \quad (2.43)$$

Now we have obtained the effective Lagrangian for the explicit chiral symmetry breaking terms. The power counting above then needs modifications accordingly. Based on the naive dimensional analysis, \mathcal{L}_M has the same chiral order as $\mathcal{L}_\phi^{(2)}$ with \mathcal{M} as $\mathcal{O}(p^2)$.

Collecting all the pieces above, the lowest order chiral effective Lagrangian for Goldstone bosons reads

$$\mathcal{L}^{(2)} = \frac{F_\phi^2}{4} \langle \partial_\mu U \partial_\mu U^\dagger \rangle + \frac{F_\phi^2 B_0}{2} \langle M U^\dagger + U M^\dagger \rangle, \quad (2.44)$$

where the corresponding power counting evaluated via the order of momenta and masses of Goldstone bosons is

$$U, U^\dagger \sim \mathcal{O}(p^0), \quad \partial_\mu \sim \mathcal{O}(p^1), \quad M \sim \mathcal{O}(p^2). \quad (2.45)$$

2.2.3 External sources

Once the interaction of interest involves external sources, such as scalar(s), pseudoscalar(p), vector(v_μ) and axial-vector(a_μ), one needs to include these external sources explicitly into the QCD Lagrangian 2.6. In this case, the QCD Lagrangian with external sources satisfying Lorentz, spin, charge conjugate and time reversal invariance which was given by Gasser and Leutwyler in Ref. [46, 47] reads,

$$\mathcal{L}_{QCD}^{ex} = \mathcal{L}_{QCD}^0 + \bar{q}(\gamma_\mu v^\mu + \gamma_\mu \gamma_5 a^\mu)q - \bar{q}(s - i\gamma_5 p)q, \quad (2.46)$$

where the external fields v^μ , a^μ , s and p denote eight vector currents and axial-vector currents, as well as the scalar and pseudoscalar source, which read

$$v^\mu = \sum_{a=1}^8 \frac{\lambda_a}{2} v_a^\mu, \quad a^\mu = \sum_{a=1}^8 \frac{\lambda_a}{2} a_a^\mu, \quad s = \sum_{a=1}^8 \lambda_a s_a, \quad p = \sum_{a=1}^8 \lambda_a p_a. \quad (2.47)$$

Note here we have omitted the singlet vector current $v_{(s)}^\mu$. All the external fields above are hermitian, color neutral 3×3 matrices in flavor space. One can easily find that the ordinary QCD Lagrangian can be recovered when $v_\mu = a_\mu = p = 0$, $s = \mathcal{M}$.

Following the same method above, one can construct the most general chiral effective Lagrangian. Taking into account chiral symmetry and its spontaneous breaking, it is much easier to rewrite the Lagrangian with left- and right-handed currents similar to Eq. 2.10, Eq. 2.11, Eq. 2.16, Eq. 2.17, which reads

$$\begin{aligned} \bar{q}\gamma^\mu(v_\mu + \gamma_5 a_\mu)q &= \frac{1}{2}\bar{q}\gamma^\mu(r_\mu + l_\mu + \gamma_5(r_\mu - l_\mu))q \\ &= \bar{q}_R\gamma^\mu r_\mu q_R + \bar{q}_L\gamma^\mu l_\mu q_L, \end{aligned} \quad (2.48)$$

in which

$$r_\mu = v_\mu + a_\mu, \quad l_\mu = v_\mu - a_\mu. \quad (2.49)$$

The rest piece of \mathcal{L}_{QCD}^{ex} containing external scalar and pseudoscalar sources can be rewritten similarly as

$$\bar{q}(s - i\gamma_5 p)q = \bar{q}_L(s - i\gamma_5 p)q_L + \bar{q}_R(s - i\gamma_5 p)q_R. \quad (2.50)$$

With Eq. 2.48 and Eq. 2.50, the \mathcal{L}_{QCD}^{ex} finally reads

$$\begin{aligned}\mathcal{L}_{QCD}^{ex} = & \mathcal{L}_{QCD}^0 + \bar{q}_R \gamma^\mu r_\mu q_R + \bar{q}_L \gamma^\mu l_\mu q_L \\ & - \bar{q}_L (s - i\gamma_5 p) q_L - \bar{q}_R (s - i\gamma_5 p) q_R.\end{aligned}\tag{2.51}$$

The \mathcal{L}_{QCD}^{ex} now exhibits a local $U_L(3) \times U_R(3)$ symmetry in the presence of external sources, indicating that \mathcal{L}_{QCD}^{ex} is invariant under $SU_L(3) \times SU_R(3)$ gauge transformation,

$$q_R \mapsto R(x)q_R, \quad q_L \mapsto L(x)q_L, \quad R(x), L(x) \in SU(3),\tag{2.52}$$

under the conditions that external sources transform as

$$\begin{aligned}r_\mu & \mapsto R(x)r_\mu R(x)^\dagger + iR(x)\partial_\mu R(x)^\dagger, \\ l_\mu & \mapsto L(x)l_\mu L(x)^\dagger + iL(x)\partial_\mu L(x)^\dagger, \\ s + ip & \mapsto R(x)(s + ip)L(x)^\dagger, \\ s - ip & \mapsto L(x)(s - ip)R(x)^\dagger.\end{aligned}\tag{2.53}$$

Similar to what is done for a gauge theory like QED, one can write the covariant derivative for the field U in the effective Lagrangian containing external sources

$$D_\mu U = \partial_\mu U - ir_\mu U + il_\mu U.\tag{2.54}$$

And it is straightforward to prove that $D_\mu U$ transforms in the same way as U

$$U \mapsto R(x)UL(x)^\dagger, \quad D_\mu U \mapsto R(x)D_\mu UL(x)^\dagger,\tag{2.55}$$

which is also the requirement of a gauge theory.

The external sources lead to extra building blocks, i.e., the field strength tensor $f_{\mu\nu}^L$ and $f_{\mu\nu}^R$ respect to the corresponding gauge field,

$$\begin{aligned}f_L^{\mu\nu} & = \partial_\mu l_\nu - \partial_\nu l_\mu - i[l_\mu, l_\nu], \\ f_R^{\mu\nu} & = \partial_\mu r_\nu - \partial_\nu r_\mu - i[r_\mu, r_\nu].\end{aligned}\tag{2.56}$$

The remaining scalar and pseudoscalar sources are collected in

$$\chi = 2B_0(s + ip).\tag{2.57}$$

In conclusion, the effective Lagrangian for the modified QCD with external sources will contain $U, D_\mu U, f_L^{\mu\nu}, f_R^{\mu\nu}, \chi$

as building blocks

$$\mathcal{L}_{\text{eff}}^{ex} = \mathcal{L}_{\text{eff}}^{ex}(U, D_\mu U, f_L^{\mu\nu}, f_R^{\mu\nu}, \chi, \dots). \quad (2.58)$$

And in the chiral counting scheme, these building blocks are counted as

$$U \sim \mathcal{O}(p^0), \quad D_\mu U, r_\mu, l_\mu \sim \mathcal{O}(p), \quad f_L^{\mu\nu}, f_R^{\mu\nu}, \chi \sim \mathcal{O}(p^2). \quad (2.59)$$

In accordance with the chiral order of each building block, the lowest order effective Lagrangian containing external sources has almost the same form as Eq. 2.44

$$\mathcal{L}^{(2)} = \frac{F_\phi^2}{4} \langle D_\mu U D_\mu U^\dagger \rangle + \frac{F_\phi^2}{4} \langle \chi U^\dagger + U \chi^\dagger \rangle. \quad (2.60)$$

2.2.4 Chiral effective Lagrangian at NLO in the meson sector

In the above subsections, we introduced briefly the construction of effective Lagrangians in chiral perturbation theory. Meanwhile, the lowest order effective Lagrangian, with and without external sources are presented as an example. Following the same idea, Gasser and Leutwyler further constructed the chiral effective Lagrangian at $\mathcal{O}(p^4)$ [47] for meson-meson interactions, which reads

$$\begin{aligned} \mathcal{L}_4 = & L_1 \{ \text{Tr}[D_\mu U (D^\mu U)^\dagger] \}^2 + L_2 \text{Tr}[D_\mu U (D_n u U)^\dagger] \text{Tr}[D^\mu U (D^n u U)^\dagger] \\ & + L_3 \text{Tr}[D_\mu U (D^\mu U)^\dagger D_\nu U (D^\nu U)^\dagger] + L_4 \text{Tr}[D_\mu U (D^\mu U)^\dagger] \text{Tr}[\chi U^\dagger + U \chi^\dagger] \\ & + L_5 \text{Tr}[D_\mu U (D^\mu U)^\dagger (\chi U^\dagger + U \chi^\dagger)] + L_6 [\text{Tr}(\chi U^\dagger + U \chi^\dagger)]^2 \\ & + L_7 [\text{Tr}(\chi U^\dagger - U \chi^\dagger)]^2 + L_8 \text{Tr}(U \chi^\dagger U \chi^\dagger + \chi U^\dagger \chi U^\dagger) \\ & - i L_9 \text{Tr}[f_{\mu\nu}^R D^\mu U (D^\nu U)^\dagger + f_{\mu\nu}^L (D^\mu U)^\dagger D^\nu U] + L_{10} \text{Tr}[U f_{\mu\nu}^L U^\dagger f_R^{\mu\nu}] \\ & + H_1 \text{Tr}(f_{\mu\nu}^R f_R^{\mu\nu} + f_{\mu\nu}^L f_L^{\mu\nu}) + H_2 \text{Tr}(\chi \chi^\dagger) \end{aligned} \quad (2.61)$$

where $f_{\mu\nu}^R, f_{\mu\nu}^L$ are the field strength tensors defined in Eq. 2.56 and $D_\mu U$ the covariant derivative defined in Eq. 2.54. The L_i are low energy constants which, in principal, could be calculated from QCD. However, practically, these parameters are determined by fitting to observables.

Table 2.1: Two scenarios of central values of L_i with $\mu = 0.77 \text{ GeV}$ from NLO fits [10].

	L_1^r	L_2^r	L_3^r	L_4^r	L_5^r	L_6^r	L_7^r	L_8^r
(I)(10^{-3})	1.11	1.05	-3.82	1.87	1.22	1.46	-0.39	0.65
(II)(10^{-3})	1.00	1.48	-3.82	0.30	1.23	0.14	-0.27	0.55

The values of these low energy constants are necessary for numerical analysis of chiral amplitudes. In Ref. [10] the authors updated the values of L_i with global fits to a number of related observables and presented two sets of values obtained from different fitting strategies. The set (I) are obtained via a fit without constraints, while the

set (II) is managed to be compatible with the results obtained from lattice QCD simulations on L_4^r and L_6^r . It is obvious that the two scenarios really differ, especially the values of L_4 and L_6 , which as a consequence leads to significant differences for certain observables such as the scattering length and the chiral amplitude of $\eta\pi \rightarrow \eta\pi$. For a detailed discussion of the influence on observables of these two sets of values, we refer to Ref. [75].

2.3 Chiral effective field theory for meson-baryon interactions

2.3.1 The lowest order effective lagrangian

The success of chiral perturbation theory in the meson sector illuminates the way to the solutions of non-perturbation QCD in the low energy regime. Thus the application to interactions involving baryons is naturally expected. In this section, we concentrate on the description of the dynamics containing a single baryon in initial and final states at low energies in the framework of chiral perturbation theory. The interaction of multi-baryons are beyond the concern of this work, for a review of which we refer to Refs. [52, 56].

The method of constructing the effective chiral Lagrangian for meson-baryon interactions is in principle the same as that for meson-meson interactions. The biggest difference is that the baryon mass at the chiral limit does not vanish, which makes the baryon mass a hard scale counted as $\mathcal{O}(1)$ in chiral dimension analysis. This feature further leads to the breaking of power counting rules when loop diagrams containing internal baryons are involved. Besides, contrary to the meson sector, performing the Hermitian of B does not go back to B , i.e., $U^{-1} = U^\dagger$ but $B \neq B^\dagger$.

Now we will take the interaction of baryon octet with $J^P = 1/2^+$ and Goldstone bosons as an example. The ground state octet of baryons can be collected in a 3×3 traceless matrix as

$$B = \sum_{a=1}^8 \frac{\lambda_a}{\sqrt{2}} B_a = \begin{pmatrix} \frac{1}{\sqrt{2}}\Sigma^0 + \frac{1}{\sqrt{6}}\Lambda & \Sigma^+ & p^+ \\ \Sigma^- & -\frac{1}{\sqrt{2}}\Sigma^0 + \frac{1}{\sqrt{6}}\Lambda & n^0 \\ \Xi^- & \Xi^0 & -\frac{2}{\sqrt{6}}\Lambda \end{pmatrix}. \quad (2.62)$$

For the building blocks for mesons in the construction of effective chiral Lagrangian for meson-baryon interactions, it is more convenient to introduce the standard non-linear realization [70, 71] for Goldstone bosons $u = \sqrt{U}$. Similar to the cases for pure mesonic interactions, besides the baryon field B and meson field u , the building blocks of the effective chiral Lagrangian for meson-baryon interactions should of course include the covariant derivatives of both fields,

$$\begin{aligned} D_\mu B &= \partial_\mu B + [\Gamma_\mu, B] \\ \Gamma_\mu &= \frac{1}{2} \{u^\dagger \partial_\mu u + u \partial_\mu u^\dagger\} \\ u_\mu &= i \{u^\dagger \partial_\mu u - u \partial_\mu u^\dagger\} \end{aligned} \quad (2.63)$$

in which Γ_μ is also known as chiral connection.

With all the building blocks mentioned above, $B, \bar{B}, D_\mu B, u, u_\mu$, together with the baryon mass at the chiral limit m_0 and Clifford Algebra $\Gamma_i \in \{1, \gamma_5, \gamma_\mu, \gamma_5 \gamma_\mu, \sigma_{\mu\nu}\}$, we are ready to write the most general effective chiral Lagrangian for meson-baryon interactions. The chiral dimensions for these building blocks are

$$B, \bar{B}, D_\mu B \sim \mathcal{O}(1), \quad (i\not{D} - m_0)B \sim \mathcal{O}(p) \quad (2.64)$$

$$1, \gamma_\mu, \gamma_5 \gamma_\mu, \sigma_{\mu\nu} \sim \mathcal{O}(1), \quad \gamma_5 \sim \mathcal{O}(p). \quad (2.65)$$

In accordance with the power counting rule of Eq. 2.64 and Eq. 2.65, the effective Lagrangian can be organized as

$$\mathcal{L}_{\phi B}^{\text{eff}} = \mathcal{L}_{\phi B}^{(1)} + \mathcal{L}_{\phi B}^{(2)} + \mathcal{L}_{\phi B}^{(3)} + \dots \quad (2.66)$$

For the lowest order, it reads

$$\mathcal{L}_{\phi B}^{(1)} = \langle \bar{B}(i\gamma^\mu D_\mu - m_0)B \rangle + \frac{D/F}{2} \langle \bar{B}\gamma^\mu \gamma_5 [u_\mu, B]_\pm \rangle, \quad (2.67)$$

in which D, F are the axial-vector coupling of the baryons to mesons. In $SU(2)$ flavor cases where only u and d quarks are taken into account, these two parameters are actually related to the axial-vector coupling of nucleon $g_A = D + F$. Similar to the L_i in Eq. 2.61, the values of D, F cannot be determined by chiral symmetry, but fit to physical observables instead. For practical applications, the common values of these two parameters comes from the semi-lepton decay of $B \rightarrow B' + e^- \bar{\nu}_e$, which leads to $D = 0.8$ and $F = 0.5$ [76].

Imitating the derivation of Eq. 2.4, one can work out the chiral order for a Feynman diagram, which reads

$$D = 4L - 2N_M - N_B + \sum_n nV_n, \quad (2.68)$$

where L denotes the number of independent loops, $N_M(N_B)$ the number of meson(baryon) internal propagators, V_n the vertices at order $\mathcal{O}(p^n)$.

2.3.2 Effective Lagrangians at NLO and NNLO

In this work, since we attempt to calculate the meson-baryon interactions up to higher orders, i.e., next-to-next-to-leading order (NNLO) or $\mathcal{O}(p^3)$, the effective chiral Lagrangian at $\mathcal{O}(p^2)$ and $\mathcal{O}(p^3)$ are necessary.

Following the method in the preceding subsection, one can easily construct the most general effective chiral Lagrangian for meson-baryon interactions with the building blocks and their corresponding chiral dimension listed in Eq. 2.64, Eq. 2.65. The most difficult and complicated point then is how to find the minimal one among all the possible expressions with the help of assumed symmetries and, more importantly, equation of motion.

The construction of chiral Lagrangian in the two flavor case was the first to complete, i.e., for pion-nucleon interaction. In Ref. [77], the Lagrangian at $\mathcal{O}(p^4)$ was presented both in the relativistic scheme and heavy baryon scheme. The three flavor chiral Lagrangian came afterwards in Ref. [78, 79, 80] for $\mathcal{O}(p^3)$ and, most recently, in Ref.[81] for $\mathcal{O}(p^4)$.

As has been mentioned before, one of the drawbacks for an EFT is that the number of terms increases rapidly along with the increase in chiral order. Taking the SU(3) flavor chiral Lagrangian for example, in the leading order(LO) counted as $\mathcal{O}(p)$, one has only three terms as in Eq. 2.67, while in the next-to-leading order(NLO), there are 16 terms and 78 terms for NNLO. And finally for the next-to-next-to-next-to-leading order(N³LO), one finds 540 terms.

In our calculation, we utilize the minimal chiral lagrangian in a covariant scheme given in Ref. [78] and Ref. [80] with the latter one as a revisited version. Since not all terms contribute in the meson-baryon interactions, we only list here those relevant. The meson-baryon Lagrangian at order $\mathcal{O}(p^2)$ relevant to meson-baryon scattering has 14 terms of the following form:

$$\begin{aligned}
\mathcal{L}_{\phi B}^{(2)} = & b_D \langle \bar{B} \{ \chi_+, B \} \rangle + b_F \langle \bar{B} [\chi_+, B] \rangle + b_0 \langle \bar{B} B \rangle \langle \chi_+ \rangle + \\
& b_1 \langle \bar{B} [u^\mu, [u_\mu, B]] \rangle + b_2 \langle \bar{B} \{ u^\mu, \{ u_\mu, B \} \} \rangle + \\
& b_3 \langle \bar{B} \{ u^\mu, [u_\mu, B] \} \rangle + b_4 \langle \bar{B} B \rangle \langle u^\mu u_\mu \rangle + \\
& i b_5 \left(\langle \bar{B} [u^\mu, [u^\nu, \gamma_\mu \vec{D}_\nu B]] \rangle - \langle \bar{B} \overleftarrow{D}_\nu [u^\nu, [u^\mu, \gamma_\mu B]] \rangle \right) + \\
& i b_6 \left(\langle \bar{B} [u^\mu, \{ u^\nu, \gamma_\mu \vec{D}_\nu B \} \rangle - \langle \bar{B} \overleftarrow{D}_\nu \{ u^\nu, [u^\mu, \gamma_\mu B] \} \rangle \right) + \\
& i b_7 \left(\langle \bar{B} \{ u^\mu, \{ u^\nu, \gamma_\mu \vec{D}_\nu B \} \} \rangle - \langle \bar{B} \overleftarrow{D}_\nu \{ u^\nu, \{ u^\mu, \gamma_\mu B \} \} \rangle \right) + \\
& i b_8 \left(\langle \bar{B} \gamma_\mu \vec{D}_\nu B \rangle - \langle \bar{B} \overleftarrow{D}_\nu \gamma_\mu B \rangle \right) \langle u^\mu u^\nu \rangle + \\
& i c_1 \langle \bar{B} \{ [u^\mu, u^\nu], \sigma_{\mu\nu} B \} \rangle + i c_2 \langle \bar{B} [[u^\mu, u^\nu], \sigma_{\mu\nu} B] \rangle + i c_3 \langle \bar{B} u^\mu \rangle \langle u^\nu \sigma_{\mu\nu} B \rangle,
\end{aligned} \tag{2.69}$$

with $\chi_\pm = u^\dagger \chi u^\dagger \pm u \chi^\dagger u$.

The meson-baryon Lagrangian contributing to $MB \rightarrow MB$ at order $\mathcal{O}(p^3)$ has 13 terms of the following form:

$$\begin{aligned}
\mathcal{L}_{MB}^{(3)} = & id_1 \left(\langle \bar{B} \gamma_\mu \vec{D}_{\nu\rho} B [u^\mu, h^{\nu\rho}] \rangle + \langle \bar{B} \overleftarrow{D}_{\nu\rho} \gamma_\mu B [u^\mu, h^{\nu\rho}] \rangle \right) + \\
& id_2 \left(\langle \bar{B} [u^\mu, h^{\nu\rho}] \gamma_\mu \vec{D}_{\nu\rho} B \rangle + \langle \bar{B} \overleftarrow{D}_{\nu\rho} [u^\mu, h^{\nu\rho}] \gamma_\mu B \rangle \right) + \\
& id_3 \left(\langle \bar{B} u^\mu \rangle \langle h^{\nu\rho} \gamma_\mu \vec{D}_{\nu\rho} B \rangle - \langle \bar{B} \overleftarrow{D}_{\nu\rho} h^{\nu\rho} \rangle \langle u^\mu \gamma_\mu B \rangle \right) + \\
& id_4 \langle \bar{B} [u_\mu, h^{\mu\nu}] \gamma_\nu B \rangle + id_5 \langle \bar{B} \gamma_\nu B [u_\mu, h^{\mu\nu}] \rangle + \\
& id_6 \left(\langle \bar{B} u_\mu \rangle \langle h^{\mu\nu} \gamma_\nu B \rangle - \langle \bar{B} h^{\mu\nu} \rangle \langle u_\mu \gamma_\nu B \rangle \right) + \\
& id_7 \left(\langle \bar{B} \sigma_{\mu\nu} \vec{D}_\rho B \{u^\mu, h^{\nu\rho}\} \rangle - \langle \bar{B} \overleftarrow{D}_\rho \sigma_{\mu\nu} B \{u^\mu, h^{\nu\rho}\} \rangle \right) + \\
& id_8 \left(\langle \bar{B} \{u^\mu, h^{\nu\rho}\} \sigma_{\mu\nu} \vec{D}_\rho B \rangle - \langle \bar{B} \overleftarrow{D}_\rho \{u^\mu, h^{\nu\rho}\} \sigma_{\mu\nu} B \rangle \right) + \\
& id_9 \left(\langle \bar{B} u^\mu \sigma_{\mu\nu} \vec{D}_\rho B h^{\nu\rho} \rangle - \langle \bar{B} \overleftarrow{D}_\rho u^\mu \sigma_{\mu\nu} B h^{\nu\rho} \rangle \right) + \\
& id_{10} \left(\langle \bar{B} \sigma_{\mu\nu} \vec{D}_\rho B \rangle - \langle \bar{B} \overleftarrow{D}_\rho \sigma_{\mu\nu} B \rangle \right) \langle u^\mu h^{\nu\rho} \rangle + \\
& d_{48} \langle \bar{B} \gamma_\mu B [\chi_-, u^\mu] \rangle + d_{49} \langle \bar{B} [\chi_-, u^\mu] \gamma_\mu B \rangle + \\
& d_{50} \left(\langle \bar{B} u^\mu \rangle \langle \chi_- \gamma_\mu B \rangle - \langle \bar{B} \chi_- \rangle \langle u^\mu \gamma_\mu B \rangle \right), \tag{2.70}
\end{aligned}$$

where $D_{\nu\rho} = D_\nu D_\rho + D_\rho D_\nu$ and $h_{\mu\nu} = D_\mu u_\nu + D_\nu u_\mu$.

For Born terms at $\mathcal{O}(p^3)$ and vertex corrections, we also need the following Lagrangian, which contributes to $B_1 \rightarrow M_1 B_2$ and has 10 terms

$$\begin{aligned}
\mathcal{L}_{BMB}^{(3)} = & d_{38} \langle \bar{B} u^\mu \gamma_5 \gamma_\mu B \chi_+ \rangle + d_{39} \langle \bar{B} \chi_+ \gamma_5 \gamma_\mu B u^\mu \rangle + d_{40} \langle \bar{B} u^\mu \gamma_5 \gamma_\mu B \rangle \langle \chi_+ \rangle + d_{41} \langle \bar{B} \gamma_5 \gamma_\mu B u^\mu \rangle \langle \chi_+ \rangle \\
& + d_{42} \langle \bar{B} \gamma_5 \gamma_\mu B \rangle \langle u^\mu \chi_+ \rangle + d_{43} \langle \bar{B} \gamma_5 \gamma_\mu B \{u^\mu, \chi_+\} \rangle + d_{44} \langle \bar{B} \{u^\mu, \chi_+\} \gamma_5 \gamma_\mu B \rangle \\
& + d_{45} \langle \bar{B} \{ \chi_-, \gamma_5 B \} \rangle + d_{46} \langle \bar{B} [\chi_-, \gamma_5 B] \rangle + d_{47} \langle \bar{B} \gamma_5 B \rangle \langle \chi_- \rangle. \tag{2.71}
\end{aligned}$$

2.3.3 Power counting breaking

In the preceding section, we have mentioned that the biggest difference between the chiral perturbation theory in the pure meson sector and meson-baryon sector is that the baryon mass at the chiral limit does not vanish. The non-vanishing baryon mass at the chiral limit yields terms which break the power counting rules in Eq.2.68. This problem was first noticed in Ref. [82] when the authors firstly attempt to extend chiral perturbation theory to elastic πN scattering.

Solutions of this issue has been discussed for about three decades. The first and direct solution to restore the power counting rules is to perform the extension in the baryon sector under the heavy baryon approximation, which is known as heavy baryon ChPT(HBChPT) [83]. The essential idea of this heavy baryon approximation is that since the violation of power counting rules comes from the fact that baryon momentum contains both a hard

scale and a soft scale, one then needs to separate the two parts manifestly,

$$p^\mu = m_B v^\mu + k^\mu, \quad (2.72)$$

where v^μ denotes the baryon velocity with $v^2 = 1$. The second term of the decomposition above k^μ denotes the residual momentum and one has $v \cdot k \ll m_B$. In this way, derivations on the baryon field are divided explicitly where the baryon mass is treated as a hard scale and the residual momentum k^μ as a pure soft scale. Therefore, higher order contributions are suppressed by k/Λ , together with k/m_0 instead of p/Λ , which are strictly small quantities for expansion. In this way, one achieves a systematic expansion in powers of derivatives.

The baryon field B should also be decomposed into a light piece and a heavy piece in the same way as its derivative $\partial_\mu B$ with the projection operator $P_{v\pm}$

$$P_{v\pm} = \frac{1 \pm \not{v}}{2},$$

$$B = \mathcal{B}_v + \mathcal{H}_v, \quad (2.73)$$

$$\mathcal{B}_v = P_{v+} B, \quad \mathcal{H}_v = P_{v-} B.$$

The derivative on the so-called heavy baryon field $\partial_\mu \mathcal{B}_v$ then generates the residual momentum k_μ , which as mentioned is a pure small quantity, with which one can rewrite the covariant effective chiral Lagrangian in Eq. 2.67 in this heavy baryon scheme. Weinberg has proved in Ref. [84, 85] that the HB ChPT is the non-relativistic approximation of the covariant Baryon ChPT with the baryon velocity $v^\mu = (1, 0, 0, 0)$.

Since the HB ChPT solves the power counting breaking problem, it is then successfully applied to study the phenomena related to nucleons [52]. However, the drawbacks and limitations of HB ChPT are also obvious. As a non-relativistic theory, the power counting rule is restored at a cost of manifest Lorentz invariance. The non-relativistic expansion in HB ChPT modifies the analytical property of baryon propagator, resulting in divergences in certain parts of the low energy regime [86, 87]. A direct example is the nucleon pole in πN scattering. On the other hand, in order to restore Lorentz invariance, one has to include $1/m_0$ corrections in the effective Lagrangian, resulting in more terms compared to the covariant scheme at a given order, which makes the calculation quite complicated.

The so-called infrared regularization(IR) scheme which keeps manifest Lorentz invariance was proposed by Ellis and Tang [88]. The basic idea of this regularization is to rewrite the loop integral after Feynman parametrization into two parts, i.e., irregular part and regular part,

$$I(p) = \int_0^1 dz \cdots = \int_0^\infty dz \cdots - \int_1^\infty dz \cdots. \quad (2.74)$$

The first part, so-called infrared integral, satisfies power counting rule, while the remainder, known as the regular part is just ordinary Taylor expansion and can be absorbed into LECs.

The IR scheme reserves the power counting rule and Lorentz invariance simultaneously. But the decomposition again modifies the analyticity of loop integral. Besides, not all of the regular parts to be subtracted violate the power counting rule. This breaking effect is supposed to be of minor importance but later studies of baryon magnet momentum [89, 90] challenge this assumption. Another example is the nucleon mass where a unphysical cut appears. In particular, this treatment makes a dispersion relation no longer available because of extra cuts [86, 89].

The third solution is the so-called extended-on-mass-shell(EOMS) scheme, which was proposed by Gegelia and Fuchs et al [91]. Since all the power counting breaking terms are contained in the regular part of Feynman integration and can be absorbed into LECs, the authors proposed to subtract them explicitly instead of the whole regular part. In other words, the idea of this scheme is that the power counting breaking terms could be treated as part of the re-normalization of LECs. This is actually quite similar to the treatment of UV-divergence in the minimal subtraction scheme(\overline{MS}) or the modified version \widetilde{MS} . For a given LEC, the re-normalization in the EOMS scheme reads

$$L_i = L_i^r + L_i^d R + L_i^{\text{PCB}} \quad (2.75)$$

where L_i^r denotes the bare value of L_i , $R = \frac{2}{\epsilon} + \gamma_E - 1 - \ln(4\pi)$ with γ_E the Euler constant the UV divergence from loops. In this way, the L_i^d , L_i^{PCB} absorbs all the UV divergence and power counting breaking terms respectively for the corresponding order.

In practical applications, these power counting breaking terms could be extracted out before Feynman integration. One needs first to perform Feynman parametrization for the amplitude of a given loop diagram and then expand the amplitude in terms of small quantities, such as meson masses, momenta et al. Since one can easily work out the chiral dimension D of this given loop diagram in accordance with the power counting rule, all terms in the expansion with chiral order lower than D are supposed to violate the power counting rule. Finally the power counting terms to be subtracted from the amplitudes can be easily obtained by integration over feynman parameters. In this scheme, neither power counting nor Lorentz invariance is a problem. Besides, it has been illustrated that the EOMS scheme owns an extra advantage that it converges relatively faster [90, 92, 93].

2.4 Unitarity in hadron-hadron interactions

In the preceding section, we briefly introduced chiral perturbation theory and the construction of effective chiral lagrangian for both pure mesonic interactions as well as those involving a single baryon. Shortly after the foundation of ChPT, it has turned out to be a huge success in describing these interactions. A large number of physical observables calculated theoretically in the framework of ChPT are quite consistent with their experimental values, such as the masses and decay constants of Goldstone bosons, $\pi\pi$ and πK scattering [46, 47]. In the single baryon system, M. Mojžiš [94] and N. Fettes et al. [95] calculated the threshold parameters and scattering amplitudes of pion-nucleon scattering within the HB CHPT mentioned in the previous section.

However, even though it is a powerful tool for low-energy strong interactions, ChPT is essentially a pertur-

bation method based on the expansion of small quantities like momenta and meson masses. As a consequence, dealing with non-perturbation phenomena, typically resonances, is beyond its capacity. In 1990s, people realized that pure chiral perturbation theory can never reproduce a resonance in a perturbation framework at any finite order because of the large rescattering effect, which is essentially non-perturbative [83, 96, 52, 88, 86]. One can find examples such as $\rho(770)$ in $\pi\pi$ scattering, $\Delta(1232)$ in πN scattering and $\Lambda(1405)$ in $\bar{K}N$ scattering. On the other hand, ChPT actually cannot be applied to covering the energy region near these resonances (the so-called resonance region) unless these excited mesons or baryons are included explicitly in the degrees of freedom. Thus these resonances are in fact the upper boundary of the applicable range.

A proper approach of resummation or unitarization of chiral perturbation theory is strongly needed. In 1990, Weinberg proposed one solution [84], that one can first work out the effective potential with ChPT and then iterate it into the Lippmann-Schwinger equation to calculate the S-matrix. It succeeded. In Refs. [97, 98] this approach was applied to $\bar{K}N$ scattering where the coupled channel Lippmann-Schwinger equation was solved with potentials from the lowest order and next-to-leading order Lagrangians respectively. By taking all the open channels, that is, K^-p , \bar{K}^0n , $\pi^0\Lambda$, $\pi^0\Sigma$, $\pi^-\Sigma^+$, $\pi^+\Sigma^-$ into account, a good agreement with the experimental data including the total cross sections for the K^-p elastic and inelastic scattering channels mentioned above can be achieved by fitting only a few parameters.

In Refs. [99, 100], a more technically simplified method based on the Bethe-Salpeter equation was proposed. In this approach, a good description of the experimental data was obtained via the lowest order Lagrangian and coupled channel effects together with a cutoff method for regularizing the intermediate meson-baryon loop. The so-called on shell approximation was applied, which makes the Bethe-Salpeter equation an algebraic equation instead of a integral one. Then in Ref. [101], where a unitary approach based on subtracted dispersion relations was proposed, now known as the N/D approach. This approach was then applied to the strangeness $S = -1$ meson-baryon interaction in Ref. [102], where more dynamically generated resonances like $\Lambda(1670)$ and $\Sigma(1620)$ were studied. The discussion of this unitary method was continued in Ref. [41].

2.4.1 Unitary relation

Before we start this section, it is necessary to specify the definition of various symbols for a scattering process. We show in Fig. 2.1 the standard definition for a two-body scattering process, where p, p', q, q' are the four-momenta of incoming and outgoing particles. On the other hand, it is more convenient to utilize the Mandelstam variables s, t, u , which are pure Lorentz scalars, instead of the four-momentum. They are defined as

$$\begin{aligned}
s &= (p + q)^2 = (p' + q')^2, \\
t &= (p - p')^2 = (q - q')^2, \\
u &= (p - q')^2 = (p' - q)^2.
\end{aligned}
\tag{2.76}$$

With the Mandelstam variables, the module of momentum $|\vec{q}_{cm}|$ in the center mass of frame can be expressed as

$$q_{cm} = \frac{\sqrt{(s - (M + m)^2)(s - (M - m)^2)}}{2\sqrt{s}}, \quad (2.77)$$

with M, m the masses for the two incoming or outgoing particles.

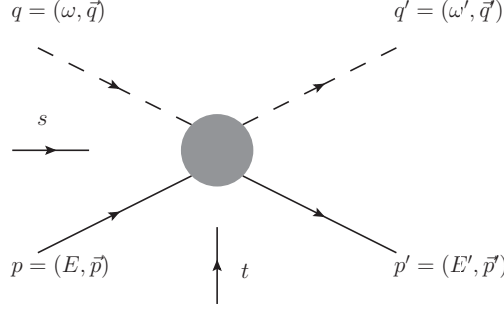


Figure 2.1: Kinematics of meson-baryon scattering.

Considering the conservation of total angular momentum in the scattering process, it is more convenient to perform the partial wave decomposition first on the scattering amplitudes, which is essentially the projection of the amplitude with given angular momentum J

$$T(s, t, u) = \sum (2J + 1) T_J(s) P_J(\cos \theta), \quad (2.78)$$

where T_J denotes the scattering amplitudes with total angular momentum J and P_J the Legendre polynomials, θ is the scattering angle in the center of mass frame.

Unitarity is one of properties that must be satisfied by S-matrix, which as a matter of fact comes from the conservation of probability, i.e., $S \cdot S^\dagger = 1$. Taking the meson-meson interactions with two coupled channels as an example, the S-matrix for a given J can be parameterized as a 2×2 unitary matrix:

$$S_J = \begin{pmatrix} \eta e^{2i\delta_1} & i\sqrt{1-\eta^2} e^{i(\delta_1+\delta_2)} \\ i\sqrt{1-\eta^2} e^{i(\delta_1+\delta_2)} & \eta e^{2i\delta_2} \end{pmatrix}, \quad (2.79)$$

in which η is the inelasticity and δ_1, δ_2 the phase shifts of corresponding channels.

Conventionally, the relation of S-matrix and the partial wave amplitudes T^J is defined as

$$\begin{aligned} S_{11}^J &= 1 + 2i\sigma_1 T_{11}^J, \\ S_{22}^J &= 1 + 2i\sigma_2 T_{22}^J, \\ S_{12}^J &= S_{21}^J = 2i\sqrt{\sigma_1\sigma_2} T_{12}^J, \end{aligned} \quad (2.80)$$

where $\sigma_i = 2 \frac{q_i}{\sqrt{s}}$. Note that the convention for the relation of S-matrix and T-matrix may be different for different

processes. For instance, for meson-baryon interactions, the phase space σ_i has an extra factor of $\frac{1}{8\pi}$, i.e., $\sigma_i = \frac{q_i}{4\pi\sqrt{s}}$.

With Eq. 2.79 and Eq. 2.80, the unitary relation for T-matrix of momentum J can be expressed in matrix form as

$$\text{Im}T_J = T_J \Sigma T_J^*, \quad (2.81)$$

with

$$\Sigma = \begin{pmatrix} \sigma_1 \theta(s - s_1^{th}) & 0 \\ 0 & \sigma_2 \theta(s - s_2^{th}) \end{pmatrix}, \quad (2.82)$$

where s_i^{th} denotes the threshold for channel i. The step function comes from the opening at the threshold of phase space of corresponding channel.

One point to be noted is that the unitary relation actually cannot be exactly satisfied by the amplitudes obtained in ChPT, but only in a perturbative way. This is because the unitary relation in Eq. 2.81 is linear on the left hand side but quadratic on the other side. Taking the amplitude for meson-meson interactions as an example, it can be organized as $T = T_2 + T_4 + \dots$ according to the power counting rule. The unitary relation can only be satisfied at any given order:

$$\text{Im}T_2 = 0, \quad (2.83)$$

$$\text{Im}T_4 = T_2 \Sigma T_2.$$

Immediately one can find a simple unitary method based on this exact perturbative unitarity, that is, the Inverse Amplitude Method(IAM). Starting from the unitary relation in Eq. 2.81, one can divide the inverse of the unitary amplitude into its real part and imaginary part

$$T^{-1} = \text{Re}T^{-1} - i\Sigma, \quad (2.84)$$

in which T^{-1} on the right hand side can be approximated with the perturbation amplitude in ChPT. Finally one can obtain the unitary amplitude which reads

$$\text{Re}T^{-1} \simeq T_2^{-1}(1 - (\text{Re}T_4)T_2^{-1}), \quad (2.85)$$

$$T \simeq T_2(T_2 - T_4)^{-1}T_2,$$

where Eq. 2.83 has been applied for simplification. This unitary method has been successfully applied to describe the phase shifts of $\pi\pi$ and πK scattering [103] and was able to generate resonances such as σ , ρ and K^* .

2.4.2 Bethe-Salpeter equation

In order to take the rescattering effect into account, the scattering equation is applied which can be expressed schematically as

$$\begin{aligned}
 T &= V + VGV + VGVGV + \dots \\
 &= V + VG(V + VGV + \dots) \\
 &= V + VGT,
 \end{aligned} \tag{2.86}$$

where V the arbitrary potential for scattering, which is usually obtained from ChPT, and G contains the propagators of two intermediate particles. Note both V and T have been projected to a given partial wave and the subscript J has been omitted here and afterwards in this subsection for simplification.

Based on Eq. 2.86, one well established relativistic equation is the Bathe-Salpeter equation(BSE) proposed in Ref.[104], which reads

$$T(p_1, p_2, p'_1, p'_2) = V(p_1, p_2, p'_1, p'_2) + \int \frac{d^4k}{(2\pi)^4} V(p_1, p_2, k, P - k)G(k, P - k)T(k, P - k, p'_1, p'_2) \tag{2.87}$$

where p_1, p_2, p'_1, p'_2 are the momenta of incoming and outgoing particles, $P = p_1 + p_2 = p'_1 + p'_2$ the total momentum, k the momentum of intermediate particle as shown in Fig. 2.2. With all these definitions and taking meson-meson interactions for an example, G can be expressed as

$$G = i \frac{1}{k^2 - m^2 + i\epsilon} \frac{1}{(P - k)^2 - M^2 + i\epsilon} \tag{2.88}$$

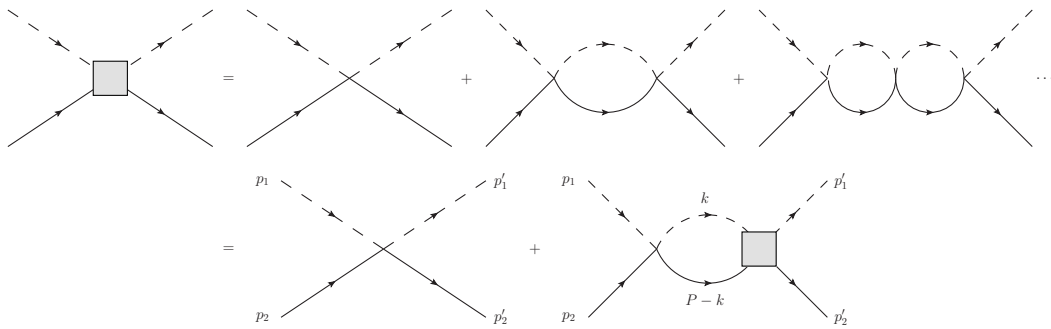


Figure 2.2: Kinematics of meson-baryon scattering.

Obviously, the Bethe-Salpeter equation in Eq. 2.87 is an integral equation, the solution of which is quite a tough task. One will need the discretization of the integral and the knowledge of principle values(see the solution of Lippmann-Schwinger Equation or Kadyshevsky equation), which is beyond the concern of this work. In this work, we will follow the treatment in Ref. [100] and simplify the integral equation into an algebra equation with the on-mass shell approximation.

The basic idea is to divide the potential V and scattering amplitude T inside the integral kernel into the on-shell parts and off-shell parts and put the two propagators in the rescattering process on their mass shell. For the potential V of a given partial wave, the decomposition can be approximately expressed as

$$V(p_1, p_2, p'_1, p'_2) = V_{on}(P^2) + (p_1^2 - m_1^2)V_{off}^{(1)}(P^2) + (p_2^2 - m_2^2)V_{off}^{(2)}(P^2) \\ + (p_1'^2 - m_1'^2)V_{off}^{(3)}(P^2) + (p_2'^2 - m_2'^2)V_{off}^{(4)}(P^2), \quad (2.89)$$

with $P = p_1 + p_2 = p'_1 + p'_2$ again the total momentum. Obviously, V_{on} and $V_{off}^{(i)}$ in Eq. 2.89 are independent of the integral variables. Note that here in order to make the left hand side of Eq. 2.89 strictly equal to the right hand side, only separable potentials are allowed like, for example, the Weinberg-Tomozawa term. Otherwise it is only a approximation of a Taylor expansion over the off-shell parts $p^2 \rightarrow m^2$ under the approximate on-shell condition.

Performing the same decomposition for T , the BS equation becomes now

$$T_{on} = V_{on} + \int \frac{d^4k}{(2\pi)^4} \frac{V_{on}T_{on}}{(k^2 - m^2)[(P - k)^2 - M^2]} \\ + \int \frac{d^4k}{(2\pi)^4} \frac{V_{off}^{(3)}T_{on} + V_{on}T_{off}^{(1)} + (k^2 - m^2)V_{off}^{(3)}T_{off}^{(1)}}{(P - k)^2 - M^2} \\ + \int \frac{d^4k}{(2\pi)^4} \frac{V_{off}^{(4)}T_{on} + V_{on}T_{off}^{(2)} + ((P - k)^2 - M^2)V_{off}^{(4)}T_{off}^{(2)}}{k^2 - m^2} \\ + \int \frac{d^4k}{(2\pi)^4} (V_{off}^{(4)}T_{off}^{(1)} + V_{off}^{(3)}T_{off}^{(2)}). \quad (2.90)$$

Similarly, all T_{on} and T_{off} are also independent of the integral variables and thus can be moved out from the integrand. The second term in Eq. 2.90 only contains the on-shell parts of V and T . After integration, the remaining three pieces containing off-shell parts leads to chiral logarithms or divergences, both of which can be absorbed by the renormalization of couplings and masses [99]. Hence they can be neglected in the calculation.

With all the discussions above, the BS equation now becomes an ordinary algebraic equation

$$T = V + VGT, \quad (2.91)$$

with G the scalar loop integral

$$G(s) = i \int \frac{d^4k}{(2\pi)^4} \frac{1}{k^2 - m^2 + i\epsilon} \frac{1}{(P - k)^2 - M^2 + i\epsilon}. \quad (2.92)$$

However, the scalar loop integral is actually divergent in the four dimensional Minkowski space. There are two widely used methods for regulating this divergence. One is the cutoff method, in which one gives the upper limit of the integration interval a finite value instead of infinity. Usually one needs to integrate the energy component out first and introduce a proper form factor. For practical applications, the cutoff method is very convenient since we only need to handle a numerical integration. But on the other hand, it works at the sacrifice of the analyticity

of loop integral, because it does not fulfill the dispersion relation in Eq. 2.100.

$$G_{CUT}(s) = \int_0^{q_{max}} \frac{d^3q}{(2\pi)^3} \frac{1}{4E_M E_m} \frac{1}{\sqrt{s} - E_M - E_m + i\epsilon}, \quad (2.93)$$

where q_{max} denotes the cutoff value, $E_{M(m)} = \sqrt{q^2 + M^2(m^2)}$ and $M(m)$ the energy and masses of two propagating hadrons.

The other method is the dimensional regularization method(DRM). One first transforms the 4-dimensional integral into d-dimension and then performs Feynman parametrization, wick rotation and shift the momentum. In this way, the loop integral can be finally simplified as a polynomial of Gamma function via the Beta function

$$B(x, y) = \int_0^\infty \frac{t^{x-1} dt}{(1+t)^{x+y}} = \frac{\Gamma(x)\Gamma(y)}{\Gamma(x+y)}. \quad (2.94)$$

In this way, the divergence is contained in the Gamma functions with $\epsilon = d-4 \rightarrow 0$ and can be extracted explicitly via ordinary algebraic operations. The divergent part reads

$$\delta G = \frac{\mu^\epsilon}{16\pi^2} \left(\frac{1}{\epsilon} - \frac{1}{2} [\ln(4\pi) - \Gamma'(1) + 1] \right), \quad (2.95)$$

where μ is the regularization scale. This convention is also known as minimal subtraction scheme(\overline{MS}).

Utilizing the dimensional regularization and omitting the ultra-violet divergence, the finite part of G can be expressed as

$$\begin{aligned} G_{\overline{MS}}(s) = & \frac{1}{16\pi^2} \left[\frac{m^2 - M^2 + s}{2s} \log \left(\frac{m^2}{M^2} \right) \right. \\ & - \frac{q}{\sqrt{s}} (\log[2q\sqrt{s} + m^2 - M^2 - s] + \log[2q\sqrt{s} - m^2 + M^2 - s]) \\ & - \log[2q\sqrt{s} + m^2 - M^2 + s] - \log[2q\sqrt{s} - m^2 + M^2 + s]) \\ & \left. + \left(\log \left(\frac{M^2}{\mu^2} \right) + a \right) \right]. \end{aligned} \quad (2.96)$$

Note that the a here denotes the subtraction constant.

Practically both the subtraction constant a and cutoff momentum q_{max} should be treated as free parameters and determined via fits to experimental observables. This is because the potential is always truncated at a finite order and these two parameters actually contain contributions from higher orders.

However, the subtraction constant and the cutoff momentum can also be treated model independently. Conventionally one can choose the scale of chiral symmetry breaking, i.e., the mass of $\rho(770)$ or 1GeV for the cutoff momentum. For the subtraction constant, it could be treated as a function of the regularization scale $a = a(\mu)$, which can then be obtained by setting $G(\mu) = 0$ manifestly or requiring the $G(s)$ at threshold equal to that calculated in the cutoff scheme.

One can easily prove that the T-matrix obtained from the BS equation automatically satisfies the unitary relation

for a real potential. From Eq. 2.91, one can find

$$T^{-1} = V^{-1} + G \quad (2.97)$$

which is exactly matched to Eq. 2.84 with $\text{Re}T^{-1} = V^{-1}$ and $\text{Im}G_i = -\sigma_i/2$ ¹.

The method combined ChPT and the Bethe-Salpeter equation with the on-shell approximation is now known as chiral unitary theory(UChPT). The application in, for example, Ref. [100] has proved that the UChPT is a powerful tool for the study on hadron-hadron interactions, especially covering the resonance region. It can dynamically generate the resonances of our interest with very few free parameters. In most cases, there will be only one free parameter, the subtraction constant a or the cutoff momentum q_{max} , besides the LECs in chiral Lagrangians.

However, one may find that in the re-summation of the loop chain for the BS equation, only s channel vertices are involved. As a consequence, potentials containing the born term and the crossed born term are not appropriate for such a resummation. Generally speaking the solution of the BS equation are not crossing symmetric. Further more, potentials containing box diagrams or any once iterated diagrams involving born terms(and crossed ones) are also not proper for the UChPT.

2.4.3 Unitarity in general

As has been mentioned in the previous subsection, although UChPT is quite a simple and powerful approach, the loss of crossing symmetry makes it unsuitable for applications involving potentials at loop level. In this subsection, we will introduce a more general unitary method which was proposed by J. A. Oller and Ulf-G. Meissner in Ref.[41].

The starting point is the unitary relation in Eq. 2.84, from which one finds the discontinuity for T_{ij} when crossing the real axis

$$\text{Im}T_{ij}^{-1}(s) = \rho_i(s)\theta(s - s_{th})\delta_{ij}. \quad (2.98)$$

with $\rho_i = -\frac{\sigma_i}{2} = -\frac{q_{cm}}{8\pi W}$. According to the Cauchy theorem, $T_{ij}^{-1}(s)$ can be expressed with once subtracted dispersion relation as

$$T_{ij}^{-1}(s) = \delta_{ij}g_i(s) + \mathcal{T}_{ij}^{-1}(s), \quad (2.99)$$

with

$$g_i(s) = \left(\tilde{a} + \frac{s - s_0}{\pi} \int_{s_{th}}^{\infty} ds' \frac{\rho_i(s')}{(s' - s)(s' - s_0)} \right), \quad (2.100)$$

where \tilde{a} is again the subtraction constant and s_0 the subtraction point. $\mathcal{T}(s)$ above denotes the remaining part of T after subtracting the right hand cut, which includes contributions from local and pole terms and crossed diagrams. Compared to Eq. 2.97, one can immediately find that $g(s)$ is exactly the once subtracted dispersion relation for $G(s)$ since $\text{Im}G = -\frac{\sigma(s)}{2}\theta(s - s_{th})$. Also note that here we also required that the T-matrix above does not contain

¹Here, the convention is switched to be matched to Eq. 2.96.

the left hand cut.

The basic idea of this general unitary method is to match the remaining part \mathcal{T} simultaneously with the perturbation amplitudes from ChPT and guarantee that it does not contain the unitary cut. One first rewrites Eq. 2.99 as

$$T(s) = [I + \mathcal{T}(s) \cdot g(s)]^{-1} \cdot \mathcal{T}(s), \quad (2.101)$$

where I is the unit matrix. The equation is expressed in matrix form to be more general. The resummation of the right hand cut contribution can be expressed as the expansion of Eq. 2.101, which is

$$T(s) = \mathcal{T}(s) - \mathcal{T}(s) \cdot g(s) \cdot \mathcal{T}(s) + \dots \quad (2.102)$$

Now we are able to find the explicit matching relation between \mathcal{T} and the perturbation amplitudes at the i -th order $T^{(i)}$ from ChPT. Take meson-meson interaction as an example. Since $g(s)$ is counted as $\mathcal{O}(1)$ and only even order terms are allowed according to power counting rules, the lowest order of the right hand cut is $T^{(2)} \cdot g(s) \cdot T^{(2)}$, which is at order $\mathcal{O}(p^4)$. Thus at the lowest order, $T(s) = T^{(2)} + \mathcal{O}(p^4)$ is free of loops and unitary cut, which indicates that the remaining part $\mathcal{T}^{(2)}(s)$ is exactly $T^{(2)}$.

Substituting $\mathcal{T}^{(2)}(s) = T^{(2)}(s)$ into Eq. 2.101, one can obtain the unitary amplitudes

$$T(s) = [I + T^{(2)}(s) \cdot g(s)]^{-1} \cdot T^{(2)}(s). \quad (2.103)$$

This method can be applied to calculate the unitary amplitudes at any given order. For higher order involving loop contributions, for instance, the $\mathcal{O}(p^4)$ for meson-meson interactions, the remaining part $\mathcal{T}(s)$ is

$$\mathcal{T}^{(4)}(s) = T^{(4)}(s) + T^{(2)}(s) \cdot g(s) \cdot T^{(2)}(s), \quad (2.104)$$

where the last term guarantees $\mathcal{T}(s)$ free of right hand cuts.

As a summary, we introduced a general scheme to unitarize the amplitudes, which is particularly convenient when considering higher order contributions up to loop level. However, at loop level, amplitudes usually contain complicated analytical structures including a variety of right hand cuts and left hand cuts. To restore the strict unitary relation, one will have to make some approximations for the perturbation amplitude via subtracting the left hand piece or, the most simple method, subtracting the whole imaginary part from the perturbation amplitude.

2.4.4 Resonances

Once we take rescattering effects into account via the resummation of unitary cuts, resonances can then be generated dynamically. The resonance behaves as a pole of unitary amplitude for a given partial wave in the complex plane of \sqrt{s} . The pole on the real axis corresponds to a bound state while those with finite imaginary parts reso-

nances.

One point to be noted is that although a resonance rises up as a pole of unitary amplitude, there are also other processes which could lead to enhancement on the complex plane. For example, threshold effect because of the step function of phase space may result in peaks but not singularities at threshold. These kinds of phenomena are known as cusps, which can be distinguished from a resonance by the residue of the unitary amplitude at the pole position. Another kind of enhancement is caused by the kinematical effect such as the triangle singularity. When the three propagators are approximately on their mass shell, a peak will appear. Compared to a resonance, these kinds of singularities are actually a perturbation effect. One can find quite a large number of discussion on these topics and here I only refer to Ref. [105] as an example for interested readers, where a triangle singularity explanation was given for the $f_2(1810)$.

On the other hand, we are also faced with one problem that the unitary T-matrix is as a matter of fact a multi-valued complex function due to the q_{cm} in the scalar loop integral of Eq. 2.96. For an arbitrary complex number z , we have $z = ze^{2\pi i}$. Thus, the q_{cm} as a square root of a complex number will naturally lead to two values, \sqrt{z} and $\sqrt{z}e^{\pi i}$. As a consequence, for each single channel, one will have two so-called Riemann sheets.

The function on the first Riemann sheet is defined by the requirement of $0 \leq \theta \leq 2\pi$. With the unitary relation in Eq. 2.97, we can write the unitary cut for $G^I(s)$ where the superscript denotes the first Riemann sheet

$$\text{Im}G_i(\sqrt{s}) = \frac{1}{2i}(G_i^I(\sqrt{s} + i0) - G_i^I(\sqrt{s} - i0)) = -\sigma_i/2 = -\frac{q_{cm}}{8\pi\sqrt{s}}, \quad (2.105)$$

where 0 here refers to a positive infinitesimal. The G on the second Riemann sheet G^{II} is then defined as

$$G^{II}(\sqrt{s} + i0) \equiv G^I(\sqrt{s} - i0). \quad (2.106)$$

With Eq. 2.105 and Eq. 2.106, one can finally obtain the relation between G^I and G^{II}

$$G^{II}(\sqrt{s}) = G^I(\sqrt{s}) + i\sigma_i. \quad (2.107)$$

Note that all the momentum in both sides of the above equation are calculated in the first Riemann sheet.

One may also define the G on the so-called physical Riemann sheet via

$$G_{ph} = \begin{cases} G^I(\sqrt{s}), & \text{Re}[\sqrt{s}] < \sqrt{s_{th}}; \\ G^I(\sqrt{s}), & \text{Re}[\sqrt{s}] > \sqrt{s_{th}}, \text{Im}[\sqrt{s}] > 0; \\ G^{II}(\sqrt{s}), & \text{Re}[\sqrt{s}] > \sqrt{s_{th}}, \text{Im}[\sqrt{s}] < 0. \end{cases} \quad (2.108)$$

The physical Riemann sheet is directly connected to the physical real axis and thus related to the pole structure for physical observables. For practical applications, one can directly search for poles on this physical Riemann sheet.

Assuming that there exists a pole at $\sqrt{s_0} = M - i\Gamma/2$ with M, Γ the mass and width of the resonance, one

can perform a Laurent expansion for the T-matrix element T_{ij} over $\sqrt{s} - \sqrt{s_0}$, which reads

$$T(\sqrt{s})_{ij} = \frac{g_i g_j}{\sqrt{s} - \sqrt{s_0}} + c_1 + c_2(\sqrt{s} - \sqrt{s_0}) + \dots, \quad (2.109)$$

where g_i denotes the coupling of the resonance to the i -th channel, which indicates the relative importance of different coupled channels to the resonance. c_i 's are complex coefficients. Note that the first term is just the familiar Breit-Wigner term for a scattering amplitude.

Chapter 3

Dynamically generated excited charmed baryons

In the preceding chapters, we introduced the theoretical framework for low energy dynamics of hadrons, i.e., chiral perturbation theory and its unitary approach(UChPT). In this chapter we will apply UChPT to study the interactions between Goldstone bosons and heavy baryons containing one single charm quark, and the internal structure of the dynamically generated states in these interactions.

3.1 Introduction

As has been mentioned in section. 1.3, ordinary mesons consist of a pair of quark and anti-quark while baryons contain three quarks. Except for only a few anomalies, for instance, the lowest lying scalar nonet such as $a_0(980)$, $f_0(980)$, $f_0(500)$, $K_0^*(700)$ and the excited baryons like $\Lambda(1405)$, most hadrons can be explained via the naive quark model [5] till the end of last century. However, with the development of accelerator techniques, the exotic XYZ states were discovered one by one, the first of which is the famous $X(3872)$ states in 2003 by the Belle Collaboration [106]. Some of these exotic hadrons contain apparently extra pairs of quark and anti-quark, such as $Z_c(4430)$ [107] and $Z_c(3900)$ [108] for heavy mesons or the most recently discovered heavy baryons, pentaquark states P_c by the LHCb Collaboration. For a review of this topic, we refer to Ref. [109].

Compared to the case of heavy meson states, the spectrum for the exotic heavy-flavor baryon sector is much less complete, partly because production cross sections of exotic baryons are small. Up to now, there are only a few experimental observations of excited charmed and bottom baryons (see Ref. [110] for a recent and comprehensive review). In the charmed baryon sector, various collaborations have observed a number of excited states, including $\Lambda_c(2595)$, $\Xi_c(2790)$ with $J^P = 1/2^-$ and $\Lambda_c(2625)$, $\Xi_c(2815)$ with $J^P = 3/2^-$ [5]. While in the bottom baryon sector, the LHCb Collaboration has reported two excited Λ_b states, $\Lambda_b(5912)$ and $\Lambda_b(5920)$ [111]. The CDF Collaboration then confirmed the second state [112].

These variety of discoveries has attracted worldwide attention of physicists. Theoretical explanations based on different kinds of models such as weakly bound molecular states or contact multi-quark states, i.e., tetra-quark or penta-quark states, have been proposed based on chiral symmetry, unitarity and heavy quark symmetry, the last of which is particularly helpful in such a case. Besides, considering that most of these exotic states are located quite close to the thresholds of some two-body channels, one can naturally expect significant coupled channel effects. A series of work [2, 4, 113, 114, 115] have proposed that these excited charmed or bottom baryons are not the traditional orbital excited states, or at least not completely. These studies provide instead a interpretation from the point of view of dynamically generated states, or molecule via different approaches including the unitary chiral approach(UChPT), the hidden gauge symmetry approach or EFT based on heavy quark symmetry. As a matter of fact, such a molecular interpretation has been successfully applied for the exceptions mentioned at the beginning of this section, e.g., the scalar nonet and $\Lambda(1405)$.

In the present work, we apply the unitary chiral approach to study the interactions between the ground-state charmed baryons and the pseudoscalar mesons with effective chiral Lagrangians up to next-to-leading order(NLO). Heavy quark spin symmetry is applied to build a relation between the potentials for $J^P = 1/2^+$ and $J^P = 3/2^+$. We search for poles on the complex plane to identify dynamically generated states. Besides, we investigate the impact of different regularization schemes to regularize the loop function in the UChPT, in which corrections from the heavy quark symmetry are taken into account. This work was published in Ref. [11].

3.2 Framework

In the standard quark model, the ground state singly charmed baryons(see Fig. 1.3), can be grouped into two SU(3) representations, i.e., an anti-triplet and a sextet according to the two light quarks as

$$3 \times 3 = \bar{3} + 6, \quad (3.1)$$

where the heavy quark is treated as a spectator. Charmed baryons belonging to these two representations should be treated separately.

The chiral Lagrangian for the leading order interaction between the sextet or anti-triplet and a pseudoscalar meson in a covariant scheme is provided in Refs. [113, 116]:

$$\mathcal{L} = \frac{i}{16f_0^2} \text{Tr}(\bar{H}_{[\bar{3}]}(x)\gamma^\mu [H_{[\bar{3}]}(x), [\phi(x), (\partial_\mu\phi(x))]_-]_+) \quad (3.2)$$

$$+ \frac{i}{16f_0^2} \text{Tr}(\bar{H}_{[6]}(x)\gamma^\mu [H_{[6]}(x), [\phi(x), (\partial_\mu\phi(x))]_-]_+), \quad (3.3)$$

where f_0 is the pseudoscalar decay constant at the chiral limit, ϕ the familiar pseudoscalar octet, $H_{[\bar{3}]}$ and $H_{[6]}$

collect the charmed baryons, respectively:

$$\phi = \sqrt{2} \begin{pmatrix} \frac{\pi^0}{\sqrt{2}} + \frac{\eta}{\sqrt{6}} & \pi^+ & K^+ \\ \pi^- & -\frac{\pi^0}{\sqrt{2}} + \frac{\eta}{\sqrt{6}} & K^0 \\ K^- & \bar{K}^0 & -\frac{2}{\sqrt{6}}\eta \end{pmatrix}, \quad (3.4)$$

$$H_{[3]} = \begin{pmatrix} 0 & \Lambda_c^+ & \Xi_c^+ \\ -\Lambda_c^+ & 0 & \Xi_c^0 \\ -\Xi_c^+ & -\Xi_c^0 & 0 \end{pmatrix}, \quad (3.5)$$

$$H_{[6]} = \begin{pmatrix} \Sigma_c^{++} & \frac{\Sigma_c^+}{\sqrt{2}} & \frac{\Xi_c'^+}{\sqrt{2}} \\ \frac{\Sigma_c^+}{\sqrt{2}} & \Sigma_c^0 & \frac{\Xi_c'^0}{\sqrt{2}} \\ \frac{\Xi_c'^+}{\sqrt{2}} & \frac{\Xi_c'^0}{\sqrt{2}} & \Omega_c^0 \end{pmatrix}. \quad (3.6)$$

With the Lagrangian of Eq. 3.2, one can easily obtain the interaction kernel for the $\phi(p_2)B(p_1) \rightarrow \phi(p_4)B(p_3)$ process of our interest where p_i 's are the four momenta of the respective particles

$$V = \frac{C_{ij}^{(I,S)}}{4f_0^2} \gamma^\mu (p_2^\mu + p_4^\mu) \approx \frac{C_{ij}^{(I,S)}}{4f_0^2} (E_2 + E_4), \quad (3.7)$$

where $C_{ij}^{(I,S)}$ denote the Clebsch-Gordan coefficients given in the Appendix. A. Note that in the expression above, we have neglected the three momenta component since in the present study we are only interested in the energy region close to the thresholds of the respective coupled channels.

In the framework of UChPT, the Bethe-Salpeter equation is applied to resum the unitary cut. With the on-shell approximation discussed in the preceding chapter, the BS equation can be simplified as an ordinary algebraic equation in Eq. 2.91. We put it here again for convenience.

$$T = V + VGT, \quad (3.8)$$

where V denotes the kernel in Eq. 3.7 and G the familiar scalar integral in Eq. 2.92. We have introduced two regularization schemes, dimensional regularization scheme and cutoff scheme, to regulate the divergence in Eq. 3.10 and Eq. 2.93. However, in Ref. [117], the authors proposed a new regularization scheme based on heavy quark symmetry, or the HQS scheme in short, which manifestly satisfies both the chiral power counting and the heavy-quark spin and flavor symmetry up to $1/M_H$ with M_H a generic heavy-hadron mass. In the HQS scheme, the scalar integral reads

$$G_{HQS} = G_{\overline{MS}} - \frac{2\mathring{M}}{16\pi^2} \left(\log \left(\frac{\mathring{M}^2}{\mu^2} \right) - 2 \right) + \frac{2m_{\text{sub}}}{16\pi^2} \left(\log \left(\frac{\mathring{M}^2}{\mu^2} \right) + a \right), \quad (3.9)$$

$$G_{\overline{MS}}(s, M^2, m^2) = \frac{2M}{16\pi^2} \left[\frac{m^2 - M^2 + s}{2s} \log \left(\frac{m^2}{M^2} \right) \right. \quad (3.10)$$

$$\left. - \frac{q}{\sqrt{s}} (\log[2q\sqrt{s} + m^2 - M^2 - s] + \log[2q\sqrt{s} - m^2 + M^2 - s]) \right. \quad (3.11)$$

$$\left. - \log[2q\sqrt{s} + m^2 - M^2 + s] - \log[2q\sqrt{s} - m^2 + M^2 + s] \right) \quad (3.12)$$

$$+ \left(\log \left(\frac{M^2}{\mu^2} \right) \underline{-2} \right). \quad (3.13)$$

Note that we have moved the subtraction constant in Eq. 3.10 into the correction part and left a -2 which is underlined in the corresponding position. In the above equations, m_{sub} is a generic pseudoscalar meson mass and $\overset{\circ}{M}$ the chiral limit value of the charmed baryon masses, which can practically be taken the average values of the masses of pseudoscalar mesons and charmed baryons listed in Table 3.1. Clearly the HQS inspired regularization method is a straightforward extension of the minimal subtraction scheme, which, in spirit, is very similar to the extended-on-mass-shell scheme [91].

In Fig. 3.1, we compared the scalar loop integral from the three regularization schemes mentioned above. The subtraction constants or cutoff momentum are fixed such that $\Lambda_c(2595)$ can be reproduced having the mass measured experimentally. In the comparison, we apply the pion mass $m = 138$ MeV for the pseudoscalar meson and the regularization scale in the two dimensional regularization methods $G_{\overline{MS}}$ and $G_{HQ S}$ is chosen to be $\mu = 1$ GeV. The loop function in the exact heavy quark limit is obtained by replacing $\overset{\circ}{M}$ with M , and expanding $G_{HQ S}$ in inverse power of M up to $\mathcal{O}(1/M)$ [117]. It is clear that the scalar loop integral in the HQS inspired scheme and the cutoff scheme remain almost independent on the heavy baryon mass, indicating the conservation of heavy quark symmetry, while the strong dependence on M of the naive \overline{MS} scheme imply the breaking of the symmetry. The behaviors are consistent with the finding in heavy meson cases in Ref. [117]. To be conservative, we shall always exhibit the results of dynamically generated charmed baryons obtained in the HQS inspired scheme as well as in the cutoff scheme in the following section.

Table 3.1: Numerical values of isospin and SU(3)-multiplet averaged masses, the pion decay constant f_π , and the SU(3) averaged pseudoscalar meson decay constant f_0 (in units of MeV) [5].

$\overset{\circ}{M}_c^{[3]}$	M_{Λ_c}	M_{Ξ_c}	$\overset{\circ}{M}_c^{[6]}$	M_{Σ_c}	$M_{\Xi'_c}$	M_{Ω_c}
2408.5	2286.5	2469.5	2534.9	2453.5	2576.8	2695.2
$M_{\Sigma_c^*}$	$M_{\Xi_c^*}$	$M_{\Omega_c^*}$	$\overset{\circ}{M}_{c^*}^{[6]}$			
2517.9	2645.9	2765.9	2601.9			
m_π	m_K	m_η	m_{sub}	f_π	$f_0 = 1.17f_\pi$	
138.0	495.6	547.9	368.1	92.21	107.8	

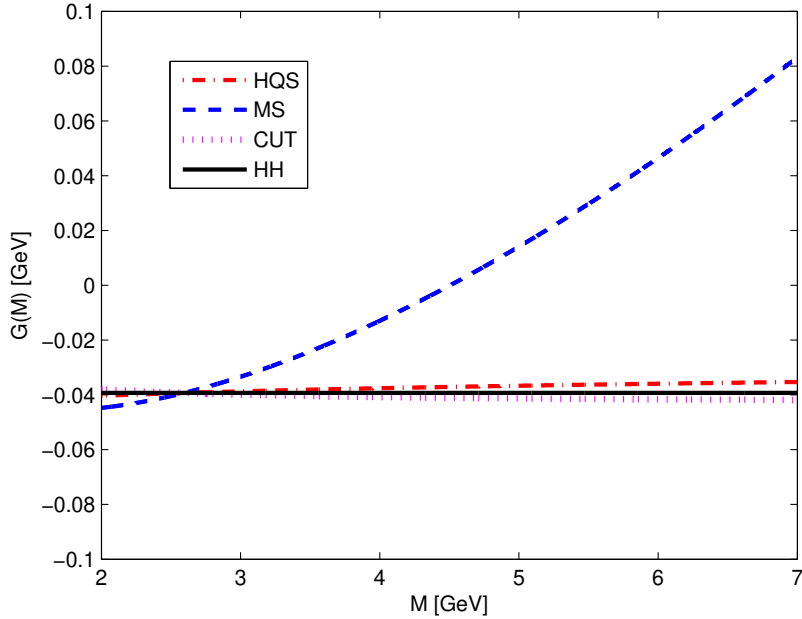


Figure 3.1: Loop function $G(M)$ as a function of the heavy hadron mass M in different regularization schemes: HQS (the heavy quark symmetry inspired scheme), $\overline{\text{MS}}$ (the modified minimal subtraction scheme), CUT (the cutoff regularization scheme), and HH (the exact heavy-quark limit). The subtraction constants or cutoff values have been fixed by reproducing $\Lambda_c(2595)$. In calculating the loop function G , the pseudoscalar meson mass is fixed at that of the pion $m = 138$ MeV and the renormalization scale in the dimensional regularization methods is fixed at $\mu = 1$ GeV.

3.3 Results and discussions

In this unitary approach, there is no free parameter in the potential V at the lowest order. The only unknown parameter exists in the scalar loop integral, i.e., the subtraction constant a in the dimensional regularization scheme or the cutoff momentum Λ in the cutoff regularization scheme. As I have mentioned in the preceding chapter, these two parameters could be treated model independently. Conventionally, one often chooses a cutoff of the order of the chiral symmetry breaking scale or mass of ρ meson, while one can fix a “natural” value for the subtraction constant by requiring the G function evaluated at threshold to be equal in both methods. Such a treatment is adequate to produce some of the dynamically generated states, which, however, in most cases will not be located exactly at the position observed experimentally. This is because the potential is only calculated up to a finite order with higher order contributions absorbed into a or Λ . In order to guarantee that the dynamically generated state coincide with its experimental counterpart, Λ or a usually needs slightly fine-tuning accordingly. One can further use Λ or a obtained to make predictions. In the present work we will follow the same line.

One can easily extend the study of the $1/2^-$ sector to the $3/2^-$ sector since heavy-quark spin symmetry implies that in the limit of infinite heavy quark masses, the interactions between a ground state baryon and a pseudoscalar meson are the same no matter whether the spin of the baryon is $1/2$ or $3/2$. As a consequence, in order to search for the excited heavy baryons with $J^P = 3/2^-$, we only need to replace the masses of the $1/2^+$ baryons by their $3/2^+$ partners (see Table 3.1). The differences will be of higher orders. Searching for poles on the complex plane,

we find the partner state $\Lambda_c^*(2625)$ in the charmed sector with the same quantum numbers as $\Lambda_c(2595)$.

It should be noted that unlike the heavy meson sector, the present lattice QCD simulations of charmed [118, 119, 120, 121, 122] or bottom [120, 123, 122] baryons still focus on the ground states with the exception of Ref. [124] and Ref. [125], where excited triply charmed and bottom states were studied, respectively. Future lattice QCD simulations of the excited singly charmed and bottom baryons will be extremely valuable to test the predictions of the present work and those of other studies.¹

3.3.1 Excited charmed baryons

Once the subtraction constant is fixed with the mass of $\Lambda_c(2595)$ with $J^P = 1/2^-$ or $\Lambda_c(2625)$ with $J^P = 3/2^-$, one can use the same constant to predict the counterparts of the dynamically generated states with different isospin and strangeness. Our calculation indicates that $\Lambda_c(2595)$ can indeed be identified as a $\Sigma_c\pi$ state, as first pointed out in Refs. [3, 113]. To account for moderate heavy-quark flavor symmetry breaking corrections, we slightly fine-tune the subtraction constant in the dimensional regularization scheme or the cutoff value in the cutoff regularization scheme so that the mass of $\Lambda_c(2595)$ is reproduced to be 2591 MeV.² The predictions are then tabulated in Tables 3.2 and 3.3.

Similar predictions are also made in Refs. [2, 4] but with different interaction kernel. In Ref. [4], a Weinberg-Tomozawa like Lagrangian based on full $SU(8) = SU(4)_f \times SU(2)$ symmetry was applied, while in Ref. [2], the transition amplitudes are obtained via vector meson or pion exchanges with corrections from box diagrams. The coupled channels to be taken into account thus differs accordingly. Taking $I = 0$ channel as an example, one finds 16 channels in the kernel of Ref. [4], 7 in Ref. [2] but 2 in the present work. In other words, we only keep the minimum number of channels to construct the LO chiral Lagrangian. One should also note that in Refs. [2, 4], the anti-triplet [3] and sextet [6] of charmed baryons are mixed up while it is not in our case. All the differences mentioned above lead to disagreements among the predictions from the three works. For example, four ($S = 0, I = 0$) states and five ($S = 0, I = 1$) states are predicted in Ref. [2]. The number of dynamically generated states in Ref. [4] is even larger. Somehow, it seems that the number of states generated is proportional to the number of coupled channels considered. As a consequence, one needs to be careful to compare our predictions with those in Refs. [2, 4].

In addition, our $\Lambda_c(2595)$ is predominantly a $\Sigma_c\pi$ state, while it is more in favor of a DN state in Ref. [2] and a D^*N state in Ref. [4]. Despite of the different dominant components, it is clear that coupled channel effects or multi quark components may not be negligible in the wave function of $\Lambda_c(2595)$.

In Table. 3.2, we have temporarily identified the states appearing at $\sqrt{s} = (2721, 0)$ MeV, $\sqrt{s} = (3069 - i12)$ MeV, $\sqrt{s} = (2827 - i55)$ MeV, and $\sqrt{s} = (3123, -i44)$ MeV as $\Lambda_c(2765)$, $\Lambda_c(2940)$, $\Xi_c(2790)$, and $\Xi_c(3123)$. These identifications are mainly based on the masses of these states [5]. Since the spin-parity's of these states are

¹We note that preliminary results on the excited state spectroscopy of singly and doubly charmed baryons have recently been presented at conferences [126, 127].

²Experimentally, $\Lambda_c(2595)$ is found at 2592.25 ± 0.28 MeV with a width of 2.6 ± 0.6 MeV [5]. We need to slightly increase f_0 to put $\Lambda_c(2595)$ exactly at this position because of the closeness of the $\Sigma_c\pi$ threshold.

not yet known, the associations of our states with their experimental counterparts should be taken with care. A second complication comes from the fact that other coupled channels other than those considered here may not be negligible as can be seen from Fig. 3.2.

In Ref. [128], $\Lambda_c(2940)$ was suggested to be a molecular state with spin-parity $J^P = 1/2^-$ or $3/2^-$, because of its proximity to the $D^{*0}p$ threshold. In Ref. [4], none of the dynamically generated states with $J^P = 1/2^-$ or $3/2^-$ can be associated to $\Lambda(2940)$. In Ref. [2], a state at 2959 MeV with a small width could be associated to the $\Lambda_c(2940)$, which, however, couples mostly to $\rho\Sigma_c$. In our present study, since the DN (D^*N) channels are not taken into account explicitly, we have found only two states at about 3050 MeV (see Tables 3.2 and 3.4), one of which we tentatively associate to $\Lambda_c^{(*)}(2940)$. However, one definitely needs to take into account the missing $D^{(*)}N$ channels to be more conclusive. It should be noted that in the molecular picture, Dong et al. have studied the strong two-body decays of $\Lambda_c(2940)$ and shown that the $J^P = 1/2^+$ assignment is favored [129]. Assuming this particular quantum number, they later studied the radiative [130] and strong three-body [131] decays of $\Lambda_c(2940)$. Molecular nature of $\Lambda_c(2940)$ has recently been studied in the framework of QCD sum rules [132], the constituent quark model [133], and the effective Lagrangian method [134], as well.

In Tables 3.4 and 3.5, we tabulate the dynamically generated states in the $3/2^-$ sector. It should be noted that compared to the $1/2^-$ sector, an extra pole is produced in the $(S, I) = (-2, 1)$ channel. On the other hand, its counterpart is found in both the $3/2^-$ and $1/2^-$ bottom sector. This seems to indicate that the breaking of heavy quark flavor symmetry is larger than that of the heavy quark spin symmetry, as naively expected.

It should be noted that to confirm the identification of the dynamically generated states with their experimental counterparts, one needs to study their decay branching ratios, since many approaches used the masses of these states to fix (some of) their parameters. Strong and radiative decays are both very important in this respect since they may probe different regions of their wave functions. In the past few years, many such studies of the decays of charmed baryons have been performed, see, e.g., Refs. [129, 130, 131, 135, 136, 137, 138, 139, 140].³

3.3.2 Further Discussions

One can certainly extend the calculation to the bottom sector with the help of heavy quark flavor symmetry as was done in the published version [11], which for simplification is not shown here. Superficially, exact heavy quark flavor symmetry would dictate that the number of dynamically states in the bottom sector and that in the charm sector is the same. A comparison in Ref. [11] shows that this is almost the case, but not exactly since heavy quark symmetry could be broken. For instance, some counterparts of the dynamically generated bottom baryons are missing in the charm sector. A closer look at these channels reveals that they simply become too broad and develop a width of $200 \sim 300$ MeV, which are not considered in our study.

The broadening of these states can be traced back partially to the weakening of the corresponding potentials and partially to the calibration of our framework to reproduce $\Lambda_c(2595)$ in the charmed sector. Since $\Lambda_c(2595)$ is

³For similar studies in the heavy-flavor mesonic sector, see, e.g., Refs. [141, 142, 143, 144, 145, 146, 147, 148].

Table 3.2: Dynamically generated charmed baryons of $J^P = 1/2^-$. The subtraction constant is fixed in a way such that $\Lambda_c(2595)$ mass is produced to be 2591 MeV with $a = -8.27$. All energies are in units of MeV and $(S, I)^M$ denotes (strangeness, isospin)^{SU(3) multiplet}.

Pole position	$(S, I)^M$	Main channels (threshold)	Exp. [5]
(2721, 0)	$(0, 0)^{[3]}$	$\Xi_c K(2965.1)$	$\Lambda_c(2765)?$
(2623, $-i12$)	$(-1, \frac{1}{2})^{[3]}$	$\Lambda_c \bar{K}(2782.1)$	
(2965, 0)	$(-2, 0)^{[3]}$	$\Xi_c \bar{K}(2965.1)$	
(2948, 0)	$(1, \frac{1}{2})^{[6]}$	$\Sigma_c K(2949.1)$	
(2674, $-i51$)	$(0, 1)^{[6]}$	$\Sigma_c \pi(2591.5)$	
(2999, $-i16$)	$(0, 1)^{[6]}$	$\Sigma_c \eta(3001.4), \Xi'_c K(3072.4)$	
(2591, 0)	$(0, 0)^{[6]}$	$\Sigma_c \pi(2591.5)$	$\Lambda_c(2595)$
(3069, $-i12$)	$(0, 0)^{[6]}$	$\Xi'_c K(3072.4)$	$\Lambda_c(2940)?$
<u>(2947, $-i34$)</u>	$(-1, \frac{3}{2})^{[6]}$	$\Sigma_c \bar{K}(2949.1)$	
(2695, 0)	$(-1, \frac{1}{2})^{[6]}$	$\Sigma_c \bar{K}(2949.1)$	
(2827, $-i55$)	$(-1, \frac{1}{2})^{[6]}$	$\Xi'_c \pi(2714.7)$	$\Xi_c(2790)?$
<u>(3123, $-i44$)</u>	$(-1, \frac{1}{2})^{[6]}$	$\Omega_c K(3190.8)$	$\Xi_c(3123)?$
(2946, 0)	$(-2, 0)^{[6]}$	$\Xi'_c \bar{K}(3072.4), \Omega_c \eta(3243.1)$	

Table 3.3: Same as Table 3.2, but obtained in the cutoff regularization scheme with $\Lambda = 1.35$ GeV.

Pole positions	$(S, I)^M$	Main channels (threshold)	Exp. [5]
(2707, 0)	$(0, 0)^{[3]}$	$\Xi_c K(2965.1)$	$\Lambda_c(2765)?$
(2622, $-i12$)	$(-1, \frac{1}{2})^{[3]}$	$\Lambda_c \bar{K}(2782.1)$	
<u>(2965, 0)</u>	$(-2, 0)^{[3]}$	$\Xi_c \bar{K}(2965.1)$	
<u>(2949, 0)</u>	$(1, \frac{1}{2})^{[6]}$	$\Sigma_c K(2949.1)$	
(2672, $-i53$)	$(0, 1)^{[6]}$	$\Sigma_c \pi(2591.5)$	
<u>(2996, $-i21$)</u>	$(0, 1)^{[6]}$	$\Sigma_c \eta(3001.4)$	
(2591, 0)	$(0, 0)^{[6]}$	$\Sigma_c \pi(2591.5)$	$\Lambda_c(2595)$
(3072, $-i15$)	$(0, 0)^{[6]}$	$\Xi'_c K(3072.4)$	$\Lambda_c(2940)?$
<u>(2946, $-i35$)</u>	$(-1, \frac{3}{2})^{[6]}$	$\Sigma_c \bar{K}(2949.1)$	
(2683, 0)	$(-1, \frac{1}{2})^{[6]}$	$\Sigma_c \bar{K}(2949.1)$	
(2813, $-i44$)	$(-1, \frac{1}{2})^{[6]}$	$\Xi'_c \pi(2714.7)$	$\Xi_c(2790)?$
(3121, $-i61$)	$(-1, \frac{1}{2})^{[6]}$	$\Omega_c K(3190.8)$	$\Xi_c(3123)?$
(2909, 0)	$(-2, 0)^{[6]}$	$\Xi'_c K(3072.4)$	

much closer to the threshold of its main coupled channel than $\Lambda_b(5912)$, the calibration implies a weaker potential in the charm sector than in the bottom sector. Due to this weakening, the dynamical generation of some charmed baryons requires a slight readjustment of the potential by changing either f_0 and a slightly within a few percent. Otherwise, they will show up as cusps. The pole positions of these states have been underlined to denote such a

Table 3.4: Dynamically generated charmed baryons of $J^P = 3/2^-$. The subtraction constant is fixed in a way such that $\Lambda_c^*(2625)$ mass is produced to be 2625 MeV with $a = -12.0$. All energies are in units of MeV and $(S, I)^M$ denotes (strangeness, isospin)^{SU(3) multiplet}.

Pole position	$(S, I)^M$	Main channels (threshold)	Exp. [5]
(2952, 0)	$(1, \frac{1}{2})^{[6]}$	$\Sigma_c^* K(3013.5)$	
(2685, $-i15$)	$(0, 1)^{[6]}$	$\Sigma_c^* \pi(2655.9)$	
(2977, $-i23$)	$(0, 1)^{[6]}$	$\Sigma_c^* \eta(3065.8)$	
(2625, 0)	$(0, 0)^{[6]}$	$\Sigma_c^* \pi(2655.9)$	$\Lambda_c^*(2625)$
(3066, $-i19$)	$(0, 0)^{[6]}$	$\Xi_c^* K(3141.5)$	
(2968, $-i33$)	$(-1, \frac{3}{2})^{[6]}$	$\Sigma_c^* \bar{K}(3013.5)$	
(2656, 0)	$(-1, \frac{1}{2})^{[6]}$	$\Sigma_c^* \bar{K}(3013.5)$	
(2827, $-i17$)	$(-1, \frac{1}{2})^{[6]}$	$\Xi_c^* \pi(2783.9)$	$\Xi_c^*(2815)?$
(3113, $-i45$)	$(-1, \frac{1}{2})^{[6]}$	$\Omega_c^* K(3261.5)$	
(3118, $-i80$)	$(-2, 1)^{[6]}$	$\Omega_c^* \pi(2903.9)$	
(2885, 0)	$(-2, 0)^{[6]}$	$\Xi_c^* \bar{K}(3141.5)$	

Table 3.5: Same as Table 3.2, but obtained in the cutoff regularization scheme with $\Lambda = 2.13$ GeV.

Pole position	$(S, I)^M$	Main channels (threshold)	Exp. [5]
(2962, 0)	$(1, \frac{1}{2})^{[6]}$	$\Sigma_c^* K(3013.5)$	
(2684, $-i15$)	$(0, 1)^{[6]}$	$\Sigma_c^* \pi(2655.9)$	
(2980, $-i28$)	$(0, 1)^{[6]}$	$\Sigma_c^* \eta(3065.8)$	
(2625, 0)	$(0, 0)^{[6]}$	$\Sigma_c^* \pi(2655.9)$	$\Lambda_c^*(2625)$
(3059, $-i22$)	$(0, 0)^{[6]}$	$\Xi_c^* K(3141.5)$	
(2974, $-i33$)	$(-1, \frac{3}{2})^{[6]}$	$\Sigma_c^* \bar{K}(3013.5)$	
(2653, 0)	$(-1, \frac{1}{2})^{[6]}$	$\Sigma_c^* \bar{K}(3013.5)$	
(2816, $-i13$)	$(-1, \frac{1}{2})^{[6]}$	$\Xi_c^* \pi(2783.9)$	$\Xi_c^*(2815)?$
(3093, $-i51$)	$(-1, \frac{1}{2})^{[6]}$	$\Omega_c^* K(3261.5)$	
(3103, $-i74$)	$(-2, 1)^{[6]}$	$\Omega_c^* \pi(2903.9)$	
(2858, 0)	$(-2, 0)^{[6]}$	$\Xi_c^* \bar{K}(3141.5)$	

fine-tuning.

One should note that we have used an averaged pseudoscalar decay constant, $f_0 = 1.17f_\pi$, in our calculations. Using the pion decay constant, $f_0 = f_\pi$, will not change qualitatively our results and conclusions, but can shift the predicted baryon masses by a few tens of MeV depending on the particular channel. In addition, the differences between the results obtained in the dimensional regularization scheme and those obtained in the cutoff regularization scheme also indicate inherent theoretical uncertainties of the UChPT method, which can be as large as 30 to 40 MeV depending on the channels. It should be mentioned that though formally, the dimensional regularization scheme might be preferred to the cutoff regularization scheme, they yield quite similar results in our present work,

both in terms of heavy-quark symmetry conservation and in terms of prediction of dynamically generated states once the relevant parameters are fixed in such a way that $\Lambda_c(2595)$ and $\Lambda_b(5912)$ are produced.

As mentioned previously, compared to the studies of Refs. [2, 4, 114, 115], we have only considered the minimum number of coupled channels dictated by chiral symmetry and its breaking. Such an approach is only appropriate if close to the dynamically generated states, no other coupled channels with the same quantum numbers exist. Otherwise, one may need to take into account those channels involving either vector mesons (light or heavy) and non-charmed baryons. As can be seen from Fig. 3.2, it is clear that for the dynamical generation of $\Lambda_c(2595)$, our minimum coupled channel space indeed includes the most relevant channels, i.e., the $\Sigma_c\pi$, while the next closest coupled channels excluded in our space, the ND , are roughly 200 MeV above, respectively. On the other hand, the $\Lambda_c(2940)$ state is close not only to the $\Xi'_c K$ channel taken into account in our framework but also to $\Lambda_c\omega$ and ΛD_s . As a result, our model space may be too restricted and the result should be taken with care. This might be the reason why our prediction is about 100 MeV off the experimental mass of this resonance.

3.3.3 Scattering Lengths

Scattering lengths provide vital information on the strong interaction. Although direct experimental measurements of the scattering lengths between a charmed baryon with a pseudoscalar meson cannot be foreseen in the near future, rapid developments in lattice QCD may soon fill the gap. In Tables 3.6, and 3.7, we tabulate the scattering lengths calculated in the dimensional regularization scheme, defined as

$$a_{jj} = -\frac{M_j}{4\pi(M_j + m_j)} T_{jj}^{(S,I)}, \quad (3.14)$$

for channel j with strangeness S and isospin I , where M_j and m_j are the respective baryon and meson masses of that channel. For the sake of comparison, we list the ChPT results of Ref. [116]. One should note that Ref. [116] calculated the scattering lengths up to $\mathcal{O}(p^3)$, while in our study only the leading order ($\mathcal{O}(p)$) ChPT kernel is used and in addition we work with the UChPT.

Examining the scattering lengths in the charmed sector, we notice that because of the existence of a bound state just below their respective thresholds, the scattering lengths for the $\Sigma_c K$ channel with $(S, I)^M = (1, 1/2)^{[6]}$ and for the $\Sigma_c\pi$ channel with $(S, I)^M = (0, 0)^{[6]}$ are quite large and negative, i.e., $a_{\Sigma_c K} = -8.114\text{fm}$ and $a_{\Sigma_c\pi} = -28.204\text{fm}$. Therefore, future lattice QCD study of these two channels may be able to test to what extent that the scenario of these states being dynamically generated is true.

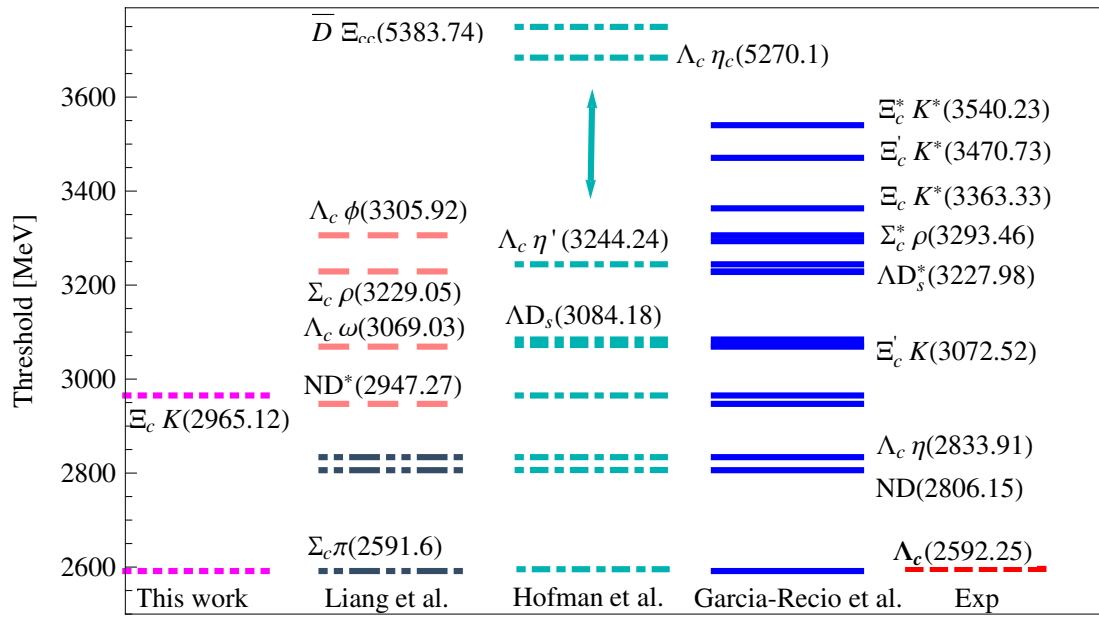


Figure 3.2: Thresholds of the coupled channels considered in different works for the singly charmed sector with $J^P = 1/2^-$ and $(S = 0, I = 0)$: Liang et al. [2], Hofmann et al. [3], Garcia-Recio et al. [4], and Exp [5]. Two model spaces denoted by dot-dot-dashed lines (PB) and dashed lines (VB), respectively, were studied in Ref. [2].

Table 3.6: ϕB scattering lengths a (in units of fm) in the charmed sector with $J^P = 1/2^-$.

$(S, I)^M$	Channel	Present work	a Ref. [116]	$(S, I)^M$	Channel	Present work	a Ref. [116]
$(1, \frac{1}{2})^{\bar{3}}$	$\Lambda_c K$	-0.135	-0.032 ± 0.038	$(1, \frac{3}{2})^{[6]}$	$\Sigma_c K$	-0.181	-0.44 ∓ 0.23
$(0, 1)^{\bar{3}}$	$\Xi_c K$	$-0.281 - i0.308$	$0.77 + i0.18$	$(1, \frac{1}{2})^{[6]}$	$\Sigma_c K$	-8.114	0.62 ± 0.12
$(0, 1)^{\bar{3}}$	$\Lambda_c \pi$	0.002	0.006	$(0, 2)^{[6]}$	$\Sigma_c \pi$	-0.119	-0.25 ∓ 0.031
$(0, 0)^{\bar{3}}$	$\Xi_c K$	$-0.338 - i0.020$	0.99 ± 0.076	$(0, 1)^{[6]}$	$\Xi'_c K$	$-0.365 - i0.097$	$(0.18 + i0.37) \mp 0.12$
$(0, 0)^{\bar{3}}$	$\Lambda_c \eta$	-0.281	$(0.35 + i0.19) \pm 0.044$	$(0, 1)^{[6]}$	$\Sigma_c \eta$	$-0.787 - i0.942$	$(0.18 + i0.2) \mp 0.034$
$(-1, \frac{3}{2})^{\bar{3}}$	$\Xi_c \pi$	-0.072	-0.11 ± 0.0052	$(0, 1)^{[6]}$	$\Sigma_c \pi$	0.376	0.28
$(-1, \frac{1}{2})^{\bar{3}}$	$\Xi_c \pi$	1.600	0.32 ± 0.0052	$(0, 0)^{[6]}$	$\Xi'_c K$	$-1.361 - i1.174$	$(1.4 + i0.56) \mp 0.12$
$(-1, \frac{1}{2})^{\bar{3}}$	$\Xi_c \eta$	$-0.266 - i0.197$	$(0.54 + i0.098) \pm 0.011$	$(0, 0)^{[6]}$	$\Sigma_c \pi$	-28.204	0.65 ∓ 0.078
$(-1, \frac{1}{2})^{\bar{3}}$	$\Lambda_c \bar{K}$	$-0.237 - i0.148$	$(0.79 + i0.27) \pm 0.038$	$(-1, \frac{3}{2})^{[6]}$	$\Xi'_c \pi$	-0.025	-0.19 ∓ 0.016
$(-2, 1)^{\bar{3}}$	$\Xi_c \bar{K}$	-0.141	-0.028 ± 0.038	$(-1, \frac{3}{2})^{[6]}$	$\Sigma_c \bar{K}$	$0.141 - i0.770$	$0.12 + i0.37$
$(-2, 0)^{\bar{3}}$	$\Xi_c \bar{K}$	12.014	1.7 ∓ 0.038	$(-1, \frac{1}{2})^{[6]}$	$\Xi'_c \pi$	-0.022	0.23 ∓ 0.016
$(-1, \frac{1}{2})^{[6]}$	$\Xi'_c \eta$	$-0.196 - i0.269$	$(0.55 + i0.49) \mp 0.24$	$(-2, 1)^{[6]}$	$\Omega_c \pi$	0.046	-0.062
$(-1, \frac{1}{2})^{[6]}$	$\Omega_c K$	$-0.508 - i0.160$	$(1.4 + i0.56) \mp 0.23$	$(-2, 0)^{[6]}$	$\Xi'_c \bar{K}$	-0.413	0.61 ∓ 0.12
$(-1, \frac{1}{2})^{[6]}$	$\Sigma_c \bar{K}$	$-0.345 - i0.013$	$(2.0 + i0.092) \mp 0.35$	$(-2, 0)^{[6]}$	$\Omega_c \eta$	$-0.277 - i0.015$	$(0.68 + i0.4) \mp 0.14$
$(-2, 1)^{[6]}$	$\Xi'_c \bar{K}$	$-0.088 - i0.168$	$(-0.11 + i0.37) \mp 0.12$	$(-3, \frac{1}{2})^{[6]}$	$\Omega_c \bar{K}$	-0.197	-0.33 ∓ 0.23

Table 3.7: ϕB scattering lengths a (in units of fm) in the charmed sector with $J^P = 3/2^-$.

$(S, I)^M$	Channel	Present work	a Ref. [116]	$(S, I)^M$	Channel	Present work	a Ref. [116]
$(1, \frac{3}{2})^{[6^*]}$	$\Sigma_c^* K(3013.5)$	-0.147	-0.45 ∓ 0.23	$(-1, \frac{1}{2})^{[6^*]}$	$\Xi_c^* \pi(2783.9)$	0.459	$(0.23 - 0.027i) \mp 0.016$
$(1, \frac{1}{2})^{[6^*]}$	$\Sigma_c^* K(3013.5)$	-0.683	0.63 ∓ 0.12	$(-1, \frac{1}{2})^{[6^*]}$	$\Xi_c^* \eta(3193.8)$	$-0.263 - 0.060i$	$(0.57 + 0.5i) \mp 0.24$
$(0, 2)^{[6^*]}$	$\Sigma_c^* \pi(2655.9)$	-0.104	-0.25 ∓ 0.031	$(-1, \frac{1}{2})^{[6^*]}$	$\Omega_c^* K(3261.5)$	$-0.324 - 0.036i$	$(1.4 + 0.56i) \mp 0.23$
$(0, 1)^{[6^*]}$	$\Xi_c^* K(3141.5)$	$-0.246 - 0.020i$	$(0.13 + 0.37i) \mp 0.12$	$(-1, \frac{1}{2})^{[6^*]}$	$\Sigma_c^* \bar{K}(3013.5)$	$-0.222 - 0.009i$	$(2.0 + 0.092i) \mp 0.35$
$(0, 1)^{[6^*]}$	$\Sigma_c^* \eta(3065.8)$	$-0.398 - 0.059i$	$(0.16 + 0.2i) \mp 0.034$	$(-2, 1)^{[6^*]}$	$\Xi_c^* \bar{K}(3141.5)$	$-0.199 - 0.211i$	$(-0.12 + 0.37i) \mp 0.12$
$(0, 1)^{[6^*]}$	$\Sigma_c^* \pi(2655.9)$	0.820	$0.27 - 0.021i$	$(-2, 1)^{[6^*]}$	$\Omega_c^* \pi(2903.9)$	0.085	-0.062
$(0, 0)^{[6^*]}$	$\Xi_c^* K(3141.5)$	$-0.572 - 0.072i$	$(1.5 + 0.56i) \mp 0.12$	$(-2, 0)^{[6^*]}$	$\Xi_c^* \bar{K}(3141.5)$	-0.243	$(0.52 - 0.0032i) \mp 0.12$
$(0, 0)^{[6^*]}$	$\Sigma_c^* \pi(2655.9)$	-0.761	$(0.67 + 0.032i) \mp 0.078$	$(-2, 0)^{[6^*]}$	$\Omega_c^* \eta(3313.8)$	$-0.201 - 0.005i$	$(0.64 + 0.4i) \mp 0.14$
$(-1, \frac{3}{2})^{[6^*]}$	$\Xi_c^* \pi(2783.9)$	0.022	$(-0.19 - 0.0027i) \mp 0.016$	$(-3, \frac{1}{2})^{[6^*]}$	$\Omega_c^* \bar{K}(3261.5)$	-0.157	-0.34 ∓ 0.23
$(-1, \frac{3}{2})^{[6^*]}$	$\Sigma_c^* \bar{K}(3013.5)$	$-0.539 - 0.242i$	$0.13 + 0.37i$				

3.3.4 An exploratory NLO study

In this section, we study the effects of the NLO potentials. In principle, higher order effects in the UChPT can be taken into account systematically if relevant LECs can be fixed reliably. However, in the present case, the experimental data available is not enough. Therefore, we have to turn to some phenomenological means to fix some of the LECs and vary others within their natural range to study the effects of the NLO potentials. As an exploratory study, we limit ourselves to the $1/2^-$ sector.

To reduce the number of unknown LECs, we use the following NLO Lagrangian in the heavy-meson formulation [116]:

$$\mathcal{L}_{H\Phi}^{(2)} = \bar{c}_0 Tr[\bar{H}_3 H_3] Tr[\chi_+] + \bar{c}_1 Tr[\bar{H}_3 \tilde{\chi}_+ H_3] + (\bar{c}_2 - \frac{2g_6^2 + g_2^2}{4M_0}) Tr[\bar{H}_3 v \cdot uv \cdot u H_3] \quad (3.15)$$

$$+ (\bar{c}_3 - \frac{2g_6^2 - g_2^2}{4M_0}) \bar{H}_3^{ab} v \cdot u_a^c v \cdot u_b^d H_{3,cd} + c_0 Tr[\bar{H}_6 H_6] Tr[\chi_+] + c_1 Tr[\bar{H}_6 \tilde{\chi}_+ H_6] \quad (3.16)$$

$$+ (c_2 - \frac{2g_2^2 + g_1^2}{4M_0}) Tr[\bar{H}_6 v \cdot uv \cdot u H_6] + (c_3 + \frac{2g_2^2 - g_1^2}{4M_0}) \bar{H}_6^{ab} v \cdot u_a^c v \cdot u_b^d H_{6,cd} \quad (3.17)$$

$$+ c_4 Tr[\bar{H}_6 H_6] Tr[v \cdot uv \cdot u], \quad (3.18)$$

where χ_+ and $\tilde{\chi}_+$ are defined as ,

$$\chi_{\pm} = \xi^+ \chi \xi^+ \pm \xi \chi \xi \quad (3.19)$$

$$\chi = \text{diag}(m_\pi^2, m_\pi^2, 2m_K^2 - m_\pi^2) \quad (3.20)$$

$$\tilde{\chi}_{\pm} = \chi_{\pm} - \frac{1}{3} Tr[\chi_{\pm}], \quad (3.21)$$

with $\xi = \exp(i\frac{\phi}{2f_\phi})$.

The LECs g_2 and g_4 can be fixed by reproducing the Σ_c and Σ_c^* widths, while the other g_i 's can be related to them using either quark model symmetries or heavy quark spin symmetry. The LECs \bar{c}_i and c_i are fixed using the (broken) SU(4) symmetry in Ref. [116]⁴. The LEC α' can not be determined and we will estimate its contribution below assuming a natural value within the range of $-1 \sim 1$ as in Ref. [116]. In the present work, we follow Ref. [116], and use the values determined there and reproduced in Tables 3.8, 3.9, and 3.10⁵.

In the NLO study, we fix the subtraction constant in the same way as in the LO case and search for poles on the complex plane. The results are tabulated in Table 3.11.

Compared to the LO case, we find some substantial changes when the NLO potentials are taken into account. For instance, in the charmed sector, one dynamically generated state in the anti-triplet sector disappears while a new one appears with $\alpha' = -1.0$. This implies that the NLO chiral potential has a huge impact on the predicted states in the anti-triplet sector.

⁴The matching relations between the SU(4) Lagrangian and the SU(3) one lead to 8 equations between LECs, while here we have 9 LECs to be determined. Therefore the α' is introduced.

⁵The values are slightly different from those of Ref. [116] because there relations among the LECs are stated incorrectly there.

Table 3.8: Constants in Eq. (3.15) for the anti-triplet.

$ g_1 $	$ g_2 $	$ g_3 $	$ g_4 $	$ g_5 $	$ g_6 $
0.98	0.60	0.85	1.0	1.5	0

Table 3.9: Constants in Eq. (3.15) for the anti-triplet (in units of GeV^{-1}).

\bar{c}_0	\bar{c}_1	\bar{c}_2	\bar{c}_3
-0.32	-0.52	$-1.78 + \frac{1}{3} \frac{\alpha'}{4\pi f}$	$-0.03 - \frac{1}{3} \frac{\alpha'}{4\pi f}$

Table 3.10: Constants in Eq. (3.15) for the sextet (in units of GeV^{-1}).

c_0	c_1	c_2	c_3	c_4
-0.61	-0.98	$-2.07 - 2 \frac{\alpha'}{4\pi f}$	-0.84	$\frac{\alpha'}{4\pi f}$

In the sextet sector, on the other hand, the changes are more moderate. Most states move a few tens of MeV compared to their LO counterparts with a few exceptions. However, the unknown LEC α' seems to affect a lot the predictions. In particular, when $\alpha' = -1$, many states disappear. Clearly, from the comparison with the LO results, we may conclude that $\alpha' = -1$ is not preferred.

One of the possible reasons why the results in the anti-triplet sector change more dramatically than those in the sextet sector is the following. In the sextet sector, we have refitted the subtraction constant to produce the state at (2591, 0) MeV, while no such readjustments have been made for the anti-triplet sectors. Nevertheless, one should note that even at NLO, $\Lambda_c(2595)$ appears naturally as a dynamically generated state without the need for an unnatural subtraction constant.

In fact, due to the lack of enough experimental information to have a good control on the NLO LECs, none of the above observations are surprising. In Ref. [116], Liu and Zhu already found that in many cases the NLO potentials are larger than the LO ones (see Tables I, II, III of their paper). Our studies confirmed their findings and showed that some of the LO predictions are subject to substantial modifications while some others may remain relatively stable. More experimental or lattice QCD inputs are clearly needed to check the results and clarify the situation. On one hand, one needs to be cautious about those results where higher order potentials are shown to be particularly relevant. On the other hand, one should note that the NLO contributions depend critically on the way the relevant LECs are estimated. If we had put them equal to zero, the contributions would vanish. Clearly, the LECs should be determined in a more reliable way in order to study the effects of higher order potentials.

Table 3.1.1: Dynamically generated charmed baryons of $J^P = 1/2^-$ in the NLO UChPT in comparison with those in the LO. At NLO, three values for the LEC α' have been taken. The subtraction constant is fixed in the same way as in the LO case. All energies are in units of MeV and $(S, I)^M$ denotes (strangeness, isospin)^{SU(3) multiplet}.

LO	NLO		$\alpha' = -1.0$	$(S, I)^M$	Main channels (threshold)	Exp. [5]
	$\alpha' = 0$	$\alpha' = 1.0$				
-	-	-	(2936, $-i15$)	(0, 1) ^[3]	$\Xi_c K(2965.1)$	
(2721, 0)	(2807, 0)	(2794, 0)	(2820, 0)	(0, 0) ^[3]	$\Xi_c K(2965.1)$	
(2623, $-i12$)	-	-	-	$(-1, \frac{1}{2})$ ^[3]	$\Lambda_c \bar{K}(2782.1), \Xi_c \pi(2607.5)$	
(2965, 0)	(2736, 0)	(2741, 0)	(2732, 0)	$(-2, 0)$ ^[3]	$\Xi_c \bar{K}(2965.1)$	
(2948, 0)	(2918, 0)	(2848, 0)	-	$(1, \frac{1}{2})$ ^[6]	$\Sigma_c K(2949.1)$	
(2674, $-i51$)	(2699, $-i107$)	(2702, $-i102$)	(2699, $-i105$)	(0, 1) ^[6]	$\Sigma_c \pi(2591.5)$	
(2999, $-i16$)	(2985, $-i0.01$)	(2984, $-i33$)	-	(0, 1) ^[6]	$\Sigma_c \eta(3001.4), \Xi_c' \bar{K}(3072.4)$	
(2591, 0)	(2591, 0)	(2591, 0)	(2591, 0)	(0, 0) ^[6]	$\Sigma_c \pi(2591.5)$	$\Lambda_c(2595)$
(3069, $-i12$)	(3025, $-i19$)	(2954, $-i11$)	-	(0, 0) ^[6]	$\Xi_c' K(3072.4)$	$\Lambda_c(2940)?$
(2947, $-i34$)	(2925, $-i13$)	(2857, $-i11$)	-	$(-1, \frac{3}{2})$ ^[6]	$\Sigma_c \bar{K}(2949.1)$	
(2695, 0)	(2567, 0)	(2568, 0)	(2565, 0)	$(-1, \frac{1}{2})$ ^[6]	$\Sigma_c \bar{K}(2949.1)$	
(2827, $-i55$)	(2824, $-i74$)	(2813, $-i70$)	(2836, $-i75$)	$(-1, \frac{1}{2})$ ^[6]	$\Xi_c' \pi(2714.7)$	$\Xi_c(2790)?$
(3123, $-i44$)	(3084, $-i26$)	(3038, $-i8$)	-	$(-1, \frac{1}{2})$ ^[6]	$\Omega_c K(3190.8)$	
-	-	(3005, $-i38$)	-	$(-2, 1)$ ^[6]	$\Xi_c' \bar{K}(3072.4)$	
(2946, 0)	(2815, 0)	(2821, 0)	(2809, 0)	$(-2, 0)$ ^[6]	$\Xi_c' \bar{K}(3072.4), \Omega_c \eta(3243.1)$	

3.4 The compositeness condition of $\Lambda_c(2595)$

3.4.1 Introduction

In principle, wave-functions are not observables themselves. As a result, it is difficult to pin down the exact nature of a hadronic state. The claims regarding the largest Fock component in its wave function are often model dependent. In recent years, the compositeness condition, first proposed by Weinberg to explain the deuteron as a neutron-proton bound state [149, 150], has been advocated as a model independent way to determine the relevance of hadron-hadron components in a molecular state. With renewed interests in hadron spectroscopy, this method has been extended to more deeply bound states, resonances, and higher partial waves [151, 152, 153, 154, 155, 156, 157, 158, 159, 160]. The theoretical aspects have been further discussed in [158, 161, 160]. However, for the particular case of $\Lambda_c(2595)$, the message has been a bit unclear. For instance, it was shown in Ref. [162] that $\Lambda_c(2595)$ is not predominantly a $\pi\Sigma_c$ molecular state using the effective range expansion. A similar conclusion was reached in Ref. [163], using the generalized effective range expansion taking into account CDD pole contributions. In this latter work, the effects of isospin breaking corrections were taken into account and the extended compositeness condition developed in Ref. [164] was used. Furthermore, although in the unitary approaches [2, 3, 4, 11, 113] $\Lambda_c(2595)$ is found to be of molecular nature, the dominant meson-baryon component differs.

In this section, we utilize the compositeness condition to examine the molecule interpretations for $\Lambda_c(2595)$. Following Ref. [158], the weight of a hadron-hadron component in a composite particle is defined as

$$X_i = -\text{Re} \left[g_i^2 \left[\frac{\partial G_i^{II}(s)}{\partial \sqrt{s}} \right]_{\sqrt{s}=\sqrt{s_0}} \right] \quad (3.22)$$

where $\sqrt{s_0}$ is the pole position, G_i^{II} is the loop function evaluated on the second Riemann sheet, and g_i is the coupling of the respective resonance or bound state to channel i calculated as

$$g_i^2 = \lim_{\sqrt{s} \rightarrow \sqrt{s_0}} (\sqrt{s} - \sqrt{s_0}) T_{ii}^{II}, \quad (3.23)$$

where T_{ii}^{II} is the ii element of the T amplitude on the second Riemann sheet.

The deviation of the sum of X_i from unity is related to the energy dependence of the s -wave potential,

$$\sum_i X_i = 1 - Z, \quad (3.24)$$

where

$$Z = - \sum_{ij} \left[g_i G_i^{II}(\sqrt{s}) \frac{\partial V_{ij}(\sqrt{s})}{\partial \sqrt{s}} G_j^{II}(\sqrt{s}) g_j \right]_{\sqrt{s}=\sqrt{s_0}}. \quad (3.25)$$

The quantity Z , which is also called field renormalization constant, is often attributed to the weight of the missing

channels. For a bound state on the first Riemann sheet, the compositeness $\sum_i X_i$ and Z are real numbers and related to the probability of finding state to channel i . But for a resonance on the second Riemann sheet, they become complex numbers and, therefore, a strict probabilistic interpretation is lost. However, the compositeness X_i and field renormalization constant Z_i themselves are well defined even for resonant states. In this case, X_i is still related to the squared wave function of the i th channel in a phase prescription that automatically renders the wave function to be real for bound states [158]. Thus it still can measure the weights of the molecular component for a resonant state. As for Z , it is always related to the residue of two-point scalar integral [165]. As a consequence the only problem seems to be that the complex value makes the probabilistic interpretation not straightforward, but nevertheless, X_i and Z contain important information on the structure of resonances.

In the picture advocated in Ref. [158] imaginary parts of X_i and Z are neglected. The quantity $1 - Z$ is taken to represent the compositeness of the hadronic state in terms of all the considered channels, and Z is referred to as its elementariness. Within this picture, a non-vanishing Z means that the model is an effective one. The energy dependent interaction effectively accounts for other possible interaction mechanisms not explicitly included in the s-wave hadron-hadron description. These could be other hadron-hadron interactions, or even genuine hadron components not of the molecular type (hence the appellative elementariness). Thus, a small value of Z indicates that the state is well described by the contributions explicitly considered, namely, s-wave hadron-hadron channels. However, it is not clear how to interpret Z obtained from the smooth energy dependence of the chiral potential V [159]. In addition, it should be emphasized that, for processes involving short distances, it is the wave function at the origin that matters ($g_i G_i$ for the s wave) [166]. For an extensive discussion on this issue, see Ref. [159], which concluded that to judge the relevance of each channel one has to study different physical processes.

On the other hand, in Ref. [164], it was claimed that one can formulate a meaningful compositeness relation with only positive coefficients thanks to a suitable unitary transformation of the S matrix. This in practice amounts to take the absolute value of X_i in Eq. 3.22 to quantify the probability of finding a specific component in the wave function of a hadron. Notice that the recipe advocated in Ref. [164] is not applicable to all types of poles. In particular the arguments of this reference exclude the case of virtual states or resonant signals which are an admixture between a pole and an enhanced cusp effect by the pole itself. More specifically, the probabilistic interpretation given in [164] to X_i is only valid when $\text{Re}s_0 > s_{i;th}$, with $s_{i;th}$ the corresponding threshold of channel i . This compositeness condition has been used in Ref. [167] to claim that $P_c(4450)$ might be a χ_{c1p} bound state.

We calculate the compositeness for $\Lambda_c(2595)$ within three different models in which the potentials are obtained using either chiral Lagrangian [11], the extended hidden gauge Lagrangian [2], or the $SU(6) \times HQSS$ model [168] respectively. In all the three models, the scattering amplitudes are calculated based on unitary chiral perturbation theory, which is introduced in the preceding section but differs in the number of coupled channels and how chiral symmetry and heavy quark symmetry are taken into account.

On the other hand, we follow the strategy in the previous section to apply different regularization schemes to

remove the divergence in the two-point scalar integral in the Bethe-Salpeter equation, including the heavy quark symmetry inspired one in Eq. 3.9 and the cutoff scheme in Eq. 2.93. As mentioned before, any change of the values of variables in the correction part of G_{HQ_S} is essentially equivalent to a re-adjustment of the subtraction constant in the \overline{MS} scheme for different coupled channels. Therefore we will avoid extra discussions on this point. One can also alternatively follow the regularization scheme in Ref. [168] where a natural subtraction constant is determined by requiring the unitary amplitudes reduce to only contain tree level at certain energy scale μ_0 , such as $G(\mu_0) = 0$. This scheme is later denoted as ‘‘DR-Naturalness’’.

In the following, we would like to examine how the number of coupled channels and the particular regularization scheme affect the predicted (calculated) compositeness of the $\Lambda_c(2595)$. For such a purpose, we first fix the number of coupled channels and then compare the calculated compositeness. This work was published in Ref. [169].

According to the PDG, $\Lambda_c(2595)$ has a mass of 2592.25 ± 0.28 MeV and a width of 2.6 ± 0.6 MeV [5]. Therefore, the only parameter in each of the three different approaches are fixed in such a way that the mass of $\Lambda_c(2595)$ is produced. We do not attempt to fix the width because here we only consider two-body coupled channels and work at the isospin symmetric limit, both of which can have a large effect on the width than on the mass (see an elaborate discussion in Ref. [163]).

3.4.2 16 channels

The $SU(6) \times HQSS$ model used in Ref. [4] is basically a $SU(8)$ spin-flavor extension of the $SU(3)$ chiral WT leading order meson-baryon interaction term, including ground state vector meson and $J^P = 3/2^+$ baryon as degrees of freedom. This is actually strictly correct only when coupled channels involving $cc\bar{c}$ components are neglected. These channels are OZI disconnected from those involving just one heavy quark. Note that in the heavy-quark limit, the OZI rule becomes exact because the number of charm quarks and the number of charm antiquarks are separately conserved. (For a more detailed discussion see Ref. [170]).

It is to be noted that in the 16 channels framework of the $SU(3) \times HQSS$ model, there exist two $\Lambda_c(2595)$ states, resemblance of the two $\Lambda(1405)$ states, with one of them narrower than the other [4, 168]. To make a fair comparison, we adjust the only parameter in each of the regularization schemes we study to fix the real part of the pole position. This yields the following parameters, $\alpha' = 0.97952$ for the naturalness scheme [4], $q_{\max} = 0.67898$ GeV for the cutoff scheme [2], and $a = -3.37865$ for the heavy-quark symmetry (HQS) scheme [11], which is in the present case equivalent to the modified minimal subtraction scheme.

From Table. 3.12 and Table. 3.13, one can see that among the 16 coupled channels, the most relevant three channels are $\pi\Sigma_c$, DN and D^*N . For the sibling state of $\Lambda_c(2595)$, it seems that the $\pi\Sigma_c$ channel plays the dominant role, except in the cutoff scheme of Ref. [2], where it appears as a bound state and DN and D^*N channels are more important. Whileas for the state that we assign to $\Lambda_c(2595)$, different regularization schemes yield slightly different results. The D^*N channel plays a leading role in the naturalness scheme of Ref. [4]. In

the cutoff scheme of Ref. [2], $\pi\Sigma_c$ is the dominant channel, with D^*N the next important channel. In the HQS scheme, all three channels seem to be equally important, with a large imaginary part for $X_{\pi\Sigma_c}$. On the other hand, interpreting the compositeness using the prescription of Ref. [164], we find that the weights of $\pi\Sigma_c$ inside $\Lambda_c(2595)$ are 0.11, 0.71 and 0.97 for the DR-naturalness, cutoff and DR-HQS schemes, respectively.

Clearly one can conclude that the regularization scheme plays a relevant role in the so-determined compositeness even with the same number of coupled channels and the same kernel potentials. In other words, the so-called compositeness used in the present way cannot be taken as a model-independent quantity. Similar conclusions have been reached in Ref. [161]. It needs to be noted that except in the naturalness scheme, the width of $\Lambda_c(2595)$ turns out to be much larger than its experimental counterpart. This might be due to the isospin breaking effects neglected in the present work [163].

Table 3.12: Compositeness of each of the 16 coupled channels for the narrow state corresponding to $\Lambda_c(2595)$. The only parameter in the meson-baryon loop function is fixed by reproducing the nominal $\Lambda_c(2595)$ mass with the following parameter: $\alpha' = 0.97952$ [4], $q_{\max} = 0.67898$ [2], and $a = -3.37865$ [11].

Couple channels	DR-naturalness	cutoff	DR-HQS
Fitted position	2592.25 - $i0.16$	2592.25 - $i9.18$	2592.25 - $i3.83$
$\pi\Sigma_c$	-0.024 + $i0.107(0.110)$	0.319 + $i0.637(0.712)$	-0.137 + $i0.960(0.970)$
DN	0.292 - $i0.026(0.294)$	0.025 + $i0.018(0.031)$	0.343 - $i0.277(0.441)$
$\eta\Lambda_c$	0.009 - $i0.001(0.009)$	0.004 - $i0.001(0.004)$	0.040 - $i0.042(0.058)$
D^*N	0.451 - $i0.055(0.454)$	0.155 - $i0.044(0.161)$	0.243 - $i0.302(0.388)$
$K\Xi_c$	0.001 - $i0.000(0.001)$	0.000 - $i0.000(0.000)$	0.001 - $i0.001(0.001)$
$\omega\Lambda_c$	0.001 - $i0.000(0.001)$	-0.000 - $i0.001(0.001)$	0.014 - $i0.012(0.018)$
$K\Xi'_c$	0.000 + $i0.000(0.000)$	0.000 - $i0.001(0.001)$	0.002 - $i0.001(0.002)$
$D_s\Lambda$	0.026 - $i0.003(0.026)$	0.004 - $i0.000(0.004)$	0.018 - $i0.019(0.026)$
$D_s^*\Lambda$	0.057 - $i0.006(0.057)$	0.008 - $i0.001(0.008)$	0.051 - $i0.054(0.074)$
$\rho\Sigma_c$	0.005 - $i0.000(0.005)$	-0.000 - $i0.002(0.002)$	0.007 - $i0.004(0.008)$
$\eta'\Lambda_c$	0.018 - $i0.002(0.018)$	0.003 - $i0.000(0.003)$	0.018 - $i0.019(0.026)$
$\rho\Sigma_c^*$	0.006 - $i0.001(0.006)$	0.003 - $i0.002(0.004)$	0.006 - $i0.008(0.010)$
$\phi\Lambda_c$	-0.000 - $i0.000(0.000)$	-0.000 - $i0.000(0.000)$	0.000 - $i0.000(0.000)$
$K^*\Xi_c$	0.000 + $i0.000(0.000)$	0.000 - $i0.000(0.000)$	0.001 - $i0.001(0.002)$
$K^*\Xi'_c$	0.000 - $i0.000(0.000)$	-0.000 - $i0.000(0.000)$	-0.000 - $i0.000(0.000)$
$K^*\Xi_c^*$	0.000 - $i0.000(0.000)$	0.000 - $i0.000(0.000)$	0.000 - $i0.000(0.000)$
X	0.843 + $i0.012(0.983)$	0.521 + $i0.602(0.932)$	0.607 + $i0.219(2.025)$

3.4.3 Two channels

With the two channels of $\pi\Sigma_c$ and $K\Xi'_c$, as included in the unitarized chiral approach [11], all the three regularization schemes yield consistent values for the compositeness, although all with a large imaginary part. The same

Table 3.13: Same as Table 3.12, but for the broader sibling of the $\Lambda_c(2595)$.

Couple channels	DR-naturalness	cutoff	DR-HQS
Fitted position	2606.7 - i32.4	2572.2	2627.9 - i37.4
$\pi\Sigma_c$	0.307 + i0.429(0.527)	0.041(0.041)	0.494 + i0.109(0.506)
DN	0.005 - i0.044(0.044)	0.254(0.254)	-0.115 + i0.001(0.115)
$\eta\Lambda_c$	0.000 + i0.000(0.000)	0.009(0.009)	0.014 + i0.024(0.028)
D^*N	0.048 + i0.024(0.054)	0.278(0.278)	0.322 + i0.172(0.365)
$K\Xi_c$	-0.000 + i0.000(0.000)	0.001(0.001)	-0.000 + i0.001(0.000)
$\omega\Lambda_c$	0.001 - i0.006(0.006)	0.001(0.001)	-0.005 + i0.002(0.006)
$K\Xi'_c$	0.001 - i0.005(0.005)	0.000(0.000)	-0.001 - i0.004(0.004)
$D_s\Lambda$	-0.000 + i0.001(0.001)	0.012(0.012)	0.006 + i0.011(0.013)
$D_s^*\Lambda$	0.001 + i0.002(0.003)	0.021(0.021)	0.016 + i0.029(0.033)
$\rho\Sigma_c$	0.013 - i0.027(0.030)	0.002(0.002)	0.000 - i0.012(0.012)
$\eta'\Lambda_c$	0.000 + i0.001(0.001)	0.007(0.004)	0.007 + i0.011(0.012)
$\rho\Sigma_c^*$	0.007 - i0.006(0.010)	0.002(0.002)	0.015 + i0.001(0.015)
$\phi\Lambda_c$	-0.000 - i0.000(0.000)	-0.000(0.000)	0.000 + i0.000(0.000)
$K^*\Xi_c$	0.002 - i0.004(0.004)	0.000(0.000)	0.000 - i0.002(0.002)
$K^*\Xi'_c$	0.000 - i0.002(0.002)	0.000(0.000)	0.001 - i0.001(0.002)
$K^*\Xi_c^*$	0.000 - i0.001(0.001)	0.000(0.000)	-0.000 - i0.001(0.001)
X	0.388 + i0.363(0.688)	0.616(0.616)	0.755 + i0.339(1.114)

can be said about the single channel case with $\pi\Sigma_c$, independent of what value used for the decay constant. The cutoff value needed to fit the $\Lambda_c(2495)$ position in the cutoff scheme seems to be rather natural, so can be said about the subtraction constant in the HQS scheme. On the other hand, the α' in the naturalness scheme does seem a bit small, compared to the value of 1, dictated by the naturalness arguments.

 Table 3.14: Compositeness of each of the two coupled channels for $\Lambda_c(2595)$. The only parameter in the meson-baryon loop function is fixed by reproducing the nominal $\Lambda_c(2595)$ mass with the following parameter: $\alpha' = 0.8268$ [4], $q_{\max} = 0.7969$ [2], and $a = -5.3768$ [11].

Couple channels	DR-naturalness	cutoff	DR-HQS
Fitted position	2592.25 - i12.7	2592.25 - i15.6	2592.25 - i13.5
$\pi\Sigma_c$	0.215 + i0.731(0.762)	0.196 + i0.770(0.794)	0.225 + i0.720(0.754)
$K\Xi'_c$	0.003 - i0.006(0.007)	0.001 - i0.002(0.003)	0.003 - i0.007(0.007)
X	0.218 + i0.725(0.769)	0.196 + i0.768(0.797)	0.228 + i0.713(0.761)

3.4.4 Three channels

In Ref. [2], three channels are used, namely $\pi\Sigma_c$, DN , and $\eta\Lambda_c$. Repeating what we did earlier, we see that in the naturalness method, the DN dominates, while in the HQS method, the $\pi\Sigma_c$ dominates. It is clear that the

regularization method has an impact on the dominance of the particular coupled channel. Again, we reach the same conclusion that the compositeness defined in the present work cannot be taken as a model-independent quantity.

Table 3.15: Compositeness of each of the three coupled channels for $\Lambda_c(2595)$. The only parameter in the meson-baryon loop function is fixed by reproducing the nominal $\Lambda_c(2595)$ mass with the following parameter: $\alpha' = 0.96048$ [4], $q_{\max} = 0.67535$ [2], and $a = -5.6365$ [11].

Couple channels	DR-naturalness	cutoff	DR-HQS
Fitted position	$2592.25 - i0.86$	$2592.25 - i11.4$	$2592.25 - i12.1$
$\pi\Sigma_c$	$-0.060 + i0.483(0.487)$	$0.057 + i1.002(1.004)$	$0.212 + i0.729(0.759)$
DN	$0.815 - i0.390(0.904)$	$0.136 - i0.355(0.380)$	$0.001 - i0.001(0.002)$
$\eta\Lambda_c$	$0.017 - i0.008(0.019)$	$0.002 - i0.006(0.007)$	$0.001 - i0.001(0.001)$
X	$0.772 + i0.085(1.409)$	$0.195 + i0.641(1.391)$	$0.214 + i0.727(0.761)$

3.5 N_c dependence of $\Lambda_c(2595)$

3.5.1 Introduction

In this section, we apply an alternative approach to test the dominant component of a hadronic state, that is, to study the dependence on the number of colors, N_c , of the poles associated to resonances that appear in the unitarized meson-meson [171, 172, 173, 174, 175, 176, 177] or meson-baryon [178, 179, 180] scattering amplitudes. The $1/N_c$ expansion [181, 182, 183, 184, 185, 186] is valid for the whole energy region and makes specific predictions for $q\bar{q}$ states and qqq states. A genuine $q\bar{q}$ state becomes bound as $N_c \rightarrow \infty$ with its mass scaling as $\mathcal{O}(1)$ and its width as $\mathcal{O}(1/N_c)$. Mesonic states of other nature may show different behavior [187]. The mass of a generic qqq state with two or three flavors evolves as $\mathcal{O}(N_c)$ while its widths scales as $\mathcal{O}(1)$ at leading order [182, 188, 189].

For dynamically generated mesons or molecular mesonic states, the evolution can deviate strongly from such a dependence. Compared with dynamically generated mesons, a study of dynamically generated baryonic states is complicated by the fact that flavor representations of baryons change with N_c when the number of flavors is larger than two [190, 191, 192]. Such a factor has been taken into account in the study of $\Lambda(1405)$ in Refs. [179, 180] as well as in the study of negative parity s -wave resonances [178].

In the present exploratory work, we limit ourselves to the two coupled channels scenario of $\Lambda_c(2595)$. Within the unitarized approaches, in order to obtain the large N_c evolution of dynamically generated states, we need to know how the masses of the interacting hadrons evolve as a function of N_c , how the loop function evolves, and how the couplings evolve. The latter evolution is a result of the change of the flavor representation of the baryons. In the following, we examine the evolution as a function of N_c of all the inputs in the unitary approach.

3.5.2 Baryon and meson masses

Ground-state heavy flavor baryon masses in the $1/m_Q$ and $1/N_c$ expansions have been studied in Ref. [193, 194, 195]. Up to leading order in $1/N_c$, one has

$$M_i = m_Q + \Lambda N_c + \delta_i, \quad (3.26)$$

where m_Q is the N_c independent heavy quark mass, Λ the contribution of the light u, d, s quarks, and δ_i the SU(3) breaking contributions. For the present study, we take $m_Q = m_c = 1.275$ GeV, $\Lambda = 0.3$ GeV, and δ_i is chosen such that M_i equals to its physical counterpart. The pseudoscalar meson masses scale as $\mathcal{O}(1)$ and are taken as constants, while the pseudoscalar decay constant scales as $\mathcal{O}(\sqrt{N_c})$, namely,

$$f(N_c) = f(N_c = 3) \sqrt{\frac{N_c}{3}}. \quad (3.27)$$

3.5.3 Loop function

The generic form of a meson-baryon loop function is

$$G = i \int \frac{d^4 q}{(2\pi)^4} \frac{2M_B}{[(P - q)^2 - m_\phi^2 + i\epsilon][q^2 - M_B^2 + i\epsilon]}, \quad (3.28)$$

which is logarithmically divergent, and should be renormalized using either the dimensional regularization method or the cutoff scheme. The latter is particularly useful, because it is more transparent to be extended to arbitrary N_c .

In the cutoff scheme, the loop function reads

$$G_{\text{cut}} = \int_0^\Lambda \frac{q^2 dq}{2\pi^2} \frac{E_M + E_m}{2E_M E_m} \frac{2M}{s - (E_M + E_m)^2 + i\epsilon}, \quad (3.29)$$

with $E_M = \sqrt{q^2 + M^2}$, and $E_m = \sqrt{q^2 + m^2}$.

Conventionally, one chooses a cutoff of the order of 1 GeV. When extended to arbitrary N_c , depending on the origin of this ultraviolet cutoff, there are two possible scenarios[175]. First, one can consider the value corresponding to the spontaneous chiral symmetry breaking $\Lambda \sim 4\pi f \sim 1$ GeV. Thus, the cutoff will share the same N_c dependence with the decay constant, that is, $\Lambda \sim \mathcal{O}(\sqrt{N_c})$. The second scenario is that the cutoff is the mass of a heavier qqq state integrated out in order to construct the effective theory. In this case, Λ scales as $\mathcal{O}(1)$ since the energy difference between ground state baryons and excited baryons scales as $\mathcal{O}(1)$. In the present work, we apply both interpretations, which yield consistent conclusions, as shown below.

3.5.4 Group representation-Clebsch-Gordan coefficients

In the unitary approach of Ref. [11], $\Lambda_c(2595)$ is dynamically generated from the interaction between the pseudoscalar octet and the sextet charmed baryons. In the language of the SU(3) group theory, it follows the decomposition of:

$$8 \otimes 6 = \bar{3} \oplus 6 \oplus \bar{15} \oplus \bar{24}. \quad (3.30)$$

Although the decomposition implies 4 channels in the SU(3) basis, only the $\bar{3}$ and $\bar{15}$ are relevant to the isospin zero case. Obviously, the extrapolation will be more convenient and intuitive if we transform the amplitude from the isospin basis to the SU(3) one. Using the SU(3) Clebsch-Gordan coefficients, the transformation matrix for strangeness zero and isospin zero is

$$U = \begin{pmatrix} -\frac{1}{2} & -\frac{\sqrt{3}}{2} \\ -\frac{\sqrt{3}}{2} & \frac{1}{2} \end{pmatrix} \quad (3.31)$$

in the order of $\bar{3}$ and $\bar{15}$. Now, the coefficients C_{ij} in the SU(3) basis can be obtained straightforward,

$$C_{ij}^{SU(3)} = U^\dagger C_{ij}^I U = \begin{pmatrix} -5 & 0 \\ 0 & -1 \end{pmatrix}. \quad (3.32)$$

While in the mesonic sector, the flavor representation remains the same with the increase of N_c , the situation in the baryonic sector is complicated because of the nontrivial N_c dependence. One way to extend the irreducible flavor representation from $N_c = 3$ to arbitrary N_c is the following:

$$[p, q] \rightarrow [p, q + \frac{N_c - 3}{2}], \quad (3.33)$$

where $[p, q]$ refers to the SU(3) irreducible representation. ⁶ Extrapolating to arbitrary N_c , the 6, $\bar{3}$, and $\bar{15}$ representations become ⁷

$$\begin{aligned} \text{“6”} &= [2, \frac{N_c - 3}{2}], \\ \text{“}\bar{3}\text{”} &= [0, \frac{N_c - 1}{2}], \\ \text{“}\bar{15}\text{”} &= [1, \frac{N_c + 1}{2}]. \end{aligned} \quad (3.34)$$

Following group theory [196], the coupling strengths in the SU(3) basis of arbitrary N_c should have the following form:

$$C_{ij}^{SU(3)}(N_c) = \begin{pmatrix} -5 & 0 \\ 0 & -\frac{5-N_c}{2} \end{pmatrix}, \quad (3.35)$$

⁶There are two alternative ways to perform the extension. The one adopted in the present work, referred to as the standard one in Ref. [191], has the advantage of keeping the spin, isospin, and strangeness of the original representation at $N_c = 3$.

⁷We adopt the notation that representation “ R ” reduces to R at $N_c = 3$ [190, 191, 192].

which reduces to Eq. (3.32) at $N_c = 3$.

Considering the fact that the representation of SU(3) changes with N_c , the transformation matrix U should also be N_c dependent. Using the recursion relations of Ref. [197] or the results of Ref. [198], one can easily obtain the explicit form of $U(N_c)$ for $8 \otimes "6"$.

Following the usual convention, the SU(3) Clebsch-Gordan (CG) coefficients can be expressed as the products of isoscalar factors and ordinary SU(2) CGCs.

$$\left(\begin{array}{cc|c} R_1 & R_2 & R_\gamma \\ I_1, I_{1z}, Y_1 & I_2, I_{2z}, Y_2 & I, I_{2z}, Y \end{array} \right) = \left(\begin{array}{cc|c} R_1 & R_2 & R_\gamma \\ I_1, Y_1 & I_2, Y_2 & I, Y \end{array} \right) \left(\begin{array}{cc|c} I_1 & I_2 & I \\ I_{1z} & I_{2z} & I_z \end{array} \right) \quad (3.36)$$

where the label R indicates the SU(3) representation, which can be denoted using the usual weight diagram notation (λ, μ) . γ labels degenerate representations occurring in a given product.

With the formula given in table 4 of Ref. [198], the U matrix can be derived straightforward. The first element, for instance, can be written as

$$U_{11} = \sqrt{\frac{(p+1)(\lambda-1-p)q(\lambda+\mu+1-q)(\lambda+\mu+2-q)}{\lambda(\lambda+1)(\mu+1)(\lambda+\mu+2)(\mu+p-q+2)}} \quad (3.37)$$

with

$$Y = p + q - \frac{2\lambda' + \mu'}{3}, \quad I = \frac{\mu' + p - q}{2} \quad (3.38)$$

where Y is related to a quantity called ϵ by $\epsilon = -3Y$. (λ', μ') refer to the representation labeled by " $\bar{3}$ " and " $\bar{15}$ " and their values are listed in Eq.3.34. And keep in mind that the formula above are used to calculate the isoscalar factors of " 6 " \otimes 8. We need to perform an extra step to get the U matrix for $8 \otimes "6"$ with correct convention. Finally, the U matrix can be written as

$$U(N_c) = \begin{pmatrix} -\sqrt{\frac{2}{5+N_c}} & -\sqrt{\frac{3+N_c}{5+N_c}} \\ -\sqrt{\frac{3+N_c}{5+N_c}} & \sqrt{\frac{2}{5+N_c}} \end{pmatrix}. \quad (3.39)$$

The N_c dependent coefficients in the isospin basis can then be obtained:

$$C_{ij}^I(N_c) = \begin{pmatrix} \frac{N_c-7}{2} & -\sqrt{\frac{N_c+3}{2}} \\ -\sqrt{\frac{N_c+3}{2}} & -4 \end{pmatrix}. \quad (3.40)$$

It is interesting to note that the self-interaction of $\pi\Sigma_c$ is attractive and does not change with N_c . On the other hand, the $K\Xi'_c$ self-interaction is attractive at $N_c = 3$, but becomes repulsive at $N_c > 7$. The off-diagonal transition, however, is always attractive and the strength increases with N_c .

Now it is straightforward to study the N_c dependence of the mass and width of $\Lambda_c(2595)$. In Figs. 3.3 and 3.4, we show the imaginary and real parts of $\Lambda_c(2595)$ pole position, in comparison with those of a conventional

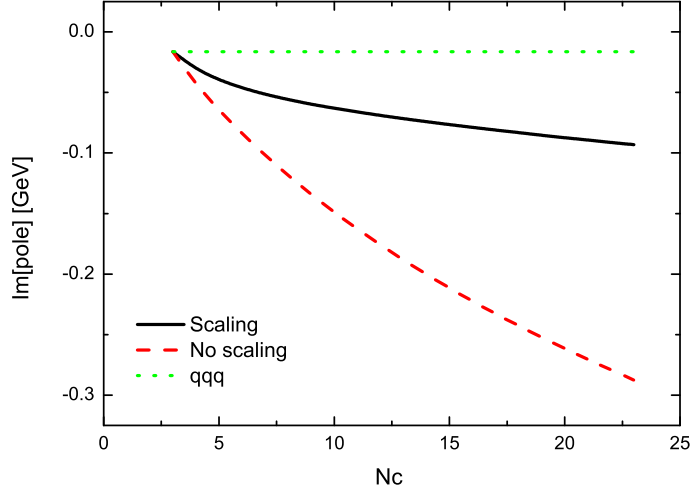


Figure 3.3: Imaginary part of the $\Lambda_c(2595)$ pole position, where “Scaling” refers to the cutoff dependence $\mathcal{O}(\sqrt{N_c/3})$, while “No scaling” refers to the use of a constant cutoff $\mathcal{O}(1)$.

qqq baryon. It is clear that they differ quite strongly from those expected for a naive qqq state. Therefore, the N_c evolution supports the conjecture that the meson-baryon component in the wave function of $\Lambda_c(2595)$ plays a relevant role.

The above analysis can be straightforwardly extended to the three-channel picture of Ref. [2] and qualitatively similar conclusions can be reached. We, however, do not attempt to study the 16 coupled channel scenario of Ref. [4], which, we believe, will yield the same conclusion.

It is interesting to note that recently lattice QCD simulations have started to probe the N_c dependence of mesonic states [199] and baryonic states [200, 201]. See, Ref. [185] for a comprehensive review. Checking the N_c dependence of $\Lambda_c(2595)$ and other proposed molecular states can help to unravel their true nature. In this sense, the present study should serve a motivation for such studies.

3.6 Summary

In this chapter, we have studied the interaction between a singly charmed baryon and a pseudoscalar meson in the unitarized chiral perturbation theory using the leading order chiral Lagrangian. It is shown that the interactions are strong enough to generate a number of dynamically generated states. Some of them can be naturally assigned to their experimental counterparts, such as $\Lambda_c(2595)$ [$\Lambda_c^*(2625)$]. An extension to bottom sector via heavy quark symmetry is straightforward. By slightly fine-tune the subtraction constant in the dimensional regularization scheme or the cutoff value in the cutoff regularization scheme, we predicted a number of additional states, whose experimental counterparts remain unknown. We strongly encourage future experiments to search for these states.

In anticipation of future lattice QCD simulation of scattering lengths, as already happened in the light baryon sector or the heavy meson sector, we have calculated the scattering lengths between the charmed baryons and the

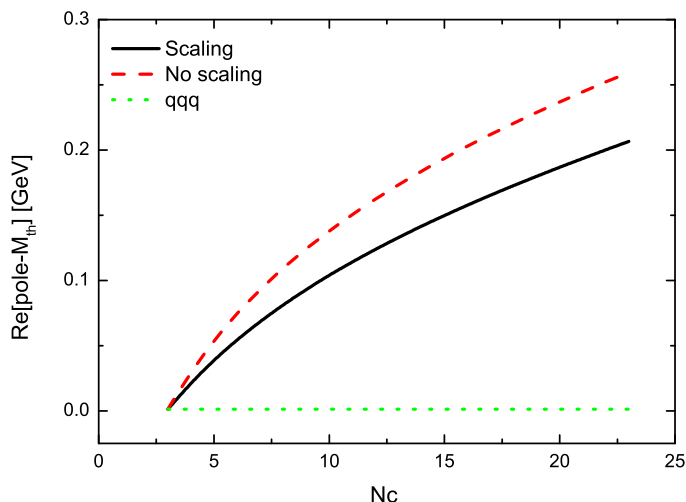


Figure 3.4: Real part of the $\Lambda_c(2595)$ pole position with respect to the $\pi\Sigma_c$ threshold, where “Scaling” refers to the cutoff dependence $\mathcal{O}(\sqrt{N_c/3})$, while “No scaling” refers to the use of a constant cutoff $\mathcal{O}(1)$.

pseudoscalar mesons. A comparison between our results and those of the $\mathcal{O}(p^3)$ ChPT study confirmed that there is indeed strong attraction in some of the coupled channels, which hint at the possible existence of dynamically generated states.

In future, the effects of higher-order potentials in the unitarized chiral perturbation theory need to be studied more carefully once relevant experimental or lattice QCD data become available. It should be noted, however, $\Lambda_c(2595)$ and their $J^P = 3/2^-$ counterparts seem to qualify as dynamically generated states even at next-to-leading order in the unitarized chiral perturbation theory.

In order to further qualify the components for the well established $\Lambda_c(2595)$ as a dynamically generated state, we also utilize two commonly accepted approaches, namely, the compositeness condition and the large N_c evolution. Our results show that although the relative importance of a coupled channel cannot be determined model independently, the basic picture that $\Lambda_c(2595)$ has relevant meson-baryon components does not change. From our study, it is clear that the commonly defined compositeness depends on the coupled channels included and the regularization scheme adopted to regularize the divergent loop function in the unitarized approaches. The molecular picture is also corroborated by our study of the dependence on the number of colors of the mass and width of $\Lambda_c(2595)$. It is shown that they differ largely from those expected for a naive qqq state, further confirming the molecular picture for $\Lambda_c(2595)$.

Chapter 4

Meson-baryon interactions up to NNLO

In this chapter we will go further into EFTs to investigate the influence from higher order contributions. Since in the preceding chapter, the NLO LECs for interactions between Goldstone bosons and charmed baryons cannot be fixed reliably, we turn to the ground-state octet baryon sector, where there are plenty of data available for a study up to next-to-next-to leading order(NNLO). We analyse the scattering amplitudes in a covariant framework, renormalizing the LECs within the EOMS scheme. A global fit to πN and KN phase shift was performed to determine the LECs, with which the scattering lengths and convergence are discussed.

4.1 Introduction

Elastic meson-baryon scattering ¹ is a fundamental process that not only can test our understanding of the strong interaction but also plays a relevant role in the studies of the properties of single and multiple baryons. For instance, one can derive from pion-nucleon scattering the nucleon sigma term, which is essential to understand the quark flavor structure of the nucleon in the scalar channel and plays an important role in direct dark matter searches [202, 203, 204, 205, 206, 207, 208]. In addition, meson-baryon scattering also provides key inputs in the construction of the chiral baryon-baryon interactions and may affect the equation of state of dense matter at high densities and therefore help to understand the so-called hyperon puzzle [209, 210, 211, 212] in explaining the existence of two-solar-mass neutron stars [213, 214]. Furthermore, meson-baryon scattering appears in the final states of heavier hadron decays and therefore becomes an integrated part in the test of the Standard Model [215, 216, 217, 218, 219] and in the search of beyond standard model physics [220]. Because of these, one has seen increasing theoretical, such as chiral perturbation theory (ChPT) [221, 222, 223, 224, 225, 7] and lattice QCD [226, 227], as well as experimental interests [228, 229, 230, 231, 232] in meson-baryon scattering in recent years.

ChPT, as a low-energy effective field theory of QCD, plays an important role in our understanding of the non-perturbative strong interaction physics [43, 46, 47, 82]. In particular, it provides a model independent framework

¹In this chapter, the mesons and baryons here refer specifically to the octet of Nambu-Goldstone bosons and the ground-state octet baryons, unless otherwise specified.

to describe the dynamics of the Nambu-Goldstone bosons interacting among themselves and with other hadrons containing light (u , d , and s) quarks. For comprehensive reviews, see, e.g., Refs. [51, 52, 53, 54, 55, 56].

The constraints imposed by chiral symmetry and its breaking are the most stringent on the self-interactions of the Nambu-Goldstone bosons and therefore ChPT has the largest predictive power in the pure mesonic sector. In the one-baryon sector, its predictive power decreases because a large number of unknown low energy constants (LECs) has to be introduced. As only a finite number of them appears in a particular process, this does not severely hamper its applicative power. A further complicating factor is the power counting breaking (PCB) issue. Namely, because of the large non-zero baryon masses m_0 in the chiral limit, lower order analytical terms appear in nominal higher order loop calculations, and therefore a consistent power counting is lost [82]. In the past three decades, several solutions have been proposed. The most studied ones are the heavy baryon ChPT [83, 52], the infrared (IR) baryon ChPT [86], and the extended-on-mass-shell (EOMS) baryon ChPT [233, 91]. For a short summary and comparison of these different schemes, see, e.g., Ref. [234]. In recent years, it has been shown that both formally and empirically, the EOMS BChPT seems to be more appealing because it satisfies all the symmetry and analyticity constraints and converges relatively faster.

Although the EOMS BChPT has been successfully applied to study pion-nucleon scattering [235, 236, 6, 237, 238, 239, 240], it has not been applied to study kaon-nucleon, or more generally, meson-baryon scattering. Our present study aims to fill this gap. It is particularly timely given the extensive studies of baryon masses [241, 242, 243, 244, 245] and the recent attempt to construct baryon-baryon interactions using covariant BChPT [246, 247, 248, 249, 250]. As mentioned above, meson-baryon scattering connects these studies and provides a non-trivial test of the consistency of BChPT.

4.2 Theoretical formalism

In this section, we explain in detail how to calculate the meson-baryon scattering amplitudes in covariant BChPT with the EOMS scheme. As pion-nucleon scattering has been studied in this framework previously [235, 236, 6, 237], we will highlight the new ingredients in extending the study from SU(2) to SU(3). For details similar to the SU(2) case, we refer the reader to Refs. [235, 236, 6, 237].

4.2.1 Scattering amplitudes and partial wave phaseshifts

In the isospin limit, the standard decomposition of the meson-baryon scattering amplitude reads [82, 251],

$$T_{MB} = \bar{u}(p', s') \left[A + \frac{1}{2}(\not{q} + \not{q}')B \right] u(p, s), \quad (4.1)$$

where $p(p')$ and $q(q')$ are the momentum of the initial (final) baryons and mesons, respectively (see Fig. 2.1).

Introducing the Mandelstam variables s, t, u , one can rewrite Eq. 4.1 in an alternative form ²

$$T_{MB} = \bar{u}(p', s') \left[D + \frac{i}{m_i + m_f} \sigma^{\mu\nu} q'_\mu q_\nu B \right] u(p, s), \quad (4.2)$$

where $\sigma^{\mu\nu} = \frac{i}{2} [\gamma^\mu, \gamma^\nu]$ and $D = A + \frac{s-u}{2(m_i+m_f)} B$. However, as noted in Ref [6], since the leading part of A and B may cancel each other, one better uses B and D to perform the low energy expansion of the scattering amplitudes when extracting the PCB terms.

The above scattering amplitudes can be projected onto specific partial waves in the following form:

$$\mathcal{T}_{MB}^{l\pm} = \frac{1}{2} (f_1^l + f_2^{l\pm}), \quad (4.3)$$

where f_1^l and f_2^l take the forms of

$$f_1^l = \frac{\sqrt{E+m_i}\sqrt{E'+m_f}}{8\pi\sqrt{s}} \left(A_l + \frac{\omega+\omega'}{2} B_l + \left(\frac{|\vec{q}|^2}{2(E+m_i)} + \frac{|\vec{q}'|^2}{2(E'+m_f)} \right) B_l \right), \quad (4.4)$$

$$f_2^l = \frac{\sqrt{E+m_i}\sqrt{E'+m_f}|\vec{q}||\vec{q}'|}{8\pi\sqrt{s}} \left(\frac{B_l}{2(E+m_i)} + \frac{B_l}{2(E'+m_f)} - \frac{A_l - \frac{\omega+\omega'}{2} B_l}{(E+m_i)(E'+m_f)} \right), \quad (4.5)$$

$$\begin{aligned} A_l(s) &= \int_{-1}^1 A(s, t) P_l(\cos \theta) d \cos \theta, \\ B_l(s) &= \int_{-1}^1 B(s, t) P_l(\cos \theta) d \cos \theta, \end{aligned} \quad (4.6)$$

where E, E', ω, ω' are the energy of the incoming and outgoing particles in the center of mass (c.m.) frame, \vec{q} and \vec{q}' are the c.m. momentum of the incoming(outgoing) mesons, m_i and m_f are the masses of the incoming and outgoing baryons. The P_l above refers to the Legendre polynomials with angular momentum l .

From the partial wave amplitudes, one can obtain the corresponding phase shifts [95]

$$\delta_{l\pm} = \arctan\{|\vec{p}| \text{Re} f_{l\pm}(s)\}. \quad (4.7)$$

In the present work, we will rely on the modern partial wave analysis of the George Washington University group [252, 253] to fix the relevant LECs. ³

²This can be easily checked by noting that $[\gamma^\mu, \gamma^\nu] q_\mu q'_\nu = 2(m_i + m_f) \not{q} - s + u$.

³For pion-nucleon scattering, one may also use the latest analysis based on the Roy-Steiner equation [254]. However, as our primary interest is to compare different formulations of BChPT, we choose to use the same data to fix the relevant LECs as those used by the previous studies [6, 7].

4.2.2 Power counting

In ChPT, the relative importance of a certain Feynman diagram contributing to a particular process is determined by its chiral order, ν , whose size is of the order of $(p/\Lambda_\chi)^\nu$, where p denotes a generic small quantity and Λ_χ the chiral symmetry breaking scale. In the one-baryon sector, where only one baryon is involved in both the initial and the final states, the chiral order for any given Feynman diagram with L loops, V_n n -th order vertices, N_M internal meson lines, and N_B internal baryon lines, is

$$\nu = 4L + \sum_n nV_n - 2N_M - N_B. \quad (4.8)$$

In the present context, the small quantities or expansion parameters are

$$s - \tilde{m}^2 \sim \mathcal{O}(p), \quad t \sim \mathcal{O}(p^2), \quad m_\pi, m_K, m_\eta \sim \mathcal{O}(p), \quad m_{N,\Lambda,\Sigma,\Xi} - \tilde{m} \sim \mathcal{O}(p^2), \quad (4.9)$$

Note that although in principle \tilde{m} here refers to m_0 , the chiral limit baryon mass, in the study of πN and KN scattering, we set $\tilde{m} = m_N$.

4.2.3 Chiral Lagrangians

In order to calculate the meson-baryon scattering amplitudes up to the leading one-loop order, i.e., $\mathcal{O}(p^3)$, we need the following meson-meson and meson-baryon Lagrangians:

$$\mathcal{L}_{\text{eff}} = \mathcal{L}_{MM}^{(2)} + \mathcal{L}_{MM}^{(4)} + \mathcal{L}_{MB}^{(1)} + \mathcal{L}_{MB}^{(2)} + \mathcal{L}_{MB}^{(3)}, \quad (4.10)$$

where the superscripts denote the chiral order. The corresponding expressions for each part of Lagrangians can be found in Chapter 2.

It should be noted that not all of the $\mathcal{O}(p^2)$ and $\mathcal{O}(p^3)$ terms contribute to a specific process. Particularly, for pion-nucleon and kaon-nucleon scattering, only 24 out of the total 37 LECs contribute. They are tabulated in Table. 4.1.

For an explicit study of the matching between SU(3) and SU(2), we refer the reader to Refs. [224, 255, 256]. In doing so, one should note that the Lagrangian in Eqs. 2.69,2.70,2.71 do not share the same Lorentz structures with those used in SU(2). To obtain the matching relations between the LECs in the SU(2) and SU(3) Lagrangian, the following relation between D_μ and the Dirac matrix γ_μ is needed, which reads:

$$\bar{\Psi} A^\mu i D_\mu \Psi + h.c. \doteq 2m \bar{\Psi} \gamma_\mu A^\mu \Psi, \quad (4.11)$$

where A^μ is an external field, and the symbol \doteq means equal up to terms of higher orders. Neglecting the possible higher order corrections, which is beyond our concern here, it is straightforward to reduce the SU(3) Lagrangian

Table 4.1: Independent (combinations of) LECs contributing to πN and KN scattering. For the sake of later reference, we introduce $\alpha_{1,\dots,8}, \beta_{1,\dots,8}, \gamma_{1,\dots,8}$ to denote different combinations of LECs. The units of the LECs are given in the last column.

πN	$KN_{I=0}$	$KN_{I=1}$	
$\alpha_1 = b_1 + b_2 + b_3 + 2b_4$	$\beta_1 = b_3 - b_4$	$\gamma_1 = b_1 + b_2 + b_4$	[GeV ⁻¹]
$\alpha_2 = b_5 + b_6 + b_7 + b_8$	$\beta_2 = 2b_6 - b_8$	$\gamma_2 = 2b_5 + 2b_7 + b_8$	[GeV ⁻²]
$\alpha_3 = c_1 + c_2$	$\beta_3 = 4c_1 + c_3$	$\gamma_3 = 4c_2 + c_3$	[GeV ⁻¹]
$\alpha_4 = 2b_0 + b_D + b_F$	$\beta_4 = b_0 - b_F$	$\gamma_4 = b_0 + b_D$	[GeV ⁻¹]
$\alpha_5 = d_2$	$\beta_5 = d_1 + d_2 + d_3$	$\gamma_5 = d_1 - d_2 - d_3$	[GeV ⁻⁴]
$\alpha_6 = d_4$	$\beta_6 = d_4 + d_5 + d_6$	$\gamma_6 = d_4 - d_5 + d_6$	[GeV ⁻²]
$\alpha_7 = d_8 + d_{10}$	$\beta_7 = d_7 - d_8 + d_{10}$	$\gamma_7 = d_7 + d_8 + d_{10}$	[GeV ⁻³]
$\alpha_8 = d_{49}$	$\beta_8 = d_{48} + d_{49} + d_{50}$	$\gamma_8 = d_{48} + d_{49} - d_{50}$	[GeV ⁻²]

to those of their SU(2) counterparts. We notice that although the application of Eq. 4.11 only leads to difference of higher orders, which could be ignored from the point of view of effective field theories, it results in a reorganization of the scattering amplitudes when divided into A and B parts. As a consequence, the explicit expressions of the tree level diagrams will be different.

We would like to point out that compared to the 9 free LECs in the πN channel in SU(2) [6], we find that only 8 of them are actually independent. All of the LECs in Eq. 2.71, which correspond to the d_{16} and d_{18} terms of Ref. [6], will eventually not contribute to the scattering amplitudes. In the $\mathcal{O}(p^3)$ Born diagrams, the contributions from the $d_{38,\dots,44}$ terms are canceled by the corrections from vertex renormalization. The remaining part, containing d_{45}, d_{46}, d_{47} , can be absorbed into those of the $d_{48,\dots,50}$ terms via

$$2m\bar{\Psi}\gamma_5\chi_-\Psi \doteq -\bar{\Psi}\gamma_5\gamma^\mu[iD_\mu, \chi_-]\Psi + \frac{g_A}{2}\bar{\Psi}[\not{p}, \chi_-]\Psi, \quad (4.12)$$

where g_A refers to the axial-vector current coupling constant. The first term on the right hand side will be canceled as the $d_{38,\dots,44}$ terms do, while the second term is in the form of the $d_{48,\dots,50}$ terms. Thus in the final scattering amplitudes, only 8 combinations of the LECs will survive, which is consistent with the HBChPT study [7].

In addition, we note that the b_5, b_6, b_7 terms in the Lagrangian (Eq. 2.69 and Eq. 2.70) are not symmetric under the exchange of the Lorentz indices μ, ν , while the b_8 term is. As a consequence, these four terms do not share the same expression. The same applies to the d_1, d_2, d_3 terms. Considering that the differences are two chiral orders higher, we supplement these terms with configurations containing exchanged Lorentz indices to make these Lagrangians symmetric with respect to the exchange of Lorentz indices. For instance, the modified b_5 and d_3 terms

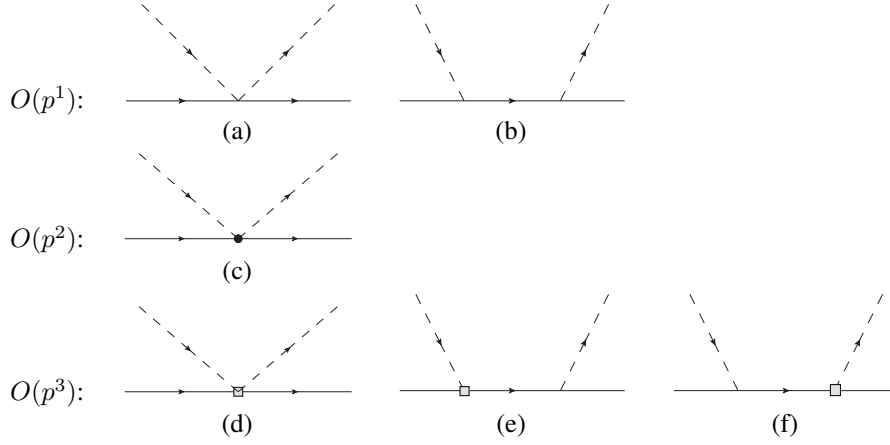


Figure 4.1: Tree level diagrams contributing to meson-baryon scattering up to $O(p^3)$. The solid lines correspond to baryons, and the dashed lines represent mesons. The vertices with filled circles and hollow blocks stem from the $\mathcal{L}_{MB}^{(2)}$ and $\mathcal{L}_{MB}^{(3)}$ Lagrangian, respectively.

finally utilized in our calculation read

$$\begin{aligned}
\mathcal{L}_{b_5} &= i \left(\langle \bar{B}[u^\mu, [u^\nu, \gamma_\mu D_\nu B]] \rangle - \langle \bar{B} \overleftarrow{D}_\nu [u^\nu, [u^\mu, \gamma_\mu B]] \rangle \right) \\
&\quad + i \left(\langle \bar{B}[u^\nu, [u^\mu, \gamma_\mu D_\nu B]] \rangle - \langle \bar{B} \overleftarrow{D}_\nu [u^\mu, [u^\nu, \gamma_\mu B]] \rangle \right), \\
\mathcal{L}_{d_3} &= i \left(\langle \bar{B} u^\mu \rangle \langle h^{\nu\rho} \gamma_\mu D_{\nu\rho} B \rangle - \langle \bar{B} \overleftarrow{D}_{\nu\rho} h^{\nu\rho} \rangle \langle u^\mu \gamma_\mu B \rangle \right) \\
&\quad - i \left(\langle \bar{B} h^{\nu\rho} \rangle \langle u^\mu \gamma_\mu D_{\nu\rho} B \rangle - \langle \bar{B} \overleftarrow{D}_{\nu\rho} u^\mu \rangle \langle h^{\nu\rho} \gamma_\mu B \rangle \right).
\end{aligned} \tag{4.13}$$

4.2.4 Feynman diagrams up to NNLO

- Tree level contact terms

The tree level contributions up to $O(p^3)$ are shown in Fig. 4.1. In the present work, we focus on the πN and KN sectors. They can be organized into the following four isospin multiplets: $\pi N^{I=3/2, 1/2}$ and $KN^{I=1, 0}$. The calculation of the contact terms is rather straightforward and the corresponding results are given in Appendix B.1.

- Tree level Born terms

In general, the amplitude for a Born diagram could be written as

$$\mathcal{A} = \frac{-\bar{u}_f \not{q}_f (\not{\mathcal{P}} - m_P) \not{q}_i u_i}{\mathcal{P}^2 - m_P^2}, \tag{4.14}$$

where u_i , \bar{u}_f refer to the spinors of the incoming or outgoing baryons, q_i and q_f are the momentum of the incoming or outgoing mesons, m_P is the mass of the baryon propagated, and \mathcal{P} is the total four momentum.

The Born terms at $O(p^3)$ can be categorized into two different groups. The first group contains the LECs $d_{38} \dots d_{44}$. They share the same expression with that of Eq. 4.14. The second group includes the LECs

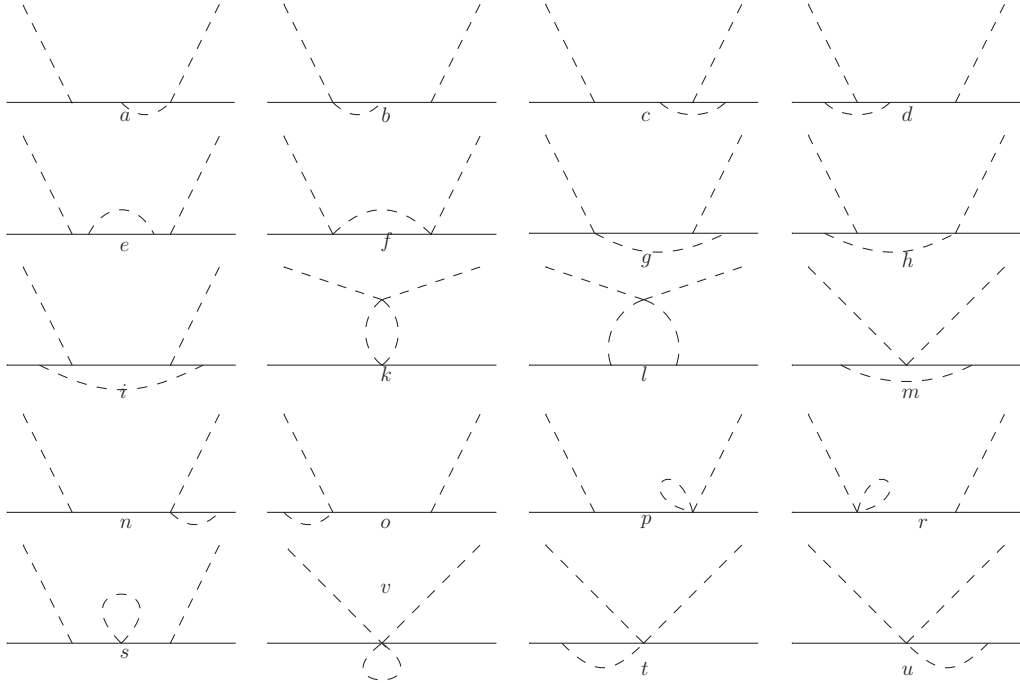


Figure 4.2: Leading one-loop contributions to meson-baryon scattering up to $O(p^3)$. Note that the wave function renormalization and crossed graphs are not shown explicitly.

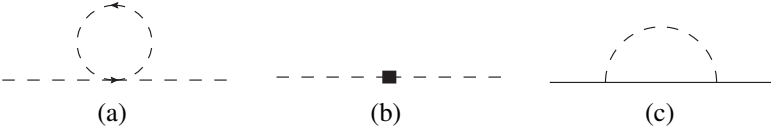


Figure 4.3: Wave function renormalization contributions to meson (dashed) and baryon (solid) fields. Counterterms from $\mathcal{L}_{MM}^{(4)}$ are denoted by the filled block.

d_{45}, d_{46}, d_{47} and the form is slightly different:

$$\mathcal{A} = \frac{i\bar{u}_f(-\not{\mathcal{P}} + m_P)\not{q}_i u_i}{\mathcal{P}^2 - m_P^2}. \quad (4.15)$$

The explicit results for the Born diagrams are given in Appendix B.2.

- Mass insertion diagrams

Mass insertions are induced by the SU(3) breaking corrections to the chiral limit baryon mass m_0 , which are of order $\mathcal{O}(p^2)$ and have the following explicit form:

$$\begin{aligned} \Delta_N &= 4m_K^2(b_0 + b_D - b_F) + 2m_\pi^2(b_0 + 2b_F), \\ \Delta_\Sigma &= 2m_\pi^2(b_0 + 2b_D) + 4b_0m_K^2, \\ \Delta_\Lambda &= \frac{2}{3}(m_K^2(6b_0 + 8b_D) + m_\pi^2(3b_0 - 2b_D)), \\ \Delta_\Xi &= 4m_K^2(b_0 + b_D + b_F) + 2m_\pi^2(b_0 - 2b_F). \end{aligned} \quad (4.16)$$

One easy way to include these corrections is to supplement the intermediate baryon mass of the Born terms with the $\mathcal{O}(p^2)$ corrections given in Eq. 4.16. The contribution from this part can be automatically included if one performs a substitution of $m_0 \rightarrow m_2 = m_0 + \Delta_B$ in the mass renormalization of baryons. Thus we will not explicitly show the contribution of this part.

- Leading one-loop diagrams

The leading one-loop contributions to meson-baryon scattering include the Feynman diagrams shown in Fig. 4.2.

The crossed diagrams, if exist, can be obtained with the same replacement rule as in the case of the crossed Born diagrams:

$$\begin{aligned} B_{Loop} &= B(s) - B(s \leftrightarrow u, M_i \leftrightarrow M_f), \\ A_{Loop} &= A(s) + A(s \leftrightarrow u, M_i \leftrightarrow M_f), \end{aligned} \quad (4.17)$$

where $M_{i,f}$ refer to the masses of incoming and outgoing mesons. In the numerical evaluation of all these loop diagrams, we adopt physical values for all the quantities appearing in the amplitudes, including decay constants and masses. Employing their chiral limit values only lead to differences of higher chiral order.

- Wave function renormalization

The wave function renormalization of the external mesons and baryons are shown in Fig. 4.3. From Fig. 4.3(a)(b),

one obtains the wave function renormalization constants for the Goldstone bosons up to NLO [55]

$$\begin{aligned}\mathcal{Z}_\pi &= 1 - \frac{1}{F_0^2} \left[8L_4(2m_K^2 + m_\pi^2) + 8L_5m_\pi^2 + \frac{1}{3}I(m_K^2) + \frac{2}{3}I(m_\pi^2) \right], \\ \mathcal{Z}_K &= 1 - \frac{1}{F_0^2} \left[8L_4(2m_K^2 + m_\pi^2) + 8L_5m_\pi^2 + \frac{1}{2}I(m_K^2) + \frac{1}{4}I(m_\pi^2) + \frac{1}{4}I(m_\eta^2) \right], \\ \mathcal{Z}_\eta &= 1 - \frac{1}{F_0^2} \left[8L_4(2m_K^2 + m_\pi^2) + \frac{8}{3}L_5m_\eta^2 + I(m_K^2) \right],\end{aligned}\quad (4.18)$$

where $I(M^2) = -\frac{M^2}{16\pi^2} \ln \frac{M^2}{\mu^2}$ is the one point function, and L_4 and L_5 are the NLO LECs of meson-meson interactions. For the baryons, as depicted in Fig. 4.3(c), the wave function renormalization constants up to $\mathcal{O}(p^3)$ are

$$\mathcal{Z}_B = 1 - (f(m_B^2) + 2m_B^2 f'(m_B^2) - 2m_B m_P g'(m_B^2)), \quad (4.19)$$

where $f(m_B^2)$ and $g(m_B^2)$ come from the baryon self-energy $-i\Sigma_{self} = -\not{P}f(\mathcal{P}^2) + m_P g(\mathcal{P}^2)$ with $\mathcal{P}^2 = s = m_B^2$ and can be written as

$$\begin{aligned}f(s) &= -\frac{i}{32\pi^2 s} \left((-m_P^2 (2s + M_\phi^2) + s (s - M_\phi^2) + m_P^4) B_0(s, m_P^2, M_\phi^2) \right. \\ &\quad \left. + (m_P^2 - s) A_0(M_\phi^2) - (s + m_P^2) A_0(m_P^2) \right), \\ g(s) &= \frac{i (M_\phi^2 (-B_0(s, m_P^2, M_\phi^2)) - A_0(m_P^2))}{16\pi^2},\end{aligned}\quad (4.20)$$

where m_P and M_ϕ refer to the masses of propagated baryons and mesons, m_B is the mass of incoming or outgoing baryons, and A_0, B_0 are the one and two point scalar functions in the Passarino-Veltman notation.

In numerical calculations, we utilize the package OneLoop [257, 258].

The above obtained scattering amplitudes still need further treatment before being employed to describe meson-baryon scattering. First, since in all the calculations above we used the physical values instead of the corresponding bare ones, the amplitudes must be properly renormalized. The procedure of renormalization is quite standard, see, e.g., Ref. [6]. We only need to point out that 1) the baryon mass normalization is implemented perturbatively and 2) the vertex renormalization is achieved via the two-body decay process, as in Ref. [237], and 3) the chiral corrections to decay constants are considered up to NLO [47]. To recover a proper power counting, we adopt the EOMS scheme.

4.3 Renormalization

The main purpose of renormalization is to compensate the corrections caused by the differences between the physical values of LECs, masses and decay constants, and the corresponding bare ones. In the present work, these corrections will promote the order of the original amplitudes by 2, leading to a contribution at the order of $\mathcal{O}(p^3)$. Thus we only need to study the $\mathcal{O}(p)$ tree level amplitudes.

4.3.1 Mass renormalization

The calculation of the diagram (e) in Fig. 4.2 shows a double pole structure in the amplitudes. This unphysical structure can be removed, as it should be, after the masses of the propagating baryons in the Born terms are correctly renormalized. Following the same power counting rule as specified above, the physical baryon masses can be expressed up to the NNLO as

$$m_{phys} = m_0 + \Delta_{N,\Lambda,\Sigma,\Xi} + \Sigma_{\mathcal{O}(p^3)}, \quad (4.21)$$

where m_0 refers to the chiral limit baryon mass, $\Delta_{N,\Lambda,\Sigma,\Xi}$ and $\Sigma_{\mathcal{O}(p^3)}$, given by Eq. 4.16 and Eq. 4.20 respectively, denote the NLO and NNLO contributions. As mentioned before, a replacement of $m_0 \rightarrow m_2 = m_0 + \Delta_{N,\Lambda,\Sigma,\Xi}$ automatically include the contributions from mass insertions.

Specifying the intermediate baryons and mesons in Eq. 4.20, the $\mathcal{O}(p^3)$ self energy reads

$$\begin{aligned} \Sigma_{\mathcal{O}(p^3)} &\equiv \Sigma(B, \Phi, P) \\ &= -i\cancel{P}f(\mathcal{P}^2) + im_Pg(\mathcal{P}^2) |_{\not{p}=m_B, \mathcal{P}^2=m_B^2} \\ &\quad - \frac{\tilde{m} \left(2\tilde{m}^2 - 2m_P\tilde{m} + M_\phi^2 + \log\left(\frac{\mu^2}{\tilde{m}^2}\right) \left(-2\tilde{m}^2 + 3m_P\tilde{m} + M_\phi^2 \right) \right)}{8\pi^2}, \end{aligned} \quad (4.22)$$

where B denote the incoming or outgoing baryon, and Φ and P represent the intermediate meson and baryon. The last term of the above equation is actually the power counting breaking term, which will be absorbed into m_2 .

Below, we list the expressions for the $\mathcal{O}(p^3)$ baryon masses:

$$\begin{aligned} \Sigma_N &= \frac{1}{12f^2} \left(\Sigma(N, \eta, N)(D - 3F)^2 + \Sigma(N, K, \Lambda)(D + 3F)^2 \right. \\ &\quad \left. + 9 \left(\Sigma(N, K, \Sigma)(D - F)^2 + \Sigma(N, \pi, N)(D + F)^2 \right) \right), \\ \Sigma_\Sigma &= \frac{1}{6f^2} \left(3\Sigma(\Sigma, K, N)(D - F)^2 + 3\Sigma(\Sigma, K, \Xi)(D + F)^2 \right. \\ &\quad \left. + 2 \left((\Sigma(\Sigma, \eta, \Sigma) + \Sigma(\Sigma, \pi, \Lambda))D^2 + 6\Sigma(\Sigma, \pi, \Sigma)F^2 \right) \right), \\ \Sigma_\Lambda &= \frac{1}{6f^2} \left(2(\Sigma(\Lambda, \eta, \Lambda) + 3\Sigma(\Lambda, \pi, \Sigma))D^2 + \Sigma(\Lambda, K, \Xi)(D - 3F)^2 \right. \\ &\quad \left. + \Sigma(\Lambda, K, N)(D + 3F)^2 \right), \\ \Sigma_\Xi &= \frac{1}{12f^2} \left(\Sigma(\Xi, K, \Lambda)(D - 3F)^2 + \Sigma(\Xi, \eta, \Xi)(D + 3F)^2 \right. \\ &\quad \left. + 9 \left(\Sigma(\Xi, \pi, \Xi)(D - F)^2 + \Sigma(\Xi, K, \Sigma)(D + F)^2 \right) \right). \end{aligned} \quad (4.23)$$

One can of course simply replace m_2 in Eq. B.10 with $m_{phys} - \Sigma_{\mathcal{O}(p^3)}$ to complete the mass renormalization, ignoring the resulting higher order differences. However, the treatment here needs to be much more careful. The series of studies on baryon masses show that with the EOMS scheme, one can achieve a pretty good and well-converged description at the complete one-loop level, which is N³LO. But when limited to NNLO, the convergence

is not as good as expected [244]. Contributions from NNLO and N^3 LO will largely cancel each other. From another point of view, the $\chi^2/d.o.f.$ from a NNLO fit is much larger than that of a N^3 LO fit, which implies a relatively unsatisfying description. As a consequence, although a direct replacement is not WRONG, it is not appropriate since the higher order contribution, N^3 LO here, to the baryon masses may worsen the description of scattering process at the order of our interest. Thus we expand the amplitudes of the Born terms after the substitution at $s = m_2^2$, in order to cancel the double pole structure strictly and avoid worsening of the convergence.

4.3.2 Vertex renormalization

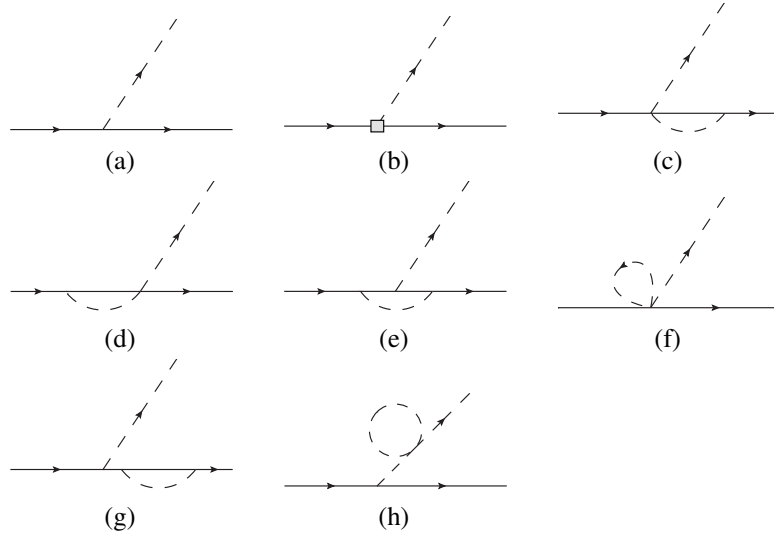


Figure 4.4: Feynman diagrams contributing to vertex renormalizations. The hollow block represents the contributions of the $O(p^3)$ vertices.

Several methods are available to renormalize the vertices. Of course, all of the renormalization methods are eventually equivalent. For instance, the authors in Ref. [6] chose to renormalize the coupling constants with the axial-vector current. In this work, we choose to achieve the vertex corrections at the one loop level via the two-body decay process, as in Ref. [237]. The two-body decays of a baryon up to $\mathcal{O}(p^3)$ are depicted in Fig. 4.4.

The renormalization of the vertices can be schematically expressed as the following:

$$C_{ph}\gamma^5\not{q}_f = C_{bare}\gamma^5\not{q}_f + C_{ph}\gamma^5\not{q}_f Z + C_{ph}\gamma^5\mathcal{A}_{loop}(s) + C_{ph}\gamma^5\not{q}_f\Delta_F. \quad (4.24)$$

The five terms on the right hand side of the above equation come from tree diagrams (a,b), wave function renormalization (g,h), one loop diagrams (c,d,e,f), and the renormalization of the decay constant, respectively, where Z refers to the wave function renormalization constants, Δ_F is the decay constant at $\mathcal{O}(p^2)$. This leads to

$$\begin{aligned} C_{bare} &= C_{ph} - C_{ph}Z - C_{ph}\Delta_F - C_{ph}\frac{\mathcal{A}_{loop}}{m_i + m_f} \\ &\equiv C_{ph} - C_{re}. \end{aligned} \quad (4.25)$$

The explicit form of \mathcal{A}_{loop} can be found in Appendix B.3.

Substituting Eq. 4.24 into the Born terms leads to

$$\begin{aligned} C_{bare}^1 C_{bare}^2 \mathcal{A}_{Born} &= (C_{ph}^1 - C_{re}^1)(C_{ph}^2 - C_{re}^2) \mathcal{A}_{Born} \\ &\simeq (C_{ph}^1 C_{ph}^2 - C_{ph}^2 C_{re}^1 - C_{ph}^1 C_{re}^2) \mathcal{A}_{Born}, \end{aligned} \quad (4.26)$$

where the last two terms in Eq.(4.26) are the correction parts we need and the $C_{re}^1 C_{re}^2 \mathcal{A}_{Born}$ has already been omitted since its order is higher.

4.3.3 Chiral corrections to the decay constants

To obtain the full meson-baryon amplitudes, one should also take into account the chiral corrections to the decay constants. In practice, one should use the bare decay constant F_0 instead of the corresponding physical ones F_π , F_K , and F_η [47].

Since the chiral corrections increase the chiral order by $\mathcal{O}(p^2)$, we only need to replace F_0 with F_π , F_K , and F_η in the tree level diagrams of order $\mathcal{O}(p^1)$.

$$\frac{\mathcal{A}_{\mathcal{O}(p^1)}}{F_0^2} = \frac{\mathcal{A}_{\mathcal{O}(p^1)}}{F_\pi^2, F_K^2, F_\eta^2} (1 - 2\Delta F_{\pi, K, \eta}), \quad (4.27)$$

where

$$\begin{aligned} \Delta F_\pi &= \frac{2(A_0(m_\pi^2) + 64\pi^2(2L_4 m_K^2 + L_4 m_\pi^2 + L_5 m_\pi^2)) + A_0(m_K^2)}{32\pi^2 F_0^2}, \\ \Delta F_K &= \frac{3A_0(m_\eta^2) + 6A_0(m_K^2) + 3A_0(m_\pi^2) + 1024\pi^2 L_4 m_K^2 + 512\pi^2 L_4 m_\pi^2 + 512\pi^2 L_5 m_K^2}{128\pi^2 F_0^2}, \\ \Delta F_\eta &= \frac{3A_0(m_K^2) + 128\pi^2(L_4(2m_K^2 + m_\pi^2) + L_5 m_\eta^2)}{32\pi^2 F_0^2}. \end{aligned} \quad (4.28)$$

4.4 Ultraviolet divergence and power counting breaking terms

As mentioned above, the one-loop integrals calculated above are ultraviolet divergent. Applying the $\overline{MS} - 1$ dimensional regularization scheme, the ultraviolet divergent part can be absorbed into the LECs at the corresponding order.

One can separate the LECs in the counter terms into their finite parts and infinite parts as,

$$L_i = L_i^r + L_i^d R, \quad (4.29)$$

where $R = \frac{2}{d-4} + \gamma_E - 1 - \ln(4\pi)$ with γ_E being the Euler constant and d the space-time dimension. The L_i^d 's are listed in Appendix B.4. All other L_i^d 's not listed are equal to zero. Note that here we approximate all the baryon masses with \tilde{m} just to simplify the expressions.

Since the chiral limit baryon mass does not vanish, the naive powering counting rule is broken when the $\overline{MS}-1$ scheme is adopted [82]. As we have mentioned above, in the covariant amplitudes, the A and B parts may cancel each other. It is better to use the modified D and B functions when one removes the PCB parts.

The power counting breaking terms are tightly related to the small quantities in the chiral expansion, which have been listed at the very beginning in Eq. 4.9. In the present work, since we are working in the $SU(3)$ case, the situation is a bit more complicated because of the mass differences among the octet baryons, which we count as $\mathcal{O}(p^2)$. To make sure the factor in front of the B part counts as a pure $\mathcal{O}(p^2)$, we rewrite the scattering amplitude in the following way:

$$\begin{aligned}
T_{MB} &= \bar{u}(p', s') \left[D + \frac{i}{m_i + m_f} \sigma^{\mu\nu} q'_\mu q_\nu B \right] u(p, s) \\
&= \bar{u}(p', s') \left[D + \frac{i}{2\tilde{m}} \sigma^{\mu\nu} q'_\mu q_\nu \frac{2\tilde{m}}{m_i + m_f} B \right] u(p, s) \\
&= \bar{u}(p', s') \left[D + \frac{i}{2\tilde{m}} \sigma^{\mu\nu} q'_\mu q_\nu \tilde{B} \right] u(p, s),
\end{aligned} \tag{4.30}$$

where $D = A + \frac{s-u}{2(m_i+m_f)}B$. Now we can see that we only need to pick up the PCB terms up to $\mathcal{O}(p^2)$ for the D functions and those up to $\mathcal{O}(p^0)$ for the \tilde{B} functions since the term $\sigma^{\mu\nu} q'_\mu q_\nu$ is of $\mathcal{O}(p^2)$.

The terms that break the power counting have been shown to originate from the regular part of the loop integrals by Becher and Leutwyler [86]. This provides a simple way to subtract the PCB terms by working out all the regular parts first. Alternatively, one can also perform the chiral expansions of small quantities directly.

Once we get rid of all the PCB terms, we obtain

$$\begin{aligned}
T' &= \bar{u}(p', s') \left[D' + \frac{i}{2\tilde{m}} \sigma^{\mu\nu} q'_\mu q_\nu \tilde{B}' \right] u(p, s), \\
&= \bar{u}(p', s') \left[D' + \frac{i}{m_i + m_f} \sigma^{\mu\nu} q'_\mu q_\nu \frac{m_i + m_f}{2\tilde{m}} \tilde{B}' \right] u(p, s).
\end{aligned} \tag{4.31}$$

The final A and B functions, where we use A_f and B_f to distinguish them from A and B , are then

$$\begin{aligned}
B_f &= \frac{m_i + m_f}{2\tilde{m}} \tilde{B}', \\
A_f &= D' - \frac{s-u}{4\tilde{m}} \tilde{B}'.
\end{aligned} \tag{4.32}$$

As shown in Ref. [91], the PCB terms are all analytical and can be absorbed into the LECs at the corresponding orders. Assuming that $\text{LEC} = \text{LEC}_b + \text{LEC}^{PCB}$, we have worked out all the power counting breaking terms, which are explicitly shown in Appendix B.5.

4.5 Results and discussion

The scattering of a pseudoscalar meson off an octet baryon can be grouped into 11 combinations of isospin and strangeness as tabulated in Table. 4.2. In the present work we focus on the πN and KN channels, because only

for these channels partial wave phase shifts are available.

Table 4.2: 11 coupled channels of meson-baryon scattering of conserved strangeness (S) and isospin (I).

(1, 1)	(1, 0)	(0, $\frac{3}{2}$)	(0, $\frac{1}{2}$)	(-1, 2)	(-1, 1)	(-1, 0)	(-2, $\frac{3}{2}$)	(-2, $\frac{1}{2}$)	(-3, 1)	(-3, 0)
KN	KN	$K\Sigma$	$K\Sigma$	$\pi\Sigma$	$\pi\Sigma$	$\pi\Sigma$	$\bar{K}\Sigma$	$\bar{K}\Sigma$	$\bar{K}\Xi$	$\bar{K}\Xi$
		πN	$K\Lambda$		$\eta\Sigma$	$\eta\Lambda$	$\pi\Xi$	$\bar{K}\Lambda$		
			ηN		$\pi\Lambda$	$\bar{K}N$		$\eta\Xi$		
			πN		$\bar{K}N$	$K\Xi$		$\pi\Xi$		
					$K\Xi$					

With the amplitudes properly renormalized, we are now ready to determine the LECs by fitting to the partial wave phase shifts. For πN , we choose the phase shifts from the analysis of WI08 [252] in the $S_{11}, S_{31}, P_{11}, P_{31}, P_{13}, P_{33}$ partial waves, where in the convention $L_{2I,2J}$, L denotes the total orbit angular momentum, I the total isospin, and J the total angular momentum. Correspondingly, the phase-shift analysis of the SP92 solution [253] in the $S_{01}, P_{01}, P_{03}, S_{11}, P_{11}, P_{13}$ partial waves are used for KN where the symbols mean $L_{I,2J}$.

For the πN channels, we choose the phase shifts with \sqrt{s} between 1082 MeV, which is slightly above the threshold, and 1130MeV, with an interval of 4 MeV. Thus totally we will have 13 points for each of the 6 partial waves. For the KN channels we follow the same strategy. Starting from 1435MeV to 1475MeV, the interval is set to be 2 MeV, with totally 20 points for each partial wave.

Since WI08 does not provide the errors for the data, we follow Refs. [259, 260] and take

$$err(\delta) = \sqrt{e_s^2 + e_r^2 \delta^2}, \quad (4.33)$$

with the systematic error $e_s = 0.1^\circ$ and the relative error $e_r = 2\%$.

Throughout the numerical study, we use the physical decay constants for the corresponding vertices. The renormalization scale μ in the loop integrals is chosen to be the average mass of the baryon octet, and the \tilde{m} , appearing in the power counting breaking terms via $s - \tilde{m}^2$, is taken to equal to the mass of the nucleon, considering that we focus now on the πN and KN channels. The physical values employed in the present work are collected in Table. 4.3.

Table 4.3: Masses and decay constants (in units of GeV) and axial-coupling constants relevant in the present work. Note the mass of the K meson is taken to be 0.493 GeV to be consistent with the SP92 data, which were originally from K^+n scattering.

m_π	m_K	m_η	m_N	m_Λ	m_Σ	m_Ξ
0.139	0.493	0.54765	0.939	1.1157	1.1934	1.3183
F_π	F_K	F_η	D	F	μ	\tilde{m}
0.0924	0.11003	0.11088	0.8	0.467	1.16	$m_N=0.939$

4.5.1 Fitting strategy one: direct fit to the phase shifts

We find that to describe the pion-nucleon scattering data, one needs to go to at least $\mathcal{O}(p^3)$. On the other hand, a reasonable reproduction of the kaon-nucleon data can already be achieved at $\mathcal{O}(p^2)$. We follow the same strategy in the first attempt to provide a simultaneous fit of both the πN and KN data.⁴

A least-of-squares fit yielded a $\chi^2/d.o.f. = 0.154$ for the 78 data points in the pion-nucleon channel. The corresponding fit results associated with errors propagated from the uncertainties of LECs are compared with the empirical data in Fig. 4.5. For the sake of comparison, we show as well the $\mathcal{O}(p^3)$ results of the SU(3) HB [225, 7] and the SU(2) EOMS BChPT [6].

Clearly, the EOMS results can describe the phase shifts quite well. Although the data are only fitted up to $\sqrt{s} = 1.13$ GeV, the phase shifts are described very well even up to $\sqrt{s} = 1.16$ GeV for some partial waves, corresponding to a momentum in the laboratory frame of $|\vec{p}_{lab}| = 200$ MeV. In addition, our calculation in SU(3) shows a compatible description compared to that in SU(2), which implies that the inclusion of strangeness has small effects on the fitting results.

We note that even with the relative large uncertainties, we cannot achieve a satisfying description of the P_{11} , P_{13} and P_{33} partial waves at higher energy regions. Particularly, in the P_{11} channel, the solution of WI08 tends to increase with energy in the higher energy region while the EOMS results, both in the SU(3) and SU(2) cases, decrease. This disagreement has already been noted in Ref. [6], where the authors pointed out that including the contribution of $\Delta(1232)$ may improve the description. Inspired by this, we have checked that in SU(3) the inclusion of the lowest order contribution from the decuplet can have the same positive effect. One can achieve a pretty good description even up to $\sqrt{s} = 1.2$ GeV, quite close to the region of the Δ resonance. For a description bridging over this Δ resonance region, one needs to include the Δ explicitly, unitarize the amplitudes, and modify the powering counting rule. For a discussion of these, we refer the reader to Ref. [237].

For the KN scattering, as noted in the HB study [225, 7], a quite good description of the phase shifts can already be achieved at NLO. In the present work, we will present two studies of the KN scattering. One is performed up to $\mathcal{O}(p^2)$ and the other is performed up to $\mathcal{O}(p^3)$ but only the loop contributions are included, because the phase shifts data are not enough to fix the relevant $\mathcal{O}(p^3)$ LECs. Other inputs in addition to the KN phase shifts are needed. The second study will be denoted by $\mathcal{O}(p^3)^*$.

In Fig. 4.6 we show our fitted results together with the experimental data. We find that in the KN channels, the error bands are very narrow for both the $\mathcal{O}(p^2)$ and $\mathcal{O}(p^3)^*$ results. In most partial waves, they are only a few percent of the corresponding phase shifts. For the sake of comparison, we show as well the HB results of Refs. [225, 7]. It is clear that the EOMS descriptions are slightly better than the HB results when extended to higher energies.

From the above discussions, it is clear that the EOMS provides a satisfactory description of both the pion-nucleon and kaon-nucleon scattering data up to $\mathcal{O}(p^3)$, while the SU(3) HB ChPT fails.

⁴As a matter of fact, different LECs contribute to πN and KN scattering independent of each other.

Table 4.4: LECs in the πN channel.

$\alpha_1[\text{GeV}^{-1}]$	$\alpha_2[\text{GeV}^{-2}]$	$\alpha_3[\text{GeV}^{-1}]$	$\alpha_4[\text{GeV}^{-1}]$	$\alpha_5[\text{GeV}^{-4}]$	$\alpha_6[\text{GeV}^{-2}]$	$\alpha_7[\text{GeV}^{-3}]$	$\alpha_8[\text{GeV}^{-2}]$	$\chi^2/d.o.f.$
-7.63(6)	1.42(2)	1.34(1)	-1.36(6)	0.61(2)	3.25(5)	1.45(3)	-0.32(13)	0.154

Table 4.5: LECs in the πN channel with $\alpha_4 = b_0 + \frac{b_D}{2} + \frac{b_F}{2}$ fixed by fitting to the baryon masses.

$\alpha_1[\text{GeV}^{-1}]$	$\alpha_2[\text{GeV}^{-2}]$	$\alpha_3[\text{GeV}^{-1}]$	$\alpha_4[\text{GeV}^{-1}]$	$\alpha_5[\text{GeV}^{-4}]$	$\alpha_6[\text{GeV}^{-2}]$	$\alpha_7[\text{GeV}^{-3}]$	$\alpha_8[\text{GeV}^{-2}]$	$\chi^2/d.o.f.$
-7.41(7)	1.56(2)	1.33(1)	-0.80	0.63(2)	3.18(6)	1.45(3)	-0.096(122)	1.26

Table 4.6: LECs in the πN channel including the lowest order decuplet contribution with $h_A = 2.9$.

$\alpha_1[\text{GeV}^{-1}]$	$\alpha_2[\text{GeV}^{-2}]$	$\alpha_3[\text{GeV}^{-1}]$	$\alpha_4[\text{GeV}^{-1}]$	$\alpha_5[\text{GeV}^{-4}]$	$\alpha_6[\text{GeV}^{-2}]$	$\alpha_7[\text{GeV}^{-3}]$	$\alpha_8[\text{GeV}^{-2}]$	C	$\chi^2/d.o.f.$
-3.737(36)	0.659(7)	0.893(4)	-0.745(21)	0.159(5)	1.066(20)	0.351(10)	0.133(34)	$\frac{h_A}{2\sqrt{2}}$	0.918

Table 4.7: πN and $K N$ scattering lengths in units of fm. Note that we did not associate any uncertainties to the $\mathcal{O}(p^3)^*$ contributions of the $K N$ channel because we have not included the tree level contributions at this order for the $K N$ channels.

Channel	$\mathcal{O}(p^1)$	$\mathcal{O}(p^2)$	$\mathcal{O}(p^3)$	Total	Huang(HB) [7]	Mai(IR) [224]	EXP
$a_{\pi N}^{3/2}$	-0.126	0.026(11)	-0.011(8)	-0.111(16)	-0.110(2)	-0.04(7)	-0.125(3) [261]
$a_{\pi N}^{1/2}$	0.212	0.025(10)	0.003(16)	0.240(22)	0.240(2)	0.07(3)	0.250 $^{+0.006}_{-0.004}$ [261]
$a_{KN}^1(\mathcal{O}(p^2))$	-0.476	0.149(1)	-/-	-0.327(1)	-0.330(5)	-0.33(32)	-0.33 [252]
$a_{KN}^0(\mathcal{O}(p^2))$	0.043	-0.057(2)	-/-	-0.014(2)	0.000(4)	0.02(64)	0.02 [252]
$a_{KN}^1(\mathcal{O}(p^3)^*)$	-0.476	1.067(5)	-0.919	-0.328(5)	-/-	-/-	-/-
$a_{KN}^0(\mathcal{O}(p^3)^*)$	0.043	0.164(2)	-0.219	-0.012(2)	-/-	-/-	-/-

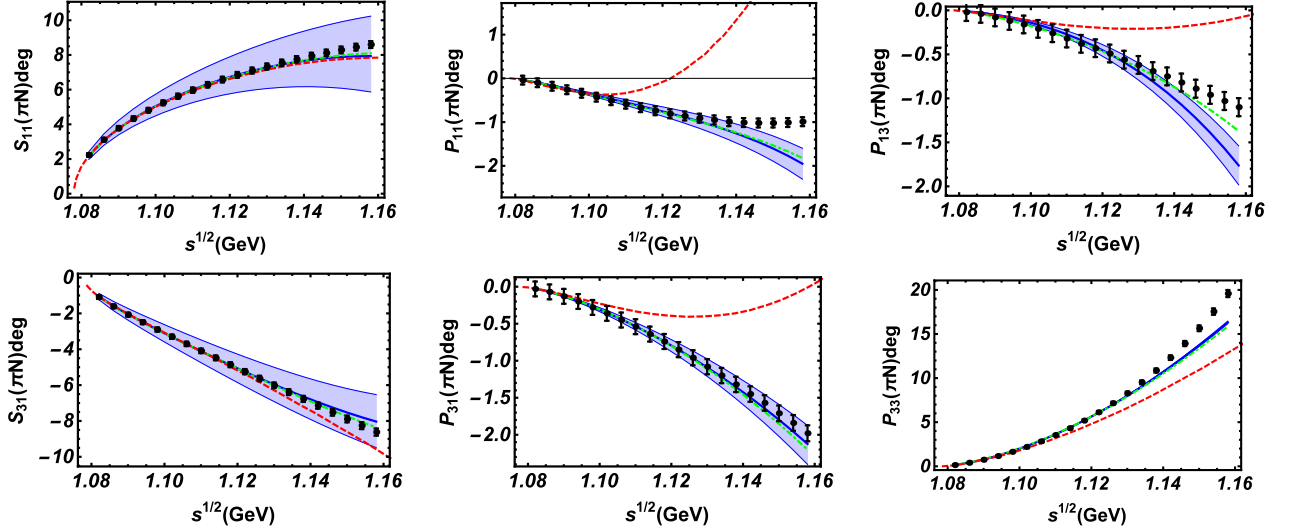


Figure 4.5: Pion-nucleon phase shifts. The blue lines denote our results and the black dots with error bars represent the WI08 solution with empirical errors given in Eq. 4.33. The blue bands correspond to the uncertainties propagated from the errors of LECs. In some partial waves, the error bands are of the size of the thickness of the lines. For the sake of comparison, we show as well the EOMS SU(2) results [6] (green dot-dashed lines) and the HB SU(3) results [7] (red dashed lines).

Table 4.8: LECs contributing to the $I = 0$ KN scattering.

	$\beta_1[\text{GeV}^{-1}]$	$\beta_2[\text{GeV}^{-2}]$	$\beta_3[\text{GeV}^{-1}]$	$\beta_4[\text{GeV}^{-1}]$	$\chi^2/d.o.f.$
$\mathcal{O}(p^2)$	-0.495(1)	0.113(0)	0.447(2)	0.136(1)	0.829
$\mathcal{O}(p^3)^*$	-0.767(1)	0.126(0)	0.604(3)	0.093(1)	0.971

Table 4.9: LECs contributing to $I = 1$ KN scattering.

	$\gamma_1[\text{GeV}^{-1}]$	$\gamma_2[\text{GeV}^{-2}]$	$\gamma_3[\text{GeV}^{-1}]$	$\gamma_4[\text{GeV}^{-1}]$	$\chi^2/d.o.f.$
$\mathcal{O}(p^2)$	-0.122(0)	0.0084(0)	0.264(1)	-0.270(1)	0.765
$\mathcal{O}(p^3)^*$	-0.419(2)	0.429(0)	0.616(1)	-0.090(3)	0.471

4.5.2 Fitting strategy two: combined study of baryon masses and meson-baryon scattering

One merit of ChPT is that it connects different observables with the same set of LECs. Thus it is interesting to explore how one observable imposes restrictions on others. In this covariant baryon ChPT framework, baryon masses and scattering process are such a pair of observables which are described by the same Lagrangian. Most of the LECs appear in both the meson-baryon scattering and the baryon masses, such as, b_0, b_D, b_F and $b_{1,\dots,8}$. A naive idea for a combined study of these two observables can be performed in two ways. First, calculating baryon masses at $\mathcal{O}(p^3)$ and using the experimental data as well as the pion-nucleon sigma term to constrain b_0, b_D, b_F , and then with these LECs fixed, study pion-nucleon and kaon-nucleon scattering. Or conversely one can study the

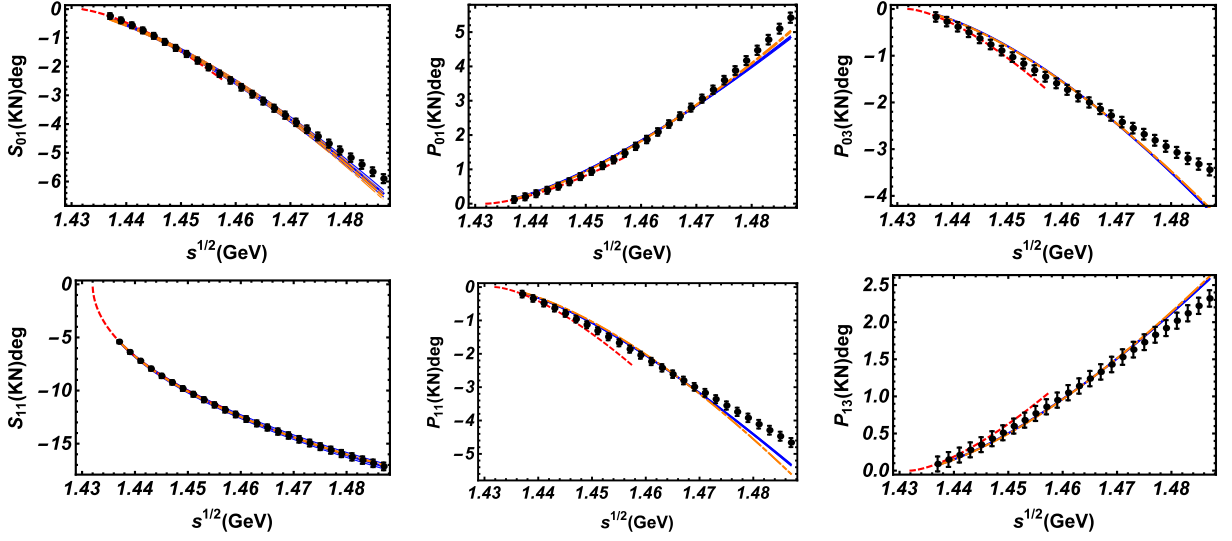


Figure 4.6: $I = 0$ (upper panel) and $I = 1$ (lower panel) KN phase shifts. The orange long-short dashed lines and blue solid lines represent our $\mathcal{O}(p^2)$ and $\mathcal{O}(p^3)^*$ results while the red dashed lines denote those of the HB ChPT [7]. The blue bands correspond to the uncertainties of the $\mathcal{O}(p^3)^*$ results propagated from the uncertainties of the LECs. The error bands of the $\mathcal{O}(p^2)$ results are not shown here to make the figures easier to read. In some partial waves, the error bands are of the size of the thickness of the lines.

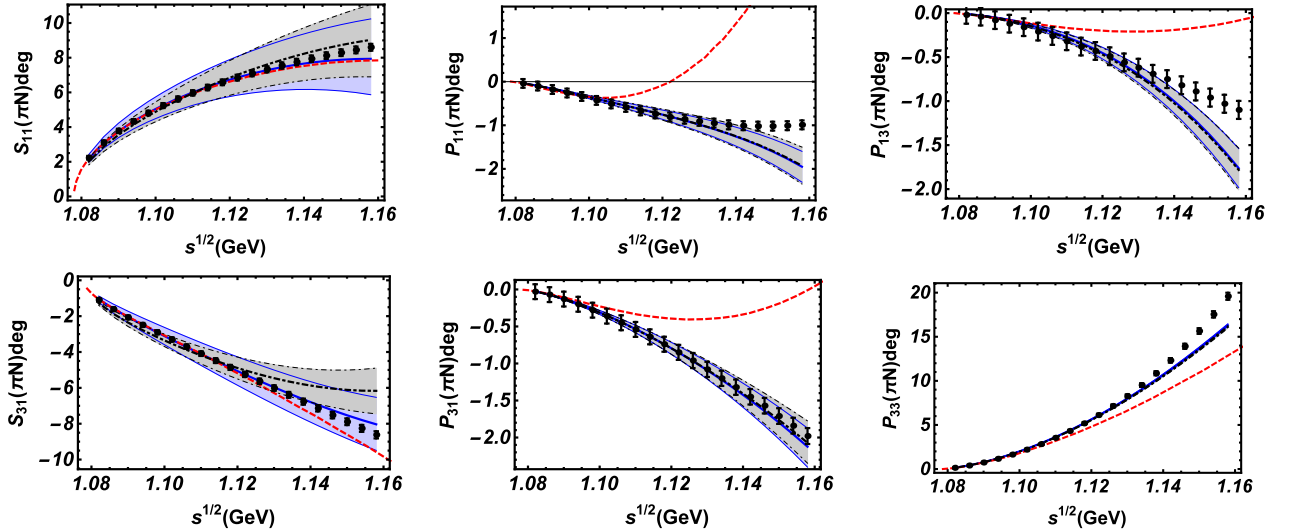


Figure 4.7: Same as Fig. 4.5, but the black dot-dashed lines associated with the black bands denote the EOMS results and their errors with b_0 , b_D , and b_F fixed by fitting to the physical (isospin averaged) octet baryon masses at NNLO. In some partial waves, the error bands are of the size of the thickness of the lines.

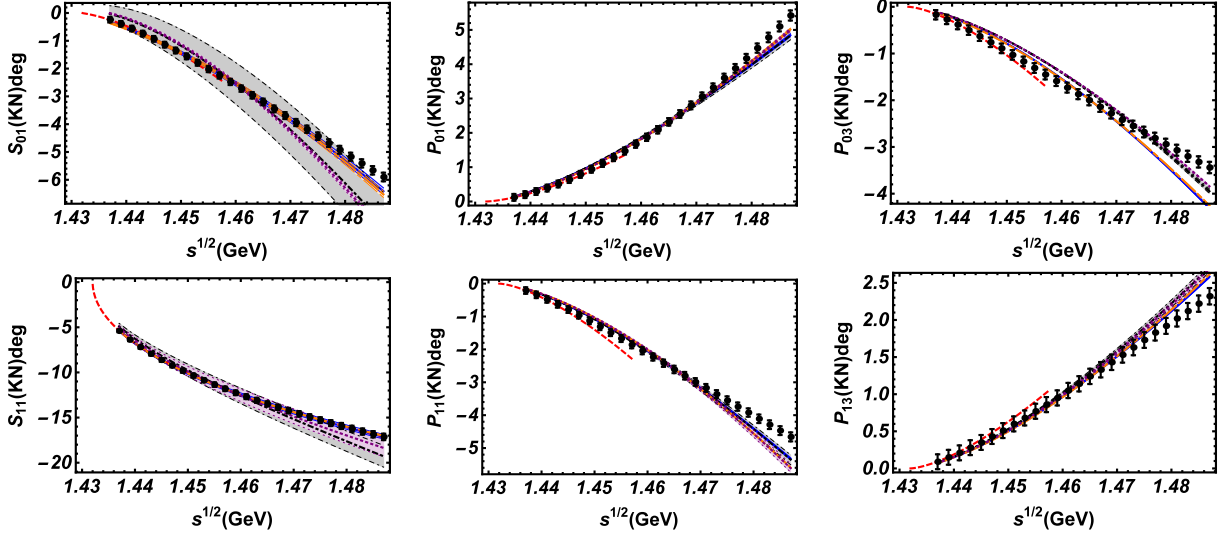


Figure 4.8: Same as Fig. 4.6, but the purple dotted lines and black dot-dashed lines denote the $\mathcal{O}(p^2)$ and $\mathcal{O}(p^3)^*$ results in the EOMS scheme with b_0 , b_D , and b_F fixed by fitting to the physical (isospin averaged) octet baryon masses at NNLO. The black bands correspond to the uncertainties of the $\mathcal{O}(p^3)^*$ results propagated from the uncertainties of the LECs. The error bands of $\mathcal{O}(p^2)$ results (purple) are not shown here to make the figures easier to read. In some partial waves, the error bands are of the size of the thickness of the lines.

baryon masses with some LECs determined via meson-baryon scattering and, furthermore, make predictions on sigma terms ⁵.

However, we note that the LECs actually contribute at different chiral orders to these two observables. In meson baryon scattering, all of these LECs appear at $\mathcal{O}(p^2)$, the second order of the chiral Lagrangian. On the other hand, b_0, b_D, b_F contribute to the baryon masses both at $\mathcal{O}(p^2)$ and $\mathcal{O}(p^4)$ via tree level as well as mass insertions, while $b_{1, \dots, 8}$ only contribute to the baryon masses via tadpole diagrams at $\mathcal{O}(p^4)$. This complicates things a lot. In principle, from the point of view of effective field theories, to achieve a fully self-consistent and combined study of baryon masses and meson-baryon scattering, one needs to renormalize the LECs in the same framework. In other words, the calculation for baryon masses and meson-baryon scattering ought to be performed up to the same order. Otherwise the LECs in these two sectors are mismatched. Thus if one tries to determine $b_{1, \dots, 8}$ through baryon masses, a calculation up to $\mathcal{O}(p^4)$ will be needed, which should be matched with scattering amplitudes also at $\mathcal{O}(p^4)$. As a consequence, the number of LECs will be too large compared with the number of data available both for baryon masses and meson-baryon scattering from experiments and lattice QCD simulations. On the other hand, if one is not so ambitious and only calculates the scattering amplitudes and baryon masses up to $\mathcal{O}(p^3)$, new problems show up. In this case, only 3 parameters (b_0, b_D, b_F) in addition to m_0 appear in the baryon masses. Although the physical baryon masses can be accurately reproduced, the study in Ref. [241] showed that it is not possible to provide a satisfactory description of the LQCD baryon masses up to this order. In addition, the constraints from baryon masses to meson-baryon scattering will be very weak because there are 24 combinations of LECs in meson-baryon scattering up to $\mathcal{O}(p^3)$.

⁵One can of course calculate the sigma terms directly from scattering amplitudes via the corresponding subthreshold parameters using the Cheng-Dashen theorem [262].

Table 4.10: LECs determined by fitting to the experimental baryon masses up to NLO in the EOMS BChPT and the corresponding fitted results, in comparison with the experimental data. All of the masses are in units of GeV.

	m_0	b_0	b_D	b_F
Fit	0.88(FIX)	-0.6232(1)	0.0570(1)	-0.4022(7)
	m_N	m_Λ	m_Σ	m_Ξ
Fit	0.9392	1.1157	1.1862	1.3272
Exp.	0.938925(645)	1.115683(6)	1.19315(430)	1.31828(343)

Taking all these into account, we calculate the baryon masses up to $\mathcal{O}(p^3)$ in the present work. Using the chiral limit baryon mass determined in Ref. [241], $m_0 = 0.880$ GeV, we determine b_0 , b_D , b_F by fitting to the experimental octet baryon masses, with the pseudoscalar decay constants fixed as explained above. The resulting LECs and the fitted octet baryon masses are given in Table. 4.10.

Table 4.11: LECs in the $I = 0$ KN channel with $\beta_4 = b_0 - b_F$ fixed by fitting to the baryon masses.

	$\beta_1[\text{GeV}^{-1}]$	$\beta_2[\text{GeV}^{-2}]$	$\beta_3[\text{GeV}^{-1}]$	$\beta_4[\text{GeV}^{-1}]$	$\chi^2/d.o.f.$
$\mathcal{O}(p^2)$	-0.284(1)	0.144(0)	0.443(3)	-0.221	4.66
$\mathcal{O}(p^3)^*$	-0.582(11)	0.153(3)	0.601(5)	-0.221	3.93

Table 4.12: LECs in the $I = 1$ KN channel with $\gamma_4 = b_0 + b_D$ fixed by fitting to the baryon masses.

	$\gamma_1[\text{GeV}^{-1}]$	$\gamma_2[\text{GeV}^{-2}]$	$\gamma_3[\text{GeV}^{-1}]$	$\gamma_4[\text{GeV}^{-1}]$	$\chi^2/d.o.f.$
$\mathcal{O}(p^2)$	-0.236(11)	-0.033(3)	0.246(5)	-0.566	1.45
$\mathcal{O}(p^3)^*$	-0.604(15)	0.364(4)	0.588(6)	-0.566	2.24

Compared to the fit up to $\mathcal{O}(p^3)$ to the scattering phase shifts, a combined fit of the baryon masses and scattering amplitudes yields a slightly worse description of the scattering phase shifts to some extent. Particularly, the fitting results are worse in the KN channel where the $\chi^2/d.o.f.$ increases by a factor of about 4 with larger error bands. This is understandable as the number of free LECs decreases. Despite of this, the negative effects do not spoil the description. For the p -wave, the descriptions of the phase shifts are of very similar quality, whether one fixes b_0, b_D, b_F or treats them as free LECs. For the s -wave, the differences are rather moderate, particularly in the low energy region. This study indicates that the EOMS BChPT is able to describe the baryon masses and meson-baryon scattering simultaneously, as it should be. Nevertheless, as mentioned at the beginning of this section, to draw a firm conclusion, more systematic studies are needed.

As for the sigma terms, we find that meson-baryon scattering up to $\mathcal{O}(p^3)$ is not very useful at this moment because the tree level contributions at $\mathcal{O}(p^3)$ in the KN channels are neglected, leading to unusually large b_D, b_F compared to an independent study of the baryon masses in, e.g., Ref. [241]. Thus we will refrain from performing such a study here.

4.5.3 Scattering lengths

Scattering lengths, also known as s -wave threshold parameters, can be predicted with the LECs determined above.

The general form of the effective range expansion reads

$$|\mathbf{p}|^{2\ell+1} \cot \delta_{l\pm}^I = \frac{1}{a_{l\pm}^I} + \frac{1}{2} r_{l\pm}^I |\mathbf{p}|^2 + \sum_{n=2}^{\infty} v_{n,l\pm}^I |\mathbf{p}|^{2n}, \quad (4.34)$$

where $|\mathbf{p}|$ refers to the three-momentum of the baryon in the c.m. frame, ℓ is the angular momentum, a is the threshold parameter, r is the effective range and v_n are the shape parameters. We can easily obtain the expression of threshold parameters from Eq. (4.34) by taking the limit of $|\mathbf{p}| \rightarrow 0$ as

$$a_{l\pm}^I = \lim_{|\mathbf{p}| \rightarrow 0} \frac{\tan \delta_{l\pm}^I}{|\mathbf{p}|^{2\ell+1}} = \lim_{|\mathbf{p}| \rightarrow 0} \frac{\text{Re} f_{l\pm}^I}{|\mathbf{p}|^{2\ell}}. \quad (4.35)$$

The scattering lengths for these channels are collected in Table. 4.7.

It is clear that our results based on the EOMS scheme are in very good agreement with the experimental data and the HB results, while the IR results [224] seem to be compatible with data only in the KN channels. We note that for the two πN channels, the LO scattering lengths, to which no unknown LECs contribute, are already compatible with the experimental data. Meanwhile the contributions of the two consecutive orders decrease order by order. Compared to the HB case [7]: $a_{\pi N}^{3/2}(\mathcal{O}(p^2)) = 0.05\text{fm}$, $a_{\pi N}^{3/2}(\mathcal{O}(p^3)) = -0.05\text{fm}$ and $a_{\pi N}^{1/2}(\mathcal{O}(p^2)) = 0.05\text{fm}$, $a_{\pi N}^{1/2}(\mathcal{O}(p^3)) = -0.03\text{fm}$, the EOMS results decrease much faster, indicating that the scattering amplitudes in this covariant framework converge faster than in the non-relativistic calculation close to threshold and the improvement is significant. In the KN channels, one can see that the NLO results can already describe the experimental data. The improvement from $\mathcal{O}(p^3)$ are so tiny that can be neglected. However, different from the πN channels, the LO scattering lengths in the KN channels are far from the corresponding experimental data. As a consequence, relatively large contributions from NLO and NNLO are naturally expected. Indeed our calculations yield extremely large values at $\mathcal{O}(p^2)$ and $\mathcal{O}(p^3)^*$ with significant cancelations. All of these point to a unsatisfying convergence even very close to threshold in the KN channels. Nonetheless, one should keep in mind that we have neglected the $\mathcal{O}(p^3)$ tree level contribution. To draw a firm conclusion, more experimental data or lattice simulations are strongly needed. More discussions can be found in the following subsection.

4.5.4 Convergence of BChPT

The convergence of SU(3) BChPT has remained an issue of heated debate for many years. See, e.g., Ref. [263] for early discussions, and Refs. [242, 264] for more recent studies of baryon magnetic moments and masses. From the latter studies, it seems that the EOMS scheme can speed up the convergence of BChPT, particularly, in the SU(3) sector. Nonetheless, even in the EOMS scheme, the convergence turns out to be relatively slow. The origin of this slow convergence in the SU(3) sector is the large expansion parameter $\frac{M_K}{\Lambda_{\chi PT}}$, which is approximately 1/2 in the

physical world. For a LQCD simulation, the situation can become even worse.

The discussion on the convergence of BChPT for meson-baryon scattering can be dated back to the first attempt in the HB scheme by M. Mojžiš [94] where the convergence of threshold parameters was studied. Afterwards N. Fettes et al. [95] worked out the pion-nucleon scattering amplitudes up to $\mathcal{O}(p^3)$. Their calculation implies that the third-order contributions are in general small in the lower energy region, while there exist large cancelations for higher energies. However, the discussion of convergence is rather limited and no firm conclusion could be drawn there. The situation was significantly improved once the full one-loop results became available [265]. They concluded that the contributions from the fourth-order are, in most partial waves, indeed not large, indicating the convergence of BChPT. Recently, the discussion on this issue based on SU(3) HBChPT were performed in Refs. [225, 7] up to $\mathcal{O}(p^3)$, where a conclusion very similar to those in SU(2) was drawn.

As well known, the HB ChPT recovers a neat power counting rule at a cost of manifestly Lorentz covariance. It suffers from the deficiency that the corresponding perturbation series fail to converge in parts of the low-energy region [86]. Thus an analysis based on covariant BChPT was strongly needed. In Ref. [236], the πN scattering amplitudes were calculated up to $\mathcal{O}(p^3)$ in SU(2) with the EOMS scheme. The authors pointed out that the convergence of the Δ -less amplitudes is questionable because there exists a large cancelation between $\mathcal{O}(p^2)$ and $\mathcal{O}(p^3)$ in almost all partial waves. However, including Δ as an explicit degree of freedom, the amplitudes turn out to present a natural convergence from subthreshold up to energies well above threshold. Very soon after this work, Chen et al. showed [6] that after promoting the calculation to $\mathcal{O}(p^4)$, the convergence pattern is reasonable even without Δ . Later in Ref. [237] a full third order calculation with explicit Δ is performed. More recent studies, such as those of Refs. [236, 238, 240], further confirmed that the convergence pattern is visibly improved in a covariant scheme via a detailed study on threshold and subthreshold parameters, associated with the extracted LECs. They also highlighted the improvements by taking the contributions of resonances such as Δ and Roper into consideration.

It is interesting to check the convergence pattern in SU(3) as well. Nevertheless, one has to be cautious about any conclusion drawn from a leading one-loop study such as the present one. We show the phase shifts of each order in Fig. 4.9 for the πN channels and Fig. 4.10 for the KN channels. For the two π -N S -waves, the LO contribution itself describes the behavior of phase shifts very well in subthreshold regions while the NLO and NNLO terms only provide visible effect at higher energies. Especially in the S_{11} partial wave, the contributions decrease order by order well above threshold, indicating a reasonable convergence. On the other hand, for all the P -waves, the contributions from the NNLO terms are smaller than those from the NLO terms. The LO terms are now of approximately the same size as NLO or even smaller because the partial wave decomposition filters out the LO contact terms. In particular, the ratio of the NNLO over NLO terms can be lower than $1/2$ for the two $J = \frac{3}{2}$ partial waves in quite a wide region above threshold. Despite the cancellation of the NLO and NNLO terms in these partial waves, these smaller ratios actually indicate a reasonable convergence. For the rest partial waves, we find a ratio of $0.7 \sim 0.8$ even very close to threshold, implying a sizable cancelation and, thus, a much slower

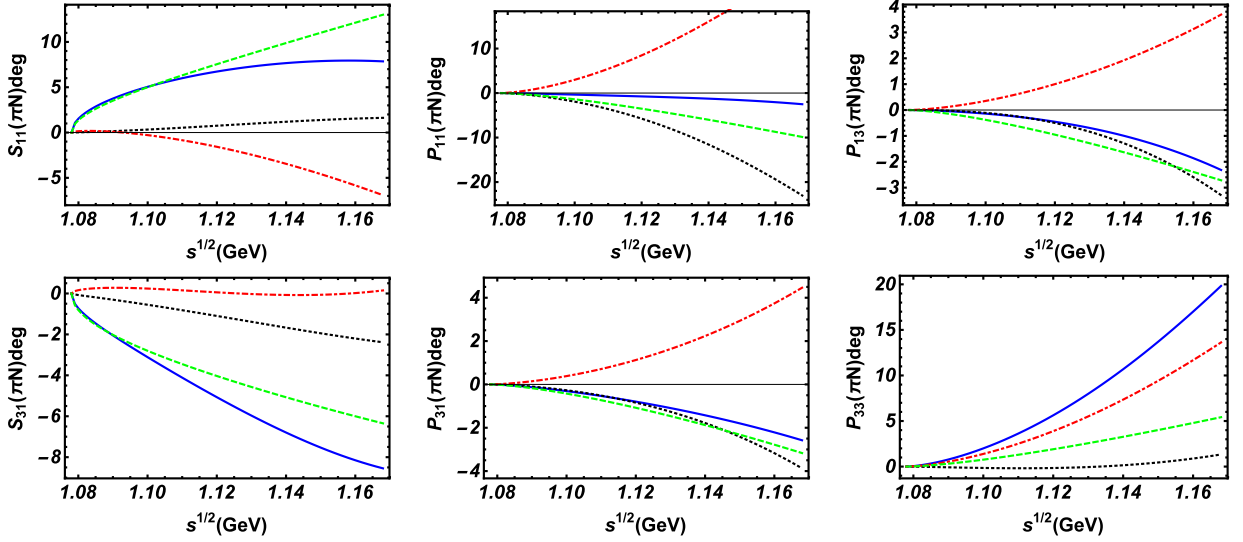


Figure 4.9: Order by order decomposition of the πN phase shifts. The blue lines donate the total results, while those of the $\mathcal{O}(p)$, $\mathcal{O}(p^2)$, and $\mathcal{O}(p^3)$ are represented by the green-dashed, red-dot-dashed, and black-dotted lines, respectively.

convergence.

For the KN channels, the LO results are in general quite small. This is not only because of the partial wave decomposition, but also because the LO Born term can only contribute via u-channel. In the two S -waves, the third order contribution is compatible with the second order and the large cancelation points to a questionable convergence. However, for most P -waves except P_{13} , the second order contribution dominates the behavior and the third order contribution is significantly smaller than the second order, implying a reasonable convergence, if we ignore the small LO contributions.

In general we do not find a fast decrease of higher order contributions and the conclusion on the convergence to be drawn here is quite similar to that in $SU(2)$. However, we would like to point out that in some P -waves for both the πN and KN channels, the chiral expansions seem to convergence at least near threshold if we only focus on the NLO and NNLO contributions. We ascribe the slower convergence of the two S -waves in the KN channels partially to the fact that we have not taken into account the $\mathcal{O}(p^3)$ tree level contributions. Inspired by the $SU(2)$ studies, we expect that the contributions of the decuplet could significantly improve the convergence pattern at least at $\mathcal{O}(p^3)$. Meanwhile a calculation up to the full one loop order is needed to test the convergence of $SU(3)$ BChPT.

4.5.5 Decuplet contributions

In this section, we evaluate the contributions of the virtual decuplet to meson-baryon scattering by including the lowest order exchange diagrams. For the construction of HBChPT and covariant BChPT with Δ or decuplet fields in general, we refer the reader to Refs. [83, 266], and Ref. [267], respectively.

In the following we show the lowest order contributions of the decuplet adopting the so-called δ -expansion [268].

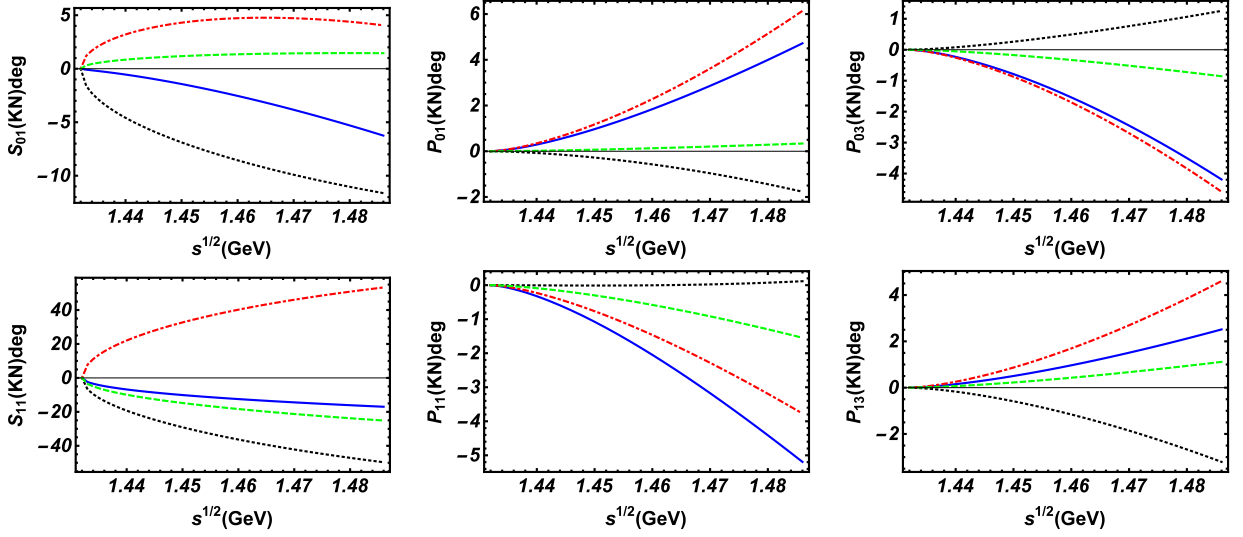


Figure 4.10: Order by order decomposition of the KN phase shifts. The blue lines donate the total results, while those of the $\mathcal{O}(p)$, $\mathcal{O}(p^2)$, and $\mathcal{O}(p^3)^*$ are represented by the green-dashed, red-dot-dashed, and black-dotted lines, respectively.



Figure 4.11: Lowest order contribution from the intermediate decuplet. The double line refers to the spin- $\frac{3}{2}$ propagator.

That is, the decuplet contributions are counted differently for energies well below the resonances or around the resonance peaks:

1. low-energy: $m_\phi \sim p$, $m_\Delta - m_N \sim p^{1/2}$
2. resonance peak: $m_\phi \sim p^2$, $m_\Delta - m_N \sim p$

At the lowest order, the decuplet exchange diagram is shown in Fig.4.11. The relevant effective Lagrangian with decuplet as explicit degrees of freedom is

$$\mathcal{L}_{\Phi BD} = \frac{i\mathcal{C}}{m_{D0}F_\Phi} \epsilon^{abc} (\partial_\alpha \bar{T}_\mu^{ade}) \gamma^{\alpha\mu\nu} B_c^e \partial_\nu \Phi_b^d + H.c. \quad (4.36)$$

where we have adopted the so-called “consistent” coupling scheme for the meson-octet-decuplet vertices [269, 270]. T is the tensor collecting the decuplet baryons, B is the baryon octet, and Φ is the Goldstone boson octet. m_{D0} here refers to the chiral limit decuplet mass. The total antisymmetric gamma matrix products are defined as

$$\gamma^{\mu\nu} = \frac{1}{2}[\gamma^\mu, \gamma^\nu], \quad \gamma^{\mu\nu\rho} = \frac{1}{2}\{\gamma^{\mu\nu}, \gamma^\rho\}. \quad (4.37)$$

Similar to the Born terms, the contribution of the decuplet exchange diagram reads

$$\begin{aligned}
B_{Born}^D(s, B_i, \Phi_i, B_f, \Phi_f, D) &= -\frac{1}{6(s-m_D^2)} \left(-m_D m_i (m_f^2 - M_f^2 + s) - m_D m_f (m_i^2 - M_i^2 + s) \right. \\
&\quad \left. + (m_f^2 - M_f^2 + s) (m_i^2 - M_i^2 + s) - 3s (m_f^2 + m_i^2 - t) - 2s m_f m_i \right), \\
A_{Born}^D(s, B_i, \Phi_i, B_f, \Phi_f, D) &= -\frac{1}{12(s-m_D^2)} \left(s (m_D (4m_f m_i - 6m_f^2 - 6m_i^2 + 6t) \right. \\
&\quad \left. + m_f (-3m_i^2 - 2M_i^2 + 2s + 3t) + m_i (-2M_f^2 - 3m_i^2 + 2s + 3t) \right. \\
&\quad \left. - 3m_f^2 m_i - 3m_f^3 \right) - m_D m_f (m_f + m_i) (m_i^2 - M_i^2 + s) \\
&\quad + (m_f^2 - M_f^2 + s) ((4m_D + m_f + m_i) (m_i^2 - M_i^2 + s) \\
&\quad \left. - m_D m_i (m_f + m_i) \right),
\end{aligned} \tag{4.38}$$

where the symbols $B_i, B_f, D, \Phi_i, \Phi_f$ refer to incoming/outgoing baryons, intermediate decuplet, and incoming/outgoing mesons. Note that in this notation, the coupling constant \mathcal{C} of the meson-octet-decuplet vertices has a factor of $2\sqrt{2}$ compared to the h_A in, for instance, Ref. [6]. Taking this into account, we set $m_{D0} = m_\Delta$ in the fitting process. The B parts of the scattering amplitudes are

$$\begin{aligned}
B_{\pi N}^{I=3/2} &= \frac{2\mathcal{C}^2(B^D(u, N, \pi, N, \pi, \Delta) - 3B^D(s, t, N, \pi, N, \pi, \Delta))}{3f^2 m_{D0}^2}, \\
B_{\pi N}^{I=1/2} &= \frac{8\mathcal{C}^2 B^D(u, N, \pi, N, \pi, \Delta)}{3f^2 m_{D0}^2},
\end{aligned} \tag{4.39}$$

$$\begin{aligned}
B_{KN}^{I=1} &= \frac{\mathcal{C}^2 B^D(u, N, K, N, K, \Sigma^*)}{3f^2 m_{D0}^2}, \\
B_{KN}^{I=0} &= \frac{\mathcal{C}^2 B^D(u, N, K, N, K, \Sigma^*)}{f^2 m_{D0}^2}.
\end{aligned} \tag{4.40}$$

The A parts can be easily obtained with the same replacement as that in the Born terms.

We first follow exactly the same fitting strategy as in the decuplet-less case except enlarging the fitting range up to 1.2GeV in the πN channel. A direct fit of these 9 parameters ($\alpha_{1,\dots,8}, \mathcal{C}$) yields a $h_A = 2.900(44)$, which is almost exactly equal to the value t determined by fitting to the Breit-Wigner width of the Δ , i.e., $\Gamma_\Delta = 118\text{MeV}$ [236, 6]. Thus we fix h_A to be exactly 2.9 and fit(refit) the LECs in the $KN(\pi N)$ channel. The fitting results are collected in Tables 4.6, 4.14, 4.13.

Taking the lowest order contribution into account, we re-plot the phase shifts with the new set of LECs. The results are shown in Figs. 4.12, 4.13. Clearly, the description is compatible with that in the SU(2) case. Compared with the results without the decuplet contributions, the description is obviously improved up to higher energies, especially for the P_{11} channel, as mentioned in the main text. Meanwhile, for the KN channel, taking the decuplet contribution into account or not does not seem to make any noticeable difference.

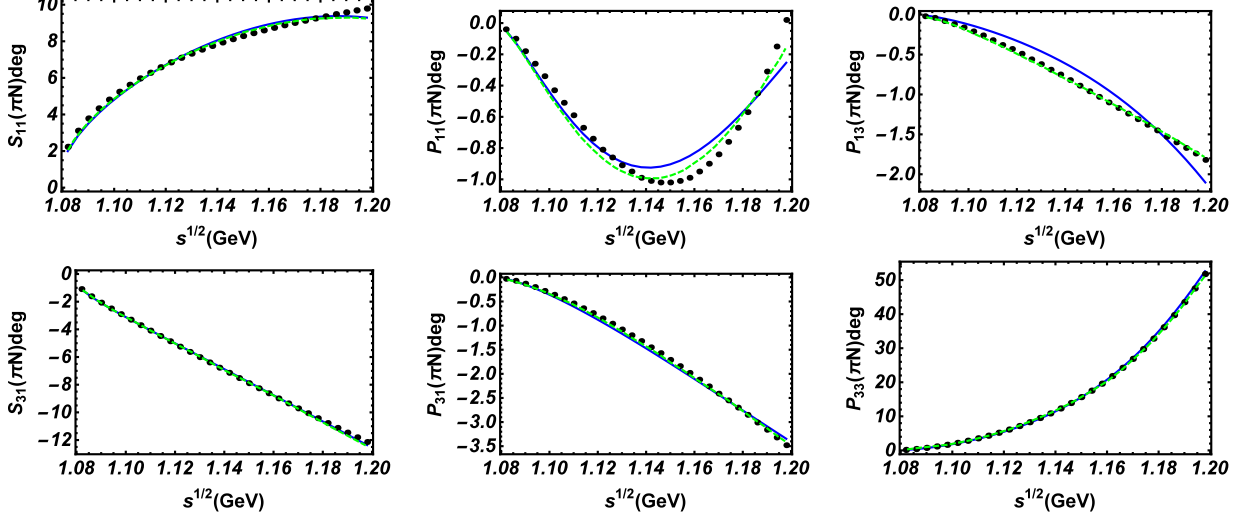


Figure 4.12: πN phase shifts with the lowest order decuplet contribution included. The blue lines are our results in SU(3) while the green dashed lines are the results in SU(2) from Ref. [6]. The black dots denote the experimental data.

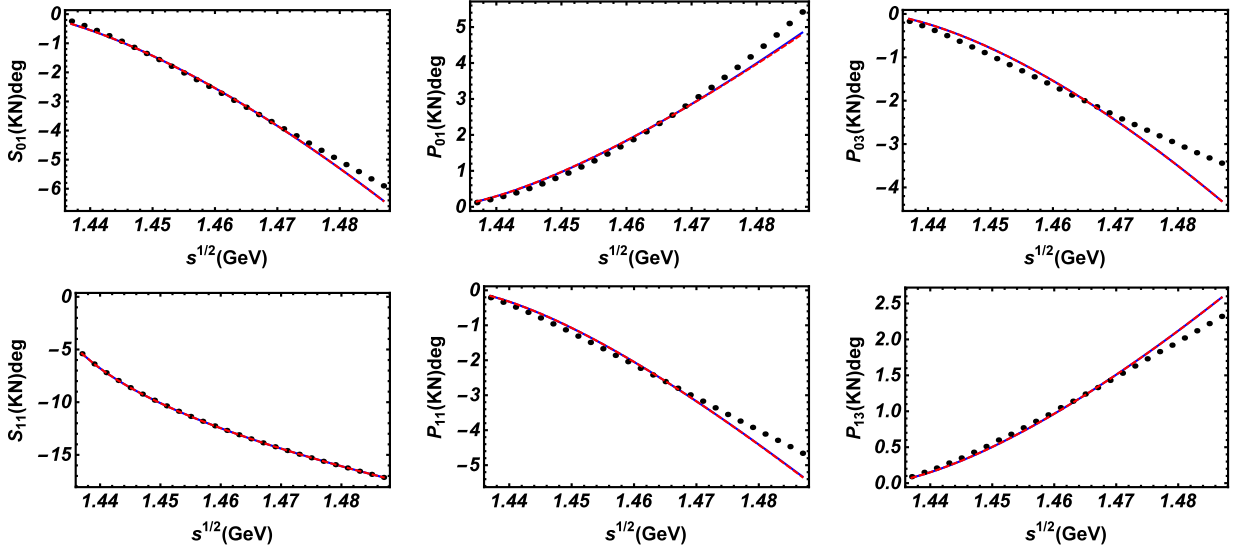


Figure 4.13: KN phase shifts with the lowest order decuplet contribution included. The blue solid lines are our results in SU(3) while the red dashed lines are the results without the decuplet contributions. The black dots denote the experimental data. The blue solid lines and the red dashed lines overlap each other.

Table 4.13: LECs in the $I = 0$ KN channel including the lowest order decuplet contribution with $h_A = 2.9$ at $\mathcal{O}(p^3)^*$.

$\beta_1[\text{GeV}^{-1}]$	$\beta_2[\text{GeV}^{-2}]$	$\beta_3[\text{GeV}^{-1}]$	$\beta_4[\text{GeV}^{-1}]$	\mathcal{C}	$\chi^2/d.o.f.$
-0.831(1)	0.1535(2)	0.608(2)	-0.055(1)	$\frac{h_A}{2\sqrt{2}}$	1.02

Table 4.14: LECs in the $I = 1$ KN channel including the lowest order decuplet contribution with $h_A = 2.9$ at $\mathcal{O}(p^3)^*$.

$\gamma_1[\text{GeV}^{-1}]$	$\gamma_2[\text{GeV}^{-2}]$	$\gamma_3[\text{GeV}^{-1}]$	$\gamma_4[\text{GeV}^{-1}]$	\mathcal{C}	$\chi^2/d.o.f.$
-0.398(22)	0.420(7)	0.615(6)	-0.103(42)	$\frac{h_A}{2\sqrt{2}}$	0.491

One interesting point is that the consideration of the decuplet contributions changes the values of LECs, similar to the case of baryon masses [242]. In the δ -expansion, the leading order decuplet contribution is counted as of $\mathcal{O}(p^{3/2})$. Up to $\mathcal{O}(p^3)$, one is supposed to include the NLO contributions, which counts of as $\mathcal{O}(p^{5/2})$. However, as shown in the SU(2) case [236], the inclusion of the NLO decuplet contribution will only introduce redundant parameters which could be absorbed into \mathcal{C} and $b_0, b_D, b_F, b_1, \dots, 8$.

4.6 Summary

In this chapter, we performed a SU(3) study of the meson-baryon elastic scattering up to $\mathcal{O}(p^3)$ in covariant baryon chiral perturbation theory. Due to lack of experimental data, we only focused on the $\pi N^{I=3/2,1/2}$ and $KN^{I=0,1}$ channels. We applied the extended-on-mass-shell (EOMS) scheme to restore the power counting and determined the corresponding low energy constants by fitting to the experimental phase shifts. We achieved a pretty good description in these channels simultaneously up to 1.16GeV for πN and 1.52GeV for KN . For πN channels, our study in SU(3) shows a compatible description as that in SU(2) and much better compared to the HB SU(3) results. For the KN channels, we found that with only phase shifts one can not uniquely determine all the LECs. Nevertheless, neglecting $\mathcal{O}(p^3)$ tree level contributions, we obtained a description in good agreement with the experimental data.

We attempted a combined study of the baryon masses and meson-baryon scattering up to $\mathcal{O}(p^3)$. We first determined b_0, b_F, b_D using the baryon masses and then kept them fixed in the fitting of the partial wave phase shifts. Our study showed indeed that the EOMS BChPT can describe simultaneously the baryon masses and meson-baryon scattering, but a firm conclusion needs more systematic studies at higher orders.

The predicted scattering lengths for the πN and KN channels are in good agreement with the HB results and the experimental data. In addition, we explored the convergence of BChPT in meson-baryon scattering. The large cancelation between the NLO and NNLO contributions implies an unsatisfying convergence rate, similar to that of the SU(2) sector up to $\mathcal{O}(p^3)$. On the other hand, since in the one baryon sector, chiral orders increase by unit of 1. It might well be the case that one will see cancelations among the contributions of even and odd adjacent orders, as one already noted in the study of decuplet masses.

The predicted phase shifts and scattering lengths for other channels listed in Table. 4.2 for the case of $\mathcal{O}(p^3)^*$ should be taken with caution since the $\mathcal{O}(p^3)$ LECs are not fully determined. Thus additional data, such as the cross sections in the $\bar{K}N$ channel, ought to be taken into account. As the interaction in this channel is by nature non-perturbative, tiled to the existence of a shallow bound state of $\bar{K}N$, $\Lambda(1405)$, we leave such a study to a future work.

Chapter 5

The $\pi\eta$ interaction and a_0 resonances in photon-photon scattering

In the previous chapters, we show how EFT improves the descriptions of experimental data order by order, and how the contradiction between the increasing number of LECs and the limited experimental data prevents further improvements of EFT moving to higher orders. In this chapter, we will turn to pure the mesonic sector to revisit the interaction of $\pi\eta - K\bar{K}$ with $I = 1$ and the two a_0 resonances in this channel, i.e., $a_0(980)$ and $a_0(1450)$, whose positions and widths have remained controversial for a long time, through the final state interactions of photon-photon scattering.

Based on chiral perturbation theory and the unitary relation, we first construct a model for the S -wave amplitudes of $\pi\eta - K\bar{K}$ interactions. Then we deduce the photon-photon scattering via the Muskhelishvili-Omnès (MO) representation [271, 272]. The parameters are fitted to the most recent measurements of photon-photon scattering data with much higher statistics from the Belle Collaboration [8], with which the two a_0 resonances are dynamically generated.

5.1 Introduction

The meson-meson interactions in the low energy regime has been one of the most challenging topics in hadron physics because of the rich spectrum of resonances in a variety of scattering process [273], such as the isoscalar $f_0(500)$ state in $\pi\pi$ scattering and $f_0(980)$ in $\pi\pi - K\bar{K}$ channel, the isovector $a_0(980)$ in $\pi\eta - K\bar{K}$ channel and the isospin one-half $K_0^*(800)$ in πK channel. These lightest scalar resonances are the first observed exotic members in low energy QCD. However, the precise knowledge for most of them are still missing.

Significant progress has been made since the proposal of ChPT [43]. Together with the unitary relation and dispersion relation, ChPT provided people a powerful tool to obtain further and much clear insights into the meson-meson scattering amplitudes. For instance, using the precise $\pi\pi$ scattering data as inputs to determine free param-

eters in the model, people are able to determine the precise pole position of $f_0(500)$ and figure out the most dominant channel for the non-perturbation effect [274]. Through this approach, one can also reproduce $f_0(980)$ with the help of $\pi\pi$ scattering data around 1 GeV [99, 275, 101, 276].

Although the unitary ChPT approach provides such a powerful tool, the disadvantage of this method is equally obvious. Scattering data are indispensable to determine the free parameters in the model. The description of the resonances are highly dependent on the statistics of the input scattering data. As a consequence for $a_0(980)$, the situation is much less clear and its pole position is still controversial [275, 101, 75, 277, 278, 279, 280] because up to now there are no direct experimental $\pi\eta$ scattering data available.

One may also note the recent lattice QCD simulations in Ref. [278]. Besides the $\pi\eta$ channel of our particular interest, $K\bar{K}$ and $\pi\eta'$ channel were also investigated. In Ref. [278], the $\pi\eta$ phase shifts and inelasticity are extracted from the energy levels via Lüscher's method and parametrizing the K matrix in various approaches. They found a pole corresponding to $a_0(980)$ in the fourth Riemann sheet, which is not directly related to the physical sheet. Chiral extrapolation of the lattice simulation was then performed by Guo et al. in Ref. [280] within ChPT in finite volume. Consistent results were observed. However, the simulation was performed with quite a large pion mass $m_\pi = 391\text{MeV}$. Whether the pole still remains in the fourth Riemann sheet after evolving from the heavy pion mass to its physical value needs more discussions.

As a consequence, the $a_0(980)$ properties have to be determined solely from final-state rescattering effects. In the PDG [1], the width of $a_0(980)$ is simply quoted as a range from 50 to 100 MeV. Besides we are more curious about on which unphysical Riemann sheets the a_0 resonances are. This information is closely tied to a better knowledge of the physical scattering T matrix and as a consequence, makes different models distinguishable.

Among the processes containing $\pi\eta$ final state interactions, the photon-photon scattering is the most popular ones. This kind of processes is actually more well-known since it is related to the so-called hadronic light-by-light contribution to the muon $g - 2$ (see, i.e. Ref. [281]). Motivated by this, measurements with quite a high statistics for the photon-photon to $\pi\eta$ process have been recently released by the Belle Collaboration [8], which provides much more precise constrains on the $\pi\eta$ scattering amplitudes. Furthermore, two unexpected points really interest us. In the data analysis afterwards, the authors reported that $a_0(980)$ is best described by a ordinary (i.e. essentially elastic) Breit-Wigner like potential. Besides, the higher resonance $a_0(1450)$ observed has much smaller mass and width, $M_{a_0(1450)} = 1316.8_{-1.0}^{+0.7}\text{MeV}$, $\Gamma = 65_{-5.4}^{+2.1}\text{MeV}$, than the averages in PDG.

Theoretically, the photon-photon to meson-meson processes are free of initial state interactions and satisfy the dispersion relation which is further constrained by the soft pion condition in the case of $\pi\eta$ [282]. In order to obtain the amplitudes, one needs to write the unitary relation and solve the resulting Muskhelishvili-Omnès (MO) equations [271, 272] for such a coupled channel scattering. Although there will not be analytical solutions, it can be solved numerically with well-established mathematical frameworks in which the polynomial ambiguities of the dispersion relation can be taken under control. As was illustrated in the seminal papers [283, 284], a predictive representation can be implemented at the level of the partial-waves with a simple modelling of the left-hand cut.

Recently after the publication of the experimental paper, these data have been re-analysed in Ref. [285] with a Muskhelishvili-Omnès (MO) construction based on a specific meson-meson T matrix model [286]. Including also the $a_2(1320)$ resonance but without $a_0(1450)$ a good description of the data up to 1.1 GeV and a qualitative description up to 1.4 GeV has been achieved. The $a_0(980)$ pole, in this model, lies on the fourth Riemann sheet, which is consistent with the lattice QCD simulations.

We perform here a global fit which takes into account both $\pi\eta$ and $K\bar{K}$ photon-photon data including all the differential cross sections up to 1.4 GeV. For the meson-meson interactions, we follow the S -wave coupled-channel T matrix model developed in ref. [75] unitarized in the way introduced in Chapter 3 but with a slightly different convention for G . The S -wave photon-photon amplitudes are then deduced from a modified MO representation with a left hand cut from cross-channel vector meson exchanges. This is quite similar to ref. [285], but we differ mainly by using chiral symmetry, which allows to fix one of the two subtraction constants through a soft pion theorem¹. The $J = 2$ partial-waves are described more phenomenological as a sum of cross-channel resonance exchanges and a direct $a_2(1320)$ Breit-Wigner amplitude. The $\gamma\gamma \rightarrow (K\bar{K})_{I=1}$ amplitudes are then combined with $I = 0$ amplitudes taken from a previous work [287] which considered $\gamma\gamma \rightarrow (\pi\pi)_{I=0,2}, (K\bar{K})_{I=0}$ in order to reconstruct the physical $K^+K^-, K^0\bar{K}^0$ amplitudes.

5.2 Framework

5.2.1 Scattering amplitudes and right hand cuts

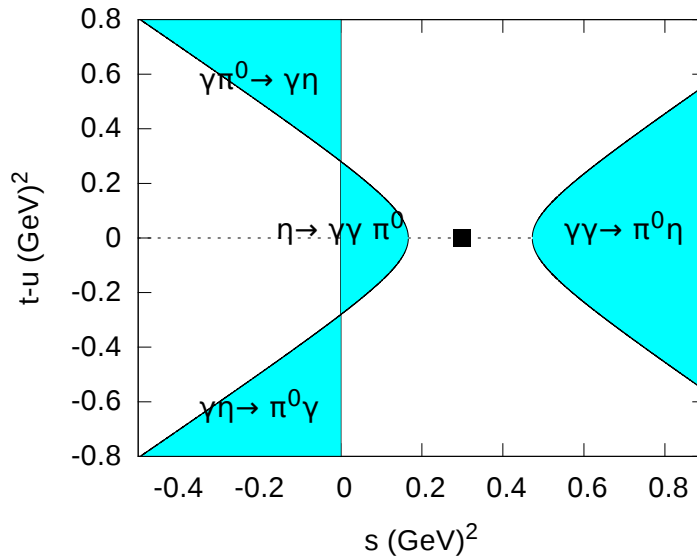


Figure 5.1: Physical regions for $\gamma\gamma \rightarrow \pi\eta, \gamma\pi \rightarrow \gamma\eta$ scattering and $\eta \rightarrow \gamma\gamma\pi^0$ decay.

¹A further difference is that the soft photon constraints at $s = 0$ are not imposed in the dispersion relations used in [285].

In the helicity basis, the amplitudes for $\gamma(q_1)\gamma(q_2) \rightarrow M_1(p_1)M_2(p_2)$ can be written in general as

$$\langle M_1(p_1)M_2(p_2)|\gamma(q_1, \lambda)\gamma(q_2, \lambda') \rangle = ie^2(2\pi)^4\delta(P_f - P_i) e^{i(\lambda-\lambda')\phi} A_{\lambda\lambda'}(s, t), \quad (5.1)$$

in which q_i, p_i are the momentum for incoming photons and outgoing mesons. s, t are Mandelstam variables defined in the usual sense

$$s = (q_1 + q_2)^2, \quad t = (q_1 - p_1)^2, \quad u = (q_1 - p_2)^2. \quad (5.2)$$

The various physical regions in the $s, t - u$ Mandelstam plane for the $\gamma\gamma \rightarrow \pi\eta, \gamma\pi \rightarrow \gamma\eta$ and $\eta \rightarrow \gamma\gamma\pi$ processes are shown on Fig. 5.1.

The amplitude above can be further deduced into tensor amplitude as

$$e^{i(\lambda-\lambda')\phi} A_{\lambda\lambda'}(s, t) = \epsilon_1^\mu(q_1, \lambda)\epsilon_2^\nu(q_2, \lambda')W_{\mu\nu}(q_1, q_2, p_1, p_2). \quad (5.3)$$

By gauge invariance, the tensor amplitude $W_{\mu\nu}$ must satisfy the two Ward identities

$$q_1^\mu W_{\mu\nu} = q_2^\nu W_{\mu\nu} = 0. \quad (5.4)$$

The tensor amplitude $W^{\mu\nu}$ can then be expressed in terms of two scalar amplitudes A, B as

$$W^{\mu\nu}(q_1, q_2, p_1, p_2) = A(s, t, u)T_1^{\mu\nu} + B(s, t, u)T_2^{\mu\nu}, \quad (5.5)$$

where

$$\begin{aligned} T_1^{\mu\nu} &= \frac{1}{2}sg^{\mu\nu} - q_1^\nu q_2^\mu \\ T_2^{\mu\nu} &= 2s\Delta^\mu \Delta^\nu + 4q_1 \cdot \Delta q_2 \cdot \Delta g^{\mu\nu} \\ &\quad - 4q_2 \cdot \Delta q_1^\nu \Delta^\mu - 4q_1 \cdot \Delta q_2^\mu \Delta^\nu, \end{aligned} \quad (5.6)$$

with $\Delta = p_1 - p_2$.

With all the formula above, the amplitudes in helicity basis are

$$\begin{aligned} A_{++} &= A_{--} = \frac{s}{2} A(s, t) + s(2m_1^2 + 2m_2^2 - s) B(s, t), \\ A_{+-} &= A_{-+} = \sin^2 \theta \lambda_{12}(s) B(s, t), \end{aligned} \quad (5.7)$$

with $\lambda_{12} = (s - (m_1 + m_2)^2)(s - (m_1 - m_2)^2)$, $\cos \theta = \frac{t-u}{\sqrt{\lambda_{12}}}$. The differential cross sections for the scattering

process of our interest then reads

$$\frac{d\sigma^{\gamma\gamma \rightarrow M_1 M_2}}{d \cos \theta} = \frac{\pi \alpha^2}{4s^2} \sqrt{\lambda_{12}(s)} (|A_{++}|^2 + |A_{+-}|^2). \quad (5.8)$$

with $\alpha \equiv \frac{e^2}{4\pi} \simeq \frac{1}{137}$ the fine structure constant.

Following the partial wave decomposition and unitary method in section 2.4, the right hand cuts for the $\gamma\gamma \rightarrow \pi\eta(K\bar{K})$ can be expressed as

$$\text{Im} \begin{pmatrix} l_{0,++}(s) \\ k_{0,++}(s) \end{pmatrix} = T_J^*(s) \Sigma(s) \begin{pmatrix} l_{0,++}(s) \\ k_{0,++}(s) \end{pmatrix}, \quad (5.9)$$

where $T_J^*(s)$ collects the meson-meson scattering amplitudes for the $\pi\eta - K\bar{K}$ coupled channel, $\Sigma(s)$ the phase space integral, $l_{0,++}$ and $k_{0,++}$ denote the partial wave amplitudes for photon-photon scattering to $\pi\eta$ and $K\bar{K}$ final states respectively. The final amplitudes $L_{\lambda\lambda'}$ and $K_{\lambda\lambda'}$ can be obtained via

$$\begin{pmatrix} L_{\lambda\lambda'} \\ K_{\lambda\lambda'} \end{pmatrix} = \sum_J (2J+1) \begin{pmatrix} l_{J,\lambda\lambda'} \\ k_{J,\lambda\lambda'} \end{pmatrix} d_{\lambda-\lambda',0}^J(\theta). \quad (5.10)$$

5.2.2 Left hand cuts

Born amplitudes

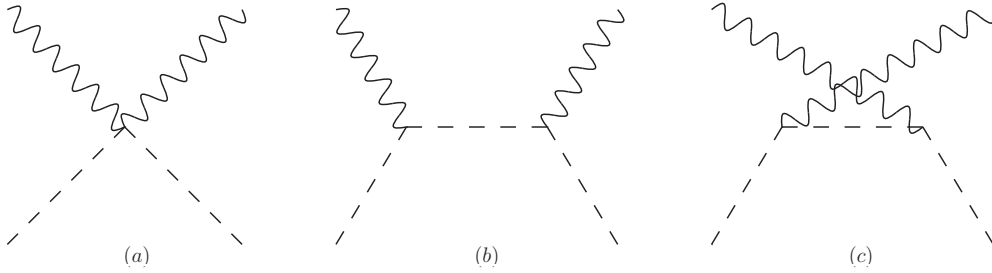


Figure 5.2: Born amplitudes of $\gamma M \rightarrow \gamma M$.

The left hand cut part in the $\gamma\gamma$ scattering comes from singularities in the cross channel as depicted in Fig. 5.2. The scalar amplitudes reduced following the decomposition mentioned above reads

$$\begin{aligned} A_P^{Born}(s, t, u) &= \frac{s}{(t - m_P^2)(u - m_P^2)}, \\ B_P^{Born}(s, t, u) &= \frac{1}{2(t - m_P^2)(u - m_P^2)}, \end{aligned} \quad (5.11)$$

with $P = K^+, \pi^+$. In the present work, since the neutral channel $\pi\eta$ is free of such terms, we only need to pay

attention to the charged channel, $K\bar{K}$, which reads

$$\begin{aligned}
k_{0,++}^{1,Born}(s) &= -\frac{2\sqrt{2}m_{K^+}^2}{s}L_{K^+}(s), \\
k_{2,++}^{1,Born}(s) &= -\frac{2m_{K^+}^2}{s\beta_{K^+}^2(s)}[(\beta_{K^+}^2(s)-3)L_{K^+}(s)+6], \\
k_{2,+ -}^{1,Born}(s) &= \frac{\sqrt{6}}{4s\beta_{K^+}^2(s)}\left[(1-\beta_{K^+}^2(s))^2L_{K^+}(s)+\frac{10}{3}\beta_{K^+}^2(s)-2\right].
\end{aligned} \tag{5.12}$$

with

$$\begin{aligned}
\beta_P(s) &= \sqrt{1-4m_P^2/s}, \\
L_{K^+}(s) &= \frac{1}{\beta_{K^+}(s)}\log\frac{1+\beta_{K^+}(s)}{1-\beta_{K^+}(s)}.
\end{aligned} \tag{5.13}$$

The superscripts for $k_{J,+}^{1,Born}$ refer to $I=1$ and the subscripts donate the total angular momentum and the helicities of initial photons.

Vector meson exchanges

Besides the QED born terms, the vector meson exchanges through cross channel will contribute to the left hand cuts in a similar way. The leading order effective Lagrangian for $V \rightarrow P\gamma$ vertex reads

$$\mathcal{L}_{VP\gamma} = eG_{VP}\epsilon^{\mu\nu\alpha\beta}F_{\mu\nu}\partial_\alpha PV_\beta, \tag{5.14}$$

in which G_{VP} denotes the couplings constants for the correspond vertices, V and P collect the vector meson nonet and pseudoscalar meson octet.

Expressions for the amplitudes of vector exchange born diagrams are straightforward,

$$W_V^{\mu\nu} = \frac{e^2G_{VP_1}G_{VP_2}}{m_V^2-t}\left(\frac{s-4t-2m_1^2-2m_2^2}{2}T_1^{\mu\nu} + \frac{1}{4}T_2^{\mu\nu}\right) + (t \leftrightarrow u), \tag{5.15}$$

where the coupling constants G_{VP_1}, G_{VP_2} for each intermediate vector propagator are related to the corresponding decay width via

$$\Gamma_{V \rightarrow P\gamma} = \alpha \frac{G_{VP}^2(m_V^2 - m_P^2)^3}{2 \cdot 3m_V^3}, \tag{5.16}$$

with $\alpha \equiv \frac{e^2}{4\pi} \simeq \frac{1}{137}$ the fine structure constant. The corresponding partial wave amplitudes for $J=0, 2$ and non-vanishing combinations of helicities are

$$\begin{aligned}
l_{0,++}^V(s) &= G_{V\pi}G_{V\eta}2s(1-m_V^2L_V(s)), \\
l_{2,++}^V(s) &= G_{V\pi}G_{V\eta}m_V^2s\left\{(1-3X_V^2(s))L_V(s) + \frac{6X_V(s)}{\sqrt{\lambda_{12}(s)}}\right\}, \\
l_{2,+ -}^V(s) &= \frac{\sqrt{6}}{8}G_{V\pi}G_{V\eta}\left\{\lambda_{12}(s)(1-X_V^2(s))^2L_V(s) - \frac{2}{3}\sqrt{\lambda_{12}(s)}X_V(s)(3X_V^2(s)-5)\right\},
\end{aligned} \tag{5.17}$$

where

$$\begin{aligned} X_V(s) &= \frac{s - m_1^2 - m_2^2 + 2m_V^2}{\sqrt{\lambda_{12}(s)}}, \\ L_V(s) &= \frac{\log(X_V(s) + 1) - \log(X_V(s) - 1)}{\sqrt{\lambda_{12}(s)}}. \end{aligned} \quad (5.18)$$

The discontinuity of L_V occurs when $X_V^2 - 1 < 0$, which leads to a left hand cut from minus infinity to s_V ,

$$s_V = -\frac{(m_1^2 - m_V^2)(m_2^2 - m_V^2)}{m_V^2}. \quad (5.19)$$

The corresponding left hand cut can then be easily calculated

$$\text{Im}[L_V(s + i\epsilon)] = -\frac{\pi}{\sqrt{\lambda_{12}(s)}}\theta(s_V - s), \quad (5.20)$$

with which the left hand cut for the whole vector meson exchange amplitudes reads

$$\begin{aligned} \frac{1}{\pi}\text{Im}[l_{0,++}^V(s)] &= 2C_{V\pi}C_{V\eta}\frac{s m_V^2}{\sqrt{\lambda_{12}(s)}}\theta(s_V - s), \\ \frac{1}{\pi}\text{Im}[l_{2,++}^V(s)] &= C_{V\pi}C_{V\eta}\frac{s m_V^2}{\sqrt{\lambda_{12}(s)}}(3X_V^2(s) - 1)\theta(s_V - s), \\ \frac{1}{\pi}\text{Im}[l_{2,+-}^V(s)] &= -\frac{\sqrt{6}}{8}C_{V\pi}C_{V\eta}\sqrt{\lambda_{12}(s)}(1 - X_V^2(s))^2\theta(s_V - s). \end{aligned} \quad (5.21)$$

Similarly, one can obtain the left hand cut for the $K\bar{K}$ channel once isospin factors are taken into account. In this case, the effective coupling constant is

$$\tilde{C}_{K^*}^{(1)} \equiv \frac{1}{\sqrt{2}}(-C_{K^*K^+}^2 + C_{K^*K^0}^2). \quad (5.22)$$

Table 5.1: Radiative widths of vector mesons and corresponding coupling constants. The relative signs of the couplings are determined assuming flavour symmetry.

	Γ (keV)	$C_{VP}(\text{GeV}^{-1})$
$\rho^0 \rightarrow \pi^0\gamma$	69(9)	0.368(24)
$\rho^0 \rightarrow \eta\gamma$	44(3)	0.789(30)
$\omega \rightarrow \pi^0\gamma$	713(26)	1.160(20)
$\omega \rightarrow \eta\gamma$	3.8(4)	0.222(11)
$\phi \rightarrow \pi^0\gamma$	5.5(2)	0.067(1)
$\phi \rightarrow \eta\gamma$	55(1)	0.345(4)
$K^{*\pm} \rightarrow K^\pm\gamma$	50(5)	0.418(22)
$K^{*0} \rightarrow K^0\gamma$	116(11)	-0.636(30)

5.2.3 Muskhelishvili-Omnès representations

The MO method is one of the most sufficient method for dealing with final state interactions. It has been applied to study $\gamma\gamma \rightarrow \pi\pi$ scattering by Gourdin and Martin [288], which is similar to the problem in the present work.

The main idea of the MO representation is first to construct an adjoint amplitude \tilde{F} in terms of the amplitude of our interest F and parts of the left hand cut F_L , with a special chosen Omnes function $\Omega(s)$. Schematically it can be expressed as

$$\tilde{F}(s) = \frac{F(s) - F_L(s)}{\Omega(s)}. \quad (5.23)$$

The Omnes function $\Omega(s)$ is constructed to only contain the same unitary cut with the final state interactions,

$$\text{Im}\Omega_J(s) = T_J(s)\Sigma(s)\Omega_J^*(s), \quad (5.24)$$

which makes the ratio $F(s)/\Omega(s)$ in the right hand side free of right hand cuts, i.e. $\text{Disc}[F(s)/\Omega(s)] = 0$. As a consequence, the dispersion relation applied on \tilde{F} will only contain the unitary cut and left hand cut part of $F(s)$, which is usually much easier to calculate.

In the present work, we follow a modified MO representation applied in Ref. [287], in which only the QED born term piece is subtracted, i.e., $F_L \equiv F_L^{\text{Born}}$. Therefore, the adjoint amplitude \tilde{F} contains both right hand cuts and left and cuts.

Model for $\pi\eta - K\bar{K}$ final state interactions

We first briefly recall the approach for the T matrix responsible for the meson-meson interactions, which is the key input in the MO representation for the photon-photon scattering. A variety of methods have been applied to investigate this issue, including the N/D method based on dispersion relations [286], a K matrix inspired approach [289], inverse amplitude method(IAM) [290] and chiral perturbation theory [290, 280]. However, as mentioned in the very beginning, the lack of direct experimental data results in inconsistent descriptions of the amplitudes from different approaches, which further leads to the ambiguity of the positions for the two a_0 resonances. In this work, we model the T matrix following the K matrix approach in Ref. [289], which has explicit matching relations to the chiral amplitudes. This kind of approach was initiated in [291], See ref. [292] for a review. Here we only briefly recall the parametrization of this approach and refer to Ref. [289] for more details.

The T matrix for the meson-meson scattering amplitudes can be written as

$$\mathbf{T}(s) = (\mathbf{1} - \mathbf{K}(s)\Phi(s))^{-1} \mathbf{K}(s), \quad (5.25)$$

where $\Phi(s)$ denotes the two-point scalar integral

$$\Phi(s) = \begin{pmatrix} \alpha_1 + \beta_1 s + 16\pi \bar{J}_{\eta\pi}(s) & 0 \\ 0 & \alpha_2 + \beta_2 s + 16\pi \bar{J}_{KK}(s) \end{pmatrix}, \quad (5.26)$$

with α_i, β_i phenomenological subtraction terms. The \mathbf{K} matrix collects the leading order and next-to-leading order potentials from ChPT, as well as a phenomenological approximation of the $\mathcal{O}(p^6)$ piece, which reads

$$\mathbf{K}(s) = \mathbf{K}_{(2)}(s) + \mathbf{K}_{(4)}(s) + \mathbf{K}_{(6)}(s), \quad (5.27)$$

where the subscripts are the chiral orders. The $\mathbf{K}_{(6)}(s)$ reads

$$\begin{aligned} [\mathbf{K}_{(6)}(s)]_{ij} &= \lambda \frac{g_i g_j}{16\pi} \left(\frac{1}{m_8^2 - s} - \frac{1}{m_8^2} \right), \\ g_1 &= \frac{\sqrt{6}}{3F_\pi^2} (c'_d(s - m_\eta^2 - m_\pi^2) + 2c'_m m_\pi^2), \\ g_2 &= \frac{1}{F_\pi^2} (c'_d(s - 2m_K^2) + 2c'_m m_K^2), \end{aligned} \quad (5.28)$$

where g_1, g_2 are derived from a resonance chiral Lagrangian [293]. In this model, there will be 7 free parameters, that is, $\alpha_1, \beta_1, \alpha_2, \beta_2, m_8, \lambda$ and the ratio c'_m/c'_d . This is essentially the same method mentioned in section. 2.4, but with an extra phenomenological $\mathcal{O}(p^6)$ piece. The ratio c'_m/c'_d is expected to be of order 1 – 2. We will use $c'_m/c'_d = 2$ as the central value and include the variation as a source of error.

For the L_i in the NLO chiral amplitudes, we apply the same values with those in Ref. [289]. Obviously, such a model which implements two-channel unitarity is mostly justified in the $a_0(980)$ region and below. We will assume that it remains qualitatively acceptable up to $E \simeq 1.4$ GeV. The T matrix is computed from Eq. 5.25 for $E \leq E_1$, $E_1 = 1.5$ GeV. In the higher energy region $E > E_1$, the T matrix is described through a simple interpolation of the phase-shifts and the inelasticity such that $\delta_{11}(\infty) = 2\pi$, $\delta_{22}(\infty) = 0$ and $\eta(\infty) = 1$. These conditions introduce a smooth cutoff in the integral equations satisfied by the matrix elements of the MO matrix and ensure the existence of a unique solution.

Amplitudes for the S-waves

With all the analytical properties, i.e., the right hand cut and left hand cut mentioned in the preceding section, we are ready to write the dispersion representation for the photon-photon to meson-meson scattering amplitudes. Since the S-wave amplitudes obey soft-photon theorems [294, 295], the ratios $l_{0++}(s)/s$ and $(k_{0++}^1(s) - k_{0++}^{1,Born}(s))/s$ remain finite when $s \rightarrow 0$. Thus they can be constructed via un-subtracted dispersion relations in terms of their

right hand cut and left hand cut as

$$\begin{aligned}
l_{0++}(s) &= s \left[\frac{1}{\pi} \int_{-\infty}^{s_V} ds' \frac{\text{Im} [l_{0++}(s')]}{s'(s'-s)} + \frac{1}{\pi} \int_{m_+^2}^{\infty} ds' \frac{\text{Im} [l_{0++}(s')]}{s'(s'-s)} \right], \\
k_{0++}^1(s) &= k_{0++}^{1,Born}(s) + s \left[\frac{1}{\pi} \int_{-\infty}^{s_{K^*}} ds' \frac{\text{Im} [k_{0++}(s')]}{s'(s'-s)} + \frac{1}{\pi} \int_{m_+^2}^{\infty} ds' \frac{\text{Im} [k_{0++}(s')]}{s'(s'-s)} \right],
\end{aligned} \tag{5.29}$$

where $m_+ = m_\pi + m_\eta$, s_V and s_{K^*} the branching points of the left hand cut for the corresponding vector meson exchange terms.

Under the assumption of two-channel unitarity the dispersion relations in Eq. 5.29 lead to a set of coupled inhomogeneous Muskhelishvili equations. They can be solved in terms of a two-channel MO matrix which satisfies a homogeneous set of coupled equations in terms of the T matrix for the $\pi\eta - K\bar{K}$ interactions. The MO representation for such a coupled channel problem is

$$\begin{pmatrix} \phi_1(s) \\ \phi_2(s) \end{pmatrix} \equiv \Omega_0^{-1}(s) \begin{pmatrix} l_{0++}(s)/s \\ (k_{0++}^1(s) - k_{0++}^{1,Born}(s))/s \end{pmatrix}, \tag{5.30}$$

where the $\Omega_0(s)$ refers to the 2×2 Omnès function satisfying

$$\Omega_0(s) = \frac{1}{\pi} \int_{m_+^2}^{\infty} \frac{ds'}{s'-s} \mathbf{T}(s) \Sigma(s) \Omega_0^*(s). \tag{5.31}$$

To obtain a unique solution of the integral equation above, boundary condition are necessary. For $s \rightarrow \infty$, asymptotic conditions on the phase-shifts are imposed. At $s = 0$ we take

$$\Omega_0(0) = \begin{pmatrix} 1 & 0 \\ 0 & 1 \end{pmatrix}. \tag{5.32}$$

Applying dispersion relations on the left hand side of Eq. 5.30, one can obtain the MO-type representation for the photon-photon scattering amplitudes

$$\begin{pmatrix} l_{0++}(s) \\ k_{0++}^1(s) \end{pmatrix} = \begin{pmatrix} 0 \\ k_{0++}^{1,Born} \end{pmatrix} + s \Omega_0(s) \begin{pmatrix} b_l + L_1(s) + R_1(s) \\ b_k + L_2(s) + R_2(s) \end{pmatrix}, \tag{5.33}$$

where the b_l , b_k denote the subtraction constants, L_i , R_i the dispersive integrals over left hand cut and right hand cut respectively, which read

$$\begin{aligned}
L_i(s) &= \frac{s - s_A}{\pi} \left\{ \int_{-\infty}^{s_V} \frac{ds'}{s'(s'-s_A)(s'-s)} \Omega_{i1}^{-1}(s') \text{Im} [l_{0++}^V(s')] + \right. \\
&\quad \left. \int_{-\infty}^{s_{K^*}} \frac{ds'}{s'(s'-s_A)(s'-s)} \Omega_{i2}^{-1}(s') \text{Im} [k_{0++}^V(s')] \right\}, \\
R_i(s) &= - \frac{s - s_A}{\pi} \int_{4m_K^2}^{\infty} \frac{ds'}{s'(s'-s_A)(s'-s)} \text{Im} [\Omega_{i2}^{-1}(s')] k_{0++}^{1,Born}(s').
\end{aligned} \tag{5.34}$$

Note that in the dispersion integral above, we have introduced the Adler zero as a subtraction point. In the soft pion limit for $\gamma\gamma \rightarrow \pi\eta$ where the four-momentum p_1 for pion vanishes, one has

$$s = m_\eta^2, \quad t = u = 0. \quad (5.35)$$

At this limit, the amplitude $\gamma\gamma \rightarrow \pi\eta$ vanishes exactly,

$$A(m_\eta^2, 0)T_1^{\mu\nu} + B(m_\eta^2, 0)T_2^{\mu\nu} = [A(m_\eta^2, 0) + 2m_\eta^2 B(m_\eta^2, 0)]T_1^{\mu\nu} = 0, \quad (5.36)$$

The expression in front of $T_1^{\mu\nu}$ is just the L_{++} helicity amplitude in the soft pion limit. Although the soft pion limit is not physical, this zero should be held in realistic cases within corrections of $\mathcal{O}(m_\pi^2)$. As a consequence, the physical L_{++} should also have a Adler zero at $s_A = m_\eta^2 + \mathcal{O}(m_\pi^2)$ with $t = u$ or $\cos\theta = 0$. Considering the decomposition

$$L_{++}(s, \cos\theta = 0) = \sum_{j \text{ even}} (2j+1) (-1)^{j/2} \frac{(j-1)!!}{j!!} l_{j,++}(s), \quad (5.37)$$

the partial waves with $J \geq 2$ are suppressed by the angular momentum barrier factor, indicating that the $J = 0$ partial wave dominates. The soft pion condition therefore implies that the $J = 0$ partial-wave should satisfy $l_{0,++}(m_\eta^2) = \mathcal{O}(m_\pi^2)$ such that an Adler zero should be present in this partial-wave amplitude,

$$l_{0,++}(s_A) = 0. \quad (5.38)$$

Under the assumption of the existence of an Adler zero in $l_{0,++}$, one can derive a relation between the two subtraction constants b_l and b_k at $s = s_A$

$$b_l = -b_k \Omega_{12}(s_A) / \Omega_{11}(s_A). \quad (5.39)$$

The b_k will finally be determined by fitting to the experimental data.

Amplitudes for the D-waves

For the $J = 2$ partial wave, one must take into account the s-channel resonance $a_2(1320)$. However, it is difficult to deal with the amplitudes fulfilling the unitary relation like the S-wave cases because in the energy region of our interest, a large variety of decay channels are open, such as $\rho\pi$, $\pi\eta$, $K\bar{K}$, $\omega\pi\pi$ and so on. Their decay branching ratios are [1]

$$\begin{aligned} B_{\eta\pi} &= (14.5 \pm 1.2)\%, & B_{K\bar{K}} &= (4.9 \pm 0.8)\%, \\ B_{\rho\pi} &= (70.1 \pm 2.7)\%, & B_{\omega\pi\pi} &= (10.6 \pm 3.2)\%. \end{aligned} \quad (5.40)$$

As a consequence, we choose to approximate the right hand cut of the D-wave amplitudes with a phenomenological Breit-Wigner approach.

The effective Lagrangians for the two vertices $\gamma\gamma \rightarrow a_2$ and $a_2 \rightarrow \pi\eta$ are

$$\begin{aligned}\mathcal{L}_{a_2\eta\pi} &= C_{\eta\pi}^{a_2} T_{\mu\nu}(x) \partial^\mu \eta(x) \partial^\nu \pi^0(x), \\ \mathcal{L}_{T\gamma\gamma} &= e^2 T_{\mu\nu}(x) \left\{ C_{\gamma\gamma}^{a_2} F^{\mu\beta}(x) F_{\beta}{}^\nu(x) + \frac{D_{\gamma\gamma}^{a_2}}{m_T^2} \partial^\mu F^{\alpha\beta}(x) \partial^\nu F_{\alpha\beta}(x) \right\},\end{aligned}\tag{5.41}$$

where $T_{\mu\nu}$ refers to the tensor field for $a_2(1320)$, $F_{\mu\nu}$ the field strength tensor, $C_{\eta\pi}^{a_2}$ and $C_{\gamma\gamma}^{a_2}$ ($D_{\gamma\gamma}^{a_2}$) the coupling constants for the corresponding vertices. The coupling constants can be determined via the partial decay widths, which read

$$\begin{aligned}\Gamma[a_2 \rightarrow \eta\pi] &= \frac{(C_{\eta\pi}^{a_2})^2 (q_{\eta\pi}(m_T^2))^5}{60\pi m_T^2}, \\ \Gamma[a_2 \rightarrow \gamma\gamma] &= \frac{e^4 m_T^3}{80\pi} \left((C_{\gamma\gamma}^{a_2})^2 + \frac{1}{6} (D_{\gamma\gamma}^{a_2})^2 \right),\end{aligned}\tag{5.42}$$

with $q_{\eta\pi}$ the momentum in the C.M. frame. Utilizing the branching ratios listed in Eq. 5.40 and the total decay width $\Gamma_{a_2} = 107 \pm 5 \text{ MeV}$ [1], the coupling constants are determined to be

$$\begin{aligned}\Gamma_{\gamma\gamma}^{a_2} &= 1.00 \pm 0.06 \text{ keV}, \\ C_{KK}^{a_2} &= -(10.5 \pm 0.9) \text{ GeV}, \\ C_{\eta\pi}^{a_2} &= (10.8 \pm 0.5) \text{ GeV}^{-1}, \\ \sqrt{(C_{\gamma\gamma}^{a_2})^2 + \frac{1}{6} (D_{\gamma\gamma}^{a_2})^2} &= (0.115 \pm 0.005) \text{ GeV}^{-1}.\end{aligned}\tag{5.43}$$

Note that although we can only obtain the absolute values for the 4 coupling constants via the partial decay widths, the relative signs can be easily determined with simple numerical experiments when fitting to the experimental data.

Collecting all the pieces above, the Breit-Wigner form amplitudes can be constructed following the same width function for the $a_2(1320)$ propagator with that applied in the experimental publication [8], which read

$$\begin{aligned}l_{2^{++}}^{BW}(s') &= \frac{D_{\gamma\gamma}^{a_2} C_{\eta\pi}^{a_2}}{60 m_T^2} \sqrt{\frac{W_2(q_{\eta\pi}(m_T^2)R)}{W_2(q_{\eta\pi}(s')R)}} \frac{s' \lambda_{\eta\pi}(s')}{m_T^2 - s' - im_T \Gamma_T(s)}, \\ l_{2^{+-}}^{BW}(s') &= \frac{\sqrt{6} C_{\gamma\gamma}^{a_2} C_{\eta\pi}^{a_2}}{60} \sqrt{\frac{W_2(q_{\eta\pi}(m_T^2)R)}{W_2(q_{\eta\pi}(s')R)}} \frac{\lambda_{\eta\pi}(s')}{m_T^2 - s' - im_T \Gamma_T(s)}.\end{aligned}\tag{5.44}$$

with

$$\begin{aligned}\Gamma_T(s) &= \sum \Gamma_{X_1 X_2}(s), \\ \Gamma_{X_1 X_2}(s) &= \Gamma_{a_2} \mathcal{B}(a_2 \rightarrow X_1 X_2) \left(\frac{q_X(s)}{q_X(m_{a_2}^2)} \right)^5 \frac{W_2(q_X(s)r_{a_2})}{W_2(q_X(m_{a_2}^2)r_{a_2})},\end{aligned}\tag{5.45}$$

Table 5.2: Parameters of the two-channel T matrix in the two fits.

	α_1	$\beta_1(\text{GeV}^{-2})$	α_2	$\beta_2(\text{GeV}^{-2})$	$m_8(\text{GeV})$	λ	χ^2
fit I	4.00(8)	-2.23(4)	-0.545(5)	0.167(6)	1.304(4)	0.47(4)	428
fit II	0.98(3)	-4.07(1)	-0.495(1)	-0.18(1)	0.900(2)	1.064(1)	439

where X_1, X_2 denote the outgoing particles, Γ_{a_2} the total decay width, $W_2(x) = 1/(9 + 3x^2 + x^4)$ the Blatt-Weisskopf related function, and $r_{a_2} = 3.09 \pm 0.53(\text{GeV}/c)^{-1}$ the effective interaction radius. For the three-body decay channel $a_2 \rightarrow \omega\pi\pi$, the decay width is $\Gamma = \Gamma_{a_2}\mathcal{B}(a_2 \rightarrow \omega\pi\pi)\frac{s}{m_{a_2}^2}$ instead.

With Eq. 5.44 and Eq. 5.17, the D-wave amplitudes for $\gamma\gamma \rightarrow \pi\eta(K\bar{K})$ are

$$\begin{aligned}
 l_{2,\lambda\lambda'}(s) &= l_{2,\lambda\lambda'}^{\text{BW}}(s) + l_{2,\lambda\lambda'}^{\text{V}}(s), \\
 k_{2,\lambda\lambda'}(s) &= -\frac{1}{\sqrt{2}}k_{2,\lambda\lambda'}^{\text{QED}}(s) + k_{2,\lambda\lambda'}^{\text{BW}}(s) + k_{2,\lambda\lambda'}^{\text{V}}(s),
 \end{aligned}
 \tag{5.46}$$

where the $-\frac{1}{\sqrt{2}}$ in front of the QED contributions comes from the isospin factor.

5.3 Results and discussions

With the S-wave and D-wave amplitudes obtained in the previous section, we are ready to fit to the experimental data. In the present work, we performed a global fit to the differential cross sections of $\gamma\gamma \rightarrow \pi\eta$ [8] which was done recently in ref. [285] and additionally, the $\gamma\gamma \rightarrow K_S K_S$ data [9]. We will restrict ourselves to the energy range $E \leq 1.4$ GeV: totally 448 differential cross section points for $\pi\eta$ ($0.85 \leq E \leq 1.39$ GeV) and 240 differential cross section points for $K_S K_S$ ($1.105 \leq E \leq 1.395$ GeV). Older data with much less statistic such as the $\gamma\gamma \rightarrow K^+ K^-$ data from the ARGUS Collaboration are omitted.

Note that to obtain the cross sections for $K_S \bar{K}_S$, we also need the amplitude for $\gamma\gamma \rightarrow (K\bar{K})_{I=0}$, which has been calculated with a similar MO representation in Ref. [287]. As a consequence, besides the 6 parameters in the T matrix for the $\pi\eta - K\bar{K}$ scattering, we have 7 extra parameters, i.e., the coupling constants $C_{\gamma\gamma}^{a_2}, D_{\gamma\gamma}^{a_2}$ to $a_2(1320)$ for the $I = 1$ channel, the coupling constants $C_{\gamma\gamma}^{f_2}, D_{\gamma\gamma}^{f_2}$ to $f_2(1270)$ for the $I = 0$ channel, the mass and width m_{a_2} and Γ_{a_2} for $a_2(1320)$, as well as the subtraction constant b_k in the MO representation. The other one b_l can then be determined via the Adler zero by Eq.5.39. Therefore, we have totally 13 parameters.

We performed a standard least squares chi square fit with the package MINUIT. At first, we have kept the T matrix parameters fixed to be one of the sets determined previously in Ref. [75] (which, in particular, used the pole positions of the two a_0 resonances as input). It was not possible to obtain a good fit of the $\gamma\gamma$ data in this manner: using these sets of parameter values one finds that the $\pi\eta$ cross sections at the $a_0(980)$ peak tends to be too large and the energy of the peak tends to be somewhat displaced compared to experiment. Relaxing the T matrix parameters, we actually obtained two distinct minimums of the total χ^2 of the global fit, as exhibited in Table. 5.2.

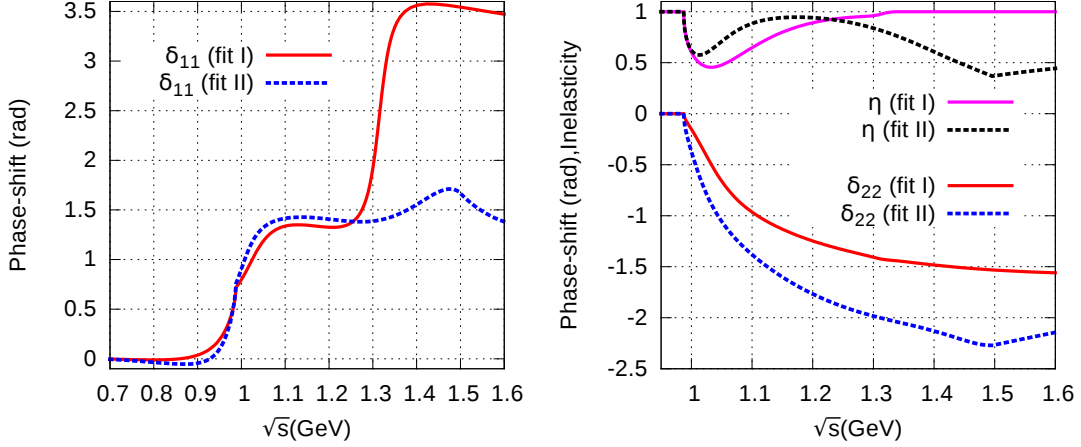


Figure 5.3: Phase-shifts and inelasticity from the two-channel T matrix model using the two sets of parameters corresponding to the two χ^2 minimums.

In Fig. 5.3 we show the phase shifts δ_{11} , δ_{22} and of the inelasticity η as a function of energy, corresponding to the two fits. At low energies, the two sets of parameters lead to similar behaviors of T matrix. One may note that the $\pi\eta$ phase shifts change sign and become negative below $K\bar{K}$ threshold. This low-energy behaviour is not anticipated in simple hadronic models of the $\pi\eta$ amplitude (e.g. [296]) but it was also observed to emerge from fitting the $\gamma\gamma$ data in ref. [297].

At higher energies, the behaviors of the two fits are significantly different. For fit I, we observe a clear sharp increase around $E \simeq 1.32\text{GeV}$ and a platform afterwards in the phase shift, indicating a narrow resonance in the usual sense. Indeed, we find a resonance pole in the T matrix located on the third Riemann sheet with the value

$$\sqrt{s_{a'_0}} = 1315(4) - i 24(3) \text{ MeV} \quad (\text{fit I}) . \quad (5.47)$$

Though a'_0 is much lower and narrower compared to the average of $a_0(1450)$ in PDG, it is quite consistent with the $a_0(Y)$ found in the best fit of the Belle Collaboration [8] via a completely different parameterization.

In fit II we also find a resonance a'_0 but this time, it locates at

$$\sqrt{s_{a'_0}} = 1421(5) - i 175(4) \text{ MeV} \quad (\text{fit II}) , \quad (5.48)$$

the mass of which is consistent with experimental value but the width is much broader.

The differential cross sections for $\gamma\gamma \rightarrow \pi\eta$ and $\gamma\gamma \rightarrow K_S K_{\bar{S}}$ are exhibited in Fig. 5.4 and Fig. 5.5 for the two set of parameters. We find both fitting results are in good agreement with the experimental data and there are no significant differences between them. Similar phenomena can be observed from the total cross sections shown in Fig. 5.6 for the two photon-photon scattering process when integrated over $\cos\theta < 0.8$ as done experimentally. Larger discrepancy is observed only at $E = 1.01\text{GeV}$ in the $\gamma\gamma \rightarrow \pi\eta$ process, which is close to the $K\bar{K}$ threshold. Our results underestimate the differential cross section at this point. Correspondingly the peak in the total cross

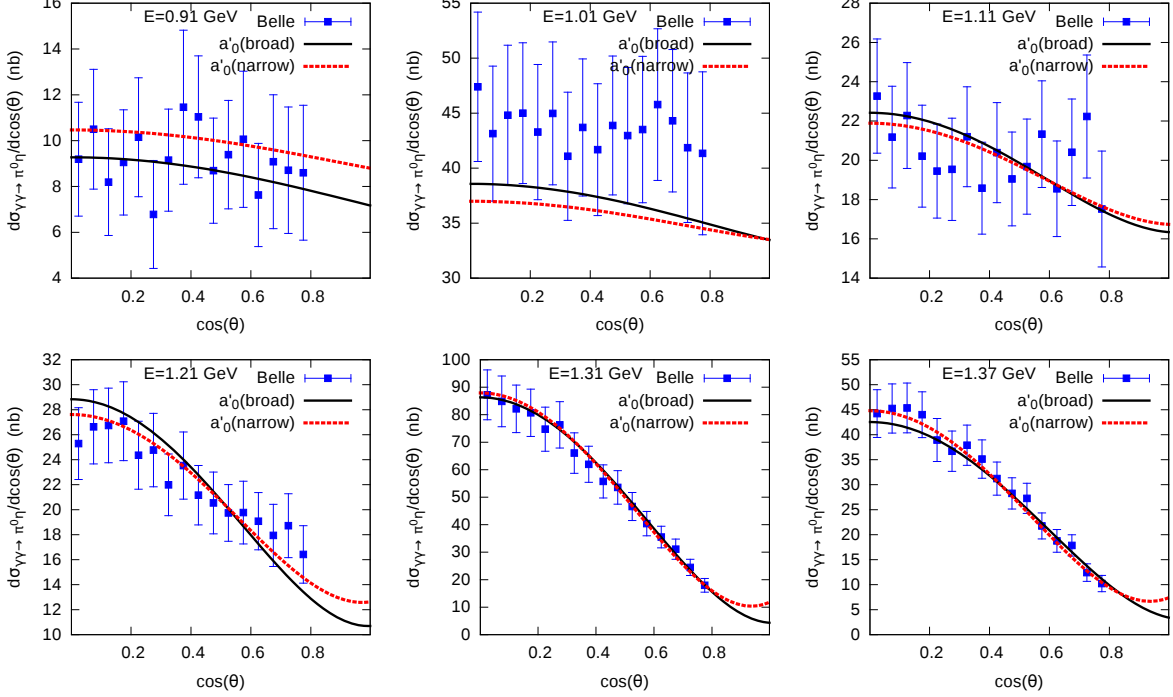


Figure 5.4: Experimental $\gamma\gamma \rightarrow \pi\eta$ differential cross sections compared with the two fits.

sections for this process seems a bit to the left compared to the experimental data. This may be because the Kaon masses applied in our calculation are not exactly the same as those in the experimental analysis. We utilize the masses of charged Kaons as those at the isospin limit $m_K = m_{K^+}$ thus the peak locates at exactly $2m_{K^+}$. Physically the different masses of charged Kaons and neutral Kaons should lead to cusp in the invariant mass distribution.

One may also notice that in the total cross sections of Fit I, no clear signal of a_0' is visible. We attribute this to the interference between the S-wave and D-wave amplitudes. We find that in fit I around $\sqrt{s} \simeq 1.32\text{GeV}$ the contribution from $l_{0,++}$ is approximately proportional to that from the $l_{2,++}$. As a consequence, the a_0 resonance effect in the S-wave is absorbed into the $a_2(1320)$ effect from D-wave and no visible effect remains. In the $K\bar{K}$ channel, the inelasticity around $\sqrt{s} \simeq 1.32\text{GeV}$ is very close to 1, indicating that in this energy region, the $K\bar{K}$ is actually decoupled. Therefore one cannot find any signal of a_0' from $K\bar{K}$ cross sections neither. We thus conclude that Fit I is not favored because of the overlap between the S-wave resonance and the D-wave one.

Now we can focus on the properties of the two a_0 resonances with the parameters from fit II. Corresponding to $a_0(980)$ observed experimentally, we find a resonance at $(1000.7, -i36.6)\text{MeV}$ on the second Riemann sheet, which locates slightly above the $K\bar{K}$ threshold. Compared to the previous studies listed in PDG [1], $a_0(980)$ in our model is closest to the one predicted by Oller in Ref. [99] via the lowest order chiral amplitudes and the one by Guo in Ref. [280] also with leading order chiral amplitude but with constrains from lattice QCD. The three $a_0(980)$ states all locate on the second Riemann sheet. However, the resonance in Ref. [280] moves to the fourth sheet when the calculation is extended up to next-to-leading order, which is consistent with the calculation in Ref. [285] and lattice QCD simulations [278]. One can obtain the coupling constants of this resonance to the $\pi\eta$

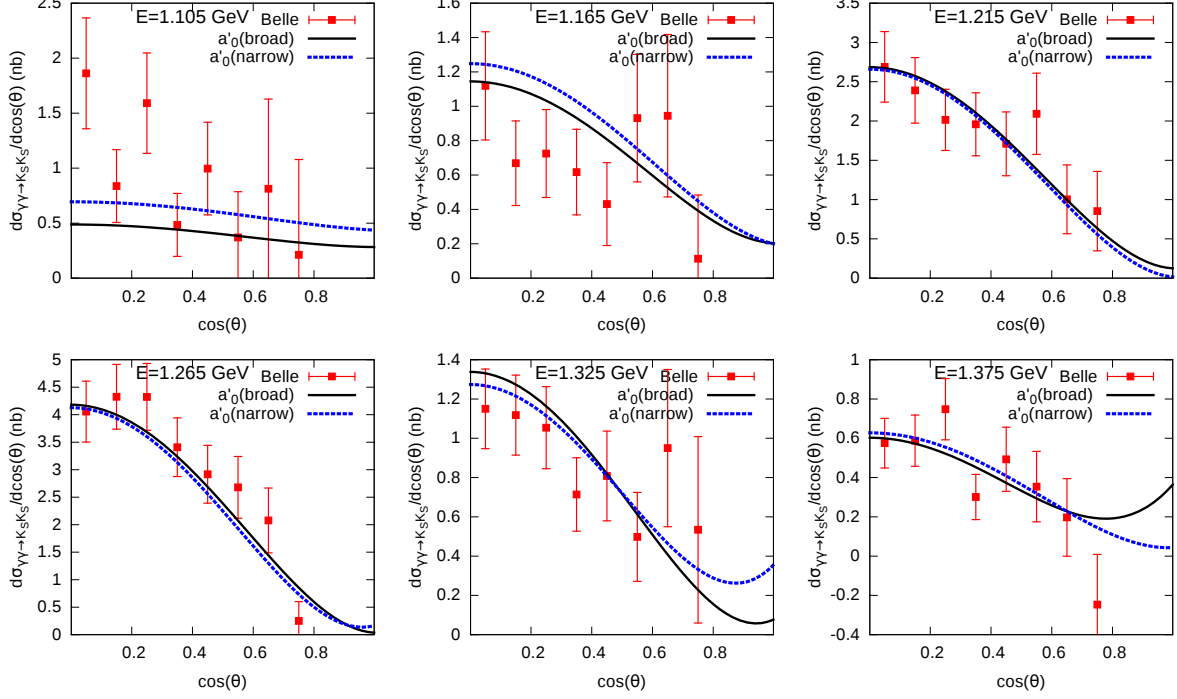


Figure 5.5: Experimental $\gamma\gamma \rightarrow K_S K_S$ differential cross sections compared with the two fits.

Table 5.3: Positions of two a_0 resonances predicted by our model, as well as the coupling constants to each channel.

	Position(MeV)	$ g_{\pi\eta} (\text{GeV})$	$ g_{K\bar{K}} (\text{GeV})$	$\Gamma_{a_0 \rightarrow \gamma\gamma}(\text{keV})$
a_0	1000.7(7) - i 36.6(1.3)(II)	2.17(2)	4.03(2)	0.52(1)
a'_0	1421(5) - i 175(4)(III)	3.15(4)	1.89(4)	1.05(5)

and $K\bar{K}$ channels via

$$\begin{aligned}
 16\pi T_{11}^{(II)}(z) \Big|_{pole} &= \frac{g_{a_0\pi\eta}^2}{z_{a_0} - z}, \\
 16\pi T_{12}^{(II)}(z) \Big|_{pole} &= \frac{g_{a_0\pi\eta} g_{a_0 K\bar{K}}}{z_{a_0} - z},
 \end{aligned} \tag{5.49}$$

where T^{II} denotes the T matrix of meson-meson interactions on the second Riemann sheet. Similarly, the coupling constants to the photon-photon amplitudes and the partial decay width can be calculated via

$$\begin{aligned}
 e^2 l_{0++}^{(II)}(z) \Big|_{pole} &= \frac{g_{a_0\gamma\gamma} g_{a_0\pi\eta}}{z_{a_0} - z}, \\
 \Gamma_{a_0 \rightarrow \gamma\gamma} &= \frac{|g_{a_0\gamma\gamma}|^2}{16\pi m_{a_0}}.
 \end{aligned} \tag{5.50}$$

The results are collected in Table. 5.3.

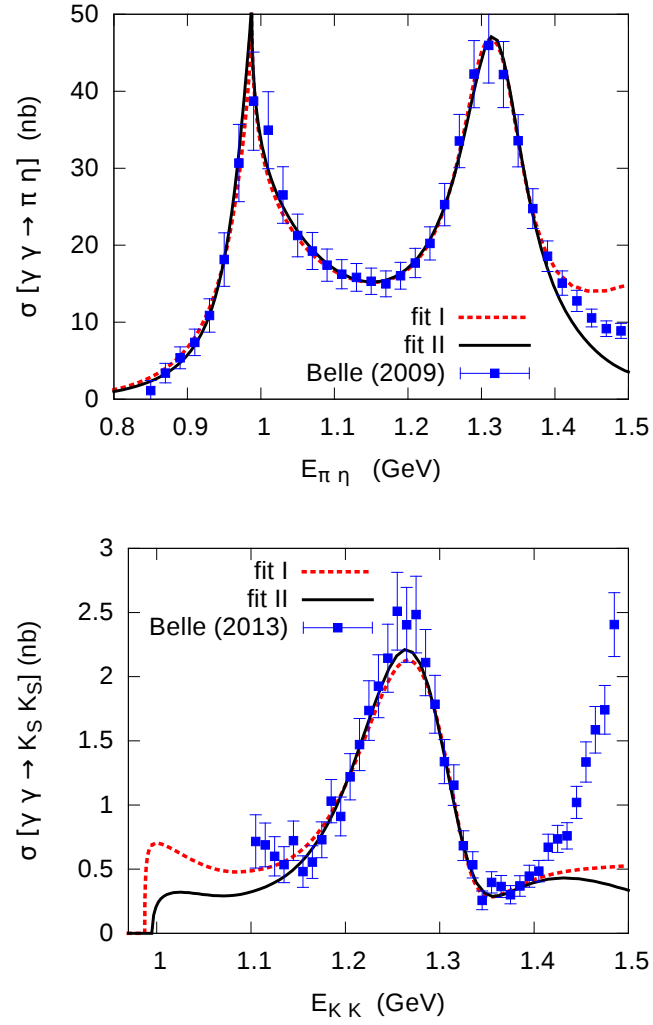


Figure 5.6: Cross sections for $\gamma\gamma \rightarrow \pi\eta, K_S K_S$ integrated in the range $|\cos\theta| < 0.8$. The data are from Refs. [8, 9], they are compared with the two fits.

5.4 Conclusion

In this chapter we revisited the scattering of meson-meson in the isovector channel as final state interactions of photon-photon scattering. We implemented a standard Muskhelishvili-Omnès representation for the $J = 0$ amplitudes in which the left hand cut is modelled from light vector meson exchanges. We followed the K matrix approach in the previous work [75], in which the underlying T matrix satisfies unitarity with two coupled channels ($\pi\eta, K\bar{K}$) and involves six phenomenological parameters. In the case of the $J = 2$ amplitudes the constraints from unitarity are more difficult to implement. Thus a crude description of Breit-Wigner form is used. In order to constrain the free parameters we fitted to both $\pi\eta$ and $K_S K_S$ data with high-statistics data below 1.4 GeV, and we found two different acceptable solutions to the minimisation. In one of our fits the S -wave amplitudes display a light and narrow a'_0 resonance similar to the one found in the Belle analysis. While this is mathematically allowed we have argued that the other fit which displays a broad a'_0 is likely to be more physical.

Concerning the $a_0(980)$ resonance, we find that a rather conventional picture i.e. a pole on the second sheet with a mass and width consistent with the PDG is compatible with both the $\pi\eta$ and the $K_S K_S$ data. This is in contrast with the Belle analysis which uses an elastic Breit-Wigner description and also with the recent analysis of Ref. [285] in which the mass and width are found to be both significantly larger than the PDG values. Data with a better energy resolution would be useful to resolve these remaining ambiguities. The $\gamma\gamma \rightarrow K^+ K^-, K_S K_S$ cross sections close to the $K\bar{K}$ thresholds are also very sensitive to the position of $a_0(980)$. Our results in this energy region are in qualitative agreement with the chiral-unitary calculations from Ref. [298] and with the estimates made in Ref. [299] but not with those from Ref. [300]. Experimental data in this near-threshold region would obviously be very constraining. Finally, it will be quite interesting to see how the pole position determined in a lattice QCD simulation [278] evolves when m_π is decreased.

Chapter 6

Summary and Outlook

In this thesis, we applied effective field theory to study three typical hadron-hadron interactions, i.e., the interaction of singly charmed baryons and Goldstone mesons, those of ground state baryons and Goldstone bosons and those of meson-meson, in each of which we focus on different points.

In the interactions between singly charmed baryons and Goldstone bosons, we mainly focus on the typical non-perturbation phenomena, resonances and their internal structures. In the leading order, under the approximation that all channels with different isospins and strangeness share one common subtraction constant which is fixed by reproducing $\Lambda_c(2595)$, we predicted a number of dynamically generated states, which are contrasted with those of other approaches and available experimental data. These results provide basic information for experimentalists, that where the resonances locate and to which channel they mainly coupled. In order to obtain a better description of the interactions, we attempted to add the next-to-leading order contributions. However, due to the lack of experimental data in these scattering process, we were not able to determine all the low energy constants in the NLO Lagrangian and could only constrain them to be of natural size. As a consequence, our model can hardly make any precise predictions at this order. Despite of this, the molecular interpretation for $\Lambda_c(2595)$ and its counterpart with $J^P = 3/1^-$ was not spoiled at NLO. More experimental data or lattice QCD simulations are highly expected. We then turned back to investigate in detail the structure of $\Lambda_c(2595)$, whose mass has been measured precisely. We first applied the compositeness rule proposed by Weinberg to analyse the components of $\Lambda_c(2595)$ as a molecular state. We found although in different models the component to each channel differs from each other, they are all in favor of a relatively large molecular picture. Besides, it is also obvious that the relative importance from the compositeness rule for each channel is not model independent. We then compared the behavior of $\Lambda_c(2595)$ in the large N_c expansion to the generic qqq baryon. Significant differences were observed, which confirmed the former conclusion.

In the second part, we mainly concentrate on the one-loop level contribution to the meson-baryon scattering, and particularly, its renormalization and convergence. The divergence in the loop diagrams and power counting breaking terms in baryon chiral perturbation theory has been discussed since people first attempted to apply EFT to

baryons. We performed a global fit which includes both πN and $K N$ scattering data, and further more, the baryon masses at the same order. Compared to the results of heavy baryon ChPT, our descriptions were in good agreement with experimental data. Besides, we took the Δ into account, after which we could obtain a good description up to a higher energy region. We then calculated the scattering lengths, which were also consistent with experimental data, and discussed the convergence of covariant baryon ChPT. However, the large number of free parameters made the fit a tough task and we were not able to determine all the related LECs. Therefore, the most interesting point in the $\bar{K}N$ channel, i.e., the double-pole structure of $\Lambda(1405)$, has not been involved yet. With the chiral amplitudes calculated in this present work and a proper unitary method, we will be able to take the non-perturbative effect into account and then determine all the LECs up to $\mathcal{O}(p^3)$ by fitting to the cross sections of $\bar{K}N$. This work is in progress.

In the last part, we combined chiral perturbation theory with dispersion relations to handle a final state interaction problem. The discussions of $\pi\eta$ interaction and the two a_0 resonances in this channel have continued for quite a long time due to the lack of direct experimental data. Lattice QCD collaborations published their results but at a quite large pion mass. With the most recent experimental data on photon-photon scattering, we were able to introduce constraints on the $\pi\eta$ interaction which appears as final state interactions. Fully taking into account the analytical properties of the amplitudes, a Muskhelishvili-Omnès version of dispersion relation was applied and an Adler zero was introduced. We fitted the $\gamma\gamma \rightarrow \pi\eta$ and $\gamma\gamma \rightarrow K_S K_S$ differential cross sections to determine the parameters in the $\pi\eta$ interaction, with which we finally obtained a $a_0(980)$ state slightly above the $K\bar{K}$ threshold and typically on the second Riemann sheet and a broader $a_0(1450)$ on third sheet. On the other hand, the amplitude of photon-photon scattering is related to the decay process $\eta \rightarrow \pi\gamma\gamma$. Since the isospin breaking effect of $\pi - \eta$ mixing plays an important role in this process, I do not present the results here.

In the three scattering processes studied in the present work, we have seen the power of EFT to interpret the experimental data and make predictions, as well the drawback, that is, the increasing number of free parameters. The phenomena in particle physics are so abundant that those involved in the present work are only tiny corners. Taking the meson-baryon interaction without heavy flavors as an example, although the double-pole structure of $\Lambda(1405)$ has been discussed for over sixty years, it still remains controversial nowadays. Besides $\Lambda(1405)$, we still have a variety of excited baryons, such as $\Lambda(1670)$, $\Lambda(1690)$, $\Sigma(1385)$, $\Omega(2012)$ and so on, whose structure needs further investigation. When interactions involves heavy flavors, either hidden or open, the variety of exotic particles, XYZ and P_c , are continually challenging our understanding of the strong interaction. The nucleon-nucleon interaction, which is the building blocks of nuclear physics, is another most challenging topic. Although non-relativistic nucleon force has been calculated up to higher orders, the covariant version falls far behind, let alone the hyperon-hyperon interactions. One can go even further beyond two-body systems to few-body systems. One interesting example is the DK , DDK , $DDDK$ systems [301, 302] where D can be replaced with D^* under heavy quark symmetry. In these few-body systems, DK can bind to form $D_{s0}^*(2317)$ and $D^{(*)}D$ to $X(3872)$ or $Z_c(3900)$. This makes the whole few-body systems bind as a series of counterparts of $D_{s0}^*(2317)$, providing a new

idea to understand hadron spectrum.

Appendix A

Clebsch-Gordan coefficients

In this section, we tabulate the Clebsch-Gordan coefficients appearing in Eq. (3.7) for the anti-triplet (Tables A.1 to A.7) and sextet (Tables A.8 to A.17) ground-state charmed or bottom baryons interacting with the pseudoscalar mesons.

Table A.1: ($S = 1, I = 1/2$)

	$\Lambda_c \mathbf{K}$
$\Lambda_c \mathbf{K}$	1

Table A.2: ($S = 0, I = 1$)

	$\Xi_c \mathbf{K}$	$\Lambda_c \pi$
$\Xi_c \mathbf{K}$	0	1
$\Lambda_c \pi$	1	0

Table A.3: ($S = 0, I = 0$)

	$\Xi_c \mathbf{K}$	$\Lambda_c \eta$
$\Xi_c \mathbf{K}$	-2	$-\sqrt{3}$
$\Lambda_c \eta$	$-\sqrt{3}$	0

Table A.4: ($S = -1, I = 3/2$)

	$\Xi_c \pi$
$\Xi_c \pi$	1

Table A.5: ($S = -1, I = 1/2$)

	$\Xi_c\pi$	$\Xi_c\eta$	$\Lambda_c\bar{K}$
$\Xi_c\pi$	-2	0	$\sqrt{3/2}$
$\Xi_c\eta$	0	0	$-\sqrt{3/2}$
$\Lambda_c\bar{K}$	$\sqrt{3/2}$	$-\sqrt{3/2}$	-1

Table A.6: ($S = -2, I = 1$)

	$\Xi_c\bar{K}$
$\Xi_c\bar{K}$	1

Table A.7: ($S = -2, I = 0$)

	$\Xi_c\bar{K}$
$\Xi_c\bar{K}$	-1

Table A.8: ($S = 1, I = 3/2$)

	$\Sigma_c\mathbf{K}$
$\Sigma_c\mathbf{K}$	2

Table A.9: ($S = 1, I = 1/2$)

	$\Sigma_c\mathbf{K}$
$\Sigma_c\mathbf{K}$	-1

Table A.10: ($S = 0, I = 2$)

	$\Sigma_c\pi$
$\Sigma_c\pi$	2

Table A.11: ($S = 0, I = 1$)

	$\Xi'_c K$	$\Sigma_c\eta$	$\Sigma_c\pi$
$\Xi'_c K$	0	$-\sqrt{3}$	$-\sqrt{2}$
$\Sigma_c\eta$	$-\sqrt{3}$	0	0
$\Sigma_c\pi$	$-\sqrt{2}$	0	-2

Table A.12: ($S = 0, I = 0$)

	$\Xi'_c\mathbf{K}$	$\Sigma_c\pi$
$\Xi'_c\mathbf{K}$	-2	$-\sqrt{3}$
$\Sigma_c\pi$	$-\sqrt{3}$	-4

Table A.13: ($S = -1, I = 3/2$)

	$\Xi'_c\pi$	$\Sigma_c\bar{K}$
$\Xi'_c\pi$	1	$\sqrt{2}$
$\Sigma_c\bar{K}$	$\sqrt{2}$	0

Table A.14: ($S = -1, I = 1/2$)

	$\Xi'_c\pi$	$\Xi'_c\eta$	$\Omega_c K$	$\Sigma_c\bar{K}$
$\Xi'_c\pi$	-2	0	$-\sqrt{3}$	$\frac{1}{\sqrt{2}}$
$\Xi'_c\eta$	0	0	$-\sqrt{3}$	$\frac{3}{\sqrt{2}}$
$\Omega_c K$	$-\sqrt{3}$	$-\sqrt{3}$	-2	0
$\Sigma_c\bar{K}$	$\frac{1}{\sqrt{2}}$	$\frac{3}{\sqrt{2}}$	0	-3

Table A.15: ($S = -2, I = 1$)

	$\Xi'_c\bar{K}$	$\Omega_c\pi$
$\Xi'_c\bar{K}$	1	$\sqrt{2}$
$\Omega_c\pi$	$\sqrt{2}$	0

Table A.16: ($S = -2, I = 0$)

	$\Xi'_c\bar{K}$	$\Omega_c\eta$
$\Xi'_c\bar{K}$	-1	$\sqrt{6}$
$\Omega_c\eta$	$\sqrt{6}$	0

Table A.17: ($S = -3, I = 1/2$)

	$\Omega_c\bar{K}$
$\Omega_c\bar{K}$	2

Appendix B

Tree amplitudes and renormalization of LECs

B.1 Tree level contact terms

In this subsection, we list the contributions of the tree-level contact terms of πN and KN scattering. To simplify the expressions, we first define

$$\begin{aligned}\nu_\pi &= (-s + m_N^2 + m_\pi^2)^2 + (m_N^2 + m_\pi^2 - u)^2, \\ \nu_K &= (-s + m_N^2 + m_K^2)^2 + (m_N^2 + m_K^2 - u)^2.\end{aligned}\tag{B.1}$$

The contributions in the respective channels are

- $\pi N^{I=3/2}$

$$\begin{aligned}B_{\pi N}^{I=3/2} &= -\frac{1}{2f^2} + \frac{2(s-u)(b_5 + b_6 + b_7 + b_8)}{f^2} - \frac{8m_N(c_1 + c_2)}{f^2} \\ &\quad - \frac{4(d_2\nu_\pi + d_4(t - 2m_\pi^2) - 2d_{49}m_\pi^2)}{f^2} - \frac{8m_N(s-u)(d_{10} + d_8)}{f^2},\end{aligned}\tag{B.2}$$

$$\begin{aligned}A_{\pi N}^{I=3/2} &= \frac{2m_\pi^2(-2b_0 + b_1 + b_2 + b_3 + 2b_4 - b_D - b_F) - t(b_1 + b_2 + b_3 + 2b_4)}{f^2} \\ &\quad + \frac{2(s-u)(c_1 + c_2)}{f^2} + \frac{2(s-u)^2(d_{10} + d_8)}{f^2}.\end{aligned}\tag{B.3}$$

- $\pi N^{I=1/2}$

$$B_{\pi N}^{I=1/2} = \frac{1}{f^2} + \frac{2(s-u)(b_5 + b_6 + b_7 + b_8)}{f^2} + \frac{16m_N(c_1 + c_2)}{f^2} - \frac{8(-d_2\nu_\pi + d_4(2m_\pi^2 - t) + 2d_{49}m_\pi^2)}{f^2} - \frac{8m_N(s-u)(d_{10} + d_8)}{f^2}, \quad (\text{B.4})$$

$$A_{\pi N}^{I=1/2} = \frac{2m_\pi^2(-2b_0 + b_1 + b_2 + b_3 + 2b_4 - b_D - b_F) - t(b_1 + b_2 + b_3 + 2b_4)}{f^2} - \frac{4(s-u)(c_1 + c_2)}{f^2} + \frac{2(s-u)^2(d_{10} + d_8)}{f^2}. \quad (\text{B.5})$$

- $KN^{I=1}$

$$B_{KN}^{I=1} = -\frac{1}{f^2} + \frac{2(2b_5 + 2b_7 + b_8)(s-u)}{f^2} - \frac{4m_N(4c_2 + c_3)}{f^2} - \frac{8m_N(s-u)(d_{10} + d_7 + d_8)}{f^2} + \frac{4(\nu_K(-d_1 + d_2 + d_3) + 2m_K^2(-d_4 + d_{48} - d_{49} + d_5 + d_{50} - d_6) + t(d_4 - d_5 + d_6))}{f^2}, \quad (\text{B.6})$$

$$A_{KN}^{I=1} = \frac{4m_K^2(-b_0 + b_1 + b_2 + b_4 - b_D) - 2t(b_1 + b_2 + b_4)}{f^2} + \frac{(s-u)(4c_2 + c_3)}{f^2} + \frac{2(s-u)^2(d_{10} + d_7 + d_8)}{f^2}. \quad (\text{B.7})$$

- $KN^{I=0}$

$$B_{KN}^{I=0} = \frac{2(b_8 - 2b_6)(s-u)}{f^2} + \frac{4m_N(4c_1 + c_3)}{f^2} - \frac{8m_N(s-u)(d_{10} + d_7 - d_8)}{f^2} + \frac{4(-\nu_K(d_1 + d_2 + d_3) + 2m_K^2(d_4 + d_{48} + d_{49} + d_5 - d_{50} + d_6) - t(d_4 + d_5 + d_6))}{f^2}, \quad (\text{B.8})$$

$$A_{KN}^{I=0} = \frac{4m_K^2(-b_0 - b_3 + b_4 + b_F) + 2t(b_3 - b_4)}{f^2} - \frac{(s-u)(4c_1 + c_3)}{f^2} + \frac{2(s-u)^2(d_{10} + d_7 - d_8)}{f^2}. \quad (\text{B.9})$$

B.2 Tree level Born diagrams

Once simplified with the on-shell condition, the amplitude for the Born diagram could be rewritten as

$$\begin{aligned} B_{Born}(s, B_i, B_f, P) &= -\frac{s + m_P(m_f + m_i) + m_f m_i}{s - m_P^2}, \\ A_{Born}(s, B_i, B_f, P) &= -\frac{m_P(-2s + m_f^2 + m_i^2) + (m_f + m_i)(m_f m_i - s)}{2(s - m_P^2)}, \end{aligned} \quad (\text{B.10})$$

where s is the invariant mass squared, m_i , and m_f are the masses of the initial and final baryons, B_i, B_f, P are the incoming, outgoing, propagating baryons respectively. For a crossed Born diagram, one can obtain the amplitude from the corresponding direct one with the following replacement $s \rightarrow u$.

For the d_{45}, d_{46}, d_{47} terms, the expressions are slightly different

$$\begin{aligned} B_{Born}^2(s, B_i, B_f, P) &= \frac{m_i + m_P}{s - m_P^2}, \\ A_{Born}^2(s, B_i, B_f, P) &= \frac{-2s + m_P(m_f - m_i) + m_f m_i + m_i^2}{2(s - m_P^2)}. \end{aligned} \quad (\text{B.11})$$

For the A parts of the Born terms, one would need to perform two replacements

$$B(s) \leftrightarrow A(s), \quad B(u) \leftrightarrow -A(u). \quad (\text{B.12})$$

The contributions of the Born diagrams are

- $\pi N_{Born}^{I=3/2}$

$$\begin{aligned} B_{\pi N}^{I=3/2} &= -\frac{B(u, N, N, N)(D + F)^2}{2f^2} \\ &+ \frac{4B(u, N, N, N)(D + F)(2d_{38}m_K^2 - d_{38}m_\pi^2 + 2d_{40}m_K^2 + d_{40}m_\pi^2 + 2d_{44}m_\pi^2)}{f^2} \\ &- \frac{4m_\pi^2 B^2(u, N, N, N)(D + F)(d_{45} + d_{46})}{f^2}. \end{aligned} \quad (\text{B.13})$$

- $\pi N_{Born}^{I=1/2}$

$$\begin{aligned} B_{\pi N}^{I=1/2} &= \frac{(D + F)^2(3B(s, N, N, N) + B(u, N, N, N))}{4f^2} \\ &- \frac{2(D + F)(3B(s, N, N, N) + B(u, N, N, N))}{f^2} (2d_{38}m_K^2 - d_{38}m_\pi^2 \\ &+ 2d_{40}m_K^2 + d_{40}m_\pi^2 + 2d_{44}m_\pi^2) \\ &+ \frac{2m_\pi^2(D + F)(d_{45} + d_{46})(3B^2(s, N, N, N) + B^2(u, N, N, N))}{f^2}. \end{aligned} \quad (\text{B.14})$$

- $KN_{Born}^{I=1}$

$$\begin{aligned}
B_{KN}^{I=1} = & -\frac{B(u, N, N, \Lambda)(D + 3F)^2 + 3B(u, N, N, \Sigma)(D - F)^2}{12f^2} \\
& -\frac{2}{3f^2} (m_\pi^2 (B(u, N, N, \Lambda)(D + 3F)(2d_{38} + d_{39} - 2d_{40} + d_{41}) \\
& + 3B(u, N, N, \Sigma)(F - D)(d_{39} + d_{41})) \\
& - 2m_K^2 (B(u, N, N, \Lambda)(D + 3F)(2d_{38} + 2d_{40} - d_{41} - d_{43} + 2d_{44}) \\
& - 3B(u, N, N, \Sigma)(F - D)(d_{41} + d_{43})) \\
& - \frac{2m_K^2 (B^2(u, N, N, \Lambda)(D + 3F)(d_{45} + 3d_{46}) - 3B^2(u, N, N, \Sigma)(F - D)(d_{45} - d_{46}))}{3f^2}.
\end{aligned} \tag{B.15}$$

- $KN_{Born}^{I=0}$

$$\begin{aligned}
B_{KN}^{I=0} = & \frac{B(u, N, N, \Lambda)(D + 3F)^2 - 9B(u, N, N, \Sigma)(D - F)^2}{12f^2} \\
& -\frac{2}{3f^2} (2m_K^2 (B(u, N, N, \Lambda)(D + 3F)(2d_{38} + 2d_{40} - d_{41} - d_{43} + 2d_{44}) \\
& + 9B(u, N, N, \Sigma)(F - D)(d_{41} + d_{43})) \\
& - m_\pi^2 (B(u, N, N, \Lambda)(D + 3F)(2d_{38} + d_{39} - 2d_{40} + d_{41}) \\
& - 9B(u, N, N, \Sigma)(F - D)(d_{39} + d_{41})) \\
& \frac{2m_K^2 (B^2(u, N, N, \Lambda)(D + 3F)(d_{45} + 3d_{46}) + 9B^2(u, N, N, \Sigma)(F - D)(d_{45} - d_{46}))}{3f^2}.
\end{aligned} \tag{B.16}$$

B.3 Vertex renormalization

To simplify the final expression, we provide the amplitudes without integrating over the intermediate momentum.

The integral can be easily performed with the help of the OneLoop package [257, 258]. The contributions are

$$Re_{ab}(B_i, B_f, \Phi, P) = \frac{-i(\not{k} + \not{q}_f)(\not{P} - \not{k} + m_P)\gamma^5 \not{k}}{(k^2 - m_\Phi^2)((P - k)^2 - m_P^2)}, \tag{B.17}$$

$$Re_{cd}(B_i, B_f, \Phi, \Phi_f, P_1, P_2) = \frac{i\gamma^5 \not{k}(\not{p}_f - \not{k} + m_2)\gamma^5 \not{q}_f(\not{P} - \not{k} + m_1)\gamma^5 \not{k}}{(k^2 - m_\Phi^2)((p_f - k)^2 - M_2^2)((P - k)^2 - M_1^2)}, \tag{B.18}$$

$$Re_{no}(B_i, B_f, \Phi,) = \frac{-i\gamma^5 \not{k}(\not{p}_f + \not{k} + m_P)(\not{q}_f + \not{k})}{(k^2 - m_\Phi^2)((p_f + k)^2 - m_P^2)}, \quad (\text{B.19})$$

$$Re_{pr}(\Phi) = \frac{i\gamma^5 \not{q}_f}{k^2 - m_\Phi^2}, \quad (\text{B.20})$$

where B_i, B_f, Φ_f refer to initial and final state baryons and mesons, Φ is the propagated meson, and P, P_1, P_2 are the propagated baryons.

In numerical calculations, when limited to πN and KN channels, only vertices listed below are needed,

$$\begin{aligned} V_{p \rightarrow \pi^0 p}^{Re} = & -\frac{\Delta F_\pi(D+F)}{2f} - \frac{(D+F)}{24f^3} (Z_B(N, \eta, N)(D-3F)^2 + Z_B(N, K, \Lambda)(D+3F)^2 \\ & + 9(Z_B(N, K, \Sigma)(D-F)^2 + Z_B(N, \pi, N)(D+F)^2)) - \frac{(D+F)Z_\Phi(\pi)}{8f} \\ & - \frac{Re_{ab}(N, N, K, \Lambda)(D+3F)}{16f^3} + \frac{Re_{ab}(N, N, K, \Sigma)(F-D)}{16f^3} - \frac{Re_{ab}(N, N, \pi, N)(D+F)}{4f^3} \\ & - \frac{Re_{cd}(N, N, \eta, \pi, N, N)(D-3F)^2(D+F)}{24f^3} - \frac{DRe_{cd}(N, N, K, \pi, \Lambda, \Sigma)(F-D)(D+3F)}{12f^3} \\ & - \frac{DRe_{cd}(N, N, K, \pi, \Sigma, \Lambda)(F-D)(D+3F)}{12f^3} - \frac{FRe_{cd}(N, N, K, \pi, \Sigma, \Sigma)(F-D)^2}{2f^3} \\ & + \frac{Re_{cd}(N, N, \pi, \pi, N, N)(D+F)^3}{8f^3} + \frac{Re_{no}(N, N, K, \Lambda)(D+3F)}{16f^3} \\ & - \frac{Re_{no}(N, N, K, \Sigma)(F-D)}{16f^3} + \frac{Re_{no}(N, N, \pi, N)(D+F)}{4f^3} \\ & + \frac{(D+F)(Re_{pr}(K) + 2Re_{pr}(\pi))}{6f^3}, \end{aligned} \quad (\text{B.21})$$

$$\begin{aligned}
V_{p \rightarrow K+\Sigma^0}^{Re} = & \frac{(F-D)\Delta F_K}{2f} - \frac{D-F}{48f^3} (Z_B(N, \eta, N)(D-3F)^2 + Z_B(N, K, \Lambda)(D+3F)^2 \\
& + 9Z_B(N, K, \Sigma)(D-F)^2 + 9Z_B(N, \pi, N)(D+F)^2 + 4Z_B(\Sigma, \eta, \Sigma)D^2 \\
& + 6Z_B(\Sigma, K, N)(D-F)^2 + 6Z_B(\Sigma, K, \Xi)(D+F)^2 + 4Z_B(\Sigma, \pi, \Lambda)D^2 + 24Z_B(\Sigma, \pi, \Sigma)F^2) \\
& - \frac{(D-F)Z_\Phi(K)}{8f} - \frac{Re_{ab}(m, \Sigma, \eta, N)(D-3F)}{16f^3} + \frac{Re_{ab}(N, \Sigma, K, \Sigma)(F-D)}{4f^3} \\
& - \frac{Re_{ab}(N, \Sigma, \pi, N)(D+F)}{16f^3} - \frac{DRe_{cd}(N, \Sigma, \eta, K, N, \Sigma)(D-3F)(F-D)}{12f^3} \\
& - \frac{Re_{cd}(N, \Sigma, K, K, \Lambda, \Xi)(D-3F)(D+3F)(D+F)}{24f^3} \\
& - \frac{Re_{cd}(N, \Sigma, K, K, \Sigma, \Xi)(F-D)(D+F)^2}{8f^3} \\
& + \frac{DRe_{cd}(N, \Sigma, \pi, K, N, \Lambda)(D+3F)(D+F)}{12f^3} + \frac{FRe_{cd}(N, \Sigma, \pi, K, N, \Sigma)(F-D)(D+F)}{2f^3} \\
& - \frac{Re_{no}(N, \Sigma, K, N)(D-F)}{8f^3} - \frac{Re_{no}(N, \Sigma, K, N)(F-D)}{4f^3} \\
& + \frac{DRe_{no}(N, \Sigma, \eta, \Sigma)}{8f^3} + \frac{DRe_{no}(N, \Sigma, \pi, \Lambda)}{8f^3} - \frac{FRe_{no}(N, \Sigma, \pi, \Sigma)}{4f^3} \\
& - \frac{(D-F)(Re_{pr}(\eta) + 2Re_{pr}(K) + Re_{pr}(\pi))}{8f^3},
\end{aligned} \tag{B.22}$$

$$\begin{aligned}
V_{p \rightarrow K+\Lambda}^{Re} = & \frac{(D+3F)\Delta F_K}{2\sqrt{3}f} + \frac{D+3F}{4\sqrt{3}f} \left(\frac{Z_B(N, \eta, N)(D-3F)^2}{12f^2} + \frac{Z_B(N, K, \Lambda)(D+3F)^2}{12f^2} \right. \\
& + \frac{3Z_B(N, K, \Sigma)(F-D)^2}{4f^2} + \frac{3Z_B(N, \pi, N)(D+F)^2}{4f^2} + \frac{Z_B(\Lambda, \eta, \Lambda)D^2}{3f^2} \\
& + \frac{Z_B(\Lambda, K, N)(D+3F)^2}{6f^2} + \frac{Z_B(\Lambda, K, \Xi)(D-3F)^2}{6f^2} + \left. \frac{Z_B(\Lambda, \pi, \Sigma)D^2}{f^2} \right) \\
& + \frac{(D+3F)Z_\Phi(K)}{8\sqrt{3}f} + \frac{3\sqrt{3}Re_{ab}(N, \Lambda, \pi, mN)(D+F)}{16f^3} \\
& - \frac{\sqrt{3}Re_{ab}(N, \Lambda, \eta, mN)(D-3F)}{16f^3} + \frac{DRe_{cd}(N, \Lambda, \eta, K, N, \Lambda)(D+3F)(D-3F)}{12\sqrt{3}f^3} \\
& + \frac{Re_{cd}(N, \Lambda, K, K, \Lambda, \Xi)(D+3F)(D-3F)^2}{24\sqrt{3}f^3} \\
& - \frac{\sqrt{3}Re_{cd}(N, \Lambda, K, K, \Sigma, \Xi)(F-D)(D+F)(D-3F)}{8f^3} \\
& + \frac{\sqrt{3}DRe_{cd}(N, \Lambda, \pi, K, N, \Sigma)(F-D)(D+F)}{4f^3} - \frac{\sqrt{3}Re_{no}(N, \Lambda, K, N)(D+3F)}{8f^3} \\
& - \frac{\sqrt{3}DRe_{no}(N, \Lambda, \eta, \Lambda)}{8f^3} + \frac{\sqrt{3}DRe_{no}(N, \Lambda, \pi, \Sigma)}{8f^3} \\
& - \frac{(D+3F)(Re_{pr}(\eta) + 2Re_{pr}(K) + Re_{pr}(\pi))}{8\sqrt{3}f^3},
\end{aligned} \tag{B.23}$$

$$V_{p \rightarrow \pi^+n}^{Re} = \sqrt{2}V_{p \rightarrow \pi^0 p}^{Re}, \quad V_{n \rightarrow \pi^-p}^{Re} = \sqrt{2}V_{p \rightarrow \pi^0 p}^{Re}, \quad V_{n \rightarrow \pi^0 n}^{Re} = -V_{p \rightarrow \pi^0 p}^{Re}, \tag{B.24}$$

$$V_{p \rightarrow K^0 \Sigma^+}^{Re} = \sqrt{2} V_{p \rightarrow K^+ \Sigma^0}^{Re}, \quad V_{n \rightarrow K^0 \Sigma^0}^{Re} = -V_{p \rightarrow K^+ \Sigma^0}^{Re}, \quad V_{n \rightarrow K^+ \Sigma^-}^{Re} = \sqrt{2} V_{p \rightarrow K^+ \Sigma^0}^{Re}, \quad (\text{B.25})$$

$$V_{n \rightarrow K^0 \Lambda^0}^{Re} = V_{p \rightarrow K^+ \Sigma^0}^{Re}. \quad (\text{B.26})$$

B.4 Divergent parts of the LECs

As mentioned in the main text, the LECs can be divided into finite parts and infinite parts as shown in Eq. (4.29),

The divergent parts absorb all the ultraviolet divergences from the loop diagrams. Their explicit expressions are

$$\begin{aligned}
c_{1d} &= -\frac{-27mDF^3 - 31mD^3F + 9mDF}{192f^2\pi^2}, \\
c_{2d} &= -\frac{-27mF^4 - 106mD^2F^2 + 18mF^2 - 19mD^4 - 6mD^2 + 9m}{768f^2\pi^2}, \\
c_{3d} &= -\frac{11mD^4 + 9mF^2D^2 + 9mD^2}{72f^2\pi^2}, \\
b_{1d} &= -\frac{207mF^4 + 738mD^2F^2 + 18mF^2 - 73mD^4 - 6mD^2 - 45m}{2304f^2\pi^2}, \\
b_{2d} &= -\frac{-45mF^4 + 90mD^2F^2 + 90mF^2 - 5mD^4 - 30mD^2 - 9m}{256f^2\pi^2}, \\
b_{3d} &= -\frac{3(3mDF^3 - mD^3F + mDF)}{32f^2\pi^2}, \\
b_{0d} &= -\frac{m(9F^2 + 13D^2)}{144f^2\pi^2}, \\
b_{4d} &= -\frac{mD^4 - 81mF^2D^2 + 27mD^2}{144f^2\pi^2}, \\
b_{Dd} &= -\frac{3mF^2 - mD^2}{32f^2\pi^2}, \\
b_{Fd} &= -\frac{5mFD}{48f^2\pi^2}, \\
b_{5d} &= -\frac{-15F^4 + 30D^2F^2 + 30F^2 + 9D^4 - 10D^2 - 15}{768f^2\pi^2}, \\
b_{6d} &= -\frac{-9DF^3 - 13D^3F + 9DF}{96f^2\pi^2}, \\
b_{7d} &= -\frac{-9D^4 + 18D^2F^2 + 18F^2 - D^4 - 6D^2 - 9}{256f^2\pi^2}, \\
b_{8d} &= -\frac{-5D^4 - 27F^2D^2 + 9D^2}{144f^2\pi^2},
\end{aligned} \quad (\text{B.27})$$

$$\begin{aligned}
d_{5d} &= -d_{48d} - \frac{9F^4 - 36DF^3 + 46D^2F^2 - 18F^2 - 20D^3F + 36DF + 17D^4 - 26D^2 - 9}{1536f^2\pi^2}, \\
d_{6d} &= d_{50d} - \frac{D^4 + 3F^2D^2 - 3D^2}{96f^2\pi^2}, \\
d_{4d} &= -d_{49d} - \frac{-9F^4 - 36DF^3 - 46D^2F^2 + 18F^2 - 20D^3F + 36DF - 17D^4 + 26D^2 + 9}{1536f^2\pi^2}, \\
d_{10d} &= \frac{b_{8d}}{4m} - \frac{5D^4 + 27F^2D^2 - 9D^2}{576f^2m\pi^2}, \\
d_{7d} &= \frac{b_{5d}}{8m} - \frac{b_{6d}}{8m} - \frac{21F^4 - 36DF^3 - 42D^2F^2 - 42F^2 - 52D^3F + 36DF - 3D^4 + 14D^2 + 21}{3072f^2m\pi^2}, \\
d_{9d} &= -\frac{b_{5d}}{2m} + \frac{b_{7d}}{2m} - \frac{3F^4 - 6D^2F^2 - 6F^2 + 3D^4 + 2D^2 + 3}{384f^2m\pi^2}, \\
d_{8d} &= \frac{b_{5d}}{8m} + \frac{b_{6d}}{8m} + \frac{b_{7d}}{8m} - \frac{21F^4 + 36DF^3 - 42D^2F^2 - 42D^2 + 52D^3F - 36DF - 3D^4 + 14D^2 + 21}{3072f^2m\pi^2}.
\end{aligned} \tag{B.28}$$

B.5 Power counting breaking terms of the one-loop diagrams

In this subsection, we list the power counting breaking terms for the πN and KN channels.

- $\pi N_{PCB}^{I=3/2}$

$$\begin{aligned}
D_{PCB} &= -\frac{1}{1152\pi^2 f^4 \tilde{m}} \left(2\tilde{m}^2 (2m_\pi^2 (369D^4 + 108D^3F + 18D^2 (43F^2 - 4) \right. \\
&\quad \left. + 12DF (25F^2 + 2) + 5F^2 (29F^2 - 8)) - t (369D^4 + 108D^3F + 9D^2 (86F^2 - 1) \right. \\
&\quad \left. + 6DF (50F^2 + 9) + F^2 (145F^2 + 3)) - \sigma^2 (171D^4 + 108D^3F + 138D^2F^2 \right. \\
&\quad \left. + 60DF^3 + 35F^4 + 63) \right),
\end{aligned} \tag{B.29}$$

$$B_{PCB} = -\frac{\tilde{m}^2 (9D^4 + 9D^3F + 2D^2F^2 - 3DF^3 + 9DF + 3F^4 - 2F^2)}{12\pi^2 f^4}. \tag{B.30}$$

- $\pi N_{PCB}^{I=1/2}$

$$\begin{aligned}
D_{PCB} &= -\frac{1}{1152\pi^2 f^4 \tilde{m}} \left(2\tilde{m}^2 (2m_\pi^2 (369D^4 + 108D^3F + 18D^2 (43F^2 - 4) \right. \\
&\quad \left. + 12DF (25F^2 + 2) + 5F^2 (29F^2 - 8)) - t (369D^4 + 108D^3F + 9D^2 (86F^2 - 1) \right. \\
&\quad \left. + 6DF (50F^2 + 9) + F^2 (145F^2 + 3)) - \sigma^2 (171D^4 + 108D^3F + 138D^2F^2 \right. \\
&\quad \left. + 60DF^3 + 35F^4 + 63) \right),
\end{aligned} \tag{B.31}$$

$$B_{PCB} = \frac{\tilde{m}^2 (9D^4 + 9D^3F + 2D^2F^2 - 3DF^3 + 9DF + 3F^4 - 2F^2)}{6\pi^2 f^4}. \quad (\text{B.32})$$

- $KN_{PCB}^{I=1}$

$$D_{PCB} = -\frac{1}{576\pi^2 f^4 \tilde{m}} (2\tilde{m}^2 (2m_K^2 (369D^4 + 18D^2 (F^2 - 3) + F^2 (85F^2 - 14)) - t (369D^4 + 9D^2 (2F^2 - 1) + F^2 (85F^2 + 3))) - \sigma^2 (171D^4 - 6D^2F^2 + 19F^4 + 63)), \quad (\text{B.33})$$

$$B_{PCB} = -\frac{i\tilde{m}^2 (27D^4 - 3D^2F^2 + 8F^4 + 3F^2)}{18\pi^2 f^4}. \quad (\text{B.34})$$

- $KN_{PCB}^{I=0}$

$$D_{PCB} = \frac{1}{144\pi^2 f^4 \tilde{m}} (F\sigma^2 (-27D^3 + 36D^2F - 15DF^2 + 4F^3) + \tilde{m}^2 (2m_K^2 (54D^3F + D^2 (9 - 378F^2) + 6D (25F^2 + 2) F - 30F^4 + 13F^2) + 3Ft (-18D^3 + 126D^2F - D (50F^2 + 9) + 10F^3))), \quad (\text{B.35})$$

$$B_{PCB} = -\frac{F\tilde{m}^2 (-27D^3 + 9D^2F + 9D (F^2 - 3) + F (F^2 - 9))}{18\pi^2 f^4}. \quad (\text{B.36})$$

In the above equations, $\sigma = s - \tilde{m}^2$. We have already set the scale μ in the \overline{MS} scheme to be equal to the chiral limit baryon mass \tilde{m} . All these power counting breaking terms are absorbed into the corresponding LECs in the

EOMS scheme, i.e.,

$$\begin{aligned}
b_0^{PCB} &= b_4^{PCB} + \frac{\tilde{m} (9D^2 (42F^2 - 1) + F^2 (30F^2 - 13))}{288\pi^2 f^2}, \\
b_D^{PCB} &= \frac{\tilde{m} (F^2 - 3D^2)}{64\pi^2 f^2}, \\
b_F^{PCB} &= -\frac{5DF\tilde{m}}{96\pi^2 f^2}, \\
b_1^{PCB} &= -\frac{\tilde{m} (333D^4 - 9D^2 (74F^2 - 7) + F^2 (5F^2 - 21))}{1152\pi^2 f^2}, \\
b_2^{PCB} &= -\frac{\tilde{m} (45D^4 - 9D^2 (10F^2 + 1) + F^2 (5F^2 + 3))}{128\pi^2 f^2}, \\
b_3^{PCB} &= -\frac{DF\tilde{m} (18D^2 + 50F^2 + 9)}{96\pi^2 f^2}, \\
b_5^{PCB} &= -\frac{-87D^4 + 46D^2 F^2 + F^4 - 15}{768\pi^2 f^2}, \\
b_6^{PCB} &= \frac{9D^3 F + 5DF^3}{96\pi^2 f^2}, \\
b_7^{PCB} &= \frac{9D^4 - 18D^2 F^2 + F^4 + 9}{256\pi^2 f^2}, \\
b_8^{PCB} &= \frac{144\pi^2 b_4^{PCB} f^2 \tilde{m} t + 2F^2 \sigma^2 (9D^2 + F^2) + 3F^2 \tilde{m}^2 t (63D^2 + 5F^2)}{144\pi^2 f^2 \sigma^2}, \\
c_1^{PCB} &= \frac{DF\tilde{m} (3D^2 - F^2 + 3)}{32\pi^2 f^2}, \\
c_2^{PCB} &= \frac{\tilde{m} (9D^4 + 2D^2 F^2 + 3F^4 - 2F^2)}{96\pi^2 f^2}, \\
c_3^{PCB} &= -\frac{F^2 \tilde{m} (9D^2 + F^2 - 9)}{72\pi^2 f^2}.
\end{aligned} \tag{B.37}$$

Bibliography

- [1] TANABASHI M, OTHERS. Review of Particle Physics[J]. Phys. Rev. D, 2018, 98(3): 030001. DOI: 10.1103/PhysRevD.98.030001.
- [2] LIANG W, UCHINO T, XIAO C, et al. Baryon states with open charm in the extended local hidden gauge approach[J]. Eur. Phys. J. A, 2015, 51(2): 16. DOI: 10.1140/epja/i2015-15016-1.
- [3] HOFMANN J, LUTZ M. Coupled-channel study of crypto-exotic baryons with charm[J]. Nucl. Phys. A, 2005, 763: 90–139. DOI: 10.1016/j.nuclphysa.2005.08.022.
- [4] GARCIA-RECIO C, MAGAS V, MIZUTANI T, et al. The s-wave charmed baryon resonances from a coupled-channel approach with heavy quark symmetry[J]. Phys. Rev. D, 2009, 79: 054004. DOI: 10.1103/PhysRevD.79.054004.
- [5] OLIVE K, OTHERS. Review of Particle Physics[J]. Chin. Phys. C, 2014, 38: 090001. DOI: 10.1088/1674-1137/38/9/090001.
- [6] CHEN Y H, YAO D L, ZHENG H. Analyses of pion-nucleon elastic scattering amplitudes up to $O(p^4)$ in extended-on-mass-shell subtraction scheme[J]. Phys. Rev. D, 2013, 87: 054019. DOI: 10.1103/PhysRevD.87.054019.
- [7] HUANG B L, ZHANG J S, LI Y D, et al. Meson-baryon scattering to one-loop order in heavy baryon chiral perturbation theory[J]. Phys. Rev. D, 2017, 96(1): 016021. DOI: 10.1103/PhysRevD.96.016021.
- [8] UEHARA S, OTHERS. High-statistics study of eta pi0 production in two-photon collisions[J]. Phys. Rev. D, 2009, 80: 032001. DOI: 10.1103/PhysRevD.80.032001.
- [9] UEHARA S, OTHERS. High-statistics study of K_S^0 pair production in two-photon collisions[J]. PTEP, 2013, 2013(12): 123C01. DOI: 10.1093/ptep/ptt097.
- [10] BIJNENS J, ECKER G. Mesonic low-energy constants[J]. Ann. Rev. Nucl. Part. Sci., 2014, 64: 149–174. DOI: 10.1146/annurev-nucl-102313-025528.
- [11] LU J X, ZHOU Y, CHEN H X, et al. Dynamically generated $J^P = 1/2^-(3/2^-)$ singly charmed and bottom heavy baryons[J]. Phys. Rev. D, 2015, 92(1): 014036. DOI: 10.1103/PhysRevD.92.014036.

- [12] AAD G, OTHERS. Observation of a new particle in the search for the Standard Model Higgs boson with the ATLAS detector at the LHC[J]. *Phys. Lett. B*, 2012, 716: 1–29. DOI: 10.1016/j.physletb.2012.08.020.
- [13] CHATRCHYAN S, OTHERS. Observation of a New Boson at a Mass of 125 GeV with the CMS Experiment at the LHC[J]. *Phys. Lett. B*, 2012, 716: 30–61. DOI: 10.1016/j.physletb.2012.08.021.
- [14] HIGGS P W. Broken Symmetries and the Masses of Gauge Bosons[J]. *Phys. Rev. Lett.*, 1964, 13: 508–509. DOI: 10.1103/PhysRevLett.13.508.
- [15] ENGLERT F, BROUT R. Broken Symmetry and the Mass of Gauge Vector Mesons[J]. *Phys. Rev. Lett.*, 1964, 13: 321–323. DOI: 10.1103/PhysRevLett.13.321.
- [16] GURALNIK G S, HAGEN C R, KIBBLE T W B. Global Conservation Laws and Massless Particles[J]. *Phys. Rev. Lett.*, 1964, 13: 585–587. DOI: 10.1103/PhysRevLett.13.585.
- [17] GLASHOW S L. Partial Symmetries of Weak Interactions[J]. *Nucl. Phys.*, 1961, 22: 579–588. DOI: 10.1016/0029-5582(61)90469-2.
- [18] WEINBERG S. A Model of Leptons[J]. *Phys. Rev. Lett.*, 1967, 19: 1264–1266. DOI: 10.1103/PhysRevLett.19.1264.
- [19] SALAM A. Elementary particle theory[C]//*Prog. Of the Nobel Symposium, 1968, Stockholm, Sweden: volume 367*. [S.l.: s.n.], 1968.
- [20] GELL-MANN M. Symmetries of baryons and mesons[J]. *Phys. Rev.*, 1962, 125: 1067–1084. DOI: 10.1103/PhysRev.125.1067.
- [21] GELL-MANN M. A Schematic Model of Baryons and Mesons[J]. *Phys. Lett.*, 1964, 8: 214–215. DOI: 10.1016/S0031-9163(64)92001-3.
- [22] ZWEIG G. An SU(3) model for strong interaction symmetry and its breaking. Version 1[M]. [S.l.: s.n.], 1964.
- [23] FRITZSCH H, GELL-MANN M. Current algebra: Quarks and what else?[J]. *eConf*, 1972, C720906V2: 135–165.
- [24] FRITZSCH H, GELL-MANN M, LEUTWYLER H. Advantages of the Color Octet Gluon Picture[J]. *Phys. Lett. B*, 1973, 47: 365–368. DOI: 10.1016/0370-2693(73)90625-4.
- [25] TKACHOV F. A Contribution to the history of quarks: Boris Struminsky’s 1965 JINR publication[M]. [S.l.: s.n.], 2009.
- [26] NAMBU Y, HAN M. Three triplets, paraquarks, and colored quarks[J]. *Phys. Rev. D*, 1974, 10: 674–683. DOI: 10.1103/PhysRevD.10.674.

- [27] YANG C N, MILLS R L. Conservation of Isotopic Spin and Isotopic Gauge Invariance[J]. Phys. Rev., 1954, 96: 191–195. DOI: 10.1103/PhysRev.96.191.
- [28] AUBERT J, OTHERS. Experimental Observation of a Heavy Particle J [J]. Phys. Rev. Lett., 1974, 33: 1404–1406. DOI: 10.1103/PhysRevLett.33.1404.
- [29] AUGUSTIN J, OTHERS. Discovery of a Narrow Resonance in e^+e^- Annihilation[J]. Phys. Rev. Lett., 1974, 33: 1406–1408. DOI: 10.1103/PhysRevLett.33.1406.
- [30] HERB S, OTHERS. Observation of a Dimuon Resonance at 9.5-GeV in 400-GeV Proton-Nucleus Collisions [J]. Phys. Rev. Lett., 1977, 39: 252–255. DOI: 10.1103/PhysRevLett.39.252.
- [31] ABE F, OTHERS. Observation of top quark production in $\bar{p}p$ collisions[J]. Phys. Rev. Lett., 1995, 74: 2626–2631. DOI: 10.1103/PhysRevLett.74.2626.
- [32] ABACHI S, OTHERS. Observation of the top quark[J]. Phys. Rev. Lett., 1995, 74: 2632–2637. DOI: 10.1103/PhysRevLett.74.2632.
- [33] GROSS D J, WILCZEK F. Ultraviolet Behavior of Nonabelian Gauge Theories[J]. Phys. Rev. Lett., 1973, 30: 1343–1346. DOI: 10.1103/PhysRevLett.30.1343.
- [34] POLITZER H D. Reliable Perturbative Results for Strong Interactions?[J]. Phys. Rev. Lett., 1973, 30: 1346–1349. DOI: 10.1103/PhysRevLett.30.1346.
- [35] WILSON K G. Confinement of Quarks[J]. Phys. Rev., 1974, D10: 2445–2459. DOI: 10.1103/PhysRevD.10.2445.
- [36] OLSEN S L, SKWARNICKI T, ZIEMINSKA D. Nonstandard heavy mesons and baryons: Experimental evidence[J]. Rev. Mod. Phys., 2018, 90(1): 015003. DOI: 10.1103/RevModPhys.90.015003.
- [37] GATtringer C, LANG C B. Quantum chromodynamics on the lattice: volume 788[M]. Berlin: Springer, 2010. DOI: 10.1007/978-3-642-01850-3.
- [38] GUO F K, HANHART C, MEIBNER U G, et al. Hadronic molecules[J]. Rev. Mod. Phys., 2018, 90(1): 015004. DOI: 10.1103/RevModPhys.90.015004.
- [39] HYODO T, NIIYAMA M. QCD and the Strange Baryon Spectrum[M]. [S.l.: s.n.], 2020.
- [40] CHEN H X, CHEN W, LIU X, et al. The hidden-charm pentaquark and tetraquark states[J]. Phys. Rept., 2016, 639: 1–121. DOI: 10.1016/j.physrep.2016.05.004.
- [41] OLLER J A, MEISSNER U G. Chiral dynamics in the presence of bound states: Kaon nucleon interactions revisited[J]. Phys. Lett., 2001, B500: 263–272. DOI: 10.1016/S0370-2693(01)00078-8.

- [42] GROSS D J. Twenty five years of asymptotic freedom[J]. Nucl. Phys. Proc. Suppl., 1999, 74: 426–446. DOI: 10.1016/S0920-5632(99)00208-X.
- [43] WEINBERG S. Phenomenological Lagrangians[J]. Physica, 1979, A96(1-2): 327–340. DOI: 10.1016/0378-4371(79)90223-1.
- [44] LEUTWYLER H. On the foundations of chiral perturbation theory[J]. Annals Phys., 1994, 235: 165–203. DOI: 10.1006/aphy.1994.1094.
- [45] D'HOKER E, WEINBERG S. General effective actions[J]. Phys. Rev., 1994, D50: R6050–R6053. DOI: 10.1103/PhysRevD.50.R6050.
- [46] GASSER J, LEUTWYLER H. Chiral Perturbation Theory to One Loop[J]. Annals Phys., 1984, 158: 142. DOI: 10.1016/0003-4916(84)90242-2.
- [47] GASSER J, LEUTWYLER H. Chiral Perturbation Theory: Expansions in the Mass of the Strange Quark [J]. Nucl. Phys., 1985, B250: 465–516. DOI: 10.1016/0550-3213(85)90492-4.
- [48] GASSER J, LEUTWYLER H. On the Low-energy Structure of QCD[J]. Phys. Lett. B, 1983, 125: 321–324. DOI: 10.1016/0370-2693(83)91293-5.
- [49] BIJNENS J, COLANGELO G, ECKER G. The Mesonic chiral Lagrangian of order p^6 [J]. JHEP, 1999, 02: 020. DOI: 10.1088/1126-6708/1999/02/020.
- [50] BIJNENS J. Chiral meson physics at two loops[J]. AIP Conf. Proc., 2005, 768(1): 153–159. DOI: 10.1063/1.1932901.
- [51] LEUTWYLER H. Principles of chiral perturbation theory[C]//Hadrons 94 Workshop. [S.l.: s.n.], 1994: 1–46.
- [52] BERNARD V, KAISER N, MEISSNER U G. Chiral dynamics in nucleons and nuclei[J]. Int. J. Mod. Phys. E, 1995, 4: 193–346. DOI: 10.1142/S0218301395000092.
- [53] PICH A. Chiral perturbation theory[J]. Rept. Prog. Phys., 1995, 58: 563–610. DOI: 10.1088/0034-4885/58/6/001.
- [54] ECKER G. Chiral perturbation theory[J]. Prog. Part. Nucl. Phys., 1995, 35: 1–80. DOI: 10.1016/0146-6410(95)00041-G.
- [55] SCHERER S. Introduction to chiral perturbation theory[J]. Adv. Nucl. Phys., 2003, 27: 277.
- [56] BERNARD V. Chiral Perturbation Theory and Baryon Properties[J]. Prog. Part. Nucl. Phys., 2008, 60: 82–160. DOI: 10.1016/j.pnpnp.2007.07.001.

- [57] GASSER J. Chiral perturbation theory[J]. Nucl. Phys. B Proc. Suppl., 2000, 86: 257–266. DOI: 10.1016/S0920-5632(00)00573-9.
- [58] BERNARD V, MEISSNER U G. Chiral perturbation theory[J]. Ann. Rev. Nucl. Part. Sci., 2007, 57: 33–60. DOI: 10.1146/annurev.nucl.56.080805.140449.
- [59] ZYLA P, OTHERS. Review of Particle Physics[J]. PTEP, 2020, 2020(8): 083C01. DOI: 10.1093/ptep/ptaa104.
- [60] ADLER S L. Axial vector vertex in spinor electrodynamics[J]. Phys. Rev., 1969, 177: 2426–2438. DOI: 10.1103/PhysRev.177.2426.
- [61] ADLER S L, BARDEEN W A. Absence of higher order corrections in the anomalous axial vector divergence equation[J]. Phys. Rev., 1969, 182: 1517–1536. DOI: 10.1103/PhysRev.182.1517.
- [62] BARDEEN W A. Anomalous Ward identities in spinor field theories[J]. Phys. Rev., 1969, 184: 1848–1857. DOI: 10.1103/PhysRev.184.1848.
- [63] BELL J S, JACKIW R. A pcac puzzle: $\pi^0 \rightarrow \gamma\gamma$ in the σ -model[J]. Il Nuovo Cimento A (1965-1970), 1969, 60(1): 47–61.
- [64] VAFA C, WITTEN E. Restrictions on Symmetry Breaking in Vector-Like Gauge Theories[J]. Nucl. Phys., 1984, B234: 173–188. DOI: 10.1016/0550-3213(84)90230-X.
- [65] NAMBU Y. Axial vector current conservation in weak interactions[J]. Phys. Rev. Lett., 1960, 4: 380–382. DOI: 10.1103/PhysRevLett.4.380.
- [66] NAMBU Y, JONA-LASINIO G. Dynamical Model of Elementary Particles Based on an Analogy with Superconductivity. I.[J]. Phys. Rev., 1961, 122: 345–358. DOI: 10.1103/PhysRev.122.345.
- [67] NAMBU Y, JONA-LASINIO G. DYNAMICAL MODEL OF ELEMENTARY PARTICLES BASED ON AN ANALOGY WITH SUPERCONDUCTIVITY. II[J]. Phys. Rev., 1961, 124: 246–254. DOI: 10.1103/PhysRev.124.246.
- [68] GOLDSTONE J. Field theories with superconductor solutions[J]. Il Nuovo Cimento (1955-1965), 1961, 19(1): 154–164.
- [69] GOLDSTONE J, SALAM A, WEINBERG S. Broken Symmetries[J]. Phys. Rev., 1962, 127: 965–970. DOI: 10.1103/PhysRev.127.965.
- [70] COLEMAN S R, WESS J, ZUMINO B. Structure of phenomenological Lagrangians. 1.[J]. Phys. Rev., 1969, 177: 2239–2247. DOI: 10.1103/PhysRev.177.2239.

- [71] CALLAN C G, Jr., COLEMAN S R, WESS J, et al. Structure of phenomenological Lagrangians. 2.[J]. Phys. Rev., 1969, 177: 2247–2250. DOI: 10.1103/PhysRev.177.2247.
- [72] GEORGI H M. Weak interactions and modern particle theory[M]. [S.l.]: Benjamin-Cummings, 1984.
- [73] GELL-MANN M. The Eightfold Way: A Theory of strong interaction symmetry[J]. CTSL-20, TID-12608, 1961. DOI: 10.2172/4008239.
- [74] OKUBO S. Note on unitary symmetry in strong interactions[J]. Prog. Theor. Phys., 1962, 27: 949–966. DOI: 10.1143/PTP.27.949.
- [75] ALBALADEJO M, MOUSSALLAM B. Form factors of the isovector scalar current and the $\eta\pi$ scattering phase shifts[J]. Eur. Phys. J. C, 2015, 75(10): 488. DOI: 10.1140/epjc/s10052-015-3715-z.
- [76] BORASOY B. Baryon axial currents[J]. Phys. Rev. D, 1999, 59: 054021. DOI: 10.1103/PhysRevD.59.054021.
- [77] FETTES N, MEISSNER U G, MOJZIS M, et al. The Chiral effective pion nucleon Lagrangian of order p^4 [J]. Annals Phys., 2000, 283: 273–302. DOI: 10.1006/aphy.2000.6059.
- [78] OLLER J A, VERBENI M, PRADES J. Meson-baryon effective chiral lagrangians to $O(q^3)$ [J]. JHEP, 2006, 09: 079. DOI: 10.1088/1126-6708/2006/09/079.
- [79] FRINK M, MEISSNER U G. On the chiral effective meson-baryon Lagrangian at third order[J]. Eur. Phys. J. A, 2006, 29: 255–260. DOI: 10.1140/epja/i2006-10105-x.
- [80] OLLER J A, VERBENI M, PRADES J. Meson-Baryon Effective Chiral Lagrangian at $O(q^3)$ Revisited [M]. [S.l.: s.n.], 2007.
- [81] JIANG S Z, CHEN Q S, LIU Y R. Meson-baryon effective chiral Lagrangians at order p^4 [J]. Phys. Rev. D, 2017, 95(1): 014012. DOI: 10.1103/PhysRevD.95.014012.
- [82] GASSER J, SAINIO M, SVARC A. Nucleons with Chiral Loops[J]. Nucl. Phys. B, 1988, 307: 779–853. DOI: 10.1016/0550-3213(88)90108-3.
- [83] JENKINS E E, MANOHAR A V. Baryon chiral perturbation theory using a heavy fermion Lagrangian[J]. Phys. Lett. B, 1991, 255: 558–562. DOI: 10.1016/0370-2693(91)90266-S.
- [84] WEINBERG S. Nuclear forces from chiral Lagrangians[J]. Phys. Lett. B, 1990, 251: 288–292. DOI: 10.1016/0370-2693(90)90938-3.
- [85] WEINBERG S. Effective chiral Lagrangians for nucleon - pion interactions and nuclear forces[J]. Nucl. Phys. B, 1991, 363: 3–18. DOI: 10.1016/0550-3213(91)90231-L.

- [86] BECHER T, LEUTWYLER H. Baryon chiral perturbation theory in manifestly Lorentz invariant form[J]. Eur. Phys. J. C, 1999, 9: 643–671. DOI: 10.1007/PL00021673.
- [87] FUCHS T, GEGELIA J, SCHERER S. Structure of the nucleon in chiral perturbation theory[J]. Eur. Phys. J. A, 2004, 19: 35–42. DOI: 10.1140/epjad/s2004-03-006-0.
- [88] ELLIS P J, TANG H B. Pion nucleon scattering in a new approach to chiral perturbation theory[J]. Phys. Rev. C, 1998, 57: 3356–3375. DOI: 10.1103/PhysRevC.57.3356.
- [89] PASCALUTSA V, HOLSTEIN B R, VANDERHAEGHEN M. A Derivative of the Gerasimov-Drell-Hearn sum rule[J]. Phys. Lett. B, 2004, 600: 239–247. DOI: 10.1016/j.physletb.2004.09.006.
- [90] GENG L, MARTIN CAMALICH J, ALVAREZ-RUSO L, et al. Leading SU(3)-breaking corrections to the baryon magnetic moments in Chiral Perturbation Theory[J]. Phys. Rev. Lett., 2008, 101: 222002. DOI: 10.1103/PhysRevLett.101.222002.
- [91] FUCHS T, GEGELIA J, JAPARIDZE G, et al. Renormalization of relativistic baryon chiral perturbation theory and power counting[J]. Phys. Rev. D, 2003, 68: 056005. DOI: 10.1103/PhysRevD.68.056005.
- [92] MARTIN CAMALICH J, GENG L, VICENTE VACAS M. The lowest-lying baryon masses in covariant SU(3)-flavor chiral perturbation theory[J]. Phys. Rev. D, 2010, 82: 074504. DOI: 10.1103/PhysRevD.82.074504.
- [93] GENG L, ALTENBUCHINGER M, WEISE W. Light quark mass dependence of the D and D_s decay constants[J]. Phys. Lett. B, 2011, 696: 390–395. DOI: 10.1016/j.physletb.2010.12.060.
- [94] MOJZIS M. Elastic πN scattering to $O(p^{**3})$ in heavy baryon chiral perturbation theory[J]. Eur. Phys. J. C, 1998, 2: 181–195. DOI: 10.1007/s100520050132.
- [95] FETTES N, MEISSNER U G, STEININGER S. Pion - nucleon scattering in chiral perturbation theory. 1. Isospin symmetric case[J]. Nucl. Phys. A, 1998, 640: 199–234. DOI: 10.1016/S0375-9474(98)00452-7.
- [96] BERNARD V, KAISER N, KAMBOR J, et al. Chiral structure of the nucleon[J]. Nucl. Phys. B, 1992, 388: 315–345. DOI: 10.1016/0550-3213(92)90615-I.
- [97] KAISER N, SIEGEL P, WEISE W. Chiral dynamics and the low-energy kaon - nucleon interaction[J]. Nucl. Phys. A, 1995, 594: 325–345. DOI: 10.1016/0375-9474(95)00362-5.
- [98] KAISER N, WAAS T, WEISE W. SU(3) chiral dynamics with coupled channels: Eta and kaon photoproduction[J]. Nucl. Phys. A, 1997, 612: 297–320. DOI: 10.1016/S0375-9474(96)00321-1.
- [99] OLLER J, OSET E. Chiral symmetry amplitudes in the S wave isoscalar and isovector channels and the σ , $f_0(980)$, $a_0(980)$ scalar mesons[J]. Nucl. Phys. A, 1997, 620: 438–456. DOI: 10.1016/S0375-9474(97)00160-7.

- [100] OSET E, RAMOS A. Nonperturbative chiral approach to s wave anti-K N interactions[J]. Nucl. Phys. A, 1998, 635: 99–120. DOI: 10.1016/S0375-9474(98)00170-5.
- [101] OLLER J, OSET E. N/D description of two meson amplitudes and chiral symmetry[J]. Phys. Rev. D, 1999, 60: 074023. DOI: 10.1103/PhysRevD.60.074023.
- [102] OSET E, RAMOS A, BENNHOLD C. Low lying $S = -1$ excited baryons and chiral symmetry[J]. Phys. Lett. B, 2002, 527: 99–105. DOI: 10.1016/S0370-2693(01)01523-4.
- [103] OLLER J, OSET E, PELAEZ J. Nonperturbative approach to effective chiral Lagrangians and meson interactions[J]. Phys. Rev. Lett., 1998, 80: 3452–3455. DOI: 10.1103/PhysRevLett.80.3452.
- [104] SALPETER E, BETHE H. A Relativistic equation for bound state problems[J]. Phys. Rev., 1951, 84: 1232–1242. DOI: 10.1103/PhysRev.84.1232.
- [105] XIE J J, GENG L S, OSET E. $f_2(1810)$ as a triangle singularity[J]. Phys. Rev. D, 2017, 95(3): 034004. DOI: 10.1103/PhysRevD.95.034004.
- [106] CHOI S, OTHERS. Observation of a narrow charmonium - like state in exclusive $B^+ \rightarrow \bar{c} K^+ \pi^+ \pi^- J/\psi$ decays[J]. Phys. Rev. Lett., 2003, 91: 262001. DOI: 10.1103/PhysRevLett.91.262001.
- [107] ABLIKIM M, OTHERS. Observation of a Charged Charmoniumlike Structure in $e^+e^- \rightarrow \pi^+\pi^- J/\psi$ at $\sqrt{s} = 4.26$ GeV[J]. Phys. Rev. Lett., 2013, 110: 252001. DOI: 10.1103/PhysRevLett.110.252001.
- [108] CHOI S, OTHERS. Observation of a resonance-like structure in the $\pi^\pm\psi'$ mass distribution in exclusive $B \rightarrow K\pi^\pm\psi'$ decays[J]. Phys. Rev. Lett., 2008, 100: 142001. DOI: 10.1103/PhysRevLett.100.142001.
- [109] GUO F K, HIDALGO-DUQUE C, NIEVES J, et al. Heavy quark symmetries and heavy meson molecules [J]. Int. J. Mod. Phys. Conf. Ser., 2014, 26: 1460070. DOI: 10.1142/S2010194514600702.
- [110] CREDE V, ROBERTS W. Progress towards understanding baryon resonances[J]. Rept. Prog. Phys., 2013, 76: 076301. DOI: 10.1088/0034-4885/76/7/076301.
- [111] AAIJ R, OTHERS. Observation of excited Λ_b^0 baryons[J]. Phys. Rev. Lett., 2012, 109: 172003. DOI: 10.1103/PhysRevLett.109.172003.
- [112] AALTONEN T A, OTHERS. Evidence for a Bottom Baryon Resonance Λ_b^{*0} in CDF Data[J]. Phys. Rev. D, 2013, 88(7): 071101. DOI: 10.1103/PhysRevD.88.071101.
- [113] LUTZ M, KOLOMEITSEV E. On charm baryon resonances and chiral symmetry[J]. Nucl. Phys. A, 2004, 730: 110–120. DOI: 10.1016/j.nuclphysa.2003.10.012.
- [114] GARCIA-RECIO C, NIEVES J, ROMANETS O, et al. Odd parity bottom-flavored baryon resonances[J]. Phys. Rev. D, 2013, 87(3): 034032. DOI: 10.1103/PhysRevD.87.034032.

- [115] LIANG W, XIAO C, OSET E. Baryon states with open beauty in the extended local hidden gauge approach [J]. *Phys. Rev. D*, 2014, 89(5): 054023. DOI: 10.1103/PhysRevD.89.054023.
- [116] LIU Z W, ZHU S L. Pseudoscalar Meson and Charmed Baryon Scattering Lengths[J]. *Phys. Rev. D*, 2012, 86: 034009. DOI: 10.1103/PhysRevD.86.034009.
- [117] ALTENBUCHINGER M, GENG L S, WEISE W. Scattering lengths of Nambu-Goldstone bosons off D mesons and dynamically generated heavy-light mesons[J]. *Phys. Rev. D*, 2014, 89(1): 014026. DOI: 10.1103/PhysRevD.89.014026.
- [118] BRICENO R A, LIN H W, BOLTON D R. Charmed-Baryon Spectroscopy from Lattice QCD with $N_f=2+1+1$ Flavors[J]. *Phys. Rev. D*, 2012, 86: 094504. DOI: 10.1103/PhysRevD.86.094504.
- [119] ALEXANDROU C, DRACH V, JANSEN K, et al. Baryon spectrum with $N_f = 2 + 1 + 1$ twisted mass fermions[J]. *Phys. Rev. D*, 2014, 90(7): 074501. DOI: 10.1103/PhysRevD.90.074501.
- [120] LIU L, LIN H W, ORGINOS K, et al. Singly and Doubly Charmed $J=1/2$ Baryon Spectrum from Lattice QCD[J]. *Phys. Rev. D*, 2010, 81: 094505. DOI: 10.1103/PhysRevD.81.094505.
- [121] NAMEKAWA Y, OTHERS. Charmed baryons at the physical point in 2+1 flavor lattice QCD[J]. *Phys. Rev. D*, 2013, 87(9): 094512. DOI: 10.1103/PhysRevD.87.094512.
- [122] BROWN Z S, DETMOLD W, MEINEL S, et al. Charmed bottom baryon spectroscopy from lattice QCD [J]. *Phys. Rev. D*, 2014, 90(9): 094507. DOI: 10.1103/PhysRevD.90.094507.
- [123] LEWIS R, WOLOSHYN R. Bottom baryons from a dynamical lattice QCD simulation[J]. *Phys. Rev. D*, 2009, 79: 014502. DOI: 10.1103/PhysRevD.79.014502.
- [124] PADMANATH M, EDWARDS R G, MATHUR N, et al. Spectroscopy of triply-charmed baryons from lattice QCD[J]. *Phys. Rev. D*, 2014, 90(7): 074504. DOI: 10.1103/PhysRevD.90.074504.
- [125] MEINEL S. Excited-state spectroscopy of triply-bottom baryons from lattice QCD[J]. *Phys. Rev. D*, 2012, 85: 114510. DOI: 10.1103/PhysRevD.85.114510.
- [126] PADMANATH M, EDWARDS R G, MATHUR N, et al. Excited-state spectroscopy of singly, doubly and triply-charmed baryons from lattice QCD[C]//6th International Workshop on Charm Physics. [S.l.: s.n.], 2013.
- [127] PADMANATH M, EDWARDS R G, MATHUR N, et al. Spectroscopy of doubly and triply-charmed baryons from lattice QCD[J]. *PoS*, 2014, LATTICE2013: 247. DOI: 10.22323/1.187.0247.
- [128] HE X G, LI X Q, LIU X, et al. $\Lambda_c(2940)^+$: A Possible molecular state?[J]. *Eur. Phys. J. C*, 2007, 51: 883–889. DOI: 10.1140/epjc/s10052-007-0347-y.

- [129] DONG Y, FAESSLER A, GUTSCHE T, et al. Strong two-body decays of the $\Lambda_c(2940)^+$ in a hadronic molecule picture[J]. Phys. Rev. D, 2010, 81: 014006. DOI: 10.1103/PhysRevD.81.014006.
- [130] DONG Y, FAESSLER A, GUTSCHE T, et al. Radiative decay of $\Lambda_c(2940)^+$ in a hadronic molecule picture [J]. Phys. Rev. D, 2010, 82: 034035. DOI: 10.1103/PhysRevD.82.034035.
- [131] DONG Y, FAESSLER A, GUTSCHE T, et al. Strong three-body decays of $\Lambda_c(2940)^+$ [J]. Phys. Rev. D, 2011, 83: 094005. DOI: 10.1103/PhysRevD.83.094005.
- [132] ZHANG J R. S -wave $D^{(*)}N$ molecular states: $\Sigma_c(2800)$ and $\Lambda_c(2940)^+$?[J]. Phys. Rev. D, 2014, 89(9): 096006. DOI: 10.1103/PhysRevD.89.096006.
- [133] ORTEGA P, ENTEM D, FERNANDEZ F. Quark model description of the $\Lambda_c(2940)^+$ as a molecular D^*N state and the possible existence of the $\Lambda_b(6248)$ [J]. Phys. Lett. B, 2013, 718: 1381–1384. DOI: 10.1016/j.physletb.2012.12.025.
- [134] HE J, YE Y T, SUN Z F, et al. The observed charmed hadron $\Lambda_c(2940)^+$ and the D^*N interaction[J]. Phys. Rev. D, 2010, 82: 114029. DOI: 10.1103/PhysRevD.82.114029.
- [135] CHENG H Y, CHUA C K. Strong Decays of Charmed Baryons in Heavy Hadron Chiral Perturbation Theory [J]. Phys. Rev. D, 2007, 75: 014006. DOI: 10.1103/PhysRevD.75.014006.
- [136] CHEN C, CHEN X L, LIU X, et al. Strong decays of charmed baryons[J]. Phys. Rev. D, 2007, 75: 094017. DOI: 10.1103/PhysRevD.75.094017.
- [137] ZHONG X H, ZHAO Q. Charmed baryon strong decays in a chiral quark model[J]. Phys. Rev. D, 2008, 77: 074008. DOI: 10.1103/PhysRevD.77.074008.
- [138] LIU L H, XIAO L Y, ZHONG X H. Charm-strange baryon strong decays in a chiral quark model[J]. Phys. Rev. D, 2012, 86: 034024. DOI: 10.1103/PhysRevD.86.034024.
- [139] YASUI S. Spectroscopy of heavy baryons with heavy-quark symmetry breaking: Transition relations at next-to-leading order[J]. Phys. Rev. D, 2015, 91(1): 014031. DOI: 10.1103/PhysRevD.91.014031.
- [140] GAMERMANN D, JIMENEZ-TEJERO C, RAMOS A. Radiative decays of dynamically generated charmed baryons[J]. Phys. Rev. D, 2011, 83: 074018. DOI: 10.1103/PhysRevD.83.074018.
- [141] GAMERMANN D, DAI L, OSET E. Radiative decay of the dynamically generated open and hidden charm scalar meson resonances $D(s_0)^*(2317)$ and $X(3700)$ [J]. Phys. Rev. C, 2007, 76: 055205. DOI: 10.1103/PhysRevC.76.055205.
- [142] LUTZ M F, SOYEUR M. Radiative and isospin-violating decays of $D(s)$ -mesons in the hadrogenesis conjecture[J]. Nucl. Phys. A, 2008, 813: 14–95. DOI: 10.1016/j.nuclphysa.2008.09.003.

- [143] DONG Y B, FAESSLER A, GUTSCHE T, et al. Estimate for the $X(3872) \rightarrow J/\psi \gamma$ decay width[J]. Phys. Rev. D, 2008, 77: 094013. DOI: 10.1103/PhysRevD.77.094013.
- [144] LIU X. Strong decays of newly observed heavy flavor hadrons[J]. Chin. Phys. C, 2009, 33: 473–480. DOI: 10.1088/1674-1137/33/6/014.
- [145] MA Y L. Estimates for $X(4350)$ Decays from the Effective Lagrangian Approach[J]. Phys. Rev. D, 2010, 82: 015013. DOI: 10.1103/PhysRevD.82.015013.
- [146] NIELSEN M, ZANETTI C. Radiative decay of the $X(3872)$ as a mixed molecule-charmonium state in QCD Sum Rules[J]. Phys. Rev. D, 2010, 82: 116002. DOI: 10.1103/PhysRevD.82.116002.
- [147] ACETI F, MOLINA R, OSET E. The $X(3872) \rightarrow J/\psi \gamma$ decay in the $D\bar{D}^*$ molecular picture[J]. Phys. Rev. D, 2012, 86: 113007. DOI: 10.1103/PhysRevD.86.113007.
- [148] DONG Y, FAESSLER A, GUTSCHE T, et al. Strong decays of molecular states Z_c^+ and $Z_c'^+$ [J]. Phys. Rev. D, 2013, 88(1): 014030. DOI: 10.1103/PhysRevD.88.014030.
- [149] WEINBERG S. Elementary particle theory of composite particles[J]. Phys. Rev., 1963, 130: 776–783. DOI: 10.1103/PhysRev.130.776.
- [150] WEINBERG S. Evidence That the Deuteron Is Not an Elementary Particle[J]. Phys. Rev., 1965, 137: B672–B678. DOI: 10.1103/PhysRev.137.B672.
- [151] HANHART C, KALASHNIKOVA Y, NEFEDIEV A. Lineshapes for composite particles with unstable constituents[J]. Phys. Rev. D, 2010, 81: 094028. DOI: 10.1103/PhysRevD.81.094028.
- [152] BARU V, HAIDENBAUER J, HANHART C, et al. Evidence that the $a(0)(980)$ and $f(0)(980)$ are not elementary particles[J]. Phys. Lett. B, 2004, 586: 53–61. DOI: 10.1016/j.physletb.2004.01.088.
- [153] CLEVEN M, GUO F K, HANHART C, et al. Bound state nature of the exotic Z_b states[J]. Eur. Phys. J. A, 2011, 47: 120. DOI: 10.1140/epja/i2011-11120-6.
- [154] GAMERMANN D, NIEVES J, OSET E, et al. Couplings in coupled channels versus wave functions: application to the $X(3872)$ resonance[J]. Phys. Rev. D, 2010, 81: 014029. DOI: 10.1103/PhysRevD.81.014029.
- [155] YAMAGATA-SEKIHARA J, NIEVES J, OSET E. Couplings in coupled channels versus wave functions in the case of resonances: application to the two $\Lambda(1405)$ states[J]. Phys. Rev. D, 2011, 83: 014003. DOI: 10.1103/PhysRevD.83.014003.
- [156] ACETI F, OSET E. Wave functions of composite hadron states and relationship to couplings of scattering amplitudes for general partial waves[J]. Phys. Rev. D, 2012, 86: 014012. DOI: 10.1103/PhysRevD.86.014012.

- [157] XIAO C, ACETI F, BAYAR M. The small $K\pi$ component in the K^* wave functions[J]. Eur. Phys. J. A, 2013, 49: 22. DOI: 10.1140/epja/i2013-13022-y.
- [158] ACETI F, DAI L, GENG L, et al. Meson-baryon components in the states of the baryon decuplet[J]. Eur. Phys. J. A, 2014, 50: 57. DOI: 10.1140/epja/i2014-14057-2.
- [159] ACETI F, OSET E, ROCA L. Composite nature of the $\Lambda(1520)$ resonance[J]. Phys. Rev. C, 2014, 90(2): 025208. DOI: 10.1103/PhysRevC.90.025208.
- [160] SEKIHARA T, HYODO T, JIDO D. Comprehensive analysis of the wave function of a hadronic resonance and its compositeness[J]. PTEP, 2015, 2015: 063D04. DOI: 10.1093/ptep/ptv081.
- [161] NAGAIHIRO H, HOSAKA A. Elementarity of composite systems[J]. Phys. Rev. C, 2014, 90(6): 065201. DOI: 10.1103/PhysRevC.90.065201.
- [162] HYODO T. Structure of Near-Threshold s-Wave Resonances[J]. Phys. Rev. Lett., 2013, 111: 132002. DOI: 10.1103/PhysRevLett.111.132002.
- [163] GUO Z H, OLLER J. Resonance on top of thresholds: the $\Lambda_c(2595)^+$ as an extremely fine-tuned state[J]. Phys. Rev. D, 2016, 93(5): 054014. DOI: 10.1103/PhysRevD.93.054014.
- [164] GUO Z H, OLLER J. Probabilistic interpretation of compositeness relation for resonances[J]. Phys. Rev. D, 2016, 93(9): 096001. DOI: 10.1103/PhysRevD.93.096001.
- [165] HYODO T, JIDO D, HOSAKA A. Compositeness of dynamically generated states in a chiral unitary approach[J]. Phys. Rev. C, 2012, 85: 015201. DOI: 10.1103/PhysRevC.85.015201.
- [166] GAMERMANN D, OSET E. Isospin breaking effects in the $X(3872)$ resonance[J]. Phys. Rev. D, 2009, 80: 014003. DOI: 10.1103/PhysRevD.80.014003.
- [167] MEIßNER U G, OLLER J A. Testing the $\chi_{c1} p$ composite nature of the $P_c(4450)$ [J]. Phys. Lett. B, 2015, 751: 59–62. DOI: 10.1016/j.physletb.2015.10.015.
- [168] GARCIA-RECIO C, HIDALGO-DUQUE C, NIEVES J, et al. Compositeness of the strange, charm, and beauty odd parity Λ states[J]. Phys. Rev. D, 2015, 92(3): 034011. DOI: 10.1103/PhysRevD.92.034011.
- [169] LU J X, CHEN H X, GUO Z H, et al. $\Lambda_c(2595)$ resonance as a dynamically generated state: The compositeness condition and the large N_c evolution[J]. Phys. Rev. D, 2016, 93(11): 114028. DOI: 10.1103/PhysRevD.93.114028.
- [170] GARCIA-RECIO C, NIEVES J, ROMANETS O, et al. Hidden charm N and Delta resonances with heavy-quark symmetry[J]. Phys. Rev. D, 2013, 87: 074034. DOI: 10.1103/PhysRevD.87.074034.

- [171] PELAEZ J. On the Nature of light scalar mesons from their large $N(c)$ behavior[J]. *Phys. Rev. Lett.*, 2004, 92: 102001. DOI: 10.1103/PhysRevLett.92.102001.
- [172] SUN Z, XIAO L, XIAO Z, et al. Model dependent analyses on the $N(c)$ dependence of the sigma pole trajectory[J]. *Mod. Phys. Lett. A*, 2007, 22: 711–718. DOI: 10.1142/S0217732307023304.
- [173] PELAEZ J, RIOS G. Nature of the $f_0(600)$ from its $N(c)$ dependence at two loops in unitarized Chiral Perturbation Theory[J]. *Phys. Rev. Lett.*, 2006, 97: 242002. DOI: 10.1103/PhysRevLett.97.242002.
- [174] GUO Z, SANZ CILLERO J, ZHENG H. Partial waves and large $N(C)$ resonance sum rules[J]. *JHEP*, 2007, 06: 030. DOI: 10.1088/1126-6708/2007/06/030.
- [175] GENG L, OSET E, PELAEZ J, et al. Nature of the axial-vector mesons from their $N(c)$ behavior within the chiral unitary approach[J]. *Eur. Phys. J. A*, 2009, 39: 81–87. DOI: 10.1140/epja/i2008-10689-y.
- [176] NIEVES J, PICH A, RUIZ ARRIOLA E. Large- N_c Properties of the rho and $f_0(600)$ Mesons from Unitary Resonance Chiral Dynamics[J]. *Phys. Rev. D*, 2011, 84: 096002. DOI: 10.1103/PhysRevD.84.096002.
- [177] LEDWIG T, NIEVES J, PICH A, et al. Large- N_c naturalness in coupled-channel meson-meson scattering [J]. *Phys. Rev. D*, 2014, 90(11): 114020. DOI: 10.1103/PhysRevD.90.114020.
- [178] GARCIA-RECIO C, NIEVES J, SALCEDO L. Large N_c Weinberg-Tomozawa interaction and negative parity s-wave baryon resonances[J]. *Phys. Rev. D*, 2006, 74: 036004. DOI: 10.1103/PhysRevD.74.036004.
- [179] ROCA L, HYODO T, JIDO D. On the nature of the $\Lambda(1405)$ and $\Lambda(1670)$ from their $N(c)$ behavior in chiral dynamics[J]. *Nucl. Phys. A*, 2008, 809: 65–87. DOI: 10.1016/j.nuclphysa.2008.05.014.
- [180] HYODO T, JIDO D, ROCA L. Structure of the (1405) baryon resonance from its large $N(c)$ behavior[J]. *Phys. Rev. D*, 2008, 77: 056010. DOI: 10.1103/PhysRevD.77.056010.
- [181] 'T HOOFT G. A Planar Diagram Theory for Strong Interactions[J]. *Nucl. Phys. B*, 1974, 72: 461. DOI: 10.1016/0550-3213(74)90154-0.
- [182] WITTEN E. Baryons in the $1/n$ Expansion[J]. *Nucl. Phys. B*, 1979, 160: 57–115. DOI: 10.1016/0550-3213(79)90232-3.
- [183] MANOHAR A V. Large N QCD[C]//Les Houches Summer School in Theoretical Physics, Session 68: Probing the Standard Model of Particle Interactions. [S.l.: s.n.], 1998: 1091–1169.
- [184] JENKINS E E. Large $N(c)$ baryons[J]. *Ann. Rev. Nucl. Part. Sci.*, 1998, 48: 81–119. DOI: 10.1146/annurev.nucl.48.1.81.
- [185] LUCINI B, PANERO M. $SU(N)$ gauge theories at large N [J]. *Phys. Rept.*, 2013, 526: 93–163. DOI: 10.1016/j.physrep.2013.01.001.

- [186] MATAGNE N, STANCU F. Baryon resonances in large N_c QCD[J]. *Rev. Mod. Phys.*, 2015, 87: 211–245. DOI: 10.1103/RevModPhys.87.211.
- [187] JAFFE R. Ordinary and extraordinary hadrons[J]. *AIP Conf. Proc.*, 2007, 964(1): 1–13. DOI: 10.1063/1.2823850.
- [188] GOITY J L. $1/N(c)$ countings in baryons[J]. *Phys. Atom. Nucl.*, 2005, 68: 624–633. DOI: 10.1134/1.1903092.
- [189] COHEN T D, DAKIN D C, NELLORE A, et al. Excited baryon decay widths in large $N(c)$ QCD[J]. *Phys. Rev. D*, 2004, 69: 056001. DOI: 10.1103/PhysRevD.69.056001.
- [190] KARL G, PATERA J, PERANTONIS S. Quantization of Chiral Solitons for Three Flavors and the Large N Limit[J]. *Phys. Lett. B*, 1986, 172: 49–52. DOI: 10.1016/0370-2693(86)90214-5.
- [191] DULINSKI Z. Large N_c Limit for Physical Quantities in $SU(3)$ Skyrme Model[J]. *Acta Phys. Polon. B*, 1988, 19: 891.
- [192] DULINSKI Z, PRASZALOWICZ M. Large N_c Limit of the Skyrme Model[J]. *Acta Phys. Polon. B*, 1988, 18: 1157.
- [193] JENKINS E E. Heavy baryon masses in the $1/m(Q)$ and $1/N(c)$ expansions[J]. *Phys. Rev. D*, 1996, 54: 4515–4531. DOI: 10.1103/PhysRevD.54.4515.
- [194] JENKINS E E. Update of heavy baryon mass predictions[J]. *Phys. Rev. D*, 1997, 55: 10–12. DOI: 10.1103/PhysRevD.55.R10.
- [195] JENKINS E E. Model-Independent Bottom Baryon Mass Predictions in the $1/N(c)$ Expansion[J]. *Phys. Rev. D*, 2008, 77: 034012. DOI: 10.1103/PhysRevD.77.034012.
- [196] HYODO T, JIDO D, HOSAKA A. Study of exotic hadrons in s-wave scatterings induced by chiral interaction in the flavor symmetric limit[J]. *Phys. Rev. D*, 2007, 75: 034002. DOI: 10.1103/PhysRevD.75.034002.
- [197] COHEN T D, LEBED R F. $SU(3)$ Clebsch-Gordan coefficients for baryon-meson coupling at arbitrary $N(c)$ [J]. *Phys. Rev. D*, 2004, 70: 096015. DOI: 10.1103/PhysRevD.70.096015.
- [198] HECHT K. The use of $SU(3)$ in the elimination of spurious center of mass states[J]. *Nucl. Phys. A*, 1971, 170(1): 34–54. DOI: 10.1016/0375-9474(71)90681-6.
- [199] BALI G S, BURSA F, CASTAGNINI L, et al. Mesons in large- N QCD[J]. *JHEP*, 2013, 06: 071. DOI: 10.1007/JHEP06(2013)071.
- [200] DEGRAND T. Lattice baryons in the $1/N$ expansion[J]. *Phys. Rev. D*, 2012, 86: 034508. DOI: 10.1103/PhysRevD.86.034508.

- [201] DEGRAND T. Lattice calculations of the spectroscopy of baryons with broken flavor SU(3) symmetry and 3, 5, or 7 colors[J]. *Phys. Rev. D*, 2014, 89(1): 014506. DOI: 10.1103/PhysRevD.89.014506.
- [202] BOTTINO A, DONATO F, FORNENGO N, et al. Implications for relic neutralinos of the theoretical uncertainties in the neutralino nucleon cross-section[J]. *Astropart. Phys.*, 2000, 13: 215–225. DOI: 10.1016/S0927-6505(99)00122-X.
- [203] BOTTINO A, DONATO F, FORNENGO N, et al. Interpreting the recent results on direct search for dark matter particles in terms of relic neutralino[J]. *Phys. Rev. D*, 2008, 78: 083520. DOI: 10.1103/PhysRevD.78.083520.
- [204] ELLIS J R, OLIVE K A, SANTOSO Y, et al. Update on the direct detection of supersymmetric dark matter [J]. *Phys. Rev. D*, 2005, 71: 095007. DOI: 10.1103/PhysRevD.71.095007.
- [205] ELLIS J R, OLIVE K A, SAVAGE C. Hadronic Uncertainties in the Elastic Scattering of Supersymmetric Dark Matter[J]. *Phys. Rev. D*, 2008, 77: 065026. DOI: 10.1103/PhysRevD.77.065026.
- [206] HILL R J, SOLON M P. Universal behavior in the scattering of heavy, weakly interacting dark matter on nuclear targets[J]. *Phys. Lett. B*, 2012, 707: 539–545. DOI: 10.1016/j.physletb.2012.01.013.
- [207] CLINE J M, KAINULAINEN K, SCOTT P, et al. Update on scalar singlet dark matter[J]. *Phys. Rev. D*, 2013, 88: 055025. DOI: 10.1103/PhysRevD.88.055025.
- [208] ELLIS J, NAGATA N, OLIVE K A. Uncertainties in WIMP Dark Matter Scattering Revisited[J]. *Eur. Phys. J. C*, 2018, 78(7): 569. DOI: 10.1140/epjc/s10052-018-6047-y.
- [209] MASSOT E, MARGUERON J, CHANFRAY G. On the maximum mass of hyperonic neutron stars[J]. *EPL*, 2012, 97(3): 39002. DOI: 10.1209/0295-5075/97/39002.
- [210] SCHULZE H J, RIJKEN T. Maximum mass of hyperon stars with the Nijmegen ES C-08 model[J]. *Phys. Rev. C*, 2011, 84: 035801. DOI: 10.1103/PhysRevC.84.035801.
- [211] HU J, LI A, TOKI H, et al. Extended quark mean-field model for neutron stars[J]. *Phys. Rev. C*, 2014, 89 (2): 025802. DOI: 10.1103/PhysRevC.89.025802.
- [212] MIYATSU T, YAMAMURO S, NAKAZATO K. A new equation of state for neutron star matter with nuclei in the crust and hyperons in the core[J]. *Astrophys. J.*, 2013, 777: 4. DOI: 10.1088/0004-637X/777/1/4.
- [213] DEMOREST P, PENNUCCI T, RANSOM S, et al. Shapiro Delay Measurement of A Two Solar Mass Neutron Star[J]. *Nature*, 2010, 467: 1081–1083. DOI: 10.1038/nature09466.
- [214] ANTONIADIS J, OTHERS. A Massive Pulsar in a Compact Relativistic Binary[J]. *Science*, 2013, 340: 6131. DOI: 10.1126/science.1233232.

- [215] OSET E, OTHERS. Weak decays of heavy hadrons into dynamically generated resonances[J]. *Int. J. Mod. Phys. E*, 2016, 25: 1630001. DOI: 10.1142/S0218301316300010.
- [216] ROCA L, MAI M, OSET E, et al. Predictions for the $\Lambda_b \rightarrow J/\psi \Lambda(1405)$ decay[J]. *Eur. Phys. J. C*, 2015, 75(5): 218. DOI: 10.1140/epjc/s10052-015-3438-1.
- [217] MIYAHARA K, HYODO T, OSET E. Weak decay of Λ_c^+ for the study of $\Lambda(1405)$ and $\Lambda(1670)$ [J]. *Phys. Rev. C*, 2015, 92(5): 055204. DOI: 10.1103/PhysRevC.92.055204.
- [218] IKENO N, OSET E. Semileptonic Λ_c decay to νl^+ and $\Lambda(1405)$ [J]. *Phys. Rev. D*, 2016, 93(1): 014021. DOI: 10.1103/PhysRevD.93.014021.
- [219] XIE J J, LIANG W H, OSET E. Hidden charm pentaquark and $\Lambda(1405)$ in the $\Lambda_b^0 \rightarrow \eta_c K^- p(\pi\Sigma)$ reaction [J]. *Phys. Lett. B*, 2018, 777: 447–452. DOI: 10.1016/j.physletb.2017.12.064.
- [220] DÖRING M, MEIBNER U G, WANG W. Chiral Dynamics and S-wave Contributions in Semileptonic B decays[J]. *JHEP*, 2013, 10: 011. DOI: 10.1007/JHEP10(2013)011.
- [221] KAISER N. Chiral corrections to kaon nucleon scattering lengths[J]. *Phys. Rev. C*, 2001, 64: 045204. DOI: 10.1103/PhysRevC.73.069902.
- [222] LIU Y R, ZHU S L. Meson-baryon scattering lengths in HB χ PT[J]. *Phys. Rev. D*, 2007, 75: 034003. DOI: 10.1103/PhysRevD.75.034003.
- [223] LIU Y R, ZHU S L. Decuplet contribution to the meson-baryon scattering lengths[J]. *Eur. Phys. J. C*, 2007, 52: 177–186. DOI: 10.1140/epjc/s10052-007-0348-x.
- [224] MAI M, BRUNS P C, KUBIS B, et al. Aspects of meson-baryon scattering in three and two-flavor chiral perturbation theory[J]. *Phys. Rev. D*, 2009, 80: 094006. DOI: 10.1103/PhysRevD.80.094006.
- [225] HUANG B L, LI Y D. Kaon-nucleon scattering to one-loop order in heavy baryon chiral perturbation theory [J]. *Phys. Rev. D*, 2015, 92(11): 114033. DOI: 10.1103/PhysRevD.95.019903.
- [226] TOROK A, BEANE S R, DETMOLD W, et al. Meson-Baryon Scattering Lengths from Mixed-Action Lattice QCD[J]. *Phys. Rev. D*, 2010, 81: 074506. DOI: 10.1103/PhysRevD.81.074506.
- [227] DETMOLD W, NICHOLSON A. Low energy scattering phase shifts for meson-baryon systems[J]. *Phys. Rev. D*, 2016, 93(11): 114511. DOI: 10.1103/PhysRevD.93.114511.
- [228] NIIYAMA M, OTHERS. Photoproduction of $\Lambda(1405)$ and $\Sigma(1385)$ on the proton at $E(\gamma) = 1.5\text{--}2.4\text{--GeV}$ [J]. *Phys. Rev. C*, 2008, 78: 035202. DOI: 10.1103/PhysRevC.78.035202.
- [229] AGAKISHIEV G, OTHERS. Baryonic resonances close to the $\bar{K}N$ threshold: the case of $\Lambda(1405)$ in pp collisions[J]. *Phys. Rev. C*, 2013, 87: 025201. DOI: 10.1103/PhysRevC.87.025201.

- [230] MORIYA K, OTHERS. Measurement of the $\Sigma\pi$ photoproduction line shapes near the $\Lambda(1405)$ [J]. *Phys. Rev. C*, 2013, 87(3): 035206. DOI: 10.1103/PhysRevC.87.035206.
- [231] MORIYA K, OTHERS. Differential Photoproduction Cross Sections of the $\Sigma^0(1385)$, $\Lambda(1405)$, and $\Lambda(1520)$ [J]. *Phys. Rev. C*, 2013, 88: 045201. DOI: 10.1103/PhysRevC.88.045201.
- [232] MORIYA K, OTHERS. Spin and parity measurement of the $\Lambda(1405)$ baryon[J]. *Phys. Rev. Lett.*, 2014, 112(8): 082004. DOI: 10.1103/PhysRevLett.112.082004.
- [233] GEGELIA J, JAPARIDZE G. Matching heavy particle approach to relativistic theory[J]. *Phys. Rev. D*, 1999, 60: 114038. DOI: 10.1103/PhysRevD.60.114038.
- [234] GENG L. Recent developments in $SU(3)$ covariant baryon chiral perturbation theory[J]. *Front. Phys. (Beijing)*, 2013, 8: 328–348. DOI: 10.1007/s11467-013-0327-7.
- [235] ALARCON J, MARTIN CAMALICH J, OLLER J. The chiral representation of the πN scattering amplitude and the pion-nucleon sigma term[J]. *Phys. Rev. D*, 2012, 85: 051503. DOI: 10.1103/PhysRevD.85.051503.
- [236] ALARCON J, MARTIN CAMALICH J, OLLER J. Improved description of the πN -scattering phenomenology in covariant baryon chiral perturbation theory[J]. *Annals Phys.*, 2013, 336: 413–461. DOI: 10.1016/j.aop.2013.06.001.
- [237] YAO D L, SIEMENS D, BERNARD V, et al. Pion-nucleon scattering in covariant baryon chiral perturbation theory with explicit Delta resonances[J]. *JHEP*, 2016, 05: 038. DOI: 10.1007/JHEP05(2016)038.
- [238] SIEMENS D, BERNARD V, EPELBAUM E, et al. Elastic pion-nucleon scattering in chiral perturbation theory: A fresh look[J]. *Phys. Rev. C*, 2016, 94(1): 014620. DOI: 10.1103/PhysRevC.94.014620.
- [239] SIEMENS D, RUIZ DE ELVIRA J, EPELBAUM E, et al. Reconciling threshold and subthreshold expansions for pion–nucleon scattering[J]. *Phys. Lett. B*, 2017, 770: 27–34. DOI: 10.1016/j.physletb.2017.04.039.
- [240] SIEMENS D, BERNARD V, EPELBAUM E, et al. Elastic and inelastic pion-nucleon scattering to fourth order in chiral perturbation theory[J]. *Phys. Rev. C*, 2017, 96(5): 055205. DOI: 10.1103/PhysRevC.96.055205.
- [241] REN X L, GENG L, MARTIN CAMALICH J, et al. Octet baryon masses in next-to-next-to-next-to-leading order covariant baryon chiral perturbation theory[J]. *JHEP*, 2012, 12: 073. DOI: 10.1007/JHEP12(2012)073.
- [242] REN X L, GENG L, MENG J, et al. Virtual decuplet effects on octet baryon masses in covariant baryon chiral perturbation theory[J]. *Phys. Rev. D*, 2013, 87(7): 074001. DOI: 10.1103/PhysRevD.87.074001.
- [243] REN X L, GENG L S, MENG J. Baryon chiral perturbation theory with Wilson fermions up to $\mathcal{O}(a^2)$ and discretization effects of latest $n_f = 2 + 1$ LQCD octet baryon masses[J]. *Eur. Phys. J. C*, 2014, 74(2): 2754. DOI: 10.1140/epjc/s10052-014-2754-1.

- [244] REN X L, GENG L S, MENG J. Decuplet baryon masses in covariant baryon chiral perturbation theory[J]. Phys. Rev. D, 2014, 89(5): 054034. DOI: 10.1103/PhysRevD.89.054034.
- [245] REN X L, GENG L S, MENG J. Scalar strangeness content of the nucleon and baryon sigma terms[J]. Phys. Rev. D, 2015, 91(5): 051502. DOI: 10.1103/PhysRevD.91.051502.
- [246] REN X L, LI K W, GENG L S, et al. Leading order relativistic chiral nucleon-nucleon interaction[J]. Chin. Phys. C, 2018, 42(1): 014103. DOI: 10.1088/1674-1137/42/1/014103.
- [247] LI K W, REN X L, GENG L S, et al. Leading order relativistic hyperon-nucleon interactions in chiral effective field theory[J]. Chin. Phys. C, 2018, 42(1): 014105. DOI: 10.1088/1674-1137/42/1/014105.
- [248] SONG J, LI K W, GENG L S. Strangeness $S=-1$ hyperon-nucleon interactions: Chiral effective field theory versus lattice QCD[J]. Phys. Rev. C, 2018, 97(6): 065201. DOI: 10.1103/PhysRevC.97.065201.
- [249] LI K W, HYODO T, GENG L S. Strangeness $S=-2$ baryon-baryon interactions in relativistic chiral effective field theory[J]. Phys. Rev. C, 2018, 98(6): 065203. DOI: 10.1103/PhysRevC.98.065203.
- [250] XIAO Y, GENG L S, REN X L. Covariant chiral nucleon-nucleon contact Lagrangian up to order $\mathcal{O}(q^4)$ [J]. Phys. Rev. C, 2019, 99(2): 024004. DOI: 10.1103/PhysRevC.99.024004.
- [251] BECHER T, LEUTWYLER H. Low energy analysis of $\pi N \rightarrow \pi N$ [J]. JHEP, 2001, 06: 017. DOI: 10.1088/1126-6708/2001/06/017.
- [252] ARNDT R, BRISCOE W, STRAKOVSKY I, et al. Extended partial-wave analysis of πN scattering data [J]. Phys. Rev. C, 2006, 74: 045205. DOI: 10.1103/PhysRevC.74.045205.
- [253] HYSLOP J, ARNDT R, ROPER L, et al. Partial wave analysis of K^+ nucleon scattering[J]. Phys. Rev. D, 1992, 46: 961–969. DOI: 10.1103/PhysRevD.46.961.
- [254] HOFERICHTER M, RUIZ DE ELVIRA J, KUBIS B, et al. Roy–Steiner-equation analysis of pion–nucleon scattering[J]. Phys. Rept., 2016, 625: 1–88. DOI: 10.1016/j.physrep.2016.02.002.
- [255] FRINK M, MEISSNER U G. Chiral extrapolations of baryon masses for unquenched three flavor lattice simulations[J]. JHEP, 2004, 07: 028. DOI: 10.1088/1126-6708/2004/07/028.
- [256] REN X L, ALVAREZ-RUSO L, GENG L S, et al. Consistency between $SU(3)$ and $SU(2)$ covariant baryon chiral perturbation theory for the nucleon mass[J]. Phys. Lett. B, 2017, 766: 325–333. DOI: 10.1016/j.physletb.2017.01.024.
- [257] VAN HAMEREN A, PAPADOPOULOS C, PITTAU R. Automated one-loop calculations: A Proof of concept[J]. JHEP, 2009, 09: 106. DOI: 10.1088/1126-6708/2009/09/106.

- [258] VAN HAMEREN A. OneLoop: For the evaluation of one-loop scalar functions[J]. *Comput. Phys. Commun.*, 2011, 182: 2427–2438. DOI: 10.1016/j.cpc.2011.06.011.
- [259] MEISSNER U G, OLLER J. Chiral unitary meson baryon dynamics in the presence of resonances: Elastic pion nucleon scattering[J]. *Nucl. Phys. A*, 2000, 673: 311–334. DOI: 10.1016/S0375-9474(00)00150-0.
- [260] ALARCON J, MARTIN CAMALICH J, OLLER J, et al. πN scattering in relativistic baryon chiral perturbation theory revisited[J]. *Phys. Rev. C*, 2011, 83: 055205. DOI: 10.1103/PhysRevC.83.055205.
- [261] SCHRODER H, OTHERS. The pion nucleon scattering lengths from pionic hydrogen and deuterium[J]. *Eur. Phys. J. C*, 2001, 21: 473–488. DOI: 10.1007/s100520100754.
- [262] CHENG T, DASHEN R F. Is $SU(2) \times SU(2)$ a better symmetry than $SU(3)$?[J]. *Phys. Rev. Lett.*, 1971, 26: 594. DOI: 10.1103/PhysRevLett.26.594.
- [263] BERNARD V, HEMMERT T R, MEISSNER U G. Cutoff schemes in chiral perturbation theory and the quark mass expansion of the nucleon mass[J]. *Nucl. Phys. A*, 2004, 732: 149–170. DOI: 10.1016/j.nuclphysa.2003.12.011.
- [264] XIAO Y, REN X L, LU J X, et al. Octet baryon magnetic moments at next-to-next-to-leading order in covariant chiral perturbation theory[J]. *Eur. Phys. J. C*, 2018, 78: 489. DOI: 10.1140/epjc/s10052-018-5960-4.
- [265] FETTES N, MEISSNER U G. Pion nucleon scattering in chiral perturbation theory. 2.: Fourth order calculation[J]. *Nucl. Phys. A*, 2000, 676: 311. DOI: 10.1016/S0375-9474(00)00199-8.
- [266] BUTLER M N, SAVAGE M J. Electromagnetic polarizability of the nucleon in chiral perturbation theory [J]. *Phys. Lett. B*, 1992, 294: 369–374. DOI: 10.1016/0370-2693(92)91535-H.
- [267] PASCALUTSA V, VANDERHAEGHEN M, YANG S N. Electromagnetic excitation of the $\Delta(1232)$ -resonance[J]. *Phys. Rept.*, 2007, 437: 125–232. DOI: 10.1016/j.physrep.2006.09.006.
- [268] PASCALUTSA V, PHILLIPS D R. Effective theory of the $\Delta(1232)$ in Compton scattering off the nucleon [J]. *Phys. Rev. C*, 2003, 67: 055202. DOI: 10.1103/PhysRevC.67.055202.
- [269] PASCALUTSA V. Quantization of an interacting spin - 3 / 2 field and the Δ isobar[J]. *Phys. Rev. D*, 1998, 58: 096002. DOI: 10.1103/PhysRevD.58.096002.
- [270] PASCALUTSA V, TIMMERMANS R. Field theory of nucleon to higher spin baryon transitions[J]. *Phys. Rev. C*, 1999, 60: 042201. DOI: 10.1103/PhysRevC.60.042201.
- [271] MUSKHELISHVILI N. Singular Integral Equations (P. Noordhof, Groningen, 1953)[M]. [S.l.: s.n.].

- [272] OMNES R. On the Solution of certain singular integral equations of quantum field theory[J]. *Nuovo Cim.*, 1958, 8: 316–326. DOI: 10.1007/BF02747746.
- [273] PATRIGNANI C, OTHERS. Review of Particle Physics[J]. *Chin. Phys. C*, 2016, 40(10): 100001. DOI: 10.1088/1674-1137/40/10/100001.
- [274] PELAEZ J. From controversy to precision on the sigma meson: a review on the status of the non-ordinary $f_0(500)$ resonance[J]. *Phys. Rept.*, 2016, 658: 1. DOI: 10.1016/j.physrep.2016.09.001.
- [275] OLLER J, OSET E, PELAEZ J. Meson meson interaction in a nonperturbative chiral approach[J]. *Phys. Rev. D*, 1999, 59: 074001. DOI: 10.1103/PhysRevD.59.074001.
- [276] ALBALADEJO M, OLLER J. Identification of a Scalar Glueball[J]. *Phys. Rev. Lett.*, 2008, 101: 252002. DOI: 10.1103/PhysRevLett.101.252002.
- [277] WOLKANOWSKI T, GIACOSA F, RISCHKE D H. $a_0(980)$ revisited[J]. *Phys. Rev. D*, 2016, 93(1): 014002. DOI: 10.1103/PhysRevD.93.014002.
- [278] DUDEK J J, EDWARDS R G, WILSON D J. An a_0 resonance in strongly coupled $\pi\eta$, $K\bar{K}$ scattering from lattice QCD[J]. *Phys. Rev. D*, 2016, 93(9): 094506. DOI: 10.1103/PhysRevD.93.094506.
- [279] GUO Z H, OLLER J. Resonances from meson-meson scattering in U(3) CHPT[J]. *Phys. Rev. D*, 2011, 84: 034005. DOI: 10.1103/PhysRevD.84.034005.
- [280] GUO Z H, LIU L, MEIßNER U G, et al. Chiral study of the $a_0(980)$ resonance and $\pi\eta$ scattering phase shifts in light of a recent lattice simulation[J]. *Phys. Rev. D*, 2017, 95(5): 054004. DOI: 10.1103/PhysRevD.95.054004.
- [281] JEGERLEHNER F, NYFFELER A. The Muon $g-2$ [J]. *Phys. Rept.*, 2009, 477: 1–110. DOI: 10.1016/j.physrep.2009.04.003.
- [282] ADLER S L. Consistency conditions on the strong interactions implied by a partially conserved axial-vector current. II[J]. *Phys. Rev.*, 1965, 139: B1638–B1643. DOI: 10.1103/PhysRev.139.B1638.
- [283] MORGAN D, PENNINGTON M. Low-energy $\gamma\gamma \rightarrow \pi\pi$ Cross-section and the QED Born Amplitude[J]. *Phys. Lett. B*, 1987, 192: 207–211. DOI: 10.1016/0370-2693(87)91169-5.
- [284] MORGAN D, PENNINGTON M. Is low-energy $\gamma\gamma \rightarrow \pi^0\pi^0$ predictable?[J]. *Phys. Lett. B*, 1991, 272: 134–138. DOI: 10.1016/0370-2693(91)91025-Q.
- [285] DANILKIN I, DEINEKA O, VANDERHAEGHEN M. Theoretical analysis of the $\gamma\gamma \rightarrow \pi^0\eta$ process[J]. *Phys. Rev. D*, 2017, 96(11): 114018. DOI: 10.1103/PhysRevD.96.114018.

- [286] DANILKIN I, GIL L, LUTZ M. Dynamical light vector mesons in low-energy scattering of Goldstone bosons[J]. Phys. Lett. B, 2011, 703: 504–509. DOI: 10.1016/j.physletb.2011.08.001.
- [287] GARCIA-MARTIN R, MOUSSALLAM B. MO analysis of the high statistics Belle results on $\gamma\gamma \rightarrow \pi^+\pi^-, \pi^0\pi^0$ with chiral constraints[J]. Eur. Phys. J. C, 2010, 70: 155–175. DOI: 10.1140/epjc/s10052-010-1471-7.
- [288] GOURDIN M, MARTIN A. Pion photon scattering[J]. IL Nuovo Cimento, 1960, 17(2): 224–243.
- [289] ALBALADEJO M, MOUSSALLAM B. Extended chiral Khuri-Treiman formalism for $\eta \rightarrow 3\pi$ and the role of the $a_0(980)$, $f_0(980)$ resonances[J]. Eur. Phys. J. C, 2017, 77(8): 508. DOI: 10.1140/epjc/s10052-017-5052-x.
- [290] GOMEZ NICOLA A, PELAEZ J. Meson meson scattering within one loop chiral perturbation theory and its unitarization[J]. Phys. Rev. D, 2002, 65: 054009. DOI: 10.1103/PhysRevD.65.054009.
- [291] DOBADO A, HERRERO M J, TRUONG T N. Unitarized Chiral Perturbation Theory for Elastic Pion-Pion Scattering[J]. Phys. Lett. B, 1990, 235: 134–140. DOI: 10.1016/0370-2693(90)90109-J.
- [292] OLLER J, OSET E, RAMOS A. Chiral unitary approach to meson meson and meson - baryon interactions and nuclear applications[J]. Prog. Part. Nucl. Phys., 2000, 45: 157–242. DOI: 10.1016/S0146-6410(00)00104-6.
- [293] ECKER G, GASSER J, PICH A, et al. The Role of Resonances in Chiral Perturbation Theory[J]. Nucl. Phys. B, 1989, 321: 311–342. DOI: 10.1016/0550-3213(89)90346-5.
- [294] LOW F. Bremsstrahlung of very low-energy quanta in elementary particle collisions[J]. Phys. Rev., 1958, 110: 974–977. DOI: 10.1103/PhysRev.110.974.
- [295] ABARBANEL H D, GOLDBERGER M L. LOW-ENERGY THEOREMS, DISPERSION RELATIONS AND SUPERCONVERGENCE SUM RULES FOR COMPTON SCATTERING[J]. Phys. Rev., 1968, 165: 1594–1609. DOI: 10.1103/PhysRev.165.1594.
- [296] BLACK D, FARIBORZ A H, SCHECHTER J. Chiral Lagrangian treatment of pi eta scattering[J]. Phys. Rev. D, 2000, 61: 074030. DOI: 10.1103/PhysRevD.61.074030.
- [297] ACHASOV N, SHESTAKOV G. Nature of the $a_0(980)$ meson in the light of photon-photon collisions[J]. Phys. Rev. D, 2010, 81: 094029. DOI: 10.1103/PhysRevD.81.094029.
- [298] OLLER J, OSET E. Theoretical study of the $\gamma\gamma \rightarrow \zeta$ meson - meson reaction[J]. Nucl. Phys. A, 1998, 629: 739–760. DOI: 10.1016/S0375-9474(97)00649-0.
- [299] ACHASOV N, SHESTAKOV G. $f_0(980)$ and $a_0(980)$ resonances near $\gamma\gamma \rightarrow K^+K^-$ and $\gamma\gamma \rightarrow K^0\bar{K}^0$ reaction thresholds[J]. JETP Lett., 2012, 96: 493–495. DOI: 10.1134/S0021364012200027.

[300] DAI L Y, PENNINGTON M R. Comprehensive amplitude analysis of $\gamma\gamma \rightarrow \pi^+\pi^-, \pi^0\pi^0$ and $\bar{K}K$ below 1.5 GeV[J]. Phys. Rev. D, 2014, 90(3): 036004. DOI: 10.1103/PhysRevD.90.036004.

[301] REN X L, MALABARBA B B, GENG L S, et al. K^* mesons with hidden charm arising from $KX(3872)$ and $KZ_c(3900)$ dynamics[J]. Phys. Lett. B, 2018, 785: 112–117. DOI: 10.1016/j.physletb.2018.08.034.

[302] WU T W, LIU M Z, GENG L S, et al. $DK, DDK,$ and $DDDK$ molecules—understanding the nature of the $D_{s0}^*(2317)$ [J]. Phys. Rev. D, 2019, 100(3): 034029. DOI: 10.1103/PhysRevD.100.034029.

Titre : Étude des interactions hadron-hadron en théorie effective des champs

Mots clés : théorie effective des champs, théorie de perturbation chirale, interactions hadron-hadron

Résumé : Les progrès techniques dont ont bénéficié les accélérateurs de particules ainsi que les détecteurs ont permis aux expérimentateurs de collecter des résultats sur un grand nombre d'interactions hadron-hadron, avec de grandes statistiques auprès d'accélérateurs tels que KEK, LHC, BEPC. Parmi les nombreuses approches utilisées pour décrire les interactions hadron-hadron à basse énergie, celles qui se basent sur la théorie effective des champs (EFT) deviennent les plus populaires. La théorie fondamentale des interactions fortes, la QCD, est perturbative aux grandes énergies (liberté asymptotique) mais pas aux basses énergies où la physique associée est dominée par le couplage fort et le confinement. Dans ce cadre, la brisure spontanée de la symétrie chirale est prise en compte et un développement perturbatif chiral est possible sur lequel sont également applicables des méthodes d'unitarisation. Des règles de comptage en puissance peuvent être introduites qui permettent la description d'une interaction hadron-hadron ordre par ordre. On peut ainsi améliorer la description de manière systématique et faire une évaluation des incertitudes.

Dans le présent travail, nous présentons tout d'abord brièvement les idées de base de la théorie effective des champs. Nous étudions ensuite trois processus de diffusion hadron-hadron, ayant chacun un intérêt particulier, dans le cadre de l'EFT. Nous montrerons ainsi la capacité de cette approche à expliquer les observables mesurées et de plus, à faire des prédictions sur des quantités qui ne le sont pas encore.

Première partie : Dans cette partie nous examinons la possibilité d'engendrer des résonances dans les interactions entre un baryon charmé ou un baryon bottom et un boson de Goldstone en utilisant un développement chiral unitarisé et en exploitant la symétrie approximative de quark lourd. Nous comparons plusieurs méthodes de régularisation pour l'intégrale de la fonction à deux points.

A l'ordre dominant, l'unique paramètre de la théorie est fixé de manière à reproduire les états $\Lambda_c(2595)$. Cette étude est ensuite étendue de manière à inclure les contributions sous-dominantes. Par ailleurs, nous avons étudié la structure du $\Lambda_c(2595)$ en utilisant le critère d'état composite de Weinberg ainsi que le développement en grand N_c .

Deuxième partie : Dans cette partie nous calculons les amplitudes d'interaction entre mésons légers et baryons de l'état fondamental dans le cadre de la théorie de perturbation chirale baryonique (BChPT) covariante et du groupe de saveur $SU(3)$ à l'ordre d'une boucle. Nous appliquons la méthode dite sur-couche étendue qui permet d'absorber à la fois les divergences ultra-violettes et les contributions qui violent la règle de comptage en puissances. Nous avons effectué, pour la première fois, un fit combiné des déphasages πN et KN . De plus, nous effectuons un fit global simultanément des déphasages méson-nucléon et des masses des baryons et nous trouvons un bon accord avec les données expérimentales. A la fin de cette partie nous discutons en détail les propriétés de convergence de la BChPT covariante.

Troisième partie : Dans cette partie nous étudions l'amplitude d'interaction d'une paire méson-méson dans l'isospin $I=1$ via le processus de production par des collisions photon-photon. Nous construisons les amplitudes de production en résolvant les équations d'Omnès-Muskhelishvili qui sont basées sur les propriétés générales d'analyticité et d'unitarité. Les mesures expérimentales de sections efficaces $\gamma\gamma \rightarrow \pi\pi$; et $\gamma\gamma \rightarrow KS$ de haute statistique effectuées récemment par la collaboration Belle nous permettent de contraindre les paramètres de notre modèle d'amplitude méson-méson (deux solutions sont trouvées) et d'en déduire les propriétés des résonances $a_0(980)$ et $a_0(1450)$ d'après leur position dans le plan complexe en énergie.

Title : Effective field theory studies of hadron-hadron interactions

Keywords : effective field theory, chiral perturbation theory, hadron-hadron interactions

Abstract : With the development of accelerator and detector techniques, experimentalists have obtained quite a large amount of data on hadron-hadron interactions with much higher statistics based on large experimental accelerators such as BEKB, LHC, BEPC and so on, revealing a large variety of phenomena for theoretical researches. In order to provide a reliable understanding on these experimental data, theorists continually investigate new models or improve the original ones. Among all the approaches for studying hadron-hadron interactions in the low energy regime, the Effective field theory(EFT) has now become one of most popular approaches. Due to the asymptotic freedom and the color confinement, the fundamental theory for the strong interaction, quantum chromodynamics(QCD) is perturbative at high energy, while at low energies it is in a strong coupled and confining regime and perturbation theory is not applicable. With the chiral symmetry and its spontaneous breaking fully taken into account, chiral perturbation theory and its unitary version make it possible to improve the descriptions order by order according to a certain power counting rule. One can thus improve the description systematically and evaluate the uncertainties.

In the present work, we first briefly introduce the main idea of effective field theory. Then we study three typical scattering processes as examples within the framework of EFT to show how EFT helps to understand experimental data and further more, its power for predicting the unmeasured ones.

Part I : In this part we investigate the interactions between singly charmed baryons and Goldstone bosons with a unitary chiral perturbation theory combined with approximate heavy quark symmetry.

We compare different regularization methods for the two-point integral. In the lowest order, we fix the only free parameter in our model by reproducing the $\Lambda_c(2595)$ and predict a number of resonances. We then extend our study to include the next-to-leading order contributions. Further more, we utilize the compositeness rules and large N_c expansion to study the structure of $\Lambda_c(2595)$ in different models.

Part II : In this part we calculate the interaction between ground state baryons and pseudoscalar meson up to one loop level with covariant SU(3) baryon chiral perturbation theory. We apply the extended-on-mass-shell scheme to absorb the Ultra-violate divergence and power counting breaking terms. For the first time we performed a combined fit for both πN and KN scattering phase shifts. Further more, we perform a global fit to meson-baryon scattering phase shifts and baryon masses and show that it can provide a reasonable description of the experimental data. In the end of this part we discuss in detail the convergence of covariant BChPT.

Part III : In this part, we study the meson-meson interaction with isospin $I = 1$ as final state interaction in photon-photon scattering. Muskhelishvili-Omnès (MO) representation based on dispersion relations and analytical properties of amplitudes are applied. The most recent experimental data on $\gamma\gamma \rightarrow \pi\pi\eta$; and $\gamma\gamma \rightarrow KS$ with much higher statistics from the Belle Collaboration are used to fix the parameters of our model, with which we calculate the position of $a_0(980)$ and $a_0(1450)$ which still remain ambiguous.